



The  
University  
Of  
Sheffield.

*FIBRE OPTIC COUPLED, INFRARED  
THERMOMETERS FOR PROCESSES  
INCURRING HARSH CONDITIONS*

Andrew David Heeley

Registration Number 150143161

This thesis is submitted in partial fulfilment of the requirements for the degree of  
Doctor of Philosophy

The University of Sheffield

Faculty of Engineering

Department of Electronic and Electrical Engineering

18<sup>th</sup> December 2019

The template used to compile this thesis was produced by Malcolm Morgan and Kayla  
Friedman for the Centre for Sustainable Development, University of Cambridge, UK





*“The socialism I believe in isn’t really politics. It is a way of living. It is humanity. I believe the only way to live and to be truly successful is by collective effort, with everyone working for each other, everyone helping each other and everyone having a share in the rewards at the end of the day. That might be asking a lot but it is the way I see football, the way I see life.”*

*Bill Shankly*



*There are those who sow divisions and those who grow visions.*

*Wisdom teaches us to live in the shelter of each other.*



## DECLARATION

I, Andrew David Heeley, confirm that this thesis is my own work and includes nothing that is the outcome of work done in collaboration except where specifically indicated in the text. I am aware of the University's Guidance on the Use of Unfair Means ([www.sheffield.ac.uk/ssid/unfair-means](http://www.sheffield.ac.uk/ssid/unfair-means)). This work has not been previously submitted, in part or whole, to any university for any degree or other qualification.

Signed:

A D Heeley

Date: 18<sup>th</sup> December 2019

Andrew David Heeley

Sheffield, UK

# *FIBRE OPTIC COUPLED, INFRARED THERMOMETERS FOR PROCESSES INCURRING HARSH CONDITIONS*

*ANDREW D HEELEY, DECEMBER 2019*

## ABSTRACT

This study undertook the development and testing of fibre optic coupled infrared thermometers (IRTs) that could substitute for thermocouples in harsh conditions that would affect contact temperature measurements deleteriously. The IRTs have been configured without photodiode cooling and signal chopping but achieved low minimum measurable temperatures, fast responses and good sensitivities. IRTs were configured with mid-wave infrared (MWIR) and short-wave infrared (SWIR) photodiodes, to measure over different temperature ranges. The thermometers had small footprints, therefore could be installed into constrained spaces and not cause interference with the process. The MWIR thermometers were substituted for thermocouples in high temperature conditions in end milling tool temperature measurements and reactive electrochemical conditions in Lithium-ion cell temperature measurements. The conditions into which the fibre optics were embedded would lead to inaccurate measurements from thermocouples, whereas the fibre optic and remotely positioned IRT offered immunity against these errors.

Calibration drift is a major problem that afflicts thermocouple temperature measurements. There has been progress towards addressing this weakness with improved thermocouples. The SWIR thermometer used a zero drift operational amplifier to minimise offset voltage, drift and noise. The IRT was coupled to a sapphire fibre optic probe that had tin deposited onto the core to form an integral fixed point temperature calibration cell. This low drift IRT provided an increment towards creating a drift-free, self-calibrating IRT that would substitute for thermocouples with integral calibration capabilities.

The feasibility of substituting thermocouples with embedded fibre optics coupled to IRTs has been demonstrated and potential improvements of these thermometers have been identified.

## ACKNOWLEDGEMENTS

First and foremost, I owe the biggest thank-you to my fiancée, Sally for supporting and encouraging me in taking the opportunity to study for a PhD that presented itself back in 2015 and putting up with my humour for so many years, besides.

I am grateful for having had the chance to pursue a PhD somewhat later in life than most students come to this level of study and to Dr. Jon Willmott as my academic supervisor for enabling that chance.

I wish to acknowledge the help and friendship offered by all those whom I have met and discussed: work, life, politics, philosophy and football with and shared lunchtime conversations with throughout The Electronic and Electrical Engineering Department and Sensor Systems Group. In no particular order: Dr. Matt Hobbs (particularly for introducing the Wednesday lunch), Dr. Nick Boone, Dr. Chengxi Zhu (Todd), Steve Dorward, Mary Stuart, Leigh Stanger, Dr. Akeel Auckloo, Matt Davies, Dr. Tom Rockett, Matt Grainger, Dr. Richard Hodgkinson and Dr. Jeng-Shui Cheong. Outside of the research group, my thanks go to Dr. Mark Sweet and Dr. Ben White particularly for sharing some of their experience and engaging with interesting lunchtime conversations. Thank-you also to Dr. Jaime Maravi Nieto for joining me in forming 'Ohm and Away' back in 2016 and the many EEE postgraduates who played alongside us. You have all added something to my experience here.

I wish to thank and acknowledge Dr. Hatim Laalej, Dr. Jon Stammers, Stephen Mann and Dr. Sabino Ayvar-Soberanos at The University of Sheffield, Advanced Manufacturing Research Centre for their assistance in testing the thermometer on an end milling machine.

I wish to thank and acknowledge Dr. Denis Cumming, Laurie Middlemiss, Josie-May Whitnear, Nikko Talplacido, Laura Wheatcroft, Megan Hoyle and Jagoda Cieslik of the University of Sheffield, Chemical and Biological Engineering department for their assistance in testing the battery cell fibre optic thermometer.

Thank you to Kayla Friedman and Malcolm Morgan of the Centre for Sustainable Development, University of Cambridge, UK for producing the Microsoft Word template used to produce this thesis.

Finally, I am truly thankful for the volunteers of Edale Mountain Rescue Team and Yorkshire Air Ambulance for rescuing me after a fall from White Edge in Derbyshire (please support these dedicated people, if you are reading this thesis) and all of the staff at Sheffield's Northern General Hospital major trauma centre & intensive care unit for achieving what "all of the King's horses and all of the King's men" could not and putting me back together in 2017, enabling me to complete this PhD.

**Funding.** This research was funded by the UK Engineering and Physical Sciences Research Council under doctoral training grant scholarship numbers EP/K503149/1 and EP/L505055/1 and grant number EP/M009106/1 Optimised Manufacturing Through Unique Innovations in Quantitative Thermal Imaging.

# CONTENTS

<b>1 INTRODUCTION .....</b>	<b>1</b>
1.1 INDUSTRIAL TEMPERATURE MEASUREMENT .....	5
1.2 INFRARED RADIATION THERMOMETER CONFIGURATIONS.....	7
1.2.1 <i>Photodiode junction operation</i> .....	7
1.2.2 <i>Transimpedance amplifier configuration</i> .....	9
1.2.3 <i>Thermometer detector and optical configuration</i> .....	12
1.3 FIBRE OPTIC MATERIALS.....	13
1.4 OBJECTIVES OF INFRARED THERMOMETER DEVELOPMENT. ....	14
1.5 SPECIFICATION FOR PROTOTYPE INFRARED THERMOMETER .....	15
1.6 RAISON D'ETRE OF THIS THESIS. ....	16
1.7 ARRANGEMENT OF THESIS .....	18
1.8 PAPERS PUBLISHED .....	19
<b>2 PRINCIPLES AND THEORY APPLICABLE TO RADIATION THERMOMETRY</b>	<b>26</b>
2.1 RADIOMETRY DEFINITIONS .....	28
2.2 BLACKBODY RADIATION CURVES .....	29
2.3 NUMERICAL INTEGRATION OF PLANCK'S LAW .....	31
2.4 WIEN'S APPROXIMATION OF PLANCK'S LAW .....	34
2.5 SAKUMA-HATTORI EQUATION.....	39
2.6 FIBRE OPTIC COUPLING .....	41
2.6.1 <i>Fibre optic materials</i> .....	42
2.6.2 <i>Fibre optic transmission equations</i> .....	44
2.7 MODELLING OF INFRARED TRANSMISSION AND POWER INCIDENT UPON DETECTOR .	48
2.8 MINIMUM TEMPERATURE MEASURABLE WITH PROTOTYPE FIBRE OPTIC THERMOMETER .....	50
2.9 TRANSIMPEDANCE AMPLIFIER AND BOOTSTRAPPING CONFIGURATIONS .....	53
<b>3 EXPERIMENTAL AND ANALYTICAL METHODS DEPLOYED .....</b>	<b>59</b>
3.1 INFRARED THERMOMETER CONFIGURATION.....	59
3.2 MODELLING OF OP-AMP NOISE AND INPUT OFFSET VOLTAGE .....	62
3.3 INFRARED FIBRE OPTIC COUPLING .....	63
3.4 THERMOMETER CHARACTERISATION AND CALIBRATION METHOD .....	64

3.5 EXPERIMENTAL CALIBRATION OF BLACKBODY SOURCES USED IN LABORATORY CHARACTERISATION OF INFRARED THERMOMETERS .....	66
3.5.1 Landcal P1200B Three-Zone Tube Furnace Calibration .....	66
3.5.2 Landcal P550P Portable Blackbody Source Calibration .....	68
3.5.3 Landcal P80P Portable Blackbody Source Calibration .....	69
3.6 ANALYSIS OF THERMOMETER CHARACTERISTICS .....	70
<b>4 END MILLING TOOL TEMPERATURE MEASUREMENT USING FIBRE OPTIC COUPLED, MID-WAVE INFRARED THERMOMETER .....</b>	<b>74</b>
4.1 INFRARED THERMOMETER CONFIGURATION .....	75
4.2 LABORATORY PROTOTYPE THERMOMETER CHARACTERISATION AGAINST BLACKBODY SOURCE TEMPERATURES .....	81
4.2.1 Thermometer output voltage characteristic .....	81
4.2.2 Thermometer voltage output noise .....	84
4.2.3 Thermometer output voltage modelling .....	87
4.2.4 Evaluation of radiation coverage of photodiode active area .....	89
4.2.5 Estimate of temperature measurement uncertainty of prototype thermometer .....	91
4.3 CONFIGURATION AND CALIBRATION OF PROTOTYPE APPLICATION IRT .....	94
4.3.1 Configuration of end milling application thermometer .....	94
4.3.2 Prototype application thermometer characterisation .....	95
4.4 APPLICATION OF IRT TO CUTTING TOOL TEMPERATURE MEASUREMENT .....	98
<b>5 DEVELOPMENT OF ZERO DRIFT, LOW TEMPERATURE RANGE, FIBRE OPTIC THERMOMETER AND APPLICATION TO BATTERY TEMPERATURE MEASUREMENTS .....</b>	<b>108</b>
5.1 ZERO DRIFT OP-AMP THERMOMETER DEVELOPMENT .....	112
5.2 COMPARISON OF LOW TEMPERATURE IRT CONFIGURATIONS USING ZERO DRIFT AND PRECISION OP-AMPS .....	114
5.2.1 Comparison of precision op-amp and zero-drift op-amp IRTs measuring steady-state temperatures .....	114
5.2.2 Characterisation of precision op-amp and zero-drift op-amp IRTs over low temperature ranges .....	115
5.2.3 Comparison of the capabilities of the IRTs to maintain 'zero' and steady-state output voltages .....	117

5.2.4 <i>Statistics Describing the Distributions of Measurements</i> .....	122
5.3 CHARACTERISATION OF LOW TEMPERATURE IRTs AGAINST BLACKBODY SOURCE...	123
5.4 APPLICATION OF PROTOTYPE IRT TO LITHIUM-ION CELL TEMPERATURE MEASUREMENTS. ....	128
5.4.1 <i>Insertion of fibre optic into Lithium ion cells coupled to low temperature IRT</i> .....	130
5.4.2 <i>Proof of concept using laboratory tests</i> .....	135
<b>6 PROTOTYPE ZERO DRIFT, FIBRE OPTIC INFRARED THERMOMETER FOR THERMOCOUPLE SUBSTITUTION .....</b>	<b>144</b>
6.1 SWIR THERMOMETER CONFIGURATION .....	145
6.2 CONFIGURATION OF FIBRE OPTIC PROBE WITH TIN COATING FORMING A PROTOTYPE INTEGRAL TEMPERATURE FIXED POINT CALIBRATION CELL .....	146
6.3 CHARACTERISATION OF SAPPHIRE FIBRE OPTIC COUPLED, SWIR THERMOMETER....	150
6.4 APPLICATION OF PROTOTYPE SWIR THERMOMETER MEASURING TEMPERATURE INFLECTIONS DURING PHASE TRANSFORMATIONS OF TIN.....	155
<b>7 CONCLUSIONS .....</b>	<b>164</b>
<b>8 FUTURE WORK TO EXTEND THE CAPABILITIES OF FIBRE OPTIC COUPLED INFRARED THERMOMETERS .....</b>	<b>171</b>
8.1 INDIUM ARSENIDE AVALANCHE PHOTODIODE TO INCREASE SENSITIVITY .....	171
8.2 TRANSIMPEDANCE AMPLIFIER WITH LOWER NOISE AND INPUT VOLTAGE OFFSET....	171
8.3 SELF-CALIBRATING FIBRE OPTIC PROBE THERMOMETER .....	172
8.4 HIGHER TEMPERATURE PROTOTYPE SWIR THERMOMETER CONFIGURATION.....	173

## LIST OF TABLES

TABLE 2.1 MINIMUM SOURCE TEMPERATURE MEASURABLE ESTIMATED FROM THE BAND RADIANCE CALCULATIONS AND MINIMUM POWER TO WHICH THE PHOTODIODE WILL RESPOND .....	52
TABLE 4.1 CONTRIBUTIONS OF CALIBRATION UNCERTAINTIES TO MEASUREMENT UNCERTAINTY (K=2) .....	92
TABLE 4.2 CONTRIBUTIONS OF MEASUREMENT UNCERTAINTIES TO MEASUREMENT UNCERTAINTY (K=2) .....	92
TABLE 5.1 COMBINATIONS OF OP-AMPS IDENTIFIED BY MODELLING AS OFFERING LOWEST OFFSET VOLTAGE AND NOISE FROM MODELLING AND SUBSEQUENTLY TESTED AT LABORATORY CONDITIONS.....	113
TABLE 5.2 MEAN, VARIANCE AND EXCESS KURTOSIS VALUES OF PRECISION OP-AMP AND ZERO DRIFT OP-AMP THERMOMETER VERSIONS.....	122

## LIST OF FIGURES

FIGURE 1.1 SCHEMATIC ILLUSTRATION OF PHOTODIODE P-N JUNCTION ENERGY LEVELS WITH NO DELIBERATE BIAS VOLTAGE APPLIED .....	8
FIGURE 1.2 SCHEMATIC DIAGRAM ILLUSTRATING TYPICAL TIA CONFIGURATION AND SMALL SIGNAL PHOTODIODE MODEL .....	10
FIGURE 2.1 SOLID ANGLE GEOMETRY.....	29
FIGURE 2.2 SPECTRAL BAND RADIANCE BETWEEN 3.0 MM AND 3.5 MM WAVELENGTHS .....	30
FIGURE 2.3 EXAMPLE BAND RADIANCE FOR THE WAVELENGTH RANGE 3.0 – 4.5 MM CALCULATED FROM NUMERICAL INTEGRATION OF PLANCK’S LAW, ASSUMING BLACKBODY CONDITIONS.....	33
FIGURE 2.4 RADIANCE CURVES CALCULATED USING PLANCK’S LAW AND WIEN APPROXIMATION .....	35
FIGURE 2.5 VARIATION OF ATTENUATION OF INFRARED BY FLUORIDE AND LOW-OH SILICA FIBRE OPTICS WITH WAVELENGTH.....	43
FIGURE 2.6 SCHEMATIC DIAGRAM ILLUSTRATING TOTAL INTERNAL REFLECTION PRINCIPLE OF TRANSMISSION ALONG FIBRE OPTIC .....	45
FIGURE 2.7 EXAMPLE NUMERICAL INTEGRATION CALCULATIONS FOR EVALUATING SPECTRAL RADIANCE, IN THIS CASE OVER THE MID-WAVE INFRARED WAVELENGTH RANGE 3.0 – 4.5 MM, TRANSMITTED BY A 230 MM LENGTH, 600 MM CORE DIAMETER ZBLAN FIBRE OPTIC.....	50
FIGURE 2.8 SCHEMATIC DIAGRAM OF BOOTSTRAPPED PHOTODIODE TIA CIRCUIT .....	54
FIGURE 3.1 SCHEMATIC DIAGRAM OF THERMOMETER BOOTSTRAPPED PHOTODIODE TIA CIRCUIT.....	60
FIGURE 3.2 SCHEMATIC DIAGRAM OF LABORATORY-BASED CONFIGURATION USED FOR CHARACTERISATION OF PROTOTYPE FIBRE OPTIC COUPLED, MID-WAVE INFRARED THERMOMETERS.....	65
FIGURE 3.3 LANDCAL P1200B BLACKBODY SOURCE CALIBRATION AGAINST TRACEABLE TRANSFER STANDARD TYPE ‘R’ THERMOCOUPLE.....	67

FIGURE 3.4 ERROR BETWEEN SET POINT AND MEASURED VALUE FOR LANDCAL P1200B BLACKBODY SOURCE CALIBRATION .....	67
FIGURE 3.5 P550P PORTABLE BLACKBODY SOURCE CALIBRATION AGAINST TRACEABLE TRANSFER STANDARD PLATINUM 100Ω RESISTANCE TEMPERATURE DETECTOR.....	68
FIGURE 3.6 ERROR BETWEEN SET POINT AND MEASURE VALUE FOR LANDCAL P550P PORTABLE BLACKBODY SOURCE CALIBRATION .....	69
FIGURE 3.7 INDICATED TEMPERATURE SET POINT AND TRANSFER STANDARD MEASURED TEMPERATURE OF P80P BLACKBODY SOURCE, AND ERROR BETWEEN INDICATED AND MEASURED TEMPERATURES .....	70
FIGURE 3.8 ERROR BETWEEN INDICATED AND MEASURED TEMPERATURES OF LANDCAL P80P BLACKBODY SOURCE.....	70
FIGURE 4.1 TOP AND BOTTOM LAYERS OF COMPACT PROTOTYPE MWIR THERMOMETER, ILLUSTRATING THE SIZE OF THE THERMOMETER PCB AND MINIMAL NUMBER OF COMPONENTS .....	78
FIGURE 4.2 CIRCUIT DIAGRAM FOR INFRARED RADIATION THERMOMETER USING BOOTSTRAPPED INASsB PHOTODIODE AND HIGH VALUE OF TRANSIMPEDANCE BUT EXCLUDING OFFSET TRIM.....	80
FIGURE 4.3 PROTOTYPE INFRARED THERMOMETER BLACKBODY SOURCE TEMPERATURE VERSUS VOLTAGE OUTPUT CHARACTERISTIC MEASURED UNDER LABORATORY CONDITIONS.....	82
FIGURE 4.4 GRAPH ILLUSTRATING $1/T$ VERSUS $Ln(V_o)$ FOR THE LABORATORY PROTOTYPE IRT AND RESIDUAL ERROR BETWEEN THE LINEAR MODEL AND MEASURED DATA .....	83
FIGURE 4.5 TYPICAL DATA RECORDED FROM THE THERMOMETER AND BLACKBODY SOURCE TEMPERATURE MEASUREMENTS, ILLUSTRATING MAGNITUDE OF NOISE AND SIGNAL, INCLUDING THE CONTINUOUSLY AVERAGED SIGNAL .....	85
FIGURE 4.6 GRAPH OF NOISE LIMITED EQUIVALENT TEMPERATURE MEASUREMENT RESOLUTION AND SIGNAL TO NOISE RATIO CALCULATED FOR PROTOTYPE SAPPHIRE FIBRE OPTIC COUPLED IRT .....	86

FIGURE 4.7 PROTOTYPE THERMOMETER MEASURED AND MODELLED OUTPUT VOLTAGE VERSUS SOURCE TEMPERATURE CURVES WITH THE STANDARD DEVIATION OF OUTPUT VOLTAGE MEASUREMENTS REPRESENTED BY ERROR BARS.....	88
FIGURE 4.8 THERMOMETER RADIANCE TEMPERATURE ERROR CALCULATED AS (TEMPERATURE MEASURED – TEMPERATURE MODELLED) AND STANDARD ERROR OF THAT CALCULATION.....	89
FIGURE 4.9 VARIATION OF FIELD OF VIEW MEASURED FOR FIBRE OPTIC THERMOMETER TO ASSESS PROPORTION OF PHOTODIODE THAT ACCEPTED RADIATION .....	91
FIGURE 4.10 $\text{InF}_3$ FIBRE OPTIC COUPLED INFRARED THERMOMETER TIA OUTPUT VOLTAGE VARIATION WITH BLACKBODY SOURCE TEMPERATURE CHARACTERISTIC.....	96
FIGURE 4.11 CHARACTERISTIC NATURAL LOGARITHM OF THE THERMOMETER OUTPUT VOLTAGE VERSUS INVERSE OF ABSOLUTE TEMPERATURE CURVE FOR THE $\text{InF}_3$ FIBRE OPTIC COUPLED PROTOTYPE INFRARED THERMOMETER FOR MACHINING APPLICATIONS.....	97
FIGURE 4.12 NOISE LIMITED EQUIVALENT TEMPERATURE RESOLUTION AND SNR OF $\text{InF}_3$ FIBRE OPTIC COUPLED PROTOTYPE IRT FOR END MILLING APPLICATION .....	98
FIGURE 4.13 MILLING MACHINE SET UP FOR TRIAL OF MWIR THERMOMETER, WITH ANNOTATION OF THE KEY FEATURES OF THE TRIAL ARRANGEMENT.....	99
FIGURE 4.14 ‘INDEXABLE’ MILLING TOOL HEAD AND CUTTING TOOL INSERTS, ILLUSTRATING PATH OF FIBRE OPTIC EMBEDDED INTO THE BACK OF THE TOOL INSERT AND THROUGH THE TOOL HEAD, THEN EXITING TO PASS ALONG THE MACHINE DRIVESHAFT TO THE THERMOMETER. ....	100
FIGURE 4.15 MEASUREMENTS AND CONTINUOUSLY AVERAGED MEAN OF CUTTING TOOL TEMPERATURE DURING END MILLING OF TITANIUM PLATE .....	102
FIGURE 4.16 THERMOCOUPLE MEASUREMENTS OF CUTTING TOOL INSERT SURFACE TEMPERATURE DURING SEPARATE TRIALS OF END MILLING OF TITANIUM PLATE. ....	103
FIGURE 5.1 SCHEMATIC DIAGRAM ILLUSTRATING CONFIGURATION USED TO TEST TWO PROTOTYPE THERMOMETERS CONCURRENTLY, VIEWING SIMILAR SOURCE TEMPERATURES .....	115

FIGURE 5.2 IRT OUTPUT VOLTAGE WITH ZERO SIGNAL; TIME SERIES DATA .....	118
FIGURE 5.3 IRT OUTPUT VOLTAGE WITH ZERO SIGNAL; HISTOGRAM OF MEASUREMENTS .....	118
FIGURE 5.4 IRT OUTPUT VOLTAGE MEASURING 700 °C; TIME SERIES DATA GRAPHS, VOI.A.M CONSECUTIVEEM LKHEM LKARGERICULT TONEEDD TILL BUT OF COURSE LEAVES OPEN THE QUESTION ED, FOR EXAMPLE: .....	119
FIGURE 5.5 IRT OUTPUT VOLTAGE MEASURING 700 °C; HISTOGRAM OF MEASUREMENTS .....	120
FIGURE 5.6 VARIATION OF BLACKBODY SOURCE TEMPERATURE AT 700 °C STEADY-STATE SET POINT AND CONCURRENT INFRARED THERMOMETER OUTPUT VOLTAGE .....	121
FIGURE 5.7 SOURCE TEMPERATURES VERSUS VOLTAGE OUTPUT CHARACTERISTICS OF ZERO DRIFT OP-AMP IRT AND PRECISION OP-AMP IRT .....	123
FIGURE 5.8 CHARACTERISTICS OF $LN(V_o)$ VARIATIONS WITH $1/T$ FOR ZERO DRIFT OP-AMP IRT AND PRECISION OP-AMP IRT .....	124
FIGURE 5.9 CHARACTERISTIC NOISE LIMITED EQUIVALENT TEMPERATURE RESOLUTION AND SNR OF ZERO DRIFT OP-AMP IRT .....	126
FIGURE 5.10 CHARACTERISTIC NOISE LIMITED EQUIVALENT TEMPERATURE RESOLUTION AND SNR PRECISION OP-AMP IRT .....	127
FIGURE 5.11 COMPONENTS OF LITHIUM-ION POUCH CELLS PRIOR TO ASSEMBLY, ILLUSTRATING THE ELECTRODES, CONTACTS, ALUMINIUM LAMINATE SHEET THAT FORMS THE POUCH CASING (PRIOR TO SEALING) AND FIBRE OPTIC FOR EMBEDDING INTO CELL. ....	132
FIGURE 5.12 ASSEMBLY OF LARGE CAPACITY POUCH CELL WITH EMBEDDED ZBLAN FIBRE OPTIC INSERTED INTO CENTRE OF ELECTRODE STACK, PRIOR TO FORMING INTO ACTIVE CELL .....	133
FIGURE 5.13 COMPLETED LARGE CAPACITY LITHIUM ION POUCH CELL WITH EMBEDDED ZBLAN FIBRE OPTIC AND THERMOCOUPLE INSERTED THROUGH OPPOSITE EDGES OF POUCH.....	134

FIGURE 5.14 MEASUREMENTS OF DUMMY POUCH CELL (CONTAINING NO ELECTROLYTE) TEMPERATURE USING ONE OF THE LOW TEMPERATURE IRTs.....	136
FIGURE 6.1 SCHEMATIC DIAGRAM OF SILVER ENCAPSULATED, TIN COATED SAPPHIRE FIBRE OPTIC CORE USED TO CREATE INTEGRAL CALIBRATION POINT ON FIBRE OPTIC PROBE .....	147
FIGURE 6.2 SINTERED TIN NANOPARTICLE COATED SAPPHIRE FIBRE OPTIC FORMING LAYERS OF METAL THAT ADHERED TO THE BARED FIBRE OPTIC SURFACE.....	149
FIGURE 6.3 SINTERED SILVER NANOPARTICLE COATED SAPPHIRE FIBRE OPTIC, ENCAPSULATING UNDERLYING LAYERS OF TIN WITHIN THE SILVER COATING .....	149
FIGURE 6.4 SINTERED TIN AND SILVER NANOPARTICLE COATED SAPPHIRE FIBRE OPTIC COUPLED TO COMPACT INFRARED THERMOMETER PRINTED CIRCUIT BOARD FOR LABORATORY TESTING OF PROTOTYPE THERMOMETER WITH INTEGRAL TIN FIXED POINT CELL.....	150
FIGURE 6.5 CHARACTERISTIC OUTPUT VOLTAGE OF THERMOMETER TRANSIMPEDANCE AMPLIFIER VERSUS BLACKBODY SOURCE TEMPERATURE CURVE. ....	151
FIGURE 6.6 CHARACTERISTIC CURVE OF THERMOMETER $LN(V_o)$ VERSUS $1/T$ OF BLACKBODY SOURCE.....	152
FIGURE 6.7 NOISE LIMITED EQUIVALENT TEMPERATURE RESOLUTION OF THE EXTENDED-INGAAS BASED THERMOMETER WITH $10\text{ M}\Omega$ TRANSIMPEDANCE .....	153
FIGURE 6.8 SIGNAL TO NOISE RATIO OF THE EXTENDED-INGAAS BASED IRT .....	154
FIGURE 6.9 SAKUMA-HATTORI CURVE FIT TO MEASURED CHARACTERISTIC OF THE INFRARED THERMOMETER BASED UPON USING THE EXTENDED-INGAAS PHOTODIODE .....	155
FIGURE 6.10 MEAN INGAAS THERMOMETER OUTPUT VOLTAGE WHILST HEATING AND COOLING TIN COATED FIBRE OPTIC THROUGH TRANSFORMATION TEMPERATURE AT $0.05\text{ }^\circ\text{C}/\text{MINUTE}$ .....	157
FIGURE 6.11 MEAN INGAAS THERMOMETER OUTPUT VOLTAGE WHILST HEATING AND COOLING TIN COATED FIBRE OPTIC THROUGH TRANSFORMATION TEMPERATURE AT $0.1\text{ }^\circ\text{C}/\text{MINUTE}$ .....	158

FIGURE 6.12 MEAN INGAAS THERMOMETER OUTPUT VOLTAGE WHILST HEATING AND COOLING TIN COATED FIBRE OPTIC THROUGH TRANSFORMATION TEMPERATURE AT 0.25 °C/MINUTE..... 158

FIGURE 8.1 CHARACTERISTIC CURVE OF 1 MΩ TRANSIMPEDANCE, SAPPHIRE FIBRE OPTIC COUPLED EXTENDED-INGAAS IRT AGAINST KNOWN BLACKBODY SOURCE TEMPERATURES..... 174

FIGURE A1.8.2 ILLUSTRATION OF 'TOP-HAT' FUNCTIONS USED TO REPRESENT PHOTODIODE PHOTSENSITIVITY AND INFRARED FIBRE OPTIC TRANSMISSION CURVES IN CALCULATIONS ..... 177

## LIST OF PAPERS PUBLISHED

1. A. D. Heeley, M. J. Hobbs, H. Laalej, and J. R. Willmott, 'Miniature Uncooled and Unchopped Fiber Optic Infrared Thermometer for Application to Cutting Tool Temperature Measurement', *Sensors*, vol. 18, no. 3188, 2018.

2. A. D. Heeley, M. J. Hobbs and J.R. Willmott, 'Prototype zero drift, fibre optic infrared thermometer for thermocouple substitution'

Submitted for publication in the MDPI published journal 'Applied Science' and undergoing peer review, June 2020.

3. A.D. Heeley, M.J. Hobbs, M. J.M. Davies and J.R. Willmott, 'Fibre optic coupled radiation thermometer with fixed-point reference: demonstrating the feasibility of a self-calibrating thermometer.'

In draft, awaiting University of Sheffield decision concerning patent application prior to publication.

## NOMENCLATURE, ABBREVIATIONS, DEFINITIONS AND ACRONYMS USED WITHIN THIS THESIS

*APD* Avalanche Photodiode

°C degrees Celsius

*Bias voltage* The voltage applied across a diode junction to reduce or increase length of the depletion region between the p and n type semiconductor materials

*DIP* Dual Inline Package

*DMM* Digital Multi-Meter

*FOV* Field of View

*InAs* Indium Arsenide semiconductor alloy used to manufacture infrared photodiodes

*InAsSb* Indium Arsenide Antimony semiconductor alloy used to manufacture infrared photodiodes

*InGaAs* Indium Gallium Arsenide semiconductor alloy used to manufacture infrared photodiodes

*Indium Fluoride, InF<sub>3</sub>* Principal material from which InF<sub>3</sub> glass fibre optic cables are manufactured

*IR* Infrared Radiation

*IRT* Infrared Radiation Thermometer

*ISOTECH* Isothermal Technology Limited, Skelmersdale, Lancashire, UK

*K* Kelvin

*Keysight* Technologies Malaysia, Penang, Malaysia

*Ln or ln* Natural logarithm ( $\log_e$ )

*log or log<sub>10</sub>* Logarithm to base 10

*LT, Linear Technology Incorporated* Linear Technology Incorporated, California, US

*Microns*  $10^{-6}\text{m}$ ,  $\mu\text{m}$

*MWIR* Medium Wavelength Infrared Radiation; nominally 3-8  $\mu\text{m}$  wavelength radiation

*Noise Limited Equivalent Temperature Resolution* The minimum temperature that can be measured for which the signal to noise ratio is unity

*Op-amp* Operational amplifier integrated circuit

*PCB* Printed Circuit Board

*PV* Photovoltaic operation mode of a photodiode for which no deliberate bias voltage is applied across the p-n junction

$R_f$  feedback resistance

*R-C* Resistor-Capacitor network in the feedback loop around the inverting input of an operational amplifier and specifically the transimpedance amplifier in the infrared thermometer circuit.

*SEDI-ATI* Fibre optic manufacturer and distributor SEDI-ATI Fibrés-Optiques, Courcouronnes, France

*SMA905* Sub-Miniature type A. The specific variant of through-ferrule type screw connector used for connecting the infrared fibre optics to photodiode mounts

*SMD* Surface Mount Device

*SNR* Signal to Noise Ratio

*TI, Texas Instruments* Texas Instruments Incorporated, New York, USA

*TIA* Transimpedance Amplifier

*V* Volts

$V_o$  Output Voltage (used in reference to the output of the transimpedance amplifier in the thermometer circuit)

*ZBLAN fibre optic* Principally Zirconium Fluoride used for manufacturing fluoride glass infrared transmitting fibre optics and typically comprising the following molar proportions of metallic fluorides: 53%  $\text{ZrF}_4$  20%  $\text{BaF}_2$  5%  $\text{LaF}_3$  4%  $\text{AlF}_3$  20%  $\text{NaF}$

# LIST OF APPENDICES

APPENDIX 1. PLANCK BLACKBODY CURVE CALCULATIONS.....	175
APPENDIX 2. EQUIPMENT USED AND FACTORY CALIBRATION UNCERTAINTIES FOR MEASURING INSTRUMENTATION.....	178
APPENDIX 3. TRACK AND COMPONENT LAYOUT DRAWINGS FOR THERMOMETER PRINTED CIRCUIT BOARD.....	186



# 1 INTRODUCTION

Reliable temperature measurements are fundamental to understanding and controlling processes in many manufacturing industries, thereby enabling improvements to processes and products to be attained [1]–[3]. Examples of the types of improvements that can be achieved by measuring and controlling temperatures to narrower ranges of uncertainty include: reduced specific energy consumption, reduced waste and by-products generated, optimised production scheduling, improved product quality with fewer defects and lower rates of rejection of finished items and improved tolerances to design characteristics (dimensions, properties, material microstructure etcetera) [1]–[7]. Improvement of temperature measurement underlies achieving precise control of the parameters above, along with many others in manufacturing. Temperature measurement improvements required include increasingly accurate and repeatable measurements with low magnitudes of uncertainties attributable to the measurement technology. The variation of metal properties with temperature-induced changes in microstructure illustrates the benefits of improved temperature control in manufacturing processes. A variation of  $\pm 10$  °C in temperature achieved during annealing of austenitic stainless steel would lead to grain size variations of  $\pm 5$   $\mu\text{m}$  and consequent variability of several MegaPascals in the yield stress to failure of the metal. Manufactured components that have undergone further machining processes, following formation of the base material within a foundation industry have further value added that is reflected in the costs of production. High volume and rapid manufacturing, as practised in many industries, requires the deployment of precise

and fast measurement and control systems to optimise productivity and efficiency, thereby minimising losses and defects. Typically, reductions of productivity losses owing to defects and energy consumption reductions of a few percentage points will translate to cost reductions of many millions of pounds for high productivity manufacturing. As an example of the impact that improved measurement and control may have: a 0.125% reduction in the number of defects in one specific process, by improvement of temperature control, led to a cost improvement of £1.5m per annum.

Temperature measurements for control of manufacturing processes are acquired by industrial thermometers that typically would be selected from: thermocouples, platinum resistance thermometers, thermistors, acoustic pyrometers, optical pyrometers and infrared radiation thermometers (IRTs). The selection of the most suitable thermometer and system configuration is dependent upon the application and measuring capability required. Thermocouples and IRTs have been used most often as industrial thermometers, owing to the limitations of the other devices [8]–[10] and the advantages that these two thermometers afford [9], [10]. Limitations of resistance thermometers and thermistors include: the maximum temperatures to which the devices may be exposed being typically less than 500 °C and often less than 100 °C; the invasive nature of the measurement devices upon the temperature field being measured; non-linearity of device response with temperature and lack of sensitivity to afford precision measurements of small temperature changes. Further techniques are more suitable for specific conditions, for example: acoustic pyrometry can be used to measure fluid temperatures but would incur errors arising from the intermediate air, gas or fluid if used remotely.

The output signal from a detector or thermometer is an analogue of the temperature to which it is exposed and this output signal is interpreted by electronic circuits that characterise it as a specific temperature, according to a calibration. The electronic analogue of the temperature measured is transmitted to a controller, affording its use in controlling the temperature of the manufacturing process or product.

Achieving repeatable, accurate and sensitive temperature measurements underlies many improvements that could be achieved but becomes increasingly difficult under harsh process conditions, for example: conditions in which high temperatures,

chemical reactions, thermo-fluid interactions, mechanical abrasion and contamination of the thermometer can occur. Each of these problems could affect the measurement, particularly if the thermometer used is susceptible to change resulting from the conditions into which it is deployed [3], [5], [11]. Sub-optimal measurements have been used to control processes, often owing to the limitations of the thermometers, for example: measurement of process temperature rather than measurement of product temperature directly [3]. Improvement of manufacturing temperature measurements, with readily deployable thermometers that measure 'better' (more accurately, faster, with higher sensitivity) than the typical configuration, would benefit manufacturing. Thermocouple temperature measurements are affected by calibration drift and irreversible hysteresis of the thermometer output with ageing and exposure to harsh process conditions [12]–[14]. Maintaining valid measurements of industrial process temperatures and product temperatures during manufacturing requires that frequent calibration checks, re-calibration and replacement of thermometers are undertaken. The process typically has to incur an outage, with consequent loss of productivity, to allow assessment or correction of thermocouples. Thermocouples have been configured with integral fixed point temperature calibration cells [15]–[17] which would allow in-operando assessment of thermocouple calibration. These developments offer some scope to overcome the ageing-related drift of thermocouples but may not address the detriment of thermoelectric stability caused by exposure to harsh conditions. The scope exists to substitute infrared thermometers with integral fixed point temperature calibration cells for thermocouples, thereby obviating the problems caused by harsh measurement conditions.

The term thermometer, used within this work, included: the coupling between the object to be measured and detector, the detector and signal conditioning that generates a measurable output signal. Ideally, thermometers could be deployed without having the depth of knowledge required presently to achieve good temperature measurements using available technologies [5].

Thermocouples are amongst the simplest thermometers used and comprise: junctions of dissimilar metal wires that form the sensing element, insulation between the wires and a protective sheath that prevents the metal wires from being affected by the

material or fluid conditions into which the thermocouple assembly has been inserted. The temperature difference arising between the sensing junction and the output terminals of the thermocouple generates an electromotive force (emf) that varies in characteristic and reproducible ways. The thermo-electric generation of emf is known as the Seebeck effect, named after the Baltic scientist Thomas Seebeck, who observed the relationship between magnetic and thermal effects occurring in dissimilar metals around 1822 (or sometimes the Seebeck-Peltier effect, to include the reverse effect, thermo-electric cooling). For a few, specific combinations of metals, the emf derived has sufficient sensitivity, linearity and magnitude to generate a useful signal and these have become the standard types of thermocouples, that have reproducible characteristics [18]. Development has afforded improved properties and led to thermocouples becoming ubiquitous for industrial temperature measurement.

The effect of infrared radiation heating the bulb of a mercury thermometer has been known to exist since white light was first dispersed into its spectral components and the temperature rise caused by each colour measured by Herschel in the early nineteenth century. Arguably knowledge of the existence of infrared radiation could be defined earlier, with the invention of the thermoscope by Galileo. Theories developed and experiments undertaken subsequently have refined the scientific understanding of infrared radiation and engineering development has improved the capability to measure the temperature of an object from its radiation. With the advent of integrated circuits and new semiconductor alloy detectors, the pace of development of temperature measurement technologies accelerated through the second half of the twentieth century and into the twenty-first century. Modern radiometric infrared thermometers achieve high accuracies, sensitivities and robust implementation at relatively low cost. The last three or four decades have witnessed smaller and lighter thermometers, with the implementation of devices using uncooled or thermo-electrically cooled array detectors in hand-held packages rather than the cumbersome and bulky units that required cryogenic cooling of previous generations [19]. It is possible to buy ergonomically designed thermometers at low cost that afford representative surface temperature measurements to be acquired for domestic or industrial equipment monitoring. Often the thermometers use so-called thermal detectors, that respond to a broad range of infrared radiation wavelengths, the total

heat incident upon them and absorbed into the sensor then induces a change in the electrical properties of the material in response. Typically, bolometers that undergo a change of electrical resistance upon exposure to radiation are used in these hand-held, domestic or medical thermometers. Thermal detectors afford simple, low-cost devices to be constructed but incur compromises of speed, accuracy and do not necessarily provide the radiometric measurement that would be expected of more expensive, scientific and industrial thermometers [19], [20]. Low cost, domestic thermometers are not suitable for more demanding applications, for example: the acquisition of reliable and accurate industrial temperature measurements, measurements from regions incurring harsh conditions or transient temperature measurements.

Development of robust and radiometric infrared thermometers remains the target of the more specialised industrial detector manufacturers and research organisations that require devices with calibrated measurement capabilities. The Sensor Systems Group within the Advanced Detector Centre at The University of Sheffield, Electronic and Electrical Engineering Department, specialise in developing novel temperature measurement systems and undertaking the metrology that underlies these systems.

## 1.1 Industrial Temperature Measurement

The 'de facto' standard approach for acquiring industrial temperature measurements in manufacturing processes has been to deploy standard type thermocouples, owing to: their ease of use, low cost, range of measurement afforded and ready availability of systems to interpret and transmit the temperature signal [3], [10], [21]–[28]. Whilst thermocouples are simple to deploy, achieving measurements that are valid, accurate and sensitive is difficult and costly, owing to a number of weaknesses that make them susceptible to error and require careful installation [21], [29].

Using thermocouples becomes increasingly problematic when undertaking measurements under harsh conditions that exacerbate the inherent weaknesses of the thermocouple detector [18]. The principal weaknesses of thermocouples are: the requirement for invasive contact with the object being measured; low sensitivity to changes and poor dynamic response; chemical reactivity of the metals; calibration drift, particularly at high temperatures and accuracy limitations. These limitations have been

ameliorated for many applications by adopting standard methods of deployment that achieve reliable measurements in specific scenarios [9], [30].

A thermocouple can only measure the temperature from surfaces immediately around it that are able to radiate to the sensing junction and of the fluid or material that it contacts and transfers heat into the sensing junction [31]. An individual thermocouple cannot measure temperature distribution but measures a mean value from the combination of the radiative, convective and conductive heat transfer arising from the conditions locally to the sensing junction. The intrusive and contact nature of thermocouples introduces measurement errors. The introduction of a contact probe of any sort into a process always interferes with both the measurement of the temperature and the process itself and can cause errors that invalidate the measurement [31], [32]. An example of such discrepancies is the measurement of a fluid stream temperature with a thermocouple, which would incur additional heating from stagnation of the fluid and present disruption of the flow stream by the thermocouple assembly [31], [33]. A 'suction pyrometer' mitigates the error from impingement heating of the sensing junction but introduces the potential for the fluid sample extracted to have a different temperature to the bulk flow [20].

Research work has been expended to develop alternative temperature measurement detectors, including various acoustic, optical, electrical, spectroscopic and infrared devices [8], [21]. IRTs have been the most widely used general temperature measurement detectors of all of the techniques developed to substitute for the ubiquitous thermocouple. The other technologies have limited use and only work for specialised applications, for example: gas temperature measurement by acoustic thermometry or radiation absorption spectroscopy [3] and thermally-induced strain by fibre Bragg grating sensors [34].

Opportunities exist to improve measurement of temperatures from objects subjected to harsh conditions by substituting for thermocouples with inert fibre optics that transmit infrared radiation to a thermometer positioned remotely from the measured object [10], [35]. Such a system would enable fast and reliable measurements of temperatures to be acquired and used in process control [3], [5], [28].

Using infrared thermometers rather than thermocouples eliminates many of the problems associated with invasive thermometers and particularly those associated with insertion or contact with the object. Infrared thermometers have installation and usage requirements to ensure that valid and accurate temperature measurements are acquired. The conditions imposed upon infrared thermometers to achieve reliable measurements primarily concern the effects of emissivity and geometrical ‘view’ factors that affect the amount of radiant energy received by the detector [36].

## 1.2 Infrared radiation thermometer configurations

An infrared radiation thermometer (IRT) typically comprises an ‘optical’ configuration (lenses, windows, filters, apertures and transmission media) to couple radiation from a source to a photosensitive detector and an electronic circuit to interpret the detector response to incoming radiation as a temperature measurement [10], [37]. The detector typically would be a photo-thermal, thermo-electric or photo-electronic (photonic) type, terminology that is defined by the type of response that the detector demonstrates to incident infrared radiation, according to the distinctions described in the following definitions. Photo-thermal detectors undergo a change of electrical properties, typically, resistance or ionic charge that varies with the absorption of heat by the detector. Thermo-electric detectors generate an electromotive force with varying temperature absorption of heat generated by incident radiation. Photonic detectors generate a photo-current by the photo-electric effect from incident electromagnetic radiation of appropriate frequency promoting charge carriers within a semiconductor junction [21]. Typical modern IRTs use semiconductor alloy photo-electronic detectors, for example, photodiodes that respond to the spectral radiance of photons absorbed that promote free electrons by generating a photo-current across the diode junction. This photo-current is measured using a transimpedance amplifier (TIA) and the resultant voltage varies in relation to the intensity of radiation absorbed.

### 1.2.1 Photodiode junction operation

Photodiodes comprise p-doped (having an abundance of positive charge carriers) and n-doped (having an abundance of negative charge carriers) semiconductor alloys formed into p-n junctions, as illustrated in figure 1.1. The boundary between the n-type

and p-type semi-conductor forms a depletion layer, from which diffusion of the free electrons and holes towards the material of opposite doping becomes counterbalanced by an equilibrium electric field and potential difference. The photodiode had no bias voltage applied, thereby minimising the generation of dark current and noise whilst maximising the sensitivity to enable measurement of low spectral radiances expected to be transmitted via fibre optic coupling.

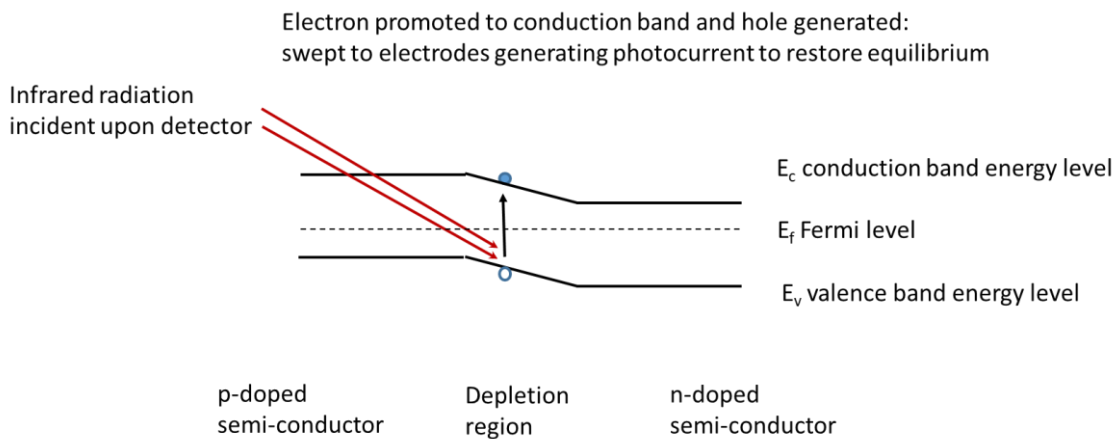


**Figure 1.1 Schematic illustration of photodiode p-n junction energy levels with no deliberate bias voltage applied**

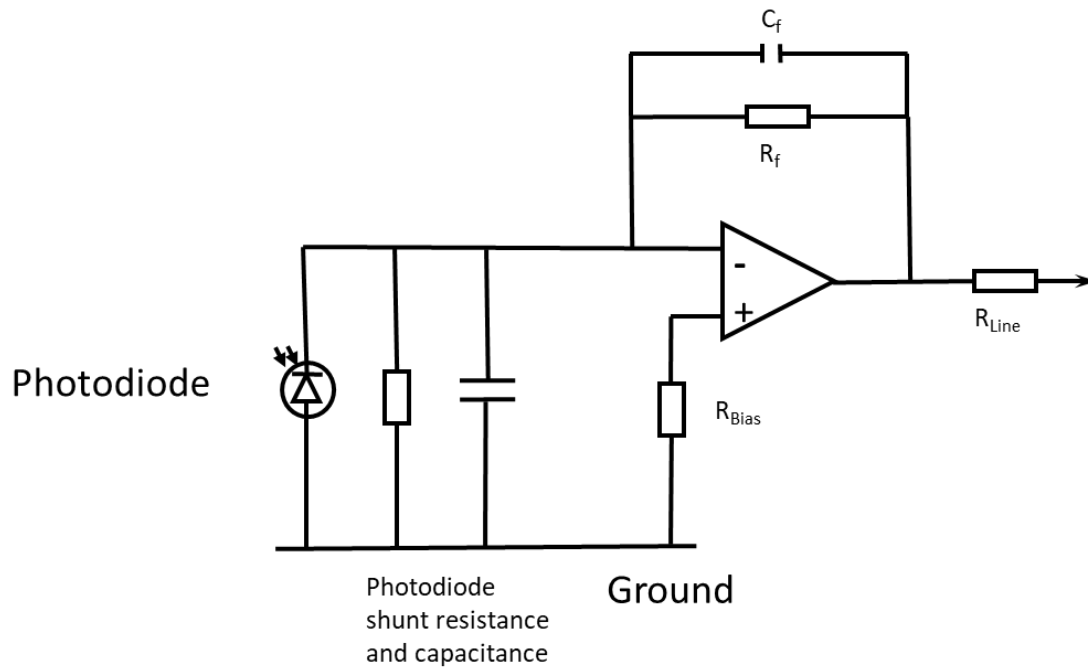
Infrared radiation of sufficient energy that falls incident upon the detector and penetrates into the semi-conductor material imparts energy into the electronic structure by the internal photo-electric effect. This energy exchange generates promotion of electrons from the valence band, over the band gap to the conduction band in the semiconductor alloy, also leaving a vacancy in the atomic lattice and a net positive charge locally. The charge carriers migrate to the cathode or anode, with either the small intrinsic or an applied potential difference being restored to equilibrium to compensate for the additional charge, thereby generating a small photocurrent. The magnitude of the photocurrent varies with the spectral radiance absorbed, therefore, the quantity of electrons promoted to the conduction band [38].

Photodiodes used for mid-wave infrared detection can have more complicated band structure, including an intrinsic material (designated as i in the descriptor of the diode) active layer between the doped p-type and n-type contact layers, that allows the detector to respond to infrared radiation with higher sensitivity. These so-called p-i-n

photodiodes have an extensive depletion region within the intrinsic layer, into which the positive and negative charge carriers flood to generate a relatively large photo-sensitive volume that enables improved efficiency of electron-hole pair generation. The intrinsic layer also introduces an intermediate energy level between the p-type and n-type semi-conductor that allows the low energy imparted by mid-wave infrared radiation to promote electrons into the conduction band directly [39], [40]. The combination of the relatively large depletion region with elevated electric field within the intrinsic layer, direct bandgap between valence and conduction band and composition of the semi-conductor alloy used provides a detector with sufficient MWIR photo-sensitivity to be usable for infrared thermometry.

### 1.2.2 Transimpedance amplifier configuration

A schematic diagram of a typical measurement system TIA is presented in figure 1.2, which illustrates a photodiode that is represented as a photocurrent source in parallel with the shunt resistance and capacitance of the photodiode. The photodiode connects to the inverting input of the transimpedance amplifier that has resistor-capacitor network in the feedback loop and grounded non-inverting input.



where:

$R_f$  is the feedback loop resistor that defines the transimpedance

$R_{Bias}$  is the op-amp input offset bias balancing resistor

$R_{Line}$  is the impedance matching resistor for the output connection

$C_f$  is the feedback loop capacitor

**Figure 1.2 Schematic diagram illustrating typical TIA configuration and small signal photodiode model**

Transimpedance amplifiers convert the photocurrent generated by the photodiode and noise present at the inverting input to an output voltage through the feedback resistor, achieving a magnitude that is measurable, typically of the order of milli-Volts to Volts for nano-Amperes to micro-Amperes of input photocurrent.

Ideally, the operational amplifier used in the TIA presents infinite impedance to the photocurrent, ensuring that the small photocurrent flows through the feedback loop, transforming to the output voltage

$$V_o = i_{ph} \times R_f$$

where:

$V_o$  is the output voltage

$i_{ph}$  is the photocurrent generated

$R_f$  is the feedback resistance

Ideally, with no photocurrent flowing, the inverting input is held at virtual ground by the grounded non-inverting input balancing the differential voltage between the inputs via the feedback loop and the output from the amplifier would be zero. Thermally induced promotion of charge carriers provides a 'dark current' from the photodiode that presents a noise signal that is amplified by the TIA. Often this noise is minimised by cooling the detector, thereby reducing the energy imparted into the charge carriers. The non-ideal characteristics of the photodiode and operational amplifier present noise and offset that lead to an output voltage being sustained without a photocurrent present at the input. The shunt resistance of the photodiode allows some of the photocurrent to flow through the photodiode to ground, rather than being amplified through the TIA, therefore representing a loss of photocurrent that does not flow through the feedback loop and an error in the output voltage achieved. This stray current will vary with the shunt resistance of the photodiode, which itself varies with temperature. The output voltage error varies and this leads to correction being required or acceptance of a variable error that increases the measurement uncertainty. The errors or uncertainties arising from Johnson noise generated by the feedback resistance and leakage of the photocurrent through the shunt resistance of the photodiode contribute the majority of the noise and measurement uncertainty. Typically, the input voltage noise and input current noise of the TIA op-amps are specified to be of the order of  $nV/\sqrt{Hz}$  and  $fA/\sqrt{Hz}$ , contributing negligibly small components to the total noise and consequent measurement uncertainty in comparison to the feedback loop and detector. High shunt resistance photodiodes, for example those made from silicon junctions, allow most of the photocurrent to flow to the TIA and generate output voltage, therefore minimising this error. The shunt resistance of photodiodes varies with alloy composition and it is known that detectors that have sensitivity to the mid-wave infrared radiation have lower shunt resistance than photodiodes that respond to higher energy photons, owing to the small band-gap between the valence and conduction bands in the semiconductor used.

### 1.2.3 Thermometer detector and optical configuration

IRTs exist that have used photo-thermal and thermo-electric detectors for example: bolometers and thermopiles, that can measure from -100 °C minimum temperature, receiving the total radiation captured by the optical configuration. These devices have an electrical property response that is measured to generate the analogue of temperature and do not need to be cooled or have the optical signal chopped to measure across a broad temperature range. These types of detectors have slow response speeds, low sensitivity and incur higher uncertainties than photonic detectors, so cannot be used readily for rapidly changing, accurate or low intensity measurements [41]. Faster and more sensitive measurements can be acquired using photonic detectors. Modern radiometric thermometers use semiconductor alloys such as: Indium Gallium Arsenide (InGaAs), Indium Arsenide (InAs), Indium Arsenide Antimony (InAsSb), Silicon and Mercury Cadmium Telluride (MCT or HgCdTe). The material used contributes to defining the photo-sensitivity curve of a detector to infrared radiation, the magnitude of photocurrent generated from incident photons and the electronic properties of the detector that dictate the circuit configuration used to measure the analogue of temperature.

Infrared radiation thermometers overcome many of the limitations of thermocouples and particularly those arising from requiring contact between the detector and the object being measured [10], [29], [36]. Using an IRT also eliminates the problems related to having the detector subjected to harsh conditions and provide long-term stability, high signal sensitivity and immunity to electro-magnetic interference because the device can be positioned remotely from the surface being measured. Infrared thermometers have been applied to many industrial temperature measurements that incur harsh conditions at the object position [9], [32], [42], [43]. There is ongoing research to apply infrared thermometers to difficult measurement conditions, for which thermocouples are used in the first instance typically, such as: measuring machine tool surface temperatures [44]–[52], battery cell temperatures [25], [53], [54] and industrial furnace control [1], [3], [4], [6], [11], [28], [55], [56].

A number of infrared thermometers use fibre optic coupling of the infrared from the measured object to the detector, enabling remote positioning of the detector and

electronics [46], [50], [51], [57], [58]. The usage of suitable fibre optics increases the capital and installation costs of a thermometer compared to a thermocouple, therefore, a more limited range of applications exist for which these more specialised optics have been justified [10], [32].

Infrared thermometers intended for accurate temperature measurements at low signal intensity that would be incurred from low temperature measurements use techniques to improve the accuracy and stability of the measurements acquired. Typically, thermometers use optical chopping of the incoming radiation to provide intermittent dark current measurement, affording offset compensation. IRTs also use thermoelectric cooling of the detector to minimize the detector dark current and drift, increase the photodiode shunt resistance [10], [59] and increase the photo-sensitivity of the detector. Accommodating these features necessitates an increased enclosure size and electronics for controlling the cooling and demodulating the signal [59].

The concept underlying the new IRT created within this project was the miniaturisation of the signal conditioning electronics and 'optical' components by eliminating the need for cooling and having a direct coupling of the source to the IRT using fibre optics, without the need for optical signal chopping. Fibre optic coupling isolated the IRT from the object undergoing measurement and eliminated physical signal chopping. The overall reduction of IRT size afforded a compact device that could be deployed into positions with limited availability of space that also incurred harsh conditions, for example, within end milling machines or Lithium ion cell test chambers.

It was necessary to couple the IRT to the heat source using fibre optics to isolate the electronics from the harsh conditions at the object undergoing measurement. The IRT was intended as a MWIR device, hence the fibre optic coupling needed to afford transmission through the appropriate range of infrared frequencies.

### 1.3 Fibre optic materials

Sapphire fibre optics are capable of operating at high temperatures, over 2000 °C, which exceeds the temperatures incurred during typical manufacturing processes and provide very good resistance to attack and degradation by chemical species [60]–[62].

Sapphire fibre optics are also brittle; therefore, require protection from excessive impact, tension, or torsion forces being incurred within the deployment. Indium Fluoride and Zirconium Fluoride (ZBLAN) glass fibre optics have lower maximum operating temperatures than sapphire but are more flexible, therefore retrofitting to existing geometries can be easier. Fluoride glass fibres also have high resistance to chemical reactions and attack except for exposure to humid conditions that would lead to degradation of the surface. Fluoride fibre optics also have broader transmission ranges than sapphire crystalline or silica glasses, extending into the mid-wave infrared, typically having cut-off wavelengths between 4.5  $\mu\text{m}$  and 5.5  $\mu\text{m}$ , thereby enabling lower temperatures to be measured than either sapphire or silica fibre optics.

Fibre-optic coupling of a radiant object to a thermometer leads to transmission losses compared to transmission through a vacuum and defines a range of wavelengths over which infrared radiation is transmitted and measured as the convolution of fibre optic transmission and the detector response curves.

## 1.4 Objectives of Infrared Thermometer Development.

The development of an infrared thermometer that used an uncooled MWIR photonic detector and received the radiant signal without optical chopping, has not been achieved successfully before. This new thermometer extended the utilisation of uncooled MWIR photodiodes by creating a calibrated infrared radiation thermometer (IRT) that was capable of measuring a wide range of temperatures. The IRTs configured with the capability of measuring over the temperature range from room temperature to a maximum of 1100 – 1200 °C (or higher, potentially) would advance temperature measurement in manufacturing, for example, applied to: machine tool and battery cell temperature measurement [25], [44], [52]–[54]. Thermometers affording measurement of higher temperatures could be applied to furnace temperature control [1], [3], [6], [11], [28], [55], [56]. Using fibre optic to couple infrared radiation onto the detector would afford having the electronic circuit positioned remotely from the harsh thermal and physical conditions at the cutting surface in machining, inside furnace chambers and the electro-chemical reaction conditions inside battery cells.

Having a thermometer that can measure from room temperature to 1100 – 1200 °C would afford improved control of heating processes and machining processes in manufacturing and electrochemical processes in batteries.

The infrared thermometers developed for use within harsh conditions have the following outline requirements to ensure that measurements are valid, effective and practical [25], [55], [62]:

- Operation without deterioration of the signal arising from changes induced by high temperature conditions such as: electronic drift, physical or optical behaviour changes and thermally-induced noise.
- Chemical inertness against the conditions and materials present in the process, for example: the reactive species present within chemical cells at elevated temperatures.
- Resilience against thermal degradation of the detector for example: thermal shock from exposure to high temperatures and fatigue arising from thermal cycling.
- Accuracy, repeatability and sensitivity of measurements acquired allied with fast response speed that exceed the capabilities of invasive sensors.
- Robustness against mechanical damage and the capability of deploying the measurement readily within the process or product being measured, and achieving cost-effective measurements.

In addition to this list of generic requirements, each application will present unique sets of conditions that combine some or all of the above requirements with specific constraints that must be satisfied to ensure the validity of measurements. The particular constraints of a process will determine the components used to make the thermometer and the temperature measurement range over which it is optimised..

## 1.5 Specification for Prototype Infrared Thermometer

The infrared thermometer must be capable of achieving measurements through a range of temperatures at sufficient resolution and accuracy to provide useful information about the processes undergoing investigation. The thermometer was also limited to having nominal physical size and mass constraints that ensured that it could be

attached to processes safely. The following summarises the specification for the prototype IRT configured:

- Temperature measurement range 20 – 1200 °C
- Temperature resolution  $\pm 1$  °C
- Response speed 1 ms
- Calibrated accuracy RMS Error < 1 %
- Nominal maximum PCB physical dimensions 30 mm x 30 mm
- Nominal maximum PCB mass 100 g
- Nominal fibre optic length 150 – 250 mm

Other limitations and specifications that were specific to an application would need to be considered as these arose, for example, the IRT response speed may need to be faster to apply the device to an explosion measurement but could be slower for measuring a battery cell temperature during charging and discharging cycles. The compromise between competing parameters would need to be determined, based upon the key measurement requirements for each application.

## 1.6 Raison d'être of this thesis.

An infrared radiation thermometer (IRT) that afforded non-invasive temperature measurement of processes incurring harsh conditions would advance temperature measurements of manufacturing operations and battery cell thermal behaviour. An IRT that deployed fibre-optic coupling between the object undergoing measurement and the thermometer, that was positioned remotely from the object, satisfied the requirements for such measurements. It would enable measurements from objects that were subjected to harsh conditions to be acquired without detriment to the thermometer. Thermometers exist that have fibre-optic coupling to enable the thermometer electronics to be positioned away from harsh conditions and these are deployed, typically with focusing optics to couple the infrared signal from a silica-based fibre-optic cable onto the detector. Using high temperature, crystalline sapphire fibre optics that are transparent to mid-wave infrared wavelengths to couple infrared radiation signals from higher temperature objects would enable deployment of a thermometer in high temperature conditions. Deploying metallic fluoride glass fibre

optic into lower temperature objects would enable the transmission of the maximum intensity of mid-wave infrared radiation possible to afford a thermometer capable of measuring the lowest possible minimum temperature. It should be possible to measure temperatures approaching room temperature without needing excessive signal filtering with such an arrangement.

The temperature ranges over which such thermometers measure could be adapted to different processes by amending the feedback resistor-capacitor (R-C) network around the TIA. Specifically, higher maximum temperature could be achieved using a smaller value feedback resistor and a lower minimum temperature could be achieved using a larger value resistor to define the transimpedance. Either of these adaptations would be likely to reduce the range of temperature measurements that one thermometer configuration could capture. It would be necessary to amend the thermometer configuration to suit specific applications and compromise between having a high maximum and low minimum temperature measurable by each configuration. The response speed of the thermometer will also be affected by using different resistor and capacitor combinations in the R-C network. Additionally, the minimum temperature that can be resolved will be affected by changes to the R-C network because of the signal filtering incurred. The operational amplifiers used to configure the thermometer could also be optimised for specific applications, potentially requiring compromise between parameters that define the thermometer characteristics. Achieving lower minimum temperature measurable may require limiting the temperature range over which the thermometer could measure without saturating the TIA operational amplifier.

IRT characterisation measurements using geometries that represented the conditions into which the thermometer would be deployed, provided practical calibrations of the prototype thermometers. This approach ensured that the practical calibrations measured under laboratory conditions should be valid for the applications.

This thesis presents the development of prototype mid-wave and short-wave infrared radiation thermometers that used infrared transmitting fibre optics to couple objects to the semiconductor photodiodes, mounted on small-sized printed circuit boards. The aspiration for the thermometers is that they can be positioned within processes and

products that incur harsh conditions but provide calibrated temperature measurements with fast response, low uncertainty and high resolution and sensitivity. Uniquely, the thermometers have been achieved without optical chopping of the radiation signal or cooling of the photodiodes; thereby, enabling the practical application of infrared radiation thermometry to substitute for thermocouples in processes that incur harsh conditions.

The thermometers used low-cost components, so could be positioned locally to the process undergoing measurement and consequential loss in too severe conditions for the device to survive would be tolerable.

## 1.7 Arrangement of Thesis

The thesis is arranged into the following chapters:

1. Introduction of the problem being addressed
  2. Background to the experimental measurements and theory of infrared temperature measurement applicable to fibre-optic coupled thermometry
  3. Experimental and analysis methods used in developing and characterising the thermometer
  4. Development and experimental characterisation of the prototype mid-wave infrared radiation thermometer and measurement of tool temperature during end milling of Titanium plate using a derivative of the prototype
  5. Development of low temperature measuring range prototype thermometer and measurement of Lithium-ion battery cell temperatures
  6. Development of short-wave infrared radiation thermometer for the measurement of temperature inflections during phase transformations of tin
  7. Conclusions
  8. Further Work
- Appendix 1. Method of integrating Planck's Law of Thermal Radiation and estimation of power incident upon photodiodes in radiation thermometers
- Appendix 2. Equipment used and factory calibration uncertainties for measuring instrumentation

## Appendix 3. Track and Component Layout Drawings for Thermometer Printed Circuit Board.

### 1.8 Papers Published

1. A. D. Heeley, M. J. Hobbs, H. Laalej, and J. R. Willmott, 'Miniature Uncooled and Unchopped Fiber Optic Infrared Thermometer for Application to Cutting Tool Temperature Measurement', *Sensors*, vol. 18, no. 3188, 2018.

2. A. D. Heeley, M. J. Hobbs and J.R. Willmott, 'Prototype zero drift, fibre optic infrared thermometer for thermocouple substitution'

Submitted for publication in the MDPI published journal 'Applied Science' and undergoing peer review, June 2020.

3. A.D. Heeley, M.J. Hobbs, M. J.M. Davies and J.R. Willmott, 'Fibre optic coupled radiation thermometer with fixed-point reference: demonstrating the feasibility of a self-calibrating thermometer.'

In draft, submission for publication pending a decision from Research and Innovation Services at The University of Sheffield concerning a potential application for patent protection.

### REFERENCES

[1] M. Evestedt and P. O. Norberg, *Precise temperature control in high quality steel reheating and annealing furnaces*, vol. 13, no. PART 1. IFAC, 2010.

[2] J. F. MacGregor and T. Kourti, "Statistical process control of multivariate processes," *Control Eng. Pract.*, vol. 3, no. 3, pp. 403–414, 1995, doi: 10.1016/0967-0661(95)00014-L.

[3] A. Queck, J. Broughton, J. Niska, C.-K. Tan, C. Steimer, and V. M. Mendive, *Advanced measurements and dynamic modelling for improved furnace operation and control*, vol. 9424. 2016.

[4] V. Battaglia et al., CO2 reduction in reheating furnaces CO2RED. 2010.

[5] A. Wolf *et al.*, "Cognitive control systems in steel processing lines for minimised energy consumption and higher product quality," 2019.

- [6] H. Pfeifer, "Industrial Furnaces-Status and Research Challenges," *Energy Procedia*, vol. 120, pp. 28–40, 2017, doi: 10.1016/j.egypro.2017.07.153.
- [7] A. K. Nair *et al.*, "Process monitoring of fibre reinforced composites using a multi-measurand fibre-optic sensor," *Sensors Actuators, B Chem.*, vol. 212, pp. 93–106, 2015, doi: 10.1016/j.snb.2015.01.085.
- [8] J. V. Nicholas and D. R. White, *Traceable Temperatures An Introduction to Temperature Measurement and Calibration*, Second Edi. John Wiley & Sons Ltd, 2001.
- [9] R. Bogue, "Sensors for extreme environments," *Sens. Rev.*, vol. 32, no. 4, pp. 267–272, 2012, doi: 10.1108/02602281211257498.
- [10] J. Dixon, "Radiation thermometry," *J Phys E Sci Instrum*, vol. 21, pp. 425–436, 1988.
- [11] H. Rawson, "Physics of glass manufacturing processes," *Phys. Technol.*, vol. 5, no. 2, pp. 91–114, 1974, doi: 10.1088/0305-4624/5/2/I03.
- [12] R. E. Bentley, "Long-term drift in mineral-insulated Nicrosil-sheathed type K thermocouples," *Sensors Actuators A. Phys.*, vol. 24, no. 1, pp. 21–26, 1990, doi: 10.1016/0924-4247(90)80043-5.
- [13] R. E. Bentley, "Irreversible thermoelectric changes in type K and type N thermocouple alloys within Nicrosil-sheathed MIMS cable," *J. Phys. D. Appl. Phys.*, vol. 22, no. 12, pp. 1908–1915, 1989, doi: 10.1088/0022-3727/22/12/017.
- [14] P. Pavlasek *et al.*, "Hysteresis Effects and Strain-Induced Homogeneity Effects in Base Metal Thermocouples," *Int. J. Thermophys.*, vol. 36, no. 2–3, pp. 467–481, 2015, doi: 10.1007/s10765-015-1841-3.
- [15] O. Ongrai, J. V. Pearce, G. MacHin, and S. J. Sweeney, "A miniature high-temperature fixed point for self-validation of type C thermocouples," *Meas. Sci. Technol.*, vol. 22, no. 10, 2011, doi: 10.1088/0957-0233/22/10/105103.
- [16] D. Tucker *et al.*, "Integrated self-validating thermocouples with a reference temperature up to 1329 °c," *Meas. Sci. Technol.*, vol. 29, no. 10, 2018, doi: 10.1088/1361-6501/aad8a8.

- [17] C. J. Elliott, A. D. Greenen, D. Tucker, T. Ford, and J. V. Pearce, "A Slimline Integrated Self-Validating Thermocouple: Initial Results," *Int. J. Thermophys.*, vol. 38, no. 9, pp. 1–10, 2017, doi: 10.1007/s10765-017-2274-y.
- [18] A. Demling, D. Ousley, and S. Stelley, "Best practices for deploying thermocouple instruments," *AIP Conf. Proc.*, vol. 1552 8, pp. 601–606, 2013, doi: 10.1063/1.4821397.
- [19] K. Keränen, J. T. Mäkinen, P. Korhonen, E. Juntunen, V. Heikkinen, and J. Mäkelä, "Infrared temperature sensor system for mobile devices," *Sensors Actuators, A Phys.*, vol. 158, no. 1, pp. 161–167, 2010, doi: 10.1016/j.sna.2009.12.023.
- [20] T. J. Claggett, R. W. Worrall, B. G. Liptak, J. E. Jamison, and K. C. Sloneker, "4.8 Miscellaneous and Discontinued Sensors," in *Temperature Measurement*, 2003, pp. 623–629.
- [21] P. R. N. Childs, J. R. Greenwood, and C. A. Long, "Review of temperature measurement," *Rev. Sci. Instrum.*, vol. 71, no. 8, pp. 2959–2978, 2000, doi: 10.1063/1.1305516.
- [22] J. P. Jones, S. P. Brookes, M. T. Whittaker, R. J. Lancaster, and B. Ward, "Assessment of Infrared Thermography for Cyclic High-Temperature Measurement and Control," *Eval. Exist. New Sens. Technol. Fatigue, Fract. Mech. Test.*, pp. 186–206, 2015, doi: 10.1520/STP158420140080.
- [23] J. Manara *et al.*, "Long wavelength infrared radiation thermometry for non-contact temperature measurements in gas turbines," *Infrared Phys. Technol.*, vol. 80, pp. 120–130, 2017, doi: 10.1016/j.infrared.2016.11.014.
- [24] B. Müller, U. Renz, and M. Bernhard, "Time resolved temperature measurements in manufacturing," *Meas. J. Int. Meas. Confed.*, vol. 34, no. 4, pp. 363–370, 2003, doi: 10.1016/j.measurement.2003.08.009.
- [25] R. Srinivasan, B. G. Carkhuff, M. H. Butler, and A. C. Baisden, "Instantaneous measurement of the internal temperature in lithium-ion rechargeable cells," *Electrochim. Acta*, vol. 56, no. 17, pp. 6198–6204, 2011, doi: 10.1016/j.electacta.2011.03.136.

- [26] H. P. G. J. Beelen, L. H. J. Raijmakers, M. C. F. Donkers, P. H. L. Notten, and H. J. Bergveld, "A comparison and accuracy analysis of impedance-based temperature estimation methods for Li-ion batteries," *Appl. Energy*, vol. 175, pp. 128–140, 2016, doi: 10.1016/j.apenergy.2016.04.103.
- [27] R. R. Richardson, P. T. Ireland, and D. A. Howey, "Battery internal temperature estimation by combined impedance and surface temperature measurement," *J. Power Sources*, vol. 265, pp. 254–261, 2014, doi: 10.1016/j.jpowsour.2014.04.129.
- [28] G. Andrews *et al.*, "Smartfire: Real-time intelligent diagnostics and optimisation of reheating furnace performance," 2010.
- [29] M. Campari and S. Garribba, "The behavior of type K thermocouples in temperature measurement: The Chromel P-Alumel thermocouples," *Rev. Sci. Instrum.*, vol. 42, no. 5, pp. 644–653, 1971, doi: 10.1063/1.1685192.
- [30] BSI, "BSI Standards Publication EN 60584-1:2013 Thermocouples Part 1 : EMF Specifications and Tolerances," *British Standard*, vol. BS EN 6058, no. 1. 2013.
- [31] S. Minn Khine, T. Houra, and M. Tagawa, "Heat-conduction error of temperature sensors in a fluid flow with nonuniform and unsteady temperature distribution," *Rev. Sci. Instrum.*, vol. 84, no. 4, 2013, doi: 10.1063/1.4801853.
- [32] A. Ghoshal, D. Le, and H. Kim, "Technological assessment of high temperature sensing systems under extreme environment," *Sens. Rev.*, vol. 32, pp. 66–71, 2012, doi: 10.1108/02602281211198476.
- [33] V. Hindasageri, R. P. Vedula, and S. V. Prabhu, "Thermocouple error correction for measuring the flame temperature with determination of emissivity and heat transfer coefficient," *Rev. Sci. Instrum.*, vol. 84, no. 2, 2013, doi: 10.1063/1.4790471.
- [34] J. Fleming, T. Amietszajew, E. McTurk, D. Greenwood, and R. Bhagat, "Development and evaluation of in-situ instrumentation for cylindrical Li-ion cells using fibre optic sensors," *HardwareX*, vol. 3, pp. 100–109, 2018, doi: 10.1016/j.ohx.2018.04.001.

- [35] Y. B. Yu and W. K. Chow, "Review on an Advanced High-Temperature Measurement Technology: The Optical Fiber Thermometry," *J. Thermodyn.*, vol. 2009, pp. 1–11, 2009, doi: 10.1155/2009/823482.
- [36] J. Hartmann, "High-temperature measurement techniques for the application in photometry, radiometry and thermometry," *Phys. Rep.*, vol. 469, no. 5–6, pp. 205–269, 2009, doi: 10.1016/j.physrep.2008.09.001.
- [37] D. Gabriel, "Temperature Measurement," *Temperature Measurement 1.0*. pp. 1–49, 1999.
- [38] A. de Sa, *Principles of Electronic Instrumentation*, First. Edward Arnold (Publishers) Ltd, London, 1981.
- [39] M. Razeghi, R. Balcerak, and Y.-S. Park, "Demonstration of Uncooled InAsSb Photodetectors for Military Sensors," 2000.
- [40] M. Razeghi, J. Piotrowski, J. Xu, J. Kim, D. Wu, and J. Wojkowski, "Long wavelength InAsSb Infrared photodetectors," 1995.
- [41] X. Zhou, "An ingaalas-ingaas two-colour detector, inas photodiode and si spad for radiation thermometry," *PQDT - UK Irel.*, no. November, 2014.
- [42] S. Gao, L. Wang, C. Feng, and K. D. Kipngetich, "Analyzing the influence of combustion gas on a gas turbine by radiation thermometry," *Infrared Phys. Technol.*, vol. 73, pp. 184–193, 2015, doi: 10.1016/j.infrared.2015.09.006.
- [43] A. H. Khalid, "Development of phosphor thermometry systems for use in development gas turbine engines," 2011.
- [44] M. Sato, T. Ueda, and H. Tanaka, "An experimental technique for the measurement of temperature on CBN tool face in end milling," *Int. J. Mach. Tools Manuf.*, vol. 47, no. 14, pp. 2071–2076, 2007, doi: 10.1016/j.ijmachtools.2007.05.006.
- [45] M. A. Davies, T. Ueda, R. M'Saoubi, B. Mullany, and A. L. Cooke, "On The Measurement of Temperature in Material Removal Processes," *CIRP Ann. - Manuf. Technol.*, vol. 56, no. 2, pp. 581–604, 2007, doi: 10.1016/j.cirp.2007.10.009.
- [46] T. Ueda, M. Sato, A. Hosokawa, and M. Ozawa, "Development of infrared radiation pyrometer with optical fibers-Two-color pyrometer with non-contact fiber

coupler," *CIRP Ann. - Manuf. Technol.*, vol. 57, no. 1, pp. 69–72, 2008, doi: 10.1016/j.cirp.2008.03.056.

[47] J. C. Heigel, E. Whinton, B. Lane, M. A. Donmez, V. Madhavan, and W. Moscoso-Kingsley, "Infrared measurement of the temperature at the tool–chip interface while machining Ti–6Al–4V," *J. Mater. Process. Technol.*, vol. 243, pp. 123–130, 2017, doi: 10.1016/j.jmatprotec.2016.11.026.

[48] J. Pujana, L. Del Campo, R. B. Pérez-Sáez, M. J. Tello, I. Gallego, and P. J. Arrazola, "Radiation thermometry applied to temperature measurement in the cutting process," *Meas. Sci. Technol.*, vol. 18, no. 11, pp. 3409–3416, 2007, doi: 10.1088/0957-0233/18/11/022.

[49] Y. Quan, H. Xu, and Z. Ke, "Research on some influence factors in high temperature measurement of metal with thermal infrared imager," *Phys. Procedia*, vol. 19, pp. 207–213, 2011, doi: 10.1016/j.phpro.2011.06.150.

[50] M. Saito and K. Kikuchi, "Infrared optical fiber sensors," *Opt. Rev.*, vol. 4, no. 5, pp. 527–538, 1997, doi: 10.1007/s10043-997-0527-x.

[51] A. Tapetado, J. Diaz-Alvarez, H. Miguelez, and C. Vazquez, "Fiber-Optic Pyrometer for Very Localized Temperature Measurements in a Turning Process," *IEEE J. Sel. Top. Quantum Electron.*, vol. 23, no. 2, 2017, doi: 10.1109/JSTQE.2016.2627553.

[52] A. Tapetado, J. Diaz-Alvarez, M. H. Miguelez, and C. Vazquez, "Two-color pyrometer for process temperature measurement during machining," *J. Light. Technol.*, vol. 34, no. 4, pp. 1380–1386, 2016, doi: 10.1109/JLT.2015.2513158.

[53] R. Srinivasan *et al.*, "Heat generation in Li-ion cells during charge and discharge," *Energy Harvest. Storage Mater. Devices, Appl. IV*, vol. 8728, no. May 2013, p. 87280E, 2013, doi: 10.1117/12.2018528.

[54] Y. Saito, "Thermal Behavior of Lithium-Ion Cells during Charge and Discharge," *J Power Sources*, vol. 244, pp. 294–299, 2013.

[55] G. R. Peacock, "Radiation Thermometers in Steel and Metals Processing," *AIP Conf. Proc.*, vol. 684, no. October, pp. 813–818, 2003, doi: 10.1063/1.1627228.

- [56] B. Grabas, "Pyrometric temperature measurements with a miniature cavity used as a blackbody in the calorimetric method for determining absorbed laser energy," *Exp. Therm. Fluid Sci.*, vol. 74, pp. 100–109, 2016, doi: 10.1016/j.expthermflusci.2015.11.022.
- [57] B. Müller and U. Renz, "Development of a fast fiber-optic two-color pyrometer for the temperature measurement of surfaces with varying emissivities," *Rev. Sci. Instrum.*, vol. 72, no. 8, pp. 3366–3374, 2001, doi: 10.1063/1.1384448.
- [58] B. Müller, U. Renz, S. Hoppe, and F. Klocke, "Radiation Thermometry at a High-Speed Turning Process," *J. Manuf. Sci. Eng.*, vol. 126, no. 3, p. 488, 2004, doi: 10.1115/1.1763188.
- [59] V. Srivastav, R. K. Sharma, R. K. Bhan, V. Dhar, and V. Venkataraman, "Exploring novel methods to achieve sensitivity limits for high operating temperature infrared detectors," *Infrared Phys. Technol.*, vol. 61, pp. 290–298, 2013, doi: 10.1016/j.infrared.2013.09.004.
- [60] SEDI-ATI Fibres Optiques, "Special Fibers," *SEDI-ATI Datasheet*. .
- [61] J. A. Savage, "Materials for Infrared Fibre Optics," *Mater. Sci. Reports*, vol. 2, no. February, pp. 99–138, 1987.
- [62] L. Schenato, A Review of Distributed Fibre Optic Sensors for Geo-Hydrological Applications, vol. 7, no. 9. 2017.

## 2 PRINCIPLES AND THEORY APPLICABLE TO RADIATION THERMOMETRY

Radiation thermometry is based upon measurement of the repeatable response of photo-sensitive devices (detectors) to incident radiation, that can be characterised in relation to the radiance temperature of the source. The incident radiation causes an electronic response or material property change in the detector. In the case of photodiodes, the interaction of infrared photons with the semiconductor materials causes the promotion of electrons and holes to the conduction band and generation of a photocurrent. The magnitude of photocurrent generated has a characteristic relationship with the intensity of infrared photons received within the wavelength range to which the detector is sensitive. The intensity of infrared radiation incident upon the photodiode depends upon the emittance with which the source object radiates and the transmission of the electro-magnetic radiation through media between the object and the receiving surface of the photodiode. In the case of a fibre optic coupled thermometer, the transmission medium between the object and photodiode is, at least, the fibre optic core and this will attenuate the intensity of radiation received by the detector compared to a blackbody transmitting through a vacuum. A thermometer characterisation or calibration is required that relates the photocurrent generated by the photodiode to a scale of known temperatures from sources having known emittances. The theory of blackbody radiation enables the relationship between the temperature of an object and the infrared radiation emitted by it to be evaluated.

The photocurrents generated within a detector are transformed to measurable voltages in a thermometer, typically using a transimpedance amplifier that amplifies the input current flowing through the feedback impedance [1]. The known emittance can then be used to characterise the consequent output voltage of a thermometer measuring the radiation that falls incident upon the detector, against the source temperature. The relationship determined between the output voltage and known temperatures can be interpolated to determine unknown temperatures of objects undergoing measurement.

The detectors used to configure thermometers reported upon in this thesis were:

- Indium Arsenide Antimony (InAsSb) alloy with response between 3.0  $\mu\text{m}$  and 5.0  $\mu\text{m}$  in the mid-wave infrared (MWIR)
- Extended range Indium Gallium Arsenide (extended-InGaAs) alloy with response between 0.9  $\mu\text{m}$  and 2.6  $\mu\text{m}$  in the short-wave infrared (SWIR)

The temperature measurement uncertainty arising from emissivity error is dependent upon the wavelength at which the infrared radiation is measured according to the relationship [2]:

$$\frac{\Delta T}{T} = \frac{\lambda T}{c_2} \frac{\Delta \epsilon}{\epsilon} \tag{Equation 2.1}$$

where:

$\Delta T$  is the error in the radiance temperature measured, K

$c_2$  is the second Planck radiation constant 0.014387752 m K

$\lambda$  is the limiting effective wavelength at which the IRT measured, m

$T$  is the absolute temperature of the object, K

$\Delta \epsilon$  is the error in relative emissivity of the object

$\epsilon$  is the relative emissivity of the object

The photodiodes were chosen to use the shortest wavelength of infrared possible that afforded measurement over the temperature ranges desired, thereby the effects of emissivity errors upon the measurement uncertainty were minimised.

## 2.1 Radiometry Definitions

Radiometry describes the set of metrology techniques that afford evaluation of the macroscopic exchange of radiation emitted by an object and received by a surface, accounting for the geometry between the two surfaces [3]. A hot object undergoing measurement and a photodiode detector undertaking its temperature measurement represent the emitting and receiving surfaces when applied to infrared radiation thermometry.

The parameters used to describe the energy exchange between surfaces have specific definitions, as follows:

- Radiance is the power emitted through all wavelengths from an object into a solid angle that subtends an area on a hemispherical surface along the normal direction and has units of  $W/m^2 \text{ sr}$
- A blackbody describes a perfect emitter or absorber of radiation, for which the temperature inferred from measurement of the radiance (the radiance temperature described below) is the actual temperature of the surface from which radiation is emitted
- Radiant emittance is the power emitted in all directions measured across the whole hemispherical surface around a surface and has units of  $W/m^2$
- Incident irradiance is the radiance emitted from an object that is subsequently received by a surface from all directions and has units of  $W/m^2$
- Spectral radiance is the radiance within the range of wavelengths from a specific wavelength to infinity and has units of  $W/m^2 \text{ sr m}$
- Band emittance is the spectral radiance emitted from a surface between two defined wavelengths and has units of  $W/m^2 \text{ sr m}$
- Radiance temperature is the apparent blackbody temperature of the surface that led to the radiance emitted from an object, that is then measured by a thermometer and has units of K
- Solid angle is the geometrical projection of an area,  $dA$  defined by an angle subtended from a point nominally at the centre of a sphere of radius,  $r$  at its surface and is defined as  $dA/r^2$  and has units of steradians. The geometric projection of solid angle is illustrated by figure 2.1, reproduced from original

content made available on Wikimedia by the original author, Sergio Mendoza, under an unrestricted creative commons public domain licence [4].

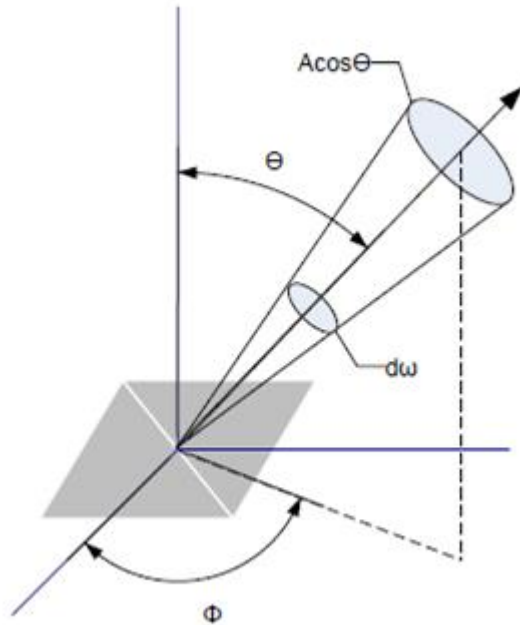


**Figure 2.1 Solid angle geometry**

## 2.2 Blackbody Radiation Curves

The band emittance of radiation from a surface is described by Planck's Law of Thermal Radiation (Planck's Law), with suitable reduction of the blackbody radiation intensity applied to account for the surface emissivity being non-blackbody in practice. The radiation intensity received by a detector may be reduced further by a 'view' factor that accounts for the geometry between the emitting object and detector.

The equations presented hereafter assume blackbody conditions and perfect radiation exchange, so are idealised assumptions of perfect emittance, transmission and incidence upon a photodiode. These assumptions would need to be amended to represent the non-ideal conditions of a real thermometer for accurate calculation of the infrared radiance that was incident upon the active area of a photodiode.

The spectral radiance of blackbody radiation is described by Planck's Law:

$$L_b(\lambda, T) = \frac{c_1}{\lambda^5} \left[ \exp\left(\frac{c_2}{\lambda T}\right) - 1 \right]^{-1} \quad \text{Equation 2.2}$$

where:

$L_b(\lambda, T)$  is the spectral radiance of wavelength,  $\lambda$  emitted by a blackbody at absolute temperature,  $T$

$c_1$  is the first radiation constant and  $c_1 = 2\pi hc^2 = 3.7417274 \times 10^{-16} \text{ J m}^2/\text{s}$

$c_2$  is the second radiation constant and  $c_2 = \frac{hc}{k_B} = 0.014387752 \text{ m K}$

$h$  is Planck's constant  $6.6261 \times 10^{-34} \text{ J s}$

$c$  is the speed of light in vacuum  $2.9979 \times 10^8 \text{ m/s}$

$k_B$  is Boltzmann's constant  $1.3806 \times 10^{-23} \text{ J/K}$

Integration of Planck's Law cannot be undertaken using analytical methods, however numerical estimation can be used to evaluate the spectral radiance between two wavelength limits. The band radiance within unit solid angle between the two wavelengths is evaluated as the difference between the one-sided integrals calculated over the range of each wavelength to infinity. The integral calculated between the arbitrary wavelengths  $3.0 \mu\text{m}$  and  $3.5 \mu\text{m}$  is illustrated in figure 2.2.

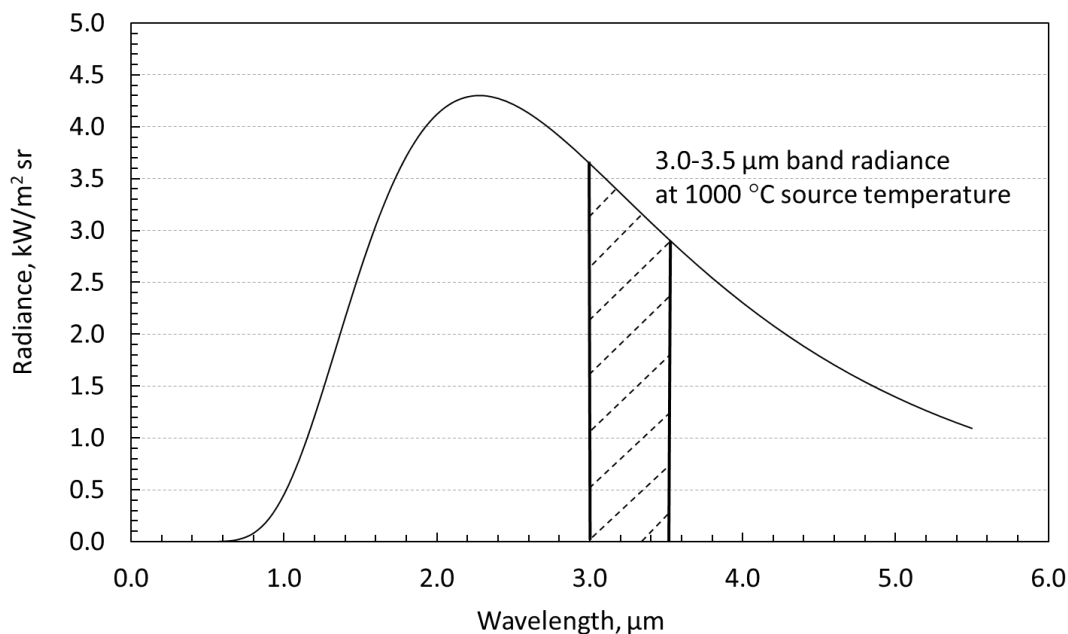


**Figure 2.2 Spectral band radiance between  $3.0 \mu\text{m}$  and  $3.5 \mu\text{m}$  wavelengths**

The power incident upon a receiving surface from a radiating surface, within the range of wavelengths defined by the integration, can be calculated by convolution of the

band radiance with the optical throughput of the system. Further convolution of the power received by the detector with the photodiode response curve afforded estimation of the photocurrent generated by the device. This calculation was useful for projecting the suitability of a proposed system for acquiring temperature measurements within a defined range and estimation of the minimum and maximum temperatures measurable by a system having known characteristics.

The following paragraphs describe the method used for estimating the intensity of radiation incident upon a photodiode in the prototype infrared thermometer and was based upon the method of Widger and Woodall [5], elaborated by Lawson [6].

## 2.3 Numerical Integration of Planck's Law

The integration of Planck's Law of thermal radiation can be solved numerically to evaluate the band radiance emitted from a source object at a temperature.

The band radiance,  $B(\lambda)$  is described by the one-sided integration of the spectral radiance that is defined by Planck's Law,  $L_\lambda$  over the wavelength range from  $\lambda$  to  $\infty$  and defines the blackbody power emitted into unit solid angle from unit area.

$$B(\lambda) = \int_{\lambda}^{\infty} L_{\lambda} d\lambda \quad \text{Equation 2.3}$$

$$B(\lambda) = \int_{\lambda}^{\infty} \frac{c_1}{\lambda^5} \left[ \exp\left(\frac{c_2}{\lambda T}\right) - 1 \right]^{-1} d\lambda \quad \text{Equation 2.4}$$

Using substitutions of the form:

$$x = \frac{c_2}{\lambda T}$$

and

$$dx = -\frac{c_2}{\lambda^2 T} d\lambda$$

substituting into the equation for band radiance:

$$B(x) = \frac{c_1 T^4}{c_2^4} \int_x^{\infty} \frac{x^3}{e^x - 1} dx \quad \text{Equation 2.5}$$

and making the substitution of an infinite series that is equivalent to the integral in equation (2.5)

$$\int_x^{\infty} \frac{x^3}{e^x - 1} dx = \sum_{n=1}^{\infty} e^{-nx} \left[ \frac{x^3}{n} + \frac{3x^2}{n^2} + \frac{6x}{n^3} + \frac{6}{n^4} \right] \quad \text{Equation 2.6}$$

enables the numerical solution of the Planck's Law equation [5], [6] as:

$$B(\lambda) = \frac{c_1 T^4}{c_2^4} \sum_{n=1}^{\infty} e^{-nx} \left[ \frac{x^3}{n} + \frac{3x^2}{n^2} + \frac{6x}{n^3} + \frac{6}{n^4} \right] \quad \text{Equation 2.7}$$

where

$$x = \frac{hc}{k\lambda T} = \frac{c_2}{\lambda T}$$

The infinite series has been demonstrated to converge with negligible truncation error for the summation  $n=1$  to  $n=10$  when  $x > 2$  [5], for which conditions the product  $\lambda T$  falls within the mid-wave infrared region of the electromagnetic spectrum at temperatures up to 1750K (circa 1475 °C).

Evaluation of the finite band radiance can then be achieved by the difference between the numerical solutions of the band radiance integrals, calculated from the specified values of  $\lambda$  to infinity, that is:

$$\int_{\lambda_1}^{\lambda_2} L_{\lambda} d\lambda = \int_{\lambda_1}^{\infty} L_{\lambda} d\lambda - \int_{\lambda_2}^{\infty} L_{\lambda} d\lambda \quad \text{Equation 2.8}$$

The numerical solution of this equation affords estimation of the radiance emitted from a blackbody source, which can then be multiplied by the fibre optic throughput to afford estimation of the power incident upon a sensor positioned remotely from the radiant source.

The band radiance calculation for any wavelength between 0.2  $\mu\text{m}$  and 6.0  $\mu\text{m}$  was undertaken in a spreadsheet and has been used to estimate the power incident upon the thermometer for each prototype configuration considered.

The fibre optic transmission curve was assumed to have a 'top-hat' profile, as illustrated by figure A1.2 of Appendix 1. The range of wavelengths between the high and low cut-off limits were assumed to be transmitted perfectly and all wavelengths outside of this pass band were assumed to be blocked fully. There was an 8% loss of the incident radiation at the fibre optic boundary, calculated according to Fresnel's Law of normal incidence. Similarly, the photodiode response curve was assumed to have a 'top-hat' profile that only generated photocurrent between the upper and lower

cut-off wavelengths. These are simplifying assumptions because the fibre optic transmission and photodiode response curves will both have increasing attenuation beyond the nominal cut-off limits and will not have such abrupt on/off characteristics. These assumptions enable the numerical solution of the equation to be realised practically using the spreadsheet calculation and represent a conservative estimate of the radiance, power incident upon the photodiode and photocurrent generated in response to the infrared signal.

An example of the blackbody band radiance calculation between 3.0  $\mu\text{m}$  and 4.5  $\mu\text{m}$  is presented in figure 2.3. This wavelength range represented the band transmitted by the ZBLAN fibre optic, over which the InAsSb photodiode chosen for the experimental work, responded at its maximum photosensitivity. The nominal high and low limits were defined as the wavelengths at which 3dB attenuation of the photosensitivity occurred. The sensitivity of the photodiode diminished rapidly beyond these limits, therefore, assuming that the photodiode had no response to wavelengths beyond these is a reasonable simplification.

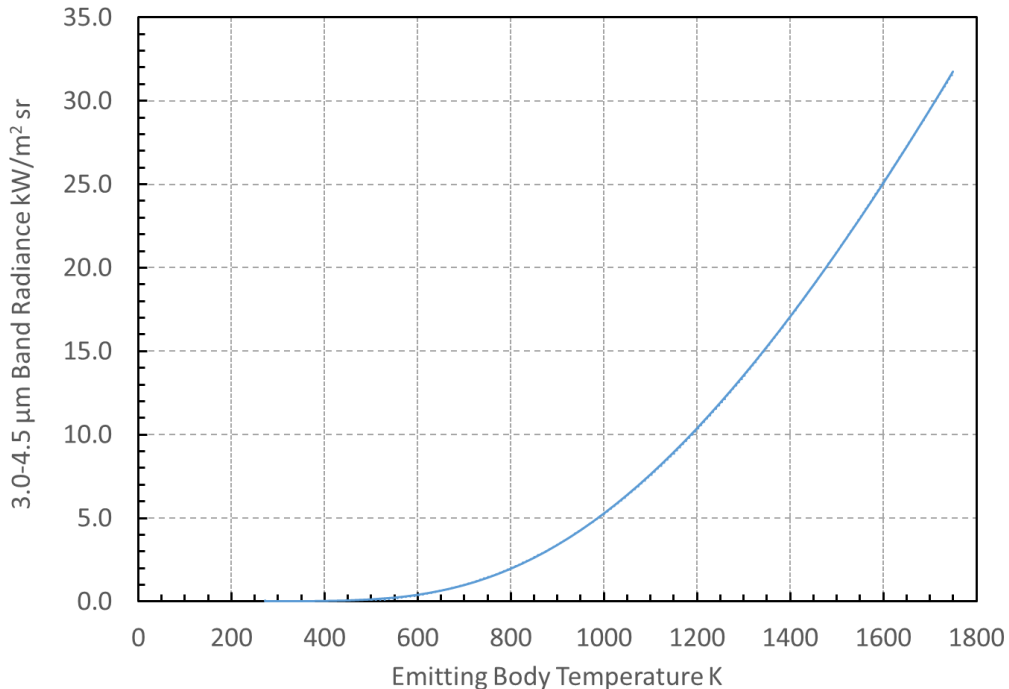


**Figure 2.3 Example band radiance for the wavelength range 3.0 – 4.5  $\mu\text{m}$  calculated from numerical integration of Planck’s Law, assuming blackbody conditions**

The band radiance and étendue (or optical throughput) calculated for a specific fibre optic coupling (see equation 2.22 presented later in this chapter) enabled the energy incident upon the photodiode to be calculated for different source temperatures and thermometer configurations (see table 2.2 presented later in this chapter). This calculation spreadsheet enabled the expected minimum temperature measurable to be estimated and the optimum configuration of photodiode and fibre optic coupling material to be selected to match the thermometer response to the application prior to assembling the components.

## 2.4 Wien's Approximation of Planck's Law

Owing to the intractability of integrating Planck's Law analytically, therefore, lacking the capability to interpolate between pairs of calibration measurements with a continuous, smooth and monotonic calibration curve, the Wien approximation has been used to simplify calculations of blackbody radiation curves. It would be feasible to embed Planck's Law calculations of band radiances into a microprocessor to afford the piecewise interpretation of measuring circuit output voltages as radiance temperatures with sufficient granularity to enable linear interpolation between known points. The Wien approximation has been used for practical calibration and characterisation of the response of a thermometer to varying temperatures to afford a continuous interpolation curve between the known points. This simplified equation approximates Planck's Law well for higher frequency, shorter wavelength, therefore higher energy infrared radiation. The Wien approximation certainly applied to the mid-wave and short-wave infrared frequencies to which the prototype thermometers configured within this work responded and higher frequencies (shorter wavelengths) for ranges of temperature measurement incurred within industrial processes [7].

The Wien approximation is based upon the assumption that the unity constant in the denominator of Planck's Law formulation can be neglected for conditions that satisfy the assumption:

$$\frac{c_2}{\lambda T} \gg 1$$

This simplification affords the elimination of the unity constant in the denominator:

$$\left[ \exp\left(\frac{c_2}{\lambda T}\right) - 1 \right]^{-1} \approx \left[ \exp - \left(\frac{c_2}{\lambda T}\right) \right] \quad \text{Equation 2.9}$$

from which, Planck's Law may be simplified to the Wien approximation:

$$L_b(\lambda, T) = \frac{c_1}{\lambda^5} \left[ \exp - \left(\frac{c_2}{\lambda T}\right) \right] \quad \text{Equation 2.10}$$

There exist ranges of wavelength and temperature conditions for which the Wien approximation and Planck's Law will differ by only 1%, favouring shorter wavelengths. The Wien approximation will estimate the intensity of radiation emitted by an object outside of the ideal constraints but will incur increased uncertainty.

Representative radiances were calculated for different temperatures through the wavelength ranges over which the SWIR and MWIR photodiodes responded, using Planck's Law and the Wien approximation. The resulting radiance curves as a function of wavelength are presented in figure 2.4

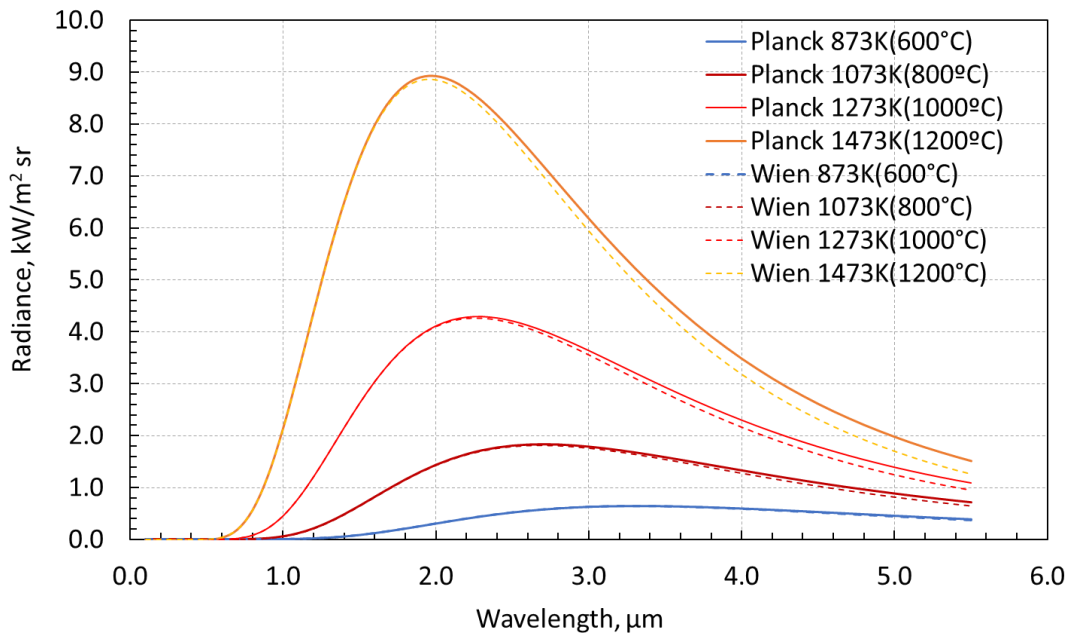


**Figure 2.4 Radiance curves calculated using Planck's Law and Wien Approximation**

The wavelength ranges of the SWIR and MWIR bands to which the extended-InGaAs and InAsSb photodiodes responded and the temperature ranges to be measured afforded Wien's approximation to be used with a maximum deviation from Planck's Law of 10% at 1000°C and 5.0 μm.

The radiance temperature of an object can be inferred by solving the inverse form of Wien's approximation, which afforded modelling the output characteristic that could be expected from an infrared thermometer and evaluation of unknown source temperatures based upon calibration to known source temperatures, as described in the following paragraph.

The Wien approximation enables the ratio of the radiance arising from an unknown temperature to the radiance from a known temperature to be evaluated and the consequent signals from a thermometer characterised to calibrate the radiance versus object temperature relationship [7]–[10]. The implementation of the Wien approximation requires knowledge of the spectral response of the thermometer to establish the monochromatic, limiting effective wavelength representation of the broad range of spectral response actually achieved, as described in the following paragraph.

Differentiation of the Wien approximation with respect to the wavelength and representation of the resulting differential change in the band radiance divided by band radiance afforded determination of the fractional change in band radiance:

$$\frac{\frac{d}{dT}[L_b(\lambda, T)]}{L_b(\lambda, T)} = \frac{\frac{c_1 c_2}{\lambda^6 T^2} \left[ \exp\left(-\frac{c_2}{\lambda T}\right) \right]}{\frac{c_1}{\lambda^5} \left[ \exp\left(-\frac{c_2}{\lambda T}\right) \right]} \quad \text{Equation 2.11}$$

Cancelling out the numerator and denominator terms from equation (2.11), the relationship describing the proportional change in band radiance simplified to:

$$\frac{\frac{d}{dT}[L_b(\lambda, T)]}{L_b(\lambda, T)} = \frac{c_2}{\lambda T^2} \quad \text{Equation 2.12}$$

The continuous interpolation equation used to calculate the radiance temperature from the measured detector output voltage would, ideally, be applied to a very narrow range of wavelengths, represented by a monochromatic central wavelength. A narrow range of wavelengths can be represented in the Wien approximation quite adequately by the mean monochromatic wavelength, without introducing significant error into the calculation. In practice, detectors can have responses over a broad range of wavelengths and temperatures, therefore, assuming the same characteristic throughout these ranges introduces greater uncertainty into the measurement. It was desirable to characterise the full range of detector response as an abstraction at a nominal monochromatic wavelength, for which the 'limiting effective wavelength' has been

defined. This mathematical abstraction to a monochromatic wavelength represents the spectral response of the thermometer through the temperature and wavelength ranges measured and is accepted for usage in multiple point calibrations within standards laboratories [7]. The relationship describing the proportional change in band radiance can be evaluated at the limiting effective wavelength without exacerbating the measurement uncertainty. The relationship between the fractional change in band radiance and limiting effective wavelength also provided metrics that can be calculated to characterise the sensitivity, uncertainty and resolution that a thermometer achieved and compare with similar metrics from other thermometers, as described in the following paragraphs.

Evaluation of the ratio of band radiances between two temperatures, convolved with the detector response curve enabled a first order expansion of the relationship between the natural logarithm of the thermometer output ( $\ln(V_o)$ ) and inverse of source absolute temperature ( $1/T$ ) to be evaluated [8]. The intercept,  $a$  and gradient,  $b$  of the linear relationship presented in equation (2.13) are evaluated from regression of the measurements plotted on a graph with  $\ln(V_o)$  on the ordinate axis and  $1/T$  on the abscissa.

$$\ln(V_o) = a + \frac{b}{T} \quad \text{Equation 2.13}$$

The limiting effective wavelength value can be evaluated from the gradient of the  $\ln(V_o) - 1/T$  curve, as presented in equation (2.14)

$$\lambda_e = \frac{c_2}{b} \quad \text{Equation 2.14}$$

where:

$\lambda_e$  is the limiting effective wavelength calculated as the representative wavelength of the thermometer

$c_2$  is the second radiation constant

$b$  is the gradient of the  $\ln(V_o)$  versus  $1/T$  curve

The sensitivity of the output voltage variation with unit temperature was defined as the percentage change of the thermometer output ( $\% \Delta V_o$ ) with varying source temperature ( $1/T$ ) and evaluated according to the relation (2.15):

$$\frac{\% \Delta V_o}{T} = \frac{c_2}{\lambda_e T^2} \quad \text{Equation 2.15}$$

Equation (2.15) enables the measurement uncertainty and noise around a mean signal to be expressed as a temperature. The noise-limited equivalent temperature resolution that defined the resolution to which measurements could be acquired using the prototype thermometer, was defined as the percentage of the output voltage that was noise divided by the output sensitivity to unit temperature variation, defined in equation (2.16) and was calculated from equation (2.17).

$$NETR = \frac{\% \text{NoiseVoltage}}{(\% \Delta V_o / ^\circ C)} \quad \text{Equation 2.16}$$

which evaluated as:

$$NETR = \frac{\left(100 \frac{\sigma}{V_o}\right)}{\left(100 \frac{c_2}{\lambda_e T^2}\right)} \quad \text{Equation 2.17}$$

where:

NETR is the Noise-limited Equivalent Temperature Resolution, °C

$\sigma$  is the sample standard deviation of noise around the mean signal (%NoiseVoltage)

$\% \Delta V_o / ^\circ C$  is the change in output voltage expected from the thermometer for a change in temperature; this value is determined from the  $\ln(V_o)$  versus  $1/T$  curve,  $\% / ^\circ C$

T is the absolute temperature of the source object being measured, K

$V_o$  is the mean output voltage value at the temperature being measured, V

The uncertainty of the measurements acquired was defined as the standard deviation of the output voltage variation and this contributes the principal component of measurement uncertainty for thermometers.

The minimum temperature measurable was defined as the temperature for which unity signal to noise ratio occurred and was evaluated as the temperature at which the magnitude of the standard deviation,  $\sigma$  equalled the mean output voltage,  $\langle V_o \rangle$ .

These parameters were calculated for the measurements acquired from the prototype thermometers during characterisation against known temperatures and used to define the nominal temperature measurement range over which measurements were maintained within defined uncertainties. The limiting effective wavelength parameter

calculated using the Wien approximation, along with the variation of the output voltage with known source temperatures enabled a Sakuma–Hattori interpolation equation to be determined. The Sakuma–Hattori equation modelled the thermometer characteristics affording interpolation of unknown temperatures from the relationship between the output voltage from the thermometer and known temperatures.

## 2.5 Sakuma-Hattori equation.

Simplifications of the response of a thermometer output signal to varying source temperature have been established that enable calibration without requiring knowledge of the spectral response of the thermometer or extensive radiance calculations. Whilst the Wien approximation simplifies the calculation of band radiance significantly, it still requires knowledge of the spectral response of the thermometer, via calculation of the limiting effective wavelength and investment of considerable effort to evaluate the integration of band radiance. One of the principal simplifications used to calibrate thermometers by many standards laboratories is the Sakuma – Hattori curve fit of thermometer output voltage variation with known source temperature variation. The Sakuma – Hattori equation that described the measured calibration points as a continuous curve, with generalised parameters, enabled the response of a thermometer to different temperature ranges and different spectral radiance ranges to be evaluated, based upon a single set of calibration measurements. This becomes very useful both for extrapolating from the calibration measurements to other ranges and fitting an interpolation curve between measurements in the absence of knowledge of the detector and thermometer details.

The Sakuma – Hattori equations are curve forms that can be fitted to data representing the signal output generated by a detector (or thermometer) versus the radiance temperature of an object being measured. The Planck form of the Sakuma – Hattori equation has been recommended by temperature measurement standards organisations for interpolating infrared thermometer calibration curves [9]. It was also recommended for estimating the uncertainties in radiance temperature measurements during infrared thermometer calibration [7]. This form of the Sakuma–Hattori equation represented the interpolation curve that provided the best fit to Planck’s Law during investigations undertaken by a number of national standards laboratories [11].

$$S(T) = \frac{C}{\left[ \exp\left(\frac{c_2}{\lambda_e T}\right) - 1 \right]}$$

**Equation 2.18**

where:

$S(T)$  is the output signal generated by a detector (or output voltage from a thermometer). The units applicable should be the detector output units, typically thermometer output voltage after amplification of the photocurrent through a transimpedance amplifier or the photocurrent generated

$C$  is a scalar coefficient that affords amplification of the range of the thermometer output to correspond with the span of the detector output

$c_2$  is the second radiation constant (0.014387752 m K)

$\lambda_e$  is a temperature-dependent effective wavelength in meter units

$T$  is the absolute temperature of the object in Kelvin units

In more generalised form and without prior knowledge of the limiting effective wavelength evaluated from manipulation of Wien's approximation, the unknowns include the scalar factor,  $C$  and the limiting effective wavelength, that can be replaced by the relation:

$$\lambda_e = A + \frac{B}{T}$$

Whereupon, the coefficients that determine the limiting effective wavelength,  $A$  and  $B$  and the scalar factor,  $C$  can be determined by fitting curves iteratively until the residual error between the modelled and measured values becomes negligible, typically having a value of less than  $10^{-6}$ . The prototype thermometers tested already had the limiting effective wavelength calculated from the Wien approximation, therefore the Sakuma–Hattori model curves determined had this constraint imposed, leaving only the scaling factor to be calculated.

The Sakuma–Hattori curve fit affords calculation of band radiance and radiance temperature similar to the Wien approximation but can be applied over a broader range of wavelengths, rather than being limited to the shorter wavelengths over which the Wien approximation is considered valid [12]. The Sakuma–Hattori equation affords a practicable method for calculation of band radiance incident upon a detector from a

source temperature and the inverse calculation to derive the radiance temperature of an object from measurements of the infrared band radiance received by a photodiode.

Calibration of a thermometer can be undertaken based upon interpolating between the measurements of known source temperatures to determine the thermometer output that would arise for any source temperature using the Sakuma – Hattori equation. The principle employs fitting the Sakuma – Hattori curve form to the measured data recorded during a multiple point calibration of the infrared thermometer and then using the coefficients determined to interpolate between the measurements. This curve fit enables a multiple point calibration to be used to characterise the thermometer and adapt the source temperature versus output curve to work through any range of source temperatures. Typically, three or more known source temperatures are used to characterise the thermometer output against temperature curve but the Sakuma – Hattori curve can be fitted with only one or two points [7], [9], [12].

The Sakuma-Hattori equation has been used to derive a characteristic for the prototype fibre optic thermometers that enabled their deployment to gather measurements from objects having temperatures outside of the laboratory calibration temperature range (100-1100 °C for the higher temperature versions and 20-80 °C for the lower temperature versions of the thermometers).

A thermometer would typically be characterised by experimental measurement, usually measuring multiple temperatures through a range over which the thermometer will be applied.

The thermometers developed within this work were coupled to objects using fibre optics, which introduced an additional consideration of the transmission medium between the emitting surface and the detector.

## 2.6 Fibre Optic Coupling

There are different fibre optic materials suitable for transmitting different wavelength ranges of infrared radiation, which have useful attributes and weaknesses. The choice made between one material or an alternative depends upon the suitability for the specific wavelengths of infrared radiation to be used and the suitability for use under the conditions at the measurement position.

### 2.6.1 Fibre optic materials

Suitable fibre optic materials used to couple the prototype thermometer to objects undergoing measurement were: sapphire ( $\text{Al}_2\text{O}_3$ ) crystalline fibre optic, Indium Fluoride ( $\text{InF}_3$ ) and ZBLAN metallic fluoride glasses. The suitability of these materials were determined upon the wavelength ranges transmitted and capability to withstand damage in deployment, specifically: the maximum temperature to which the material may be exposed being above that expected to arise at the object and the chemical inertness towards reagents present in the measurement environments.

The wavelength ranges transmitted by the fluoride glass fibre optics aligned to their usage with photodiodes that respond in the MWIR and SWIR, as illustrated in figure 2.5. Similarly, sapphire fibre optic had transmission between  $0.75\ \mu\text{m}$  and  $3.5\ \mu\text{m}$ , so aligned with the response of the photodiodes used in this study. Silica fibres formed to have low residual hydroxyl ion concentrations were incapable of transmitting the longer wavelengths of infrared required for lower temperature range measurements using MWIR photodiodes. Silica fibre optics could be used with SWIR photodiodes, such as the extended-InGaAs variant measuring the higher temperature ranges, provided that the material also had suitable properties for deployment into the conditions incurred.

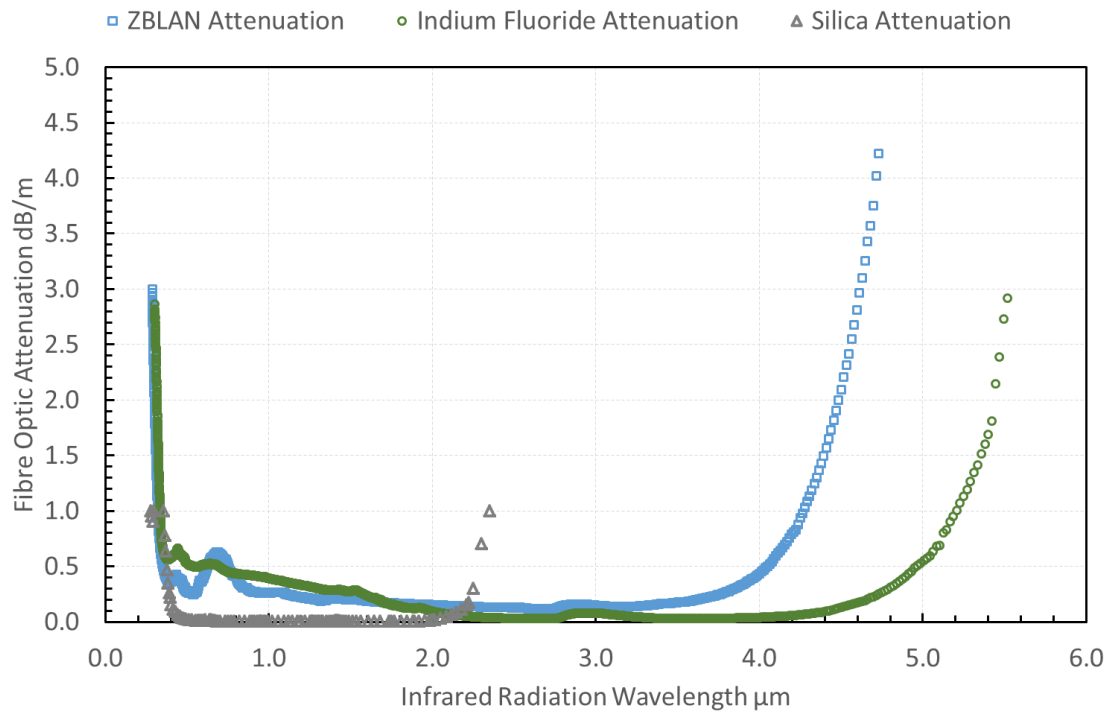


**Figure 2.5 Variation of attenuation of infrared by fluoride and low-OH silica fibre optics with wavelength**

The metallic fluoride based glass fibres have typical transmission bands extending over the range of wavelengths between 0.2 µm and 4.5 µm to 5.5 µm, thereby transmitting radiation between the ultra-violet and the mid-wave infrared (MWIR) regions of the electro-magnetic spectrum [13]. Fluoride glass fibre optics represent ideal transmission media for coupling infrared radiation from an object to either SWIR or MWIR thermometers, from the perspective of maximising transmission of the most relevant infrared radiation wavelengths. Fluoride glasses have limitations in application; typically, the maximum temperature tolerated by these fibres is circa 200 °C [13]. The manufacturer specified a maximum operating temperature of 90 °C for the versions of fluoride glass fibre used in this project.

The bend radius that the fluoride fibres can incur without fracturing also enabled these types of fibre optics to be embedded into difficult to access objects such as: heat-sealed pouch cells used to assemble Lithium-ion batteries. Fluoride glass fibre optics must be protected from exposure to any moisture because of degradation reactions that occur between the materials and water molecules or hydroxyl ions [14], [15].

Sapphire crystalline fibres transmit radiation through the range of wavelengths 0.7 – 3.5  $\mu\text{m}$  (visible through to MWIR wavelengths) that encompassed SWIR fully and overlapped with the 3.0 – 5.0  $\mu\text{m}$  MWIR photodiode response curve between 3.0  $\mu\text{m}$  and 3.5  $\mu\text{m}$ . The range of wavelengths transmitted by sapphire fibre optic would be ideal for coupling to an SWIR thermometer but only the shortest 25% of wavelengths to which the InAsSb photodiode responded. The region of overlap at the shortest wavelengths to which the InAsSb photodiode responded, suggested that the MWIR thermometer with sapphire fibre optic coupling would be more suitable for measuring higher temperature objects than those having lower temperatures.

Sapphire can withstand a maximum temperature of 2030  $^{\circ}\text{C}$  for continuous operation, therefore was used to withstand embedding into objects that incurred high temperatures. It also remains inert against many chemical reactions, hence can be used in the presence of aggressive chemicals. Sapphire fibres are brittle and have limited bend radius, so cannot be deployed into constrained spaces that require tight bends.

The physical properties of the fibre optic materials dictated their suitability for embedding into harsh conditions and the geometry necessary to achieve embedding into the object surface.

## 2.6.2 Fibre optic transmission equations.

The transmission of infrared radiation along a fibre optic utilises the principle of total internal reflection (TIR) of the radiation coupled into the fibre at the boundary of the fibre core and the immediately surrounding cladding [13]. The materials that are used to form the core of the fibre and cladding are chosen to ensure that the cladding has a lower value of refractive index than the core to ensure that TIR can be achieved. Infrared radiation is coupled into the fibre provided that the angle that the radiation subtends to the receiving surface of the fibre optic is within a limiting ‘critical’ angle, that can be derived from Snell’s Law. Any infrared radiation that enters the fibre at a planar angle that lies within the limit defined by equation (2.19) will be transmitted along the fibre:

$$\sin \theta_{max} = \frac{1}{n_0} \sqrt{n_1^2 - n_2^2} \quad \text{Equation 2.19}$$

where:

$\theta_{max}$  is the maximum angle of acceptance of radiation coupled into the fibre for which TIR will occur

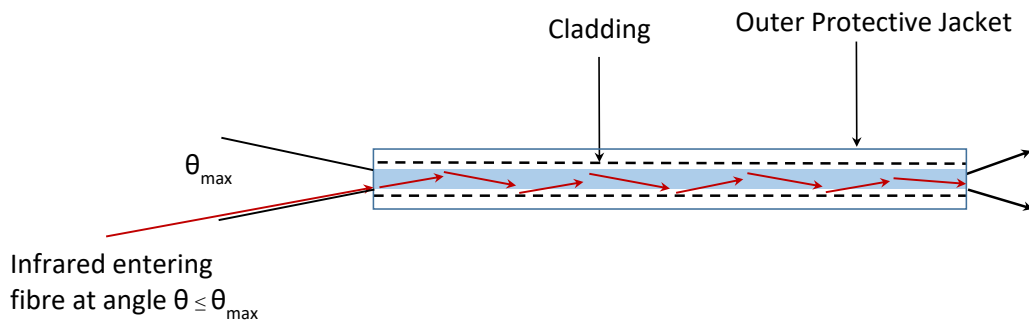
$n_0$  is the refractive index of the medium into which the fibre is immersed, typically this might be air with  $n_0 = 1.0$

$n_1$  is the refractive index of the fibre core material

$n_2$  is the refractive index of the cladding material

Equation (2.19) is valid when the condition  $n_1 > n_2$  is satisfied

The transmission principle of a fibre optic is illustrated in figure 2.6, for which the



nomenclature used in equation (2.19) applies.

**Figure 2.6 Schematic diagram illustrating total internal reflection principle of transmission along fibre optic**

The maximum angle of acceptance of infrared radiation into the fibre that is defined by equation (2.19) can then be used to define the projected solid angle that may also be referred to as the cone of acceptance of radiation entering into the fibre, as presented in equation (2.20):

$$\Omega = \pi \sin^2 \theta_{max} \qquad \text{Equation 2.20}$$

where:

$\Omega$  is the projected solid angle of radiation that can be coupled into the fibre, the cone of acceptance

$\theta_{max}$  is the maximum angle of acceptance for TIR to occur defined by equation (2.20)

Furthermore, the Numerical Aperture value can be calculated from the information pertaining to the critical angle and refractive index of the medium surrounding the fibre optic surface (typically this would be air and have refractive index,  $n_0 = 1.0$ ), according to equation (2.21):

$$NA = n_0 \sin \theta_{max} \quad \text{Equation 2.21}$$

where:

NA is the numerical aperture and the other symbols take the same meanings as used in equation (2.19)

The area of acceptance for radiation entering the receiving surface of the fibre optic is the cross-sectional area of the core. The cross-sectional area of the fibre optic core multiplied by the Numerical Aperture value of equation (2.19) defines the étendue value or optical throughput of the fibre optic. The equation defining the étendue of a fibre is presented in equation (2.22) for which the surrounding medium has been assumed to be air with refractive index  $n_0 = 1.0$ :

$$\text{Étendue} = \frac{\pi^2}{4} d^2 NA^2 \quad \text{Equation 2.22}$$

where:

$d$  is the fibre core diameter and all other symbols maintain their meanings from equations (2.19) through (2.21).

These equations represent the idealised case for fibre optic transmission, whereas there will be losses arising in practice from: impurities in the fibre material, imperfections in the glass fibre core and cladding surfaces, inhomogeneity of the fibre material and penetration of radiation into the cladding. Impurities in the glass cause absorption of radiation and often arise as residual elements from the manufacturing processes, with oxygen and hydrogen molecules, hydroxyl ions and metallic atoms being prominent causes of attenuation through specific ranges of wavelengths associated with their characteristic infrared absorption bands. Imperfections on the glass fibre core and cladding surfaces cause partial scattering of the radiation at the boundary of the two materials, rather than the reflection required for transmission and can be caused during service, for example: by bending the fibre optic and causing microscopic

fractures in the surfaces that then disperse the radiation field. Penetration of a proportion of the radiation into the cladding causes what is termed an 'evanescent field' and enables weak transmission of some radiation intensity within the cladding rather than along the core [13]. The fibre optic itself will have absorption, scattering and dispersion losses arising from the gradient of refractive index within the material and consequent differences in propagation velocity through the fibre. All of these loss mechanisms contribute towards the attenuation characteristics of the fibres that manufacturers quote, typically amounting to attenuation of the order 0.2 – 0.5 dB/m for infrared transmitting metal fluoride and sapphire fibre optics [16], [17]. The attenuation presented by a fixed length of fibre optic coupling the thermometer to the object and that has stable properties in-operando can be accounted for during calibration.

The lengths of fibre optic used for the prototype thermometers were short, up to 1 m maximum, therefore these transmission losses had negligible effect upon the intensity of radiation that would be incident upon the photodiode. The transmission of the fibre was assumed to be ideal and the intensity modelled for calculating photodiode response was assumed to be dictated by the étendue of the fibre, normal incidence coupling from air to the fibre optic and radiation source intensity. Should an application require that a long fibre optic be deployed, it would necessitate characterisation of a thermometer to establish the lower infrared signal magnitude arising through the range of temperatures measured.

It should be acknowledged that the existence of radiation losses meant that the equations governing transmission along the fibre optic core and coupling into the fibre surface used for estimation of infrared radiation intensity at the fibre optic outlet surface represented ideal conditions. The étendue equation was used to calculate the throughput of the fibre optics used to transmit an infrared signal from a source object to the prototype thermometers to afford estimation of the minimum temperature that the thermometers could measure with different fibre optics coupling radiation onto the sensors. The signal transmission achieved, therefore the estimated minimum temperature measurable by the thermometer attached to the fibre optic, would likely differ from the characteristics calculated. The object was assumed to be a blackbody

radiation source, emitting according to Planck's Law of Thermal Radiation (Planck's Law). With the caveat that the calculation represented an idealised version of the thermometer measurement, Planck's Law has been integrated numerically, according to the method presented in chapter 2.3 and the throughput of the fibre optic used to evaluate the intensity of radiation incident upon the photodiode for a range of wavelengths and source temperatures.

## 2.7 Modelling of infrared transmission and power incident upon detector

There are a number of options for fibre optic coupling that operate within the infrared range of wavelengths: chalcogenide, sapphire, fluoride glass and low hydroxyl silica can all transmit over different portions of this band. Generally, chalcogenide materials are toxic and incur damage easily from chemical reactions and high temperature, so would not be suitable for usage in harsh conditions. Low hydroxyl silica fibres have limited ranges of transmission that favour shorter wavelengths of near infrared (NIR) and attenuate SWIR or MWIR wavelength ranges. The remaining options of sapphire and fluoride glass fibre optics transmit between NIR and MWIR wavelengths, so present the best options for measuring wider ranges of temperature. Sapphire has the capability of surviving high temperature, whereas metallic fluoride glass has lower maximum operating temperature but is less prone to brittle fracture. Both materials are chemically inert or react slowly in many typical applications.

Typical attenuation curves for ZBLAN, Indium Fluoride and low hydroxyl ion Silica glass fibre optics, for which the upper limiting wavelengths of transmission were defined as 4.5  $\mu\text{m}$ , 5.5  $\mu\text{m}$  and 2.4  $\mu\text{m}$  respectively, were presented in figure 2.5 [17]. These curves illustrated the point that the cut-off of a fibre happens over a range of wavelengths and does not extinguish the signal immediately but attenuates it increasingly outside of the nominal transmission band. The effect of the attenuation curves upon the signal measured is accounted for in the calibration that measures the actual photocurrent generated for a radiance temperature, of course. Modelling affords judicious choices of components and selection of thermometer configuration for applications, prior to assembling a thermometer for an application.

Calculations were undertaken using Microsoft Excel and the details of these have been provided in appendix 1, however, an example calculation for an Indium Arsenide Antimony (InAsSb) photodiode coupled through a 425  $\mu\text{m}$  diameter sapphire fibre optic is provided in the following paragraphs to illustrate the method used.

Numerical integration of spectral radiance was undertaken, according to the method of Widger and Woodall [5], for which Planck's Law was formulated in terms of frequency and the spectral radiance at frequency  $\nu$ , can be stated:

$$L_{\nu} = \left[ \frac{2h\nu^3}{c^2} \right] \left[ \frac{1}{e^{\frac{h\nu}{kT}} - 1} \right] \quad \text{Equation 2.23}$$

where:

$L_{\nu}$  is the spectral radiance at frequency  $\nu$ ,  $\text{W}/\text{m}^2 \text{sr}$

$\nu$  is the spatial frequency of radiation,  $\text{m}^{-1}$

T is the absolute temperature, K

h, c and k are Planck's constant, the speed of light in vacuum and Boltzmann's constant, as defined previously

The spectral radiance was integrated numerically and the band radiance evaluated by the difference between the numerical integrations for two wavelengths. The numerical integrations generated a table of spectral radiance values for different temperature and wavelength products ( $\lambda T$ ) that were summed for a finite number of series expansion n to calculate the total spectral radiance within the range specified.

An example calculation for band radiance calculated between  $\lambda = 3.0 \mu\text{m}$  and  $4.5 \mu\text{m}$ ,  $T = 273 - 1750 \text{ K}$  and for series summation limits  $n = 1 - 10$  is presented in figure 2.7 In this case, the calculations represented the nominal limiting wavelengths defined by the InAsSb photodiode responsivity and fibre optic transmission curves for coupling by a ZBLAN fibre optic. The intensity incident upon a detector was multiplied by the attenuation of the signal by the optical throughput of  $600 \mu\text{m}$  diameter ZBLAN fibre optic of 230 mm length to calculate the power incident upon the InAsSb detector, this being one configuration of fibre optic thermometer considered.

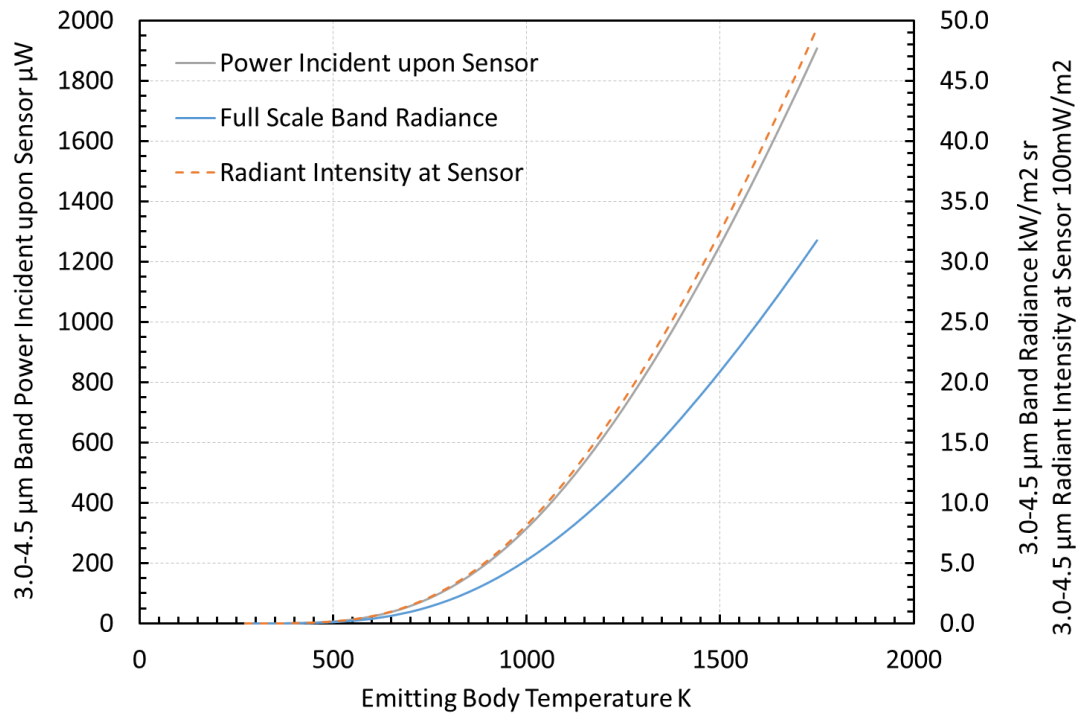


**Figure 2.7 Example numerical integration calculations for evaluating spectral radiance, in this case over the mid-wave infrared wavelength range 3.0 – 4.5  $\mu\text{m}$ , transmitted by a 230 mm length, 600  $\mu\text{m}$  core diameter ZBLAN fibre optic**

## 2.8 Minimum temperature measurable with prototype fibre optic thermometer

The minimum temperatures that could be measured by thermometers that used InAsSb or extended range Indium Gallium Arsenide (extended-InGaAs) photodiodes and were coupled to an object by infrared fibre optics, have been estimated. These estimated minima were based upon the numerical integration of Planck's Law and the resulting calculation of the band radiances and powers incident upon the photodiodes, as described within this chapter. The assumption of immediate cut-off of the fibre optic transmission curve and photodiode response curve at the upper and lower wavelengths led to the estimate of the band radiance being conservative because these curves extend beyond these nominal limits, as illustrated in figure 2.4. The partial transmission and responsivity outside of the nominal cut-off wavelengths provided additional spectral radiance and photocurrent generation, respectively. This additional power and response afforded measurement of marginally lower temperatures than

calculated, hence the estimates presented were conservative. Interpolation of the power incident upon the sensor was used to establish the source temperature that would lead to the minimum power detectable by the photodiode, specified in manufacturer's data to be: 0.15  $\mu\text{W}$  for InAsSb and 1 pW for extended-InGaAs. Using the estimation method stated, the minimum source temperatures expected to be measurable by different configurations of thermometer are presented in table 2.1.

**Table 2.1 Minimum source temperature measurable estimated from the band radiance calculations and minimum power to which the photodiode will respond**

<b>Thermometer Configuration: Photodiode and Fibre Optic</b>	<b>Fibre Optic Transmission Wavelength Range <math>\mu\text{m}</math></b>	<b>Photodiode Response Wavelength Range <math>\mu\text{m}</math></b>	<b>Nominal Convolved Wavelength Range <math>\mu\text{m}</math></b>	<b>Minimum Temperature Measurable by Detector* <math>^{\circ}\text{C}</math></b>
InAsSb 425 $\mu\text{m}$ Sapphire	0.75 – 3.5	3.0 – 5.0	3.0 – 3.5	230
InAsSb 325 $\mu\text{m}$ Sapphire	0.75 – 3.5	3.0 – 5.0	3.0 – 3.5	255
InAsSb 100 $\mu\text{m}$ Sapphire	0.75 – 3.5	3.0 – 5.0	3.0 – 3.5	470
InGaAs 425 $\mu\text{m}$ Sapphire	0.75 – 3.5	0.9 – 2.6	0.9 – 2.6	100
InAsSb 100 $\mu\text{m}$ InF <sub>3</sub>	0.31 – 5.5	3.0 – 5.0	3.0 – 5.0	185
InAsSb 100 $\mu\text{m}$ ZBLAN	0.285 – 4.5	3.0 – 5.0	3.0 – 4.5	210
InAsSb 200 $\mu\text{m}$ ZBLAN	0.285 – 4.5	3.0 – 5.0	3.0 – 4.5	135
InAsSb 450 $\mu\text{m}$ ZBLAN	0.285 – 4.5	3.0 – 5.0	3.0 – 4.5	75
InAsSb 600 $\mu\text{m}$ ZBLAN	0.285 – 4.5	3.0 – 5.0	3.0 – 4.5	50

\*Note. The minimum temperatures presented have been rounded to the nearest 5  $^{\circ}\text{C}$

A convolution of the actual transmission curve of the fibre optic and response curve of the photodiode, rather than the idealised 'top-hat' approximations used, would afford more accurate estimation of the minimum temperatures measurable by the different thermometer configurations. There would be no additional knowledge provided by undertaking this more exact calculation, just improved accuracy compared to the estimates calculated and presented in figure 2.7 and table 2.1.

## 2.9 Transimpedance amplifier and bootstrapping configurations

The photocurrents generated by the detectors used in the thermometers were transformed to measurable voltages using transimpedance amplifiers. The transimpedance amplifier configuration included a feedback loop between the output and inverting input, as illustrated by figure 1.2 of chapter 1, through which most of the photocurrent should flow to generate the output voltage. Ideally, the photocurrent would only be passed through the feedback resistor and appear as the TIA output voltage:

$$V_o = i_{ph} \times R_f$$

where:

$V_o$  is the TIA output voltage

$i_{ph}$  is the photocurrent

$R_f$  is the feedback resistance (transimpedance)

The transimpedance amplifier inputs would be held at the same voltage, ideally with the inverting input held at virtual ground with the non-inverting input connected to ground when there is no photocurrent flowing. There will always be some offset voltage between the inputs of an operational amplifier (op-amp) that leads to there being an output voltage offset from zero with no photocurrent generated by the photodiode. This offset may be compensated by applying an appropriate voltage to the non-inverting input or offset nulling connections that are provided on some op-amps. The offset can also be compensated by measuring the zero signal offset using optical signal chopping and applying a correction in the thermometer algorithm.

Attaching a photodiode with low shunt resistance (shunt impedance, more generally) to the inverting input of the transimpedance amplifier leads to non-linear response of the thermometer output with varying shunt current [18] and varying thermometer temperature, as described in chapter 1. The variation of the dark current with increased electron promotion to the conduction band at increased thermometer temperature is particularly troublesome for photodiodes that operate in the MWIR because of the small band gap necessary to achieve photosensitivity to this part of the spectrum. The smaller energy gap between valence and conduction bands in photodiodes such as the InAsSb type allows larger dark current and more drift by the random processes of thermal excitation incurred in the diode junction. The problems presented by low shunt resistance photodiodes can be compensated, at least partially, by implementing a bootstrap impedance multiplier.

The adaptation from the simple TIA of chapter 1 is illustrated in figure 2.7 that shows the addition of bootstrapping.

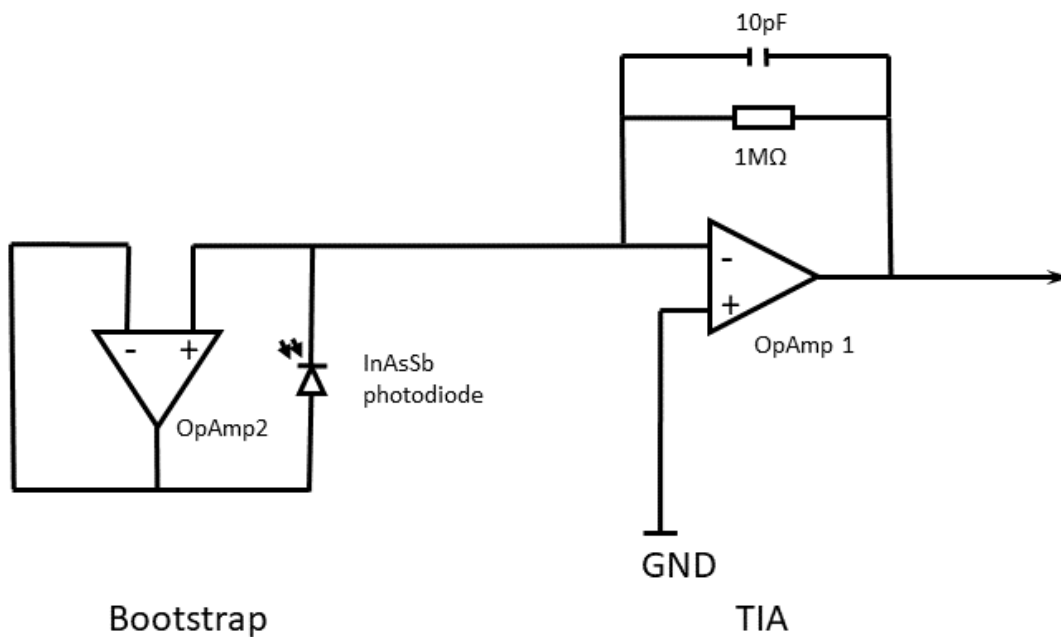


**Figure 2.8 Schematic diagram of bootstrapped photodiode TIA circuit**

The photodiode cathode and anode are held at the same voltage by the bootstrapping op-amp, thereby ensuring that it operates in photovoltaic mode, with only a small bias applied resulting from any offset in the op-amp. The shunt impedance presented by a

bootstrapped photodiode, having actual impedance,  $Z_d$  will be multiplied by a factor of the open-loop gain of the bootstrap op-amp,  $(A+1)$ . The virtual impedance is transformed to  $Z_d(A+1)$  and the resulting higher virtual impedance apparent at the transimpedance amplifier input enables the use of high resistance values in its feedback loop. The enhanced shunt impedance reduces the shunt current through the photodiode, aiming to achieve negligible magnitude and ensures that most of the photocurrent flows through the feedback loop, for a range of measurement conditions beyond that available from direct connection of the photodiode without enhancement by a virtual impedance multiplier.

The usage of a bootstrapping op-amp introduced additional noise sources from the input voltage of the bootstrap amplifier multiplied by the closed-loop gain of the feedback resistance and input current presented directly on the feedback resistance. The input voltage noise gain of the TIA input would be decreased in comparison to connecting the photodiode without the bootstrapping op-amp because the apparent detector source impedance had been increased. The noise induced by the feedback resistance and TIA input current remained unaffected by the presence of the bootstrapping amplifier [Makai & Makai paper]. Overall it has been shown that the bootstrapped TIA spectral noise would be increased marginally, for example: rising from 42  $\mu\text{V}/\text{Hz}$  to 53  $\mu\text{V}/\text{Hz}$  in experimental measurements by Makai, Makai and Balazas [Makai et al noise measurement paper].

## Summary of Chapter: Application to Radiation Thermometry

The radiance temperature of an object can be evaluated from the effect of radiation incident upon a photosensitive detector. The resulting thermometer, used with fibre optic coupling and for which the output has been calibrated against known blackbody radiance temperatures, can be deployed to acquire measurements from objects at unknown temperatures. Mid-wave and short-wave infrared radiation thermometers, expedited using InAsSb and extended-InGaAs detectors, respectively, were to be constructed and tested in laboratory conditions. The thermometers with practical calibrations would find application to temperature measurements as substitutes for thermocouples, which have been the principal choice of thermometer for embedding into objects. Coupling between the object and thermometers would be implemented

using sapphire and fluoride glass fibre optics that viewed the object surface to be measured, usually with the fibre tip inserted into a blind-end hole. The thermometers developed used transimpedance amplifiers that were configured for measurement of the voltages transformed from the photo-currents generated by the detectors. The photo-currents are characteristic of the radiant emittance received by the photodiode, which are analogues of the radiance temperature of the object. The experimental development, laboratory characterisation and application testing of the thermometers are described in the chapters that follow.

The configuration of bootstrapped photodiode connected to transimpedance amplifier was decided upon for all of the thermometers because the uncooled photodiodes had low shunt resistances and would be expected to have non-linear output with varying conditions.

## REFERENCES

- [1] G. P. Eppeldauer and R. J. Martin, "Photocurrent measurement of PC and PV HgCdTe detectors," *J. Res. Natl. Inst. Stand. Technol.*, vol. 106, no. 3, pp. 577–587, 2001, doi: 10.6028/jres.106.024.
- [2] British Standards Institute, "BS 1041-5 Temperature measurement— Part 5: Guide to selection and use of radiation pyrometers," *British Standard*, vol. 1041, no. 5. 1989.
- [3] F. E. Nicodemus, "Radiance in Optical Radiometry," *Am. J. Phys*, vol. 31, 1963.
- [4] S. Mendoza, "Solid Angle," *Wikimedia*. Accessed May 2020.  
[https://commons.wikimedia.org/wiki/File:Solid\\_angle23.png](https://commons.wikimedia.org/wiki/File:Solid_angle23.png).
- [5] W. K. Widger Jr and M. P. Woodall, "Integration of the Planck blackbody radiation function," *Bull. Am. Meteorol. Soc.*, vol. 57, no. 10, pp. 1217–1219, 1976, doi: 10.1175/1520-0477(1976)057<1217:IOTPBR>2.0.CO;2.
- [6] D. Lawson, "The Blackbody Fraction , Infinite Series and Spreadsheets," *Int. J. Eng. Educ.*, vol. 20, no. 6, pp. 984–990, 2004.

- [7] P. Saunders, "General interpolation equations for the calibration of radiation thermometers," *Metrologia*, vol. 34, no. 3, pp. 201–210, 1997, doi: 10.1088/0026-1394/34/3/1.
- [8] J. W. Hahn and C. Rhee, "Interpolation equation for the calibration of infrared pyrometers," *Metrologia*, vol. 31, no. 1, pp. 27–32, 1994, doi: 10.1088/0026-1394/31/1/005.
- [9] F. Sakuma and S. Hattori, "Establishing a practical temperature standard by using a narrow-band radiation thermometer with a silicon detector," in *TEMPERATURE: ITS MEASUREMENT AND CONTROL IN SCIENCE AND INDUSTRY, VOLUME 5, PART 1: Proceedings of the Sixth International Temperature Symposium*, 1982, vol. 5.1, pp. 421–427.
- [10] P. Saunders and D. Rod White, "Interpolation errors for radiation thermometry," *Metrologia*, vol. 41, no. 1, pp. 41–46, 2004, doi: 10.1088/0026-1394/41/1/006.
- [11] P. Saunders *et al.*, "Uncertainty budgets for calibration of radiation thermometers below the silver point," *Int. J. Thermophys.*, vol. 29, no. 3, pp. 1066–1083, 2008, doi: 10.1007/s10765-008-0385-1.
- [12] P. Saunders and D. R. White, "Physical basis of interpolation equations for radiation thermometry," *Metrologia*, vol. 40, no. 4, pp. 195–203, 2003, doi: 10.1088/0026-1394/40/4/309.
- [13] T. Katsuyama and H. Matsumura, *Infrared Optical Fibres*, 1st Editio. IOP Publishing Ltd, 1989.
- [14] J. Thomason, P. Jenkins, and L. Yang, "Glass Fibre Strength—A Review with Relation to Composite Recycling," *Fibers*, vol. 4, no. 2, p. 18, 2016, doi: 10.3390/fib4020018.
- [15] J. A. Savage, "Materials for Infrared Fibre Optics," *Mater. Sci. Reports*, vol. 2, no. February, pp. 99–138, 1987.
- [16] SEDI-ATI Fibres Optiques, "Special Fibers," *SEDI-ATI Datasheet*. .
- [17] Thorlabs Inc, "Thorlabs ZrF4 & InF3 Attenuation Comparison Spreadsheet," *Thorlabs webpage*. .

[18] J. P. Makai and J. J. Makai, "Current-to-voltage converter for linearity correction of low shunt resistance photovoltaic detectors," *Rev. Sci. Instrum.*, vol. 67, no. 6, pp. 2381–2386, 1996, doi: 10.1063/1.1147006.

# 3 EXPERIMENTAL AND ANALYTICAL METHODS DEPLOYED

## 3.1 Infrared thermometer configuration

A series of infrared radiation thermometers (IRTs) were configured to satisfy the requirements for reliable temperature measurements applied to the manufacturing processes and products that were outlined within the introduction and summarised, as follows. Accurate and repeatable temperature measurements are critical to enabling improvements in the process control, product quality and the understanding of thermal effects during manufacturing and operation [1]–[3]. The principal objective underlying the development of fibre optic coupled IRTs was enabling their substitution for thermocouples in harsh measurement conditions to improve: resilience to the severe conditions incurred, response speed, sensitivity and calibration drift during usage. The shortest wavelength ranges over which it was feasible to measure the temperature ranges required were used for the configuration of the IRTs. Using shorter wavelengths reduced the magnitude of emissivity errors that contributed to the measurement uncertainties. The prototype IRTs, used Indium Arsenide Antimony (InAsSb) photodiodes that were sensitive to radiation wavelengths within the mid-wave infrared radiation (MWIR) part of the spectrum and extended wavelength range Indium Gallium Arsenide (extended-InGaAs) photodiodes that were responsive in the short-wave infrared (SWIR) part of the spectrum. The longer wavelengths within the range of the MWIR version of the thermometer afforded the measurement of

temperatures from a minimum of approximately ambient or room temperature. The SWIR versions of the thermometer afforded a range of measurement from a minimum of approximately 100 °C. The thermometers developed were suitable for industrial temperature measurement and provided sufficiently high responsivity that enabled measurement of the low intensity infrared radiation transmitted through a fibre optic coupling. The thermometers enabled identification of relatively small changes in signal magnitude, affording sensitive measurement.

The different IRTs were configured to bootstrap the photodiode using an operational amplifier (op-amp) voltage follower and transimpedance amplifier (TIA) to transform the photocurrent to a readily measurable voltage, a configuration that followed the design of Makai and Makai [4] that was described in chapter 2.

A schematic diagram of the principal components of the bootstrapped photodiode and TIA circuit is presented in figure 3.1

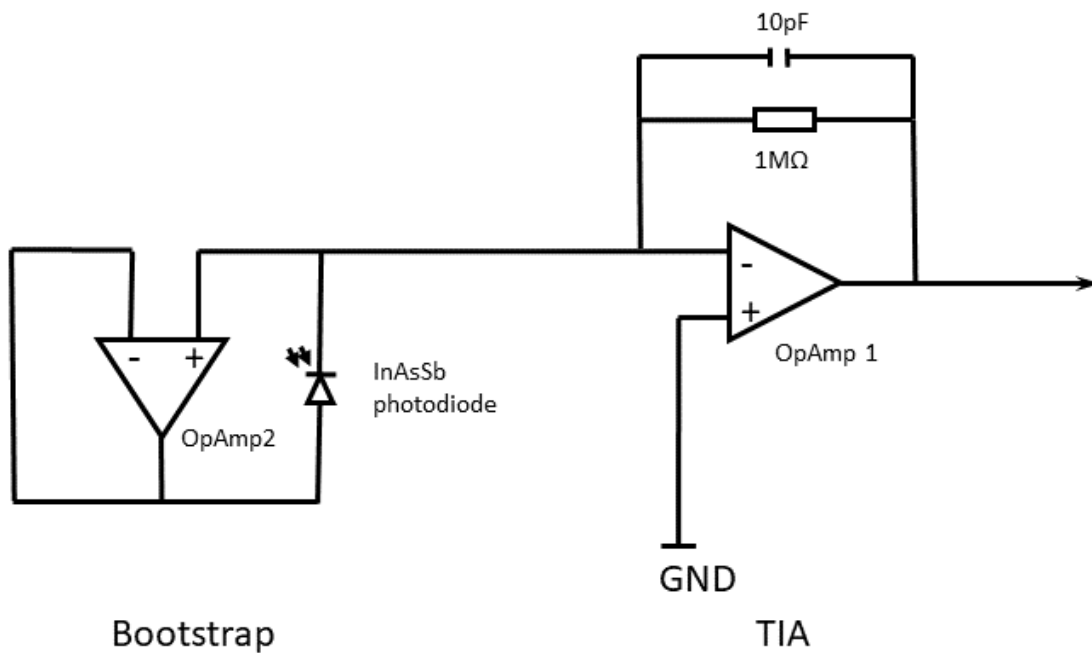


**Figure 3.1 Schematic diagram of thermometer bootstrapped photodiode TIA circuit**

The IRTs used the same circuit configuration, apart from the photodiode types and fibre optic coupling materials, that were varied between versions, according to the

temperature range to be measured. Specific variations of the circuit developed to accommodate additional features included trimming potentiometers to reduce the input offset voltage and different op-amps will be described in later chapters.

The TIA had a feedback loop comprising a resistor-capacitor (R-C) network between the output and inverting input of the op-amp and was constructed according to manufacturer guidance concerning component selection for standard designs of photodiode amplifiers [5], [6].

The InAsSb and extended-InGaAs photodiodes had low shunt resistances, achieving typical values of 120 k $\Omega$  and 14 k $\Omega$ , respectively [7], [8]. The low shunt resistances of the photodiodes limited the maximum values of transimpedance resistor that could be deployed [6], as described in chapter 2. The maximum transimpedance values limited the effective amplification of the photocurrent and the minimum temperature that could be measured by these thermometers. The low shunt resistance and constrained transimpedance values have limited the application of InAsSb and extended-InGaAs photodiodes in IRTs, particularly affecting the capability of the thermometers to measure lower temperature ranges. Photodiode cooling has been necessary to achieve useful lower temperature range measurements using such low shunt resistance photodiodes. Nominally, the requirements upon a photodiode are that it has useful: sensitivity, repeatability, accuracy and reasonable response speed to changing signals [9]–[11]. Makai and Makai developed a method for implementing a boot-strapped photodiode connected to a transimpedance amplifier [9]. This configuration enabled low shunt resistance photodiodes to be used with higher transimpedance values by elevating the apparent shunt resistance at the TIA input. The bootstrapped photodiode and high values of transimpedance enabled measurement of low intensity radiation [12].

The bootstrapping method was applied to the InAsSb photodiode to enable it to be used in a MWIR thermometer without needing cooling, or signal chopping. The extended-InGaAs photodiode used, which had response between 0.9–2.6  $\mu\text{m}$  and was used uncooled, also used the bootstrapping technique of Makai and Makai to present elevated apparent shunt resistance at the TIA input [9]

The MWIR and SWIR thermometers developed received unchopped infrared radiation, therefore the op-amp used for the TIA needed to have low input voltage offset to be able to measure low temperatures. Input bias currents would generate additional input voltage offset when passed through a large value feedback resistor, as used in the thermometer transimpedance amplifier. The op-amps chosen for the IRTs developed and described in chapter 4, satisfied these requirements. A large feedback resistance value was required to maximise the signal to noise ratio [13] which could cause high input voltage offset, if it amplified a small offset, therefore a compromise had to be found between the offset and transimpedance required to extract a signal from the noise.

### 3.2 Modelling of op-amp noise and input offset voltage

Electronic simulation software 'LTSPICE', that was provided by Linear Technologies Incorporated for modelling systems of integrated circuits, was used to simulate the response of the bootstrapped photodiode and TIA circuit to varying photo-current and the magnitude of the noise voltage arising at the output across a range of frequencies. The circuit was simulated using idealised models of each of the operational amplifiers considered for the TIA. The idealised characteristics of common op-amps have been defined and encoded as model libraries by manufacturers. The voltage output characteristics were modelled as a function of steadily increasing photocurrent, represented by a current source, for which the current magnitude was simulated as a linear increasing ramp. The noise characteristic of the circuit was simulated as the voltage arising at the output as the frequency of signal increased through ten decades between 1.0 mHz and 1.0 MHz. The limiting frequencies over which the noise characteristics were modelled were chosen to range from near d.c. to exceed the likely maximum frequency required in the temperature measurements by two orders of magnitude. The spectral noise would be a maximum at d.c. conditions and reduce at higher frequencies, therefore, including two orders of magnitude higher frequency than the nominal cut-off of the TIA R-C feedback network would provide an estimate of the noise that was too large. The noise modelling should be seen as presenting the worst-case scenario.

### 3.3 Infrared Fibre Optic Coupling

Fibre optic coupling of infrared radiation onto the photodiode of the prototype thermometer enabled the more sensitive electronics used to measure the voltage and infer the object temperature to be positioned remotely from the object undergoing measurement. This is advantageous for objects that incur harsh conditions, for example: high temperature, rapidly cycling temperature, chemical reactions or mechanical and fluid abrasion. The fibre optic materials selected for coupling the IRTs developed within this project transmitted appropriate ranges of infrared wavelengths that enabled measurement of the object temperatures and remained intact whilst subjected to the harsh physical and chemical process conditions into which the fibre optic was immersed.

MWIR Indium Fluoride and ZBLAN glass fibre optics were used to couple infrared radiation to the thermometer for mid-to-lower temperature applications for example: battery cell temperature measurement and temperature measurement of tool inserts during machining. The fluoride glass fibres were chosen for their broad range of wavelengths transmitted, that extend to  $4.5\ \mu\text{m}$  (ZBLAN) and  $5.5\ \mu\text{m}$  ( $\text{InF}_3$ ) in the mid-wave infrared, thereby enabling lower temperature objects to be measured using an MWIR Indium Arsenide Antimony photodiode and high value of transimpedance. The broader transmission bands of Indium Fluoride and ZBLAN metallic fluoride glass fibre optics compared to crystalline sapphire fibre optics enabled lower minimum resolvable temperature of circa  $30\text{-}50\ \text{°C}$  to be measured by the prototype thermometer configurations coupled to the fluoride glass fibre optics. These configurations provided thermometers that would be suitable for measurement of temperatures from near room temperature to  $1100\ \text{°C}$ , with suitable choice of op-amps and supply voltages. Filtering the raw signal with a time constant of at least  $0.1\ \text{s}$  was necessary to measure temperatures below  $200\ \text{°C}$  with the smallest diameter Indium Fluoride fibre optic ( $100\ \mu\text{m}$  diameter) that was used during initial prototype thermometer testing. The slower response necessary to enable filtering with this period, would impose an upper frequency limit upon signals that could be measured of  $5\ \text{Hz}$ , defined as half of the maximum sampling frequency to comply with the Nyquist limit for sampling a signal without incurring aliasing [14]. Longer integration or filtering time constants could be used to enable measurement of the average signal within the random noise from a low

intensity source, however this would reduce the maximum signal frequency that could be measured when receiving cyclic signals rather than the steady-state signals acquired during the laboratory characterisation measurements.

### 3.4 Thermometer characterisation and calibration method

Prototype thermometers were configured that measured the following infrared wavelengths and object temperature ranges, as described in chapters 4 to 6:

- MWIR thermometers (chapters 4 and 5):
  - 200 °C to 1000 °C
  - 30 °C to 500 °C
- SWIR thermometer (chapter 6):
  - 100 °C to 1000 °C

The voltage outputs of the prototype infrared thermometers were characterised under laboratory conditions through the range of source temperatures 50 °C to 1000 °C (for the higher temperature range versions), 20 °C to 500 °C and 20 °C to 80 °C (for the lower temperature range versions). The different temperature ranges over which prototype thermometer characterisations were undertaken required three different approximate blackbody sources, as follows:

- Ametek Land Landcal P1200B operated between 600 °C and 1000 °C
- Ametek Land Landcal P550P operated between 50 °C and 500 °C
- Ametek Land Landcal P80P operated between 20 °C and 80 °C

The characterisations were undertaken against these approximate blackbody sources, in accordance with the calibration methods for infrared thermometers defined in British Standard BS1041 part 5:1989 [15] with the adaptation that the fibre optic coupling the infrared to the thermometer was inserted into a source thermo-well, the method for which is described in the following paragraph.

The exposed end of a fibre optic was inserted into a calibration thermo-well adjacent to the radiant cavity of a blackbody source. The fibre optic had a length of the core exposed at the tip to enable the core to receive radiant heat from all surfaces immediately surrounding the fibre. The exposed and embedded fibre optic enabled multiple reflections of the radiation emitted from the source and with the length to

diameter ratio of the fibre optic exceeding five, allowed enhancement of the emissivity at the measurement position to achieve approximate blackbody cavity conditions [16], [17]. Infrared radiation from the thermo-well that was coupled into the fibre optic through the exposed end was then transmitted to the output end that was mounted into an SMA905 optical connector. The radiation was further coupled to the photodiode that was mounted on the thermometer printed circuit board (PCB) through free space, defined by the output end of the fibre in the SMA905 connector and a concentric photodiode mount, all assembled into a short length of lens tube to maintain alignment between the fibre core and photodiode. The configuration of the equipment used for prototype thermometer voltage output characterisation is represented as a schematic diagram in figure 3.2

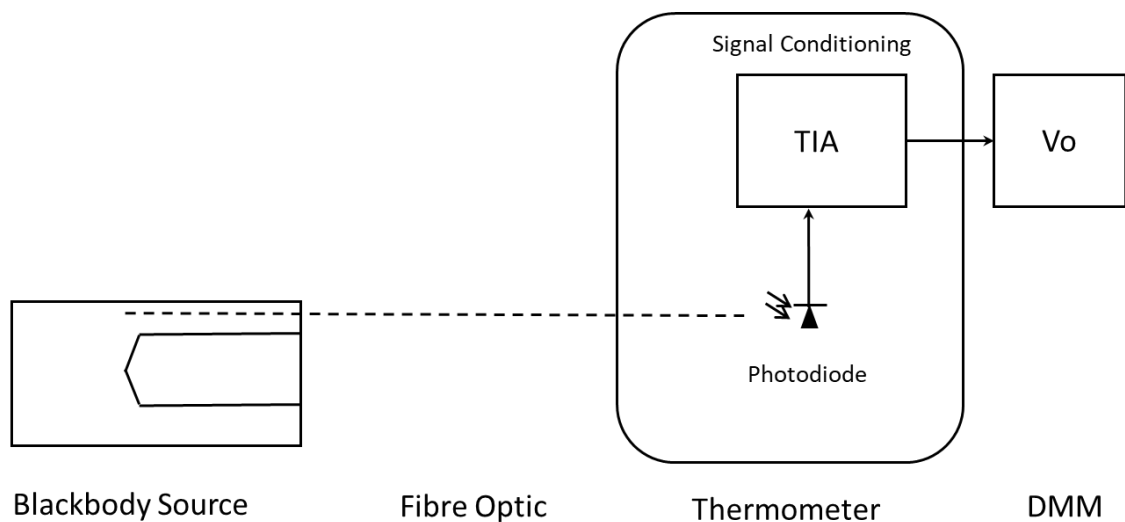


**Figure 3.2 Schematic diagram of laboratory-based configuration used for characterisation of prototype fibre optic coupled, mid-wave infrared thermometers**

The blackbody source temperature, measured by the control thermocouple and indicated by the controller unit, achieved stable measured temperature equal to the set point at each temperature and the source was allowed to achieve steady-state temperature prior to undertaking measurements.

The blackbody source temperatures were checked against thermometers that were calibrated against UK Accreditation Services traceable standards at manufacture, therefore represented transfer standards that enabled the temperature of the sources to

be calibrated prior to characterisation of the thermometers. These calibrations are presented in the following section 3.5.

### 3.5 Experimental Calibration of Blackbody Sources used in Laboratory Characterisation of Infrared Thermometers

Calibration of the approximate blackbody sources used was undertaken against the transfer standard thermometers that were calibrated to traceable national standards at manufacture, as described in appendix 2. The blackbody controller temperature set points and independently measured temperatures, and the errors between the temperature set points (SP) and measured values (MV) were evaluated. The source calibrations are presented in the following graphs.

#### 3.5.1 Landcal P1200B Three-Zone Tube Furnace Calibration

The higher temperature approximate blackbody source was calibrated using the transfer standard type 'R' Platinum-Rhodium thermocouple described in appendix 2. The thermocouple was calibrated to traceable national standards by the manufacturer (Isothermal Technology Limited) at the time of supply, so provided a valid and traceable calibration for the blackbody source. The relationship between temperature set point and temperature measured by the transfer standard thermocouple is presented in figure 3.3 and the error between the set point (SP) and measured values (MV) in figure 3.4.

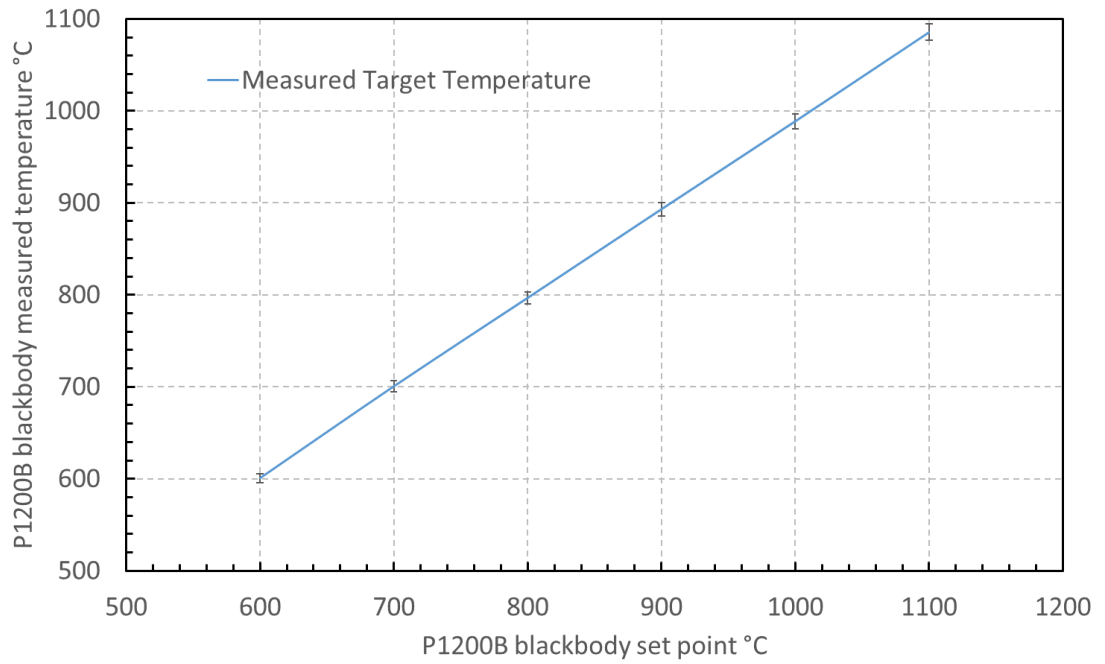


**Figure 3.3 Landcal P1200B Blackbody Source Calibration Against Traceable Transfer Standard Type 'R' Thermocouple**

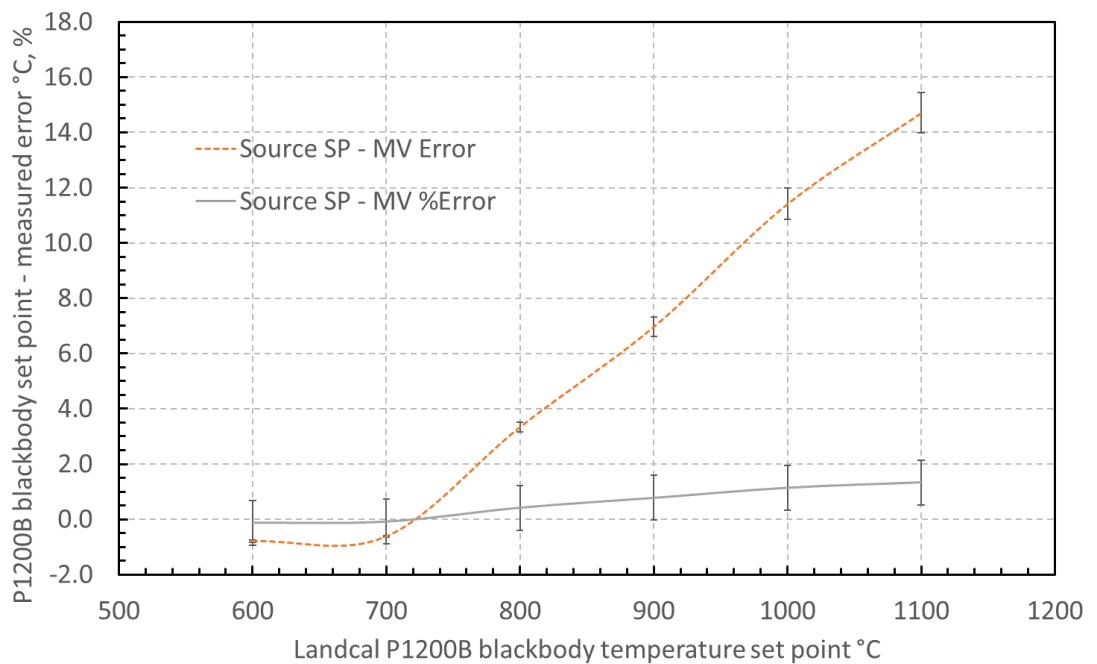
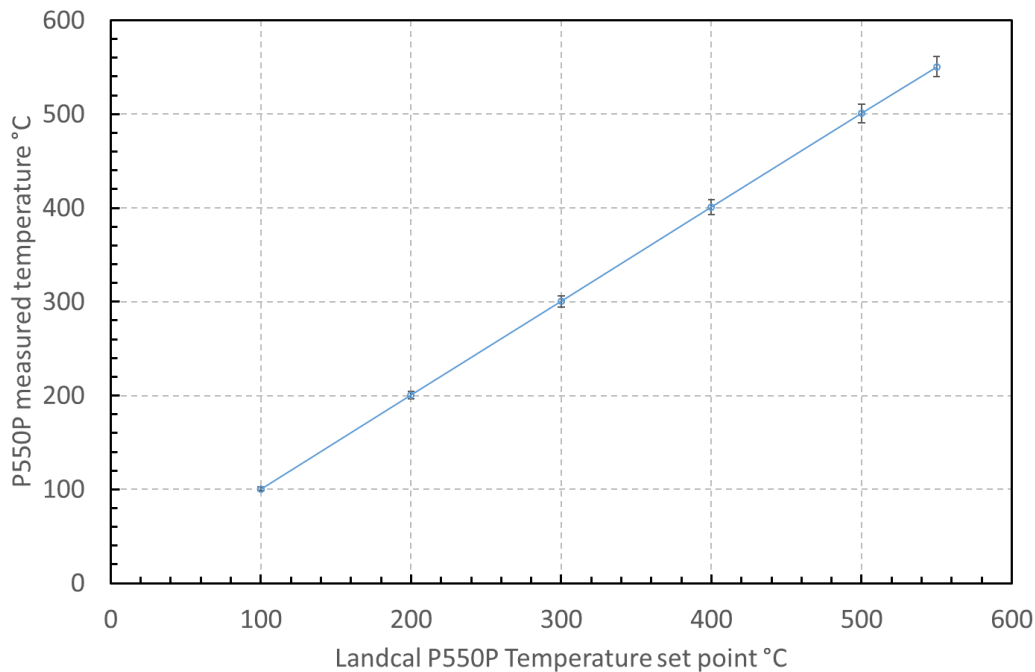


**Figure 3.4 Error between set point and measured value for Landcal P1200B Blackbody Source Calibration**

### 3.5.2 Landcal P550P Portable Blackbody Source Calibration

The lower temperature approximate blackbody source was calibrated using the transfer standard Platinum resistance temperature detector having 100  $\Omega$  resistance at 0 °C (Pt-100 RTD) and for which the traceable calibration is described in appendix 2. The Pt-100 RTD was calibrated to traceable national standards by the manufacturer (Isothermal Technology Limited, Skelmersdale, UK) at the time of supply, so provided a valid and traceable calibration for the blackbody source. The relationship between temperature set point and temperature measured by the transfer standard thermocouple is presented in figure 3.5 and the error between the set point and



measured values in figure 3.6.

**Figure 3.5 P550P Portable Blackbody Source Calibration Against Traceable Transfer Standard Platinum 100 $\Omega$  Resistance Temperature Detector**

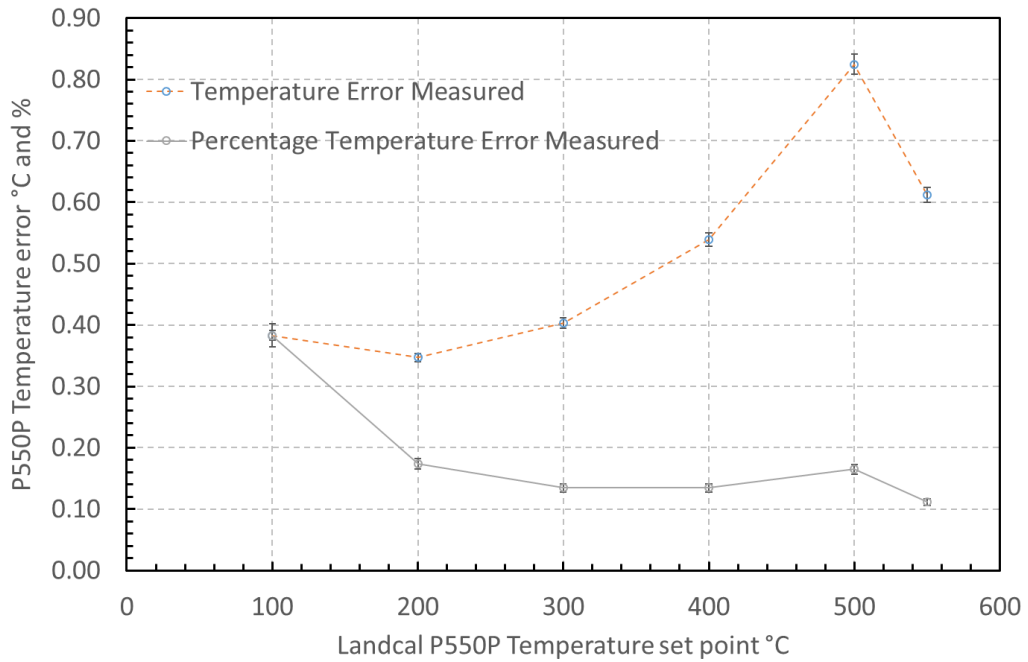
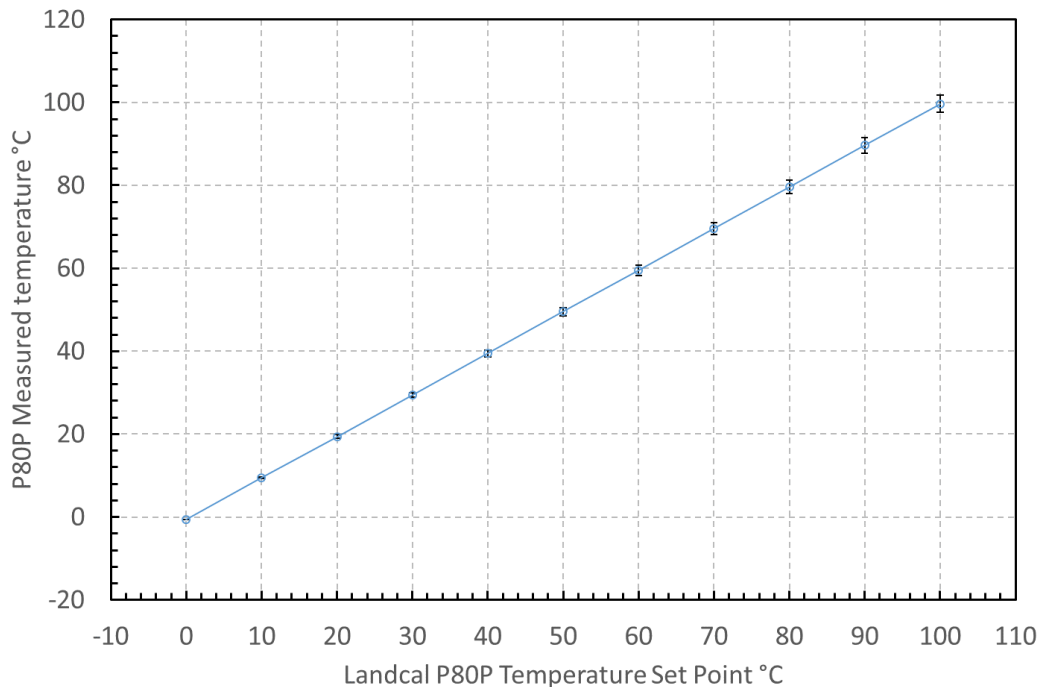


**Figure 3.6 Error between set point and measure value for Landcal P550P portable blackbody source calibration**

### 3.5.3 Landcal P80P Portable Blackbody Source Calibration

The Ametek Land Landcal P80P portable approximate blackbody source was calibrated against a transfer standard Platinum resistance thermometer having 100  $\Omega$  resistance at 0 °C (PRT-100) that had been calibrated at manufacture against standards that were traceable to national laboratory primary standards.

The calibration over the temperature range 0 – 100 °C is presented in figure 3.7 and



error curves in figure 3.8.

**Figure 3.7 Indicated temperature set point and transfer standard measured temperature of P80P blackbody source, and error between indicated and measured temperatures**

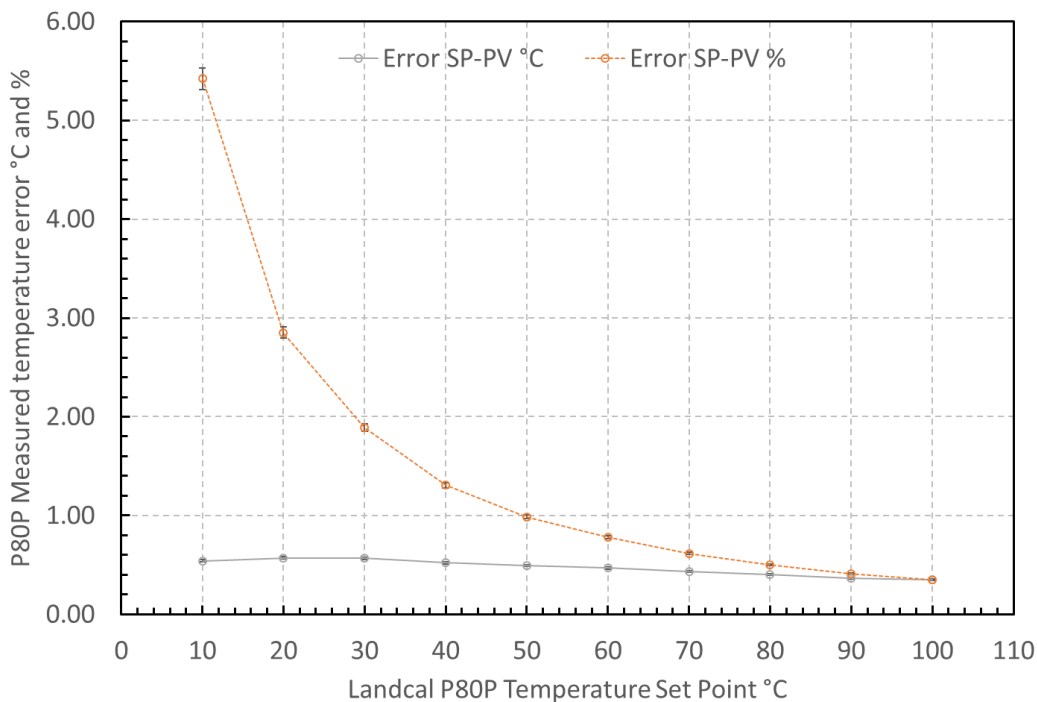


**Figure 3.8 Error between indicated and measured temperatures of Landcal P80P blackbody source**

### 3.6 Analysis of Thermometer Characteristics

Applying the Wien's approximation to Planck's Law afforded determination of the limiting effective wavelength, that is a monochromatic abstraction of the thermometer spectral response over a range of temperatures [18] and an interpolation relationship between the measured output voltage from a thermometer and the source temperature emitting infrared radiation. The characteristics were determined from the voltage output measured at known temperatures at regular intervals through the range(s) over which the thermometer measured. The higher temperature range thermometers were

characterised at 50 °C and 100 °C intervals between 100 °C and 1000 °C, the middle temperature range thermometers at 10 °C and 50 °C intervals between 100 °C and 500 °C and the lower temperature range thermometers were characterised at 5 °C and 10 °C intervals between 20 °C and 80 °C. The known temperature versus output voltage points were used to determine a Sakuma–Hattori interpolation curve [19] for the monochromatic, limiting effective wavelength, evaluated from the Wien approximation. The interpolation equation enabled any voltage between the minimum and maximum output voltages to be interpreted as a temperature between the minimum and maximum temperatures against which the thermometer was calibrated.

The relationship between the natural logarithm of the output voltage from the thermometer TIA circuit and the inverse of absolute temperature of the source was used to determine the limiting effective wavelength, sensitivity of the thermometer and noise limited equivalent temperature resolution according to the equations described in chapter 2. These data were used to develop output voltage versus source temperature models, against which the measured temperatures were compared to assess the validity and uncertainty of measurements.

## Summary of chapter

The mid-wave infrared (MWIR) and short-wave infrared (SWIR) thermometers have been configured to afford as wide a range of temperature measurements as possible, without needing photodiode cooling or signal chopping to enhance the measuring capability at low source temperatures. The transimpedance amplifier (TIA) circuit utilised a bootstrapping technique demonstrated by Makai and Makai [9] to provide a stable and elevated apparent shunt resistance at the TIA input, that was suitable for use with photodiodes having low shunt resistances.

The fibre optics were chosen to withstand the harsh conditions to which they would be subjected in each application, whilst maximising the signal and wavelength range transmitted to satisfy the temperature range over which the infrared thermometer was specified to measure. Sapphire crystalline fibre optic was preferred for higher temperature applications and low reactivity metallic fluoride glass fibre optics for lower temperature applications that required transmission of lower intensity signals.

A method of laboratory characterisation and thermometer calibration against approximate blackbody sources, based upon BS 1041-5:1989 was used and applied to the prototype thermometers. The fibre optics were inserted into thermo-wells on the blackbody sources that mimicked being embedded into blind-ended holes drilled into objects undergoing temperature measurement. The laboratory characterisation of the prototype thermometers provided practical calibrations for the application thermometers.

## REFERENCES

- [1] A. Queck, et al, 'Advanced measurements and dynamic modelling for improved furnace operation and control (DYNAMO)', European Commission Directorate-General for Research and Innovation, Final Report EUR 28146 EN, 2016. ISBN 978-92-79-62951-8 doi:10.2777/338050.
- [2] M. Evestedt and P. O. Norberg, Precise temperature control in high quality steel reheating and annealing furnaces, vol. 13, no. PART 1. IFAC, 2010.
- [3] L. H. J. Rajmakers, D. L. Danilov, R. A. Eichel, and P. H. L. Notten, 'A review on various temperature-indication methods for Li-ion batteries', *Appl. Energy*, vol. 240, no. July 2018, pp. 918–945, 2019.
- [4] J. P. Makai and J. J. Makai, 'Current-to-voltage converter for linearity correction of low shunt resistance photovoltaic detectors', *Rev. Sci. Instrum.*, vol. 67, no. 6, pp. 2381–2386, 1996.
- [5] J. Caldwell, 'TI Designs – Precision : Verified Design 1 MHz , Single-Supply , Photodiode Amplifier Reference Design', *Texas Instruments Reference Design*, no. November. pp. 1–21, 2014.
- [6] Texas Instruments Inc, 'AN-1803 Design Considerations for a Transimpedance Amplifier', *Texas Instruments Application Report SNOA515A*, vol. AN-1803. 2013.
- [7] Hamamatsu Photonics, 'InAsSb photovoltaic detector P13243-11-MA Datasheet', *Hamamatsu P13243 Series Datasheet*. 2015.
- [8] Hamamatsu Photonics, 'InGaAs PIN photodiodes G12180 data sheet', no. 4. pp. 1–8, 2018.

- [9] J. P. Makai and T. Makai, 'Low radiation level detection with room temperature InAs detector', *J. Mod. Opt.*, vol. 61, no. 14, pp. 1187–1194, 2014.
- [10] J. Dixon, 'Radiation thermometry', *J Phys E Sci Instrum*, vol. 21, pp. 425–436, 1988.
- [11] B. Müller and U. Renz, 'Development of a fast fiber-optic two-color pyrometer for the temperature measurement of surfaces with varying emissivities', *Rev. Sci. Instrum.*, vol. 72, no. 8, pp. 3366–3374, 2001.
- [12] J. P. Makai and T. Makai, 'Enhancement of the low level detection limit of radiometric quality photovoltaic and photoconductive detectors', *Metrologia*, vol. 42, no. 4, pp. 266–270, 2005.
- [13] Burr-Brown Corporation, 'Designing Photodiode Amplifier Circuits With Opa128', *Application Bulletin SBOA061*. pp. 1–4, 1994.
- [14] A. de Sa, *Principles of Electronic Instrumentation*, First. Edward Arnold (Publishers) Ltd, London, 1981.
- [15] British Standards Institute, 'BS 1041-5 Temperature measurement— Part 5: Guide to selection and use of radiation pyrometers', *British Standards Institute*, vol. 1041, no. 5. 1989.
- [16] E. M. Sparrow, L. U. Albers, and E. R. G. Eckert, 'Thermal radiation characteristics of cylindrical enclosures', *J. Heat Transfer*, vol. 84, no. 1, pp. 73–81, 1962.
- [17] J. Vollmer, 'Study of the effective thermal emittance of cylindrical cavities', *J. Opt. Soc. Am.*, vol. 47, no. 10, pp. 926–932, 1957.
- [18] P. Saunders, 'General interpolation equations for the calibration of radiation thermometers', *Metrologia*, vol. 34, no. 3, pp. 201–210, 1997.
- [19] F. Sakuma and S. Hattori, 'Establishing a practical temperature standard by using a narrow-band radiation thermometer with a silicon detector', in *TEMPERATURE: ITS MEASUREMENT AND CONTROL IN SCIENCE AND INDUSTRY, VOLUME 5, PART 1: Proceedings of the Sixth International Temperature Symposium*, 1982, vol. 5.1, pp. 421–427.

## 4 END MILLING TOOL TEMPERATURE MEASUREMENT USING FIBRE OPTIC COUPLED, MID-WAVE INFRARED THERMOMETER

The Advanced Manufacturing Research Centre (AMRC), part of the University of Sheffield that is engaged with improving manufacturing processes alongside industrial partners, required a method of measuring the temperature at the cutting surface of machine tools. Understanding the temperature history of the cutting surface during machining would assist the AMRC in developing improved tolerances for milling operations undertaken on high-value Titanium aerospace components. The research undertaken into temperature histories at AMRC often use specialised, very fine wire thermocouples embedded into the machine tools but these have limited response speeds of several milliseconds and are subject to interference from the high electromagnetic fields coupling into the wires. The potential for a fibre optic infrared radiation thermometer to substitute for thermocouples in this application would be of significant interest to the industrial partners of AMRC and manufacturers more widely.

## Part 1: Laboratory development and characterisation of prototype fibre optic coupled, mid-wave infrared thermometer

### 4.1 Infrared thermometer configuration

The first prototype infrared radiation thermometer (IRT) version used an Indium Arsenide Antimony (InAsSb) photodiode that generated a photocurrent when exposed to mid-wave infrared radiation (MWIR) between the wavelengths 3.0  $\mu\text{m}$  and 5.0  $\mu\text{m}$ . The thermometer used the bootstrapped photodiode and transimpedance amplifier configuration illustrated in figure 3.1 of chapter 3.

The effective gain of the transimpedance amplifier (TIA) was defined by the transimpedance in the resistor-capacitor (R-C) network and this was chosen to have a large value to ensure that the voltage generated from the photocurrent was measurable using benchtop instrumentation. The initial laboratory prototype version TIA had 1 M $\Omega$ , 100 k $\Omega$  and 10 k $\Omega$  feedback resistances that enabled amplification of the photocurrent in the range of nano-Amperes (nA) to micro-Amperes ( $\mu\text{A}$ ) to the measurable voltage within the range micro-Volts ( $\mu\text{V}$ ) to Volts (V) and the capability to use different grounded photodiode or bootstrapped configurations. These test features were eliminated from subsequent versions of the thermometer that were configured for application to the measurement of milling tool temperatures.

The InAsSb photodiode deployed in the prototype thermometer had a shunt resistance specified to be 120 k $\Omega$  at room temperature [1], which is a lower shunt resistance than would be encountered from Silicon photodiodes that are typically used uncooled and have shunt resistances of the order of tens of Gigaohms [2]. The use of large values of transimpedance would be necessary to achieve measurements of the weak infrared signals incident upon a photodiode from low minimum temperatures. The low shunt resistance of the MWIR photodiodes used presented problems when used with high values of transimpedance, owing to some of the photocurrent passing through the photodiode, rather than generating measurable TIA output voltage. Additionally, photodiode bias induced by offset voltage and offset voltage drift, particularly with varying thermometer temperature, would lead to higher dark current and non-linear output voltage. Typically, cooling is used to reduce the dark current and increase the shunt resistance of the photodiode, enabling larger values of transimpedance to be

used in IRTs. The prototype thermometers were intended for application in constrained spaces, so needed to operate without having photodiode cooling. The prototype IRTs used bootstrapping to increase the apparent shunt resistance presented to the TIA by the photodiode and maintain near to photovoltaic conditions. The thermally induced dark current would not be reduced by this configuration, therefore would constrain the minimum temperature to which the IRT could measure. The prototype versions of the thermometer for different applications were adapted from the laboratory prototype with improvements identified during laboratory development, characterisation and initial pilot trials. The thermometers built for applications were simplified to the minimal number and size of components on the printed circuit board (PCB), thereby achieved a compact size for installation into positions with space constraints or requiring low mass added by the thermometer for mounting onto moving equipment.

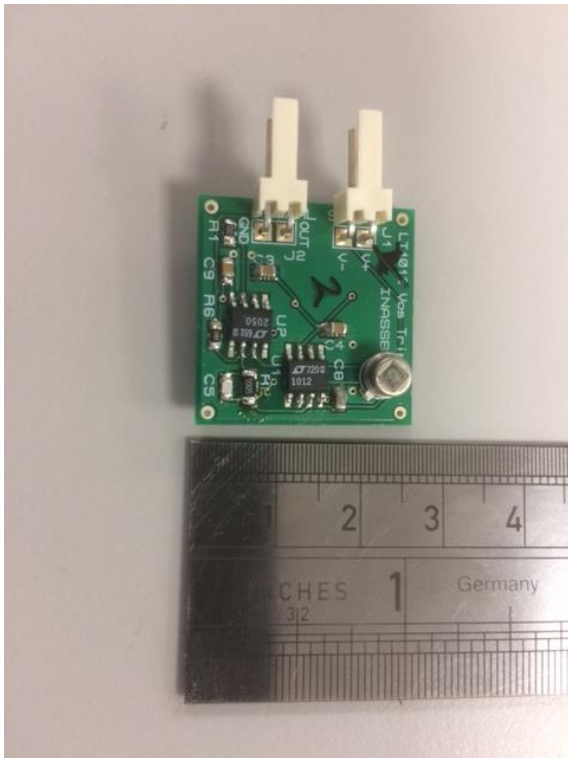
The initial prototype thermometer for applications was used to measure temperatures during end milling and configured using 1 M $\Omega$  resistance and a parallel 10 pF capacitance to form the feedback R-C network around the TIA op-amp, as used in development of the laboratory prototype version of the thermometer. The resistor was chosen to afford transimpedance of 10<sup>6</sup>  $\Omega$  to generate measurable voltages between 0.15 mV and 10 V from the minimum and maximum photocurrents delivered by the InAsSb photodiode, which were specified by the manufacturer as 150 pA and 10  $\mu$ A, respectively [1]. The R-C network had an integration time constant of 10  $\mu$ s, therefore presented a cut-off frequency of 15.9 kHz to alternating signals. For steady-state signals of the type acquired during characterisation, this integration time constant is only relevant for ensuring that averaging the measurements is undertaken over intervals of sufficient duration to identify the temperature signals from the noise.

The InAsSb photodiode was presented in a small transistor outline (TO) package, designated TO-46. The simplified circuit used for thermometers deployed into applications allowed the size of PCBs for these prototype thermometers to be reduced from the laboratory prototype, excluding consideration of the external power supply. The photodiode was chosen to be the version using the smallest transistor outline package available readily without making a bespoke detector. The photodiode also had

to be uncooled to minimise the size, whilst having the largest photosensitive area available within the package to achieve the best compromise between size, cost and measurement performance. The power supply was mounted separately to the thermometer PCB, so did not compromise the PCB size, particularly when the thermometer was operated using dry cells, for example: lightweight Lithium-ion CR2032 coin cells that were used in the end milling machine trial described later.

The use of small package sizes and dispensing with ancillary cooling and signal chopping in the thermometer enabled the PCB to have a small footprint, achieving dimensions of 25 mm x 25 mm. This size was sufficiently small to afford mounting the thermometer in locations that enabled short length fibre optics to couple the infrared to the detector, whilst isolating the thermometer from the object being measured, for example: inside a milling machine chamber. The types of location for which the thermometers were designed would not be accessible to thermometers that have larger components, for example: heatsinks for rejecting heat from cooling the photodiode and electro-mechanical chopping of the infrared signal required for use with a lock-in amplifier. The small size of the PCB and surface-mounted components, that formed the thermometer signal conditioning electronics, are illustrated in figure 4.1.

**Thermometer PCB top layer**



**Thermometer PCB bottom layer**

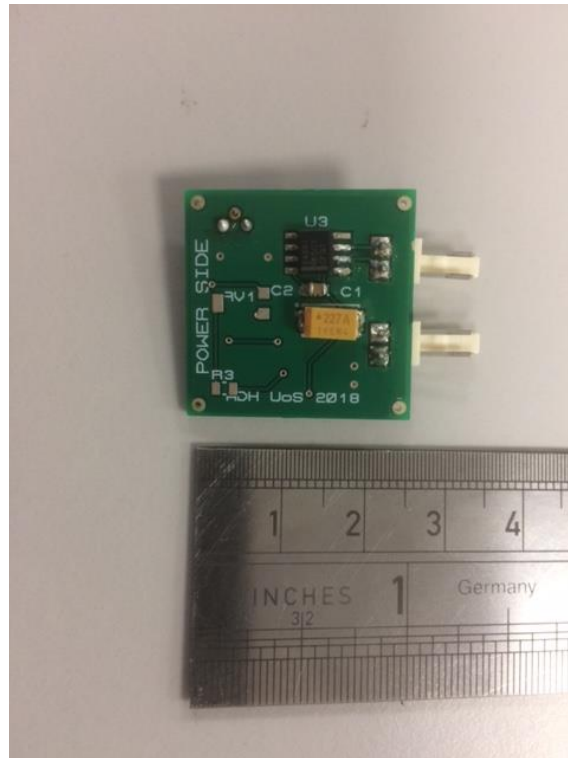


**Figure 4.1 Top and bottom layers of compact prototype MWIR thermometer, illustrating the size of the thermometer PCB and minimal number of components**

The prototype thermometers of this study were constructed manually, hence there exists scope to reduce the op-amp, discrete and connector component sizes further and use robotic soldering in manufacture. These improvements would enable the physical size of the PCB to be minimised and it would be a reasonable expectation that the physical dimensions could easily be halved. Use of low cost components was also considered a prudent compromise to ensure that total loss of thermometers from damage in harsh conditions would not be critical.

The fibre optic was terminated into an SMA905 fibre optic header that was then coupled to a TO-46 mount with the photodiode concentric with and opposite to the output end of the fibre optic core. Dow-Corning 3145 silicone adhesive sealant was used to hold the photodiode in position within the mount, thereby ensuring retention of the sensor concentric with the fibre optic core and sealing of the sub-assembly to prevent fluid, dust and debris affecting the fibre optic to photodiode coupling. The photodiode was positioned ten millimetres away from the fibre optic output to ensure

that the infrared radiation was incident over the whole active area of the photodiode. Measurements of the field of view incurred by the thermometer, described later in this chapter (see section 4.2.4) indicated that the active area of the photodiode was over-filled, therefore decreasing the intensity of radiation that was received below the maximum.

The signal to noise ratio was increased in the prototype by covering the photodiode active area fully without over-spill of the infrared radiation incident upon it, therefore utilising the maximum signal intensity possible to generate photocurrent. This improvement should afford the lowest minimum temperature measurable from each configuration of photodiode, transimpedance resistor value and fibre optic transmission band that was trialled.

The potential to measure temperatures above the maximum 1100 °C attained in laboratory characterisation, whilst also retaining the low temperature capability of the thermometer, exists with suitable choices of feedback resistance and capacitance values, op-amp used in the transimpedance amplifier, power supplies and filtering.

Further filtering to enable the temperature signal to be identified from the noise could be undertaken either during signal acquisition or post-acquisition signal processing, within an external data acquisition system.

The transimpedance resistor also contributes to the definition of the bandwidth of the circuit and may require the resistance to be reduced to accommodate capturing signals from broad bandwidth. Equally the introduction of amplifier, resistor and component noise sources affects the thermometer minimum temperature resolution, so compromises chosen to maximise one parameter need to be judicious and may need to be revised to provide optimised performance for specific requirements, for example: shorter integration time to capture higher frequency signals or higher transimpedance to capture weak signals.

The full circuit diagram of the thermometer PCB without input voltage offset trimming that was developed for the end milling machine application is presented in figure 4.2. The PCB track and component layouts for the top and bottom layers are presented in Appendix 3.

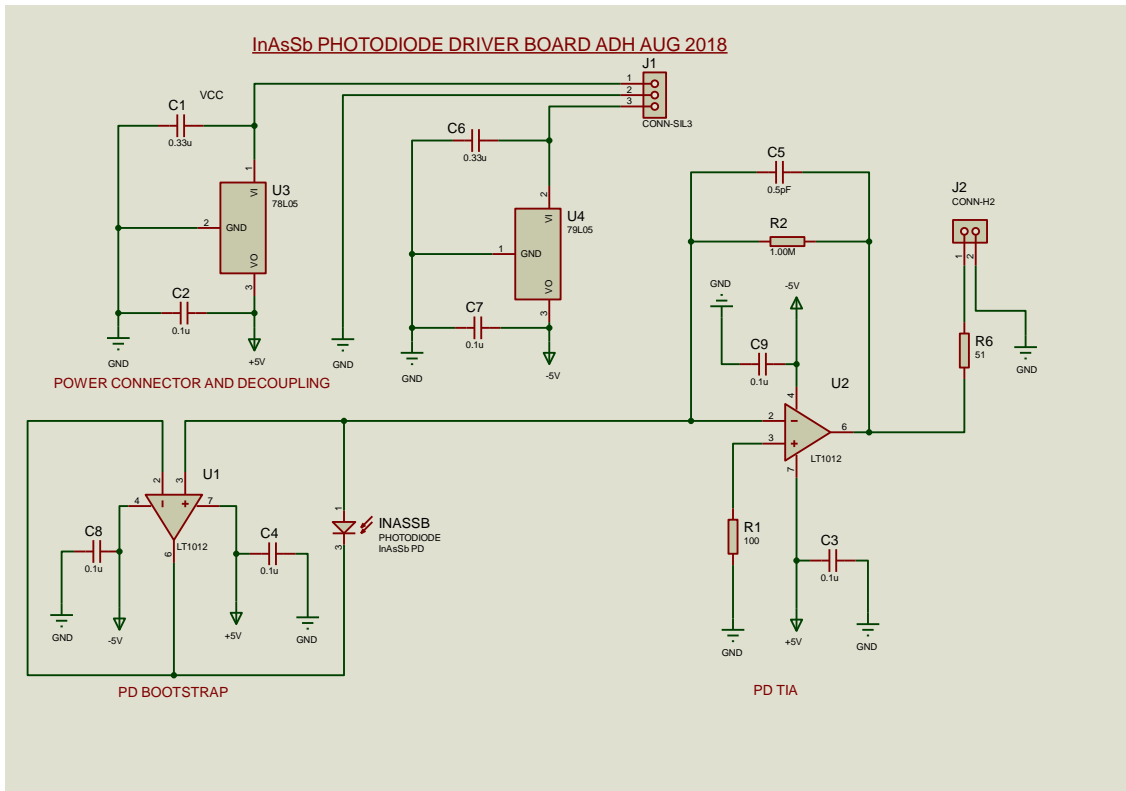


**Figure 4.2 Circuit diagram for infrared radiation thermometer using bootstrapped InAsSb photodiode and high value of transimpedance but excluding offset trim**

The prototype thermometer TIA circuits used op-amps chosen to have sufficiently low input voltage offset, voltage noise, input current noise and input bias current to enable the measurement of output signal variations of the order of 0.01 mV, whilst not incurring high costs. The op-amps used were further constrained to be capable of operating from low voltage power supplies, for example, enabling operation from paired CR2032 button cells.

This prototype was developed further to introduce an input voltage offset trim to the non-inverting input of the TIA stage to minimise this offset and source of uncertainty in the output voltage, thereby enabling subsequent amplification of the signal without constraining the range of the measurement. Variants of these PCBs were developed that used single-side voltage supply (0V and +V) to enable lightweight, coin cells or an induction loop to provide the power supply more easily. The op-amps were chosen to have the same 8-pin, small-outline integrated circuit (SOIC) footprint and pin configuration for these PCBs to afford interchangeability of the components between circuit variants.

The addition of input voltage offset trimming potentiometers for the TIA non-inverting input and certain op-amps increased the depth of the PCB to approximately 10 mm to 15 mm, owing to the height of these components mounted on the underside of the thermometer board. The 25 mm x 25 mm square footprint of the PCB was not affected by the addition of the trimming potentiometers. The additional height may be undesirable for mounting thermometers in some processes that require the PCB to present the smallest obstruction achievable but would not prevent their use in many cases where this would not be a consideration.

Each of the application thermometers configured used a derivative of the circuit illustrated in figure 4.2.

If photodiode cooling was added to the thermometer PCB, it would be possible to improve the capability of the thermometer to achieve lower minimum measurable temperature than the bootstrapped thermometer presented here. This would compromise the compact size of the thermometer PCB and disallow its use in applications that needed this advantage but may be appropriate for applications with more space available for mounting the thermometer.

## 4.2 Laboratory prototype thermometer characterisation against blackbody source temperatures

The characterisation of the laboratory prototype mid-wave infrared, fibre optic coupled, thermometer that is presented in this chapter, was undertaken according to the experimental methods described in chapter 3. Refinement of the initial laboratory prototype thermometer, following experimentation and further development led to the configuration of the small-sized prototype thermometers that were suitable for applications incurring harsh conditions.

### 4.2.1 Thermometer output voltage characteristic

The thermometer output voltage was recorded for signals that registered a continuously measurable value that could be identified above the noise, at least qualitatively. The thermometer output voltage characteristic with increasing object

temperature achieved and the estimated uncertainty around the measurement values calculated are presented in figure 4.3. The estimated uncertainty represented on figure 4.3 was the mean standard deviation of measurements recorded during calibration of the thermometer against known, steady-state temperatures.

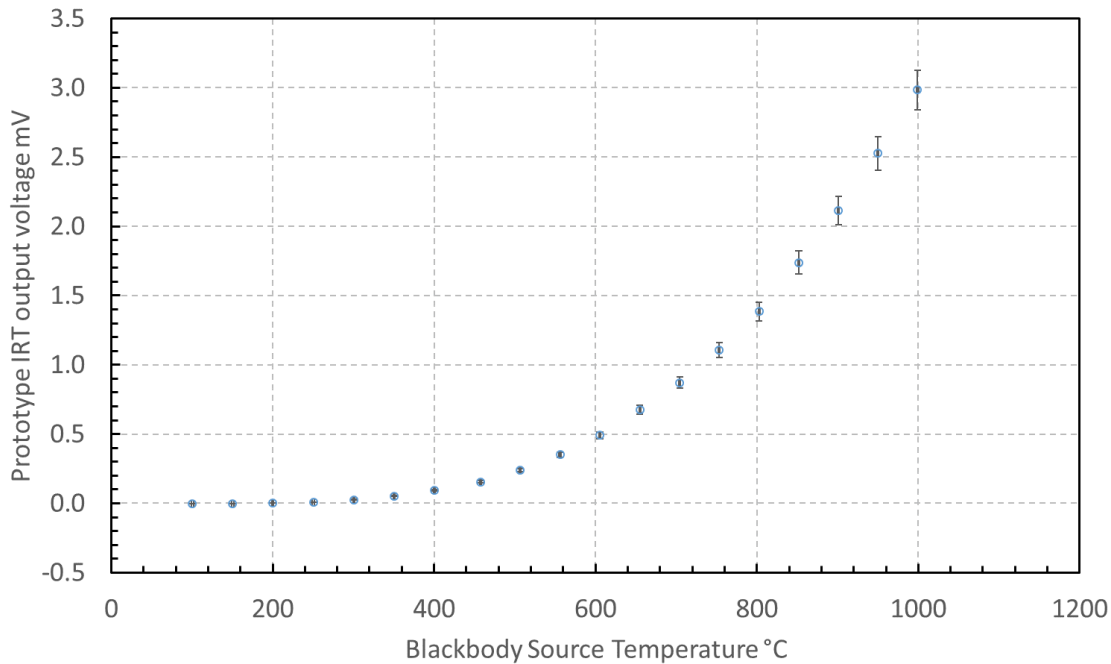


**Figure 4.3 Prototype Infrared Thermometer Blackbody Source Temperature versus Voltage Output Characteristic Measured under Laboratory Conditions**

The output voltage measured had a range between 0.0035 mV (3.5  $\mu$ V) at 200 °C and 2.982 mV at 1000 °C source temperatures. The minimum blackbody source temperature for which the prototype thermometer response exceeded the noise sufficiently to afford continuous measurement without averaging over durations of the order of seconds, was 200 °C. In principle, the minimum source temperature that the thermometer should be capable of measuring would be when the signal to noise ratio (SNR) is unity, which would suggest the minimum temperature measurable with this configuration of thermometer should be approximately 100 °C. The measurements acquired needed to be averaged continuously over several seconds duration to identify the measurement at 100 °C, therefore the thermometer would not be usable readily to measure objects at this temperature, unless the temperature was either at steady-state (as was the case for the practical calibration undertaken in laboratory characterisation) or only slowly

changing conditions. The practical minimum temperature was defined as approximately 200 °C.

The natural logarithm of the output voltage from the thermometer ( $\ln(V_o)$ ) can be characterised as an inverse function of the absolute temperature ( $1/T$ ), according to the expansion of the ratio of band radiances calculated using the Wien approximation and described in equation (2.13) of chapter 2. The  $1/T$  versus  $\ln(V_o)$  curve measured for the laboratory prototype thermometer is presented in figure 4.4.

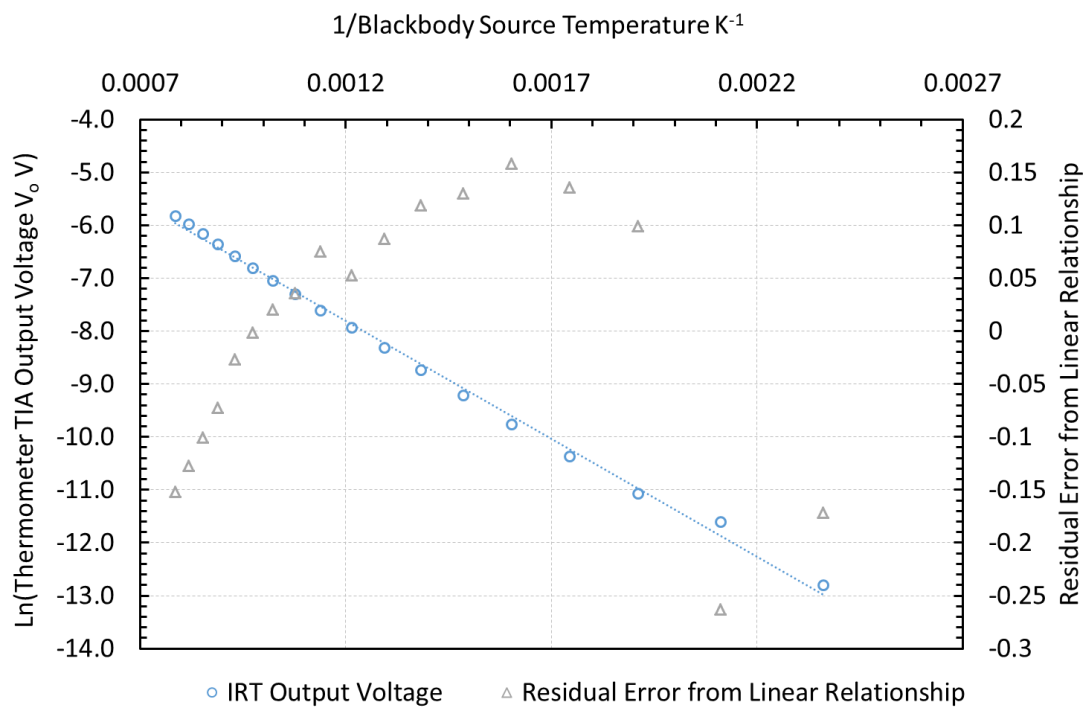


**Figure 4.4 Graph illustrating  $1/T$  versus  $\ln(V_o)$  for the laboratory prototype IRT and residual error between the linear model and measured data**

The  $1/T$  versus  $\ln(V_o)$  curve should have a linear characteristic throughout its range to the first order expansion presented by Hahn and Rhee [3] and it was evident that this relationship held true for the higher temperature measurements (smaller values of  $1/T$ ) and until the source temperature was below approximately 200 °C ( $1/T$  value of 0.0021). At lower temperatures, the noise magnitude was comparable to or greater than the signal, which led to the curvature observed in the characteristic and illustrated to the right hand side of figure 4.4. The thermometer should be used to measure

temperatures within the range where the  $1/T$  versus  $\ln(V_o)$  characteristic was approximately linear, therefore exceeding the practical minimum temperature 200 °C.

The voltage output from the prototype thermometer demonstrated low sensitivity, achieving a mean value across the range measured of 3.72  $\mu\text{V}/^\circ\text{C}$ . The infrared radiation power incident upon the photodiode and the low sensitivity of the photodiode to that incident radiation compared to other photodiodes, such as: Silicon, Mercury Cadmium Telluride and Indium Gallium Arsenide [1], [4], alongside the transimpedance used to amplify the signal, dictated the low sensitivity. Improvement of the thermometer sensitivity would require higher incident radiation power on the photodiode and higher transimpedance in the amplifier configuration. The narrow waveband over which the thermometer responded was defined by the product of the sapphire fibre optic transmission band (nominally 0.7 – 3.5  $\mu\text{m}$ ) and photodiode response band (nominally 3.0 – 5.0  $\mu\text{m}$ ) curves, resulting in the expected operating wavelength range being limited to 3.0 – 3.5  $\mu\text{m}$ . The product of the fibre optic transmission and photodiode sensitivity curves limited the radiation that was incident upon the photodiode, therefore the response of the thermometer. The theoretical minimum temperature that could be measured by the thermometer was calculated to be 227 °C, based upon estimating the transmission and response between exactly 3.0  $\mu\text{m}$  and 3.5  $\mu\text{m}$ , as described in chapter 2 and appendix 1. The minimum temperature measurable that was established by experiment is lower than the calculated value because the fibre optic transmission and photodiode response curves extended beyond the nominal cut-off wavelengths, thereby affording marginally higher infrared intensity to be transmitted and wider range of wavelengths to which the photodiode responded.

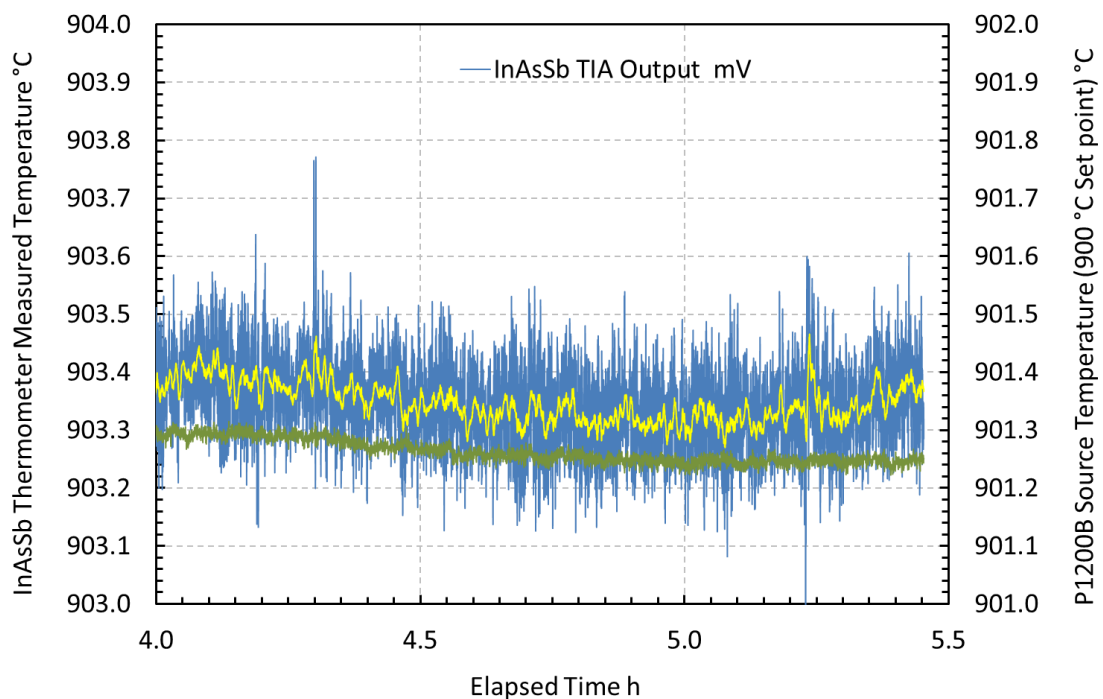
#### 4.2.2 Thermometer voltage output noise

The minimum temperature that the thermometer would measure can be defined by the resolution that the noise magnitude affords, calculated as an equivalent temperature based upon manipulating the Wien approximation, as described in chapter 2.

The noise magnitude was defined as one sample standard deviation of the signal measured and the signal to noise ratio (SNR) as the mean value of sample measurements divided by the sample standard deviation. These definitions of noise

magnitude and SNR assumed that the noise was distributed normally around a central mean value that defined the signal value. The assumption of normal distribution of the noise will be valid for shot noise and Johnson noise [5], which are the principal types associated with the thermometer.

An example of the typical data recorded from the thermometer and blackbody source temperature measurements after the source had settled at a steady-state temperature of 900 °C is presented in figure 4.5. This sample of measurements was extracted from a recording of data that started with the furnace at room temperature at zero elapsed time, to achieving stable temperature set point after approximately two hours. This figure illustrated the thermometer noise and continuously-averaged signal within the measurements at steady-state temperature over a duration of eighty minutes, with the



blackbody furnace having achieved equilibrium between heat input and losses.

**Figure 4.5 Typical data recorded from the thermometer and blackbody source temperature measurements, illustrating magnitude of noise and signal, including the continuously averaged signal**

It was evident that the noise magnitude represented deviations of less than 0.1% around the mean signal value of 903.35 °C, therefore the signal would be identified from the noise quickly at these higher temperatures. The noise at lower temperatures

represented a larger proportion of the mean signal, with the consequence that poorer resolution was achieved from the lower magnitude signals, thereby requiring longer averaging durations to identify the signal from the noise.

The noise limited temperature resolution and SNR measured for the prototype thermometer are presented in figure 4.6. The error bars illustrating the uncertainty of the noise equivalent temperature resolution calculations were representative of the standard deviation around the measurements upon which the calculations were based.

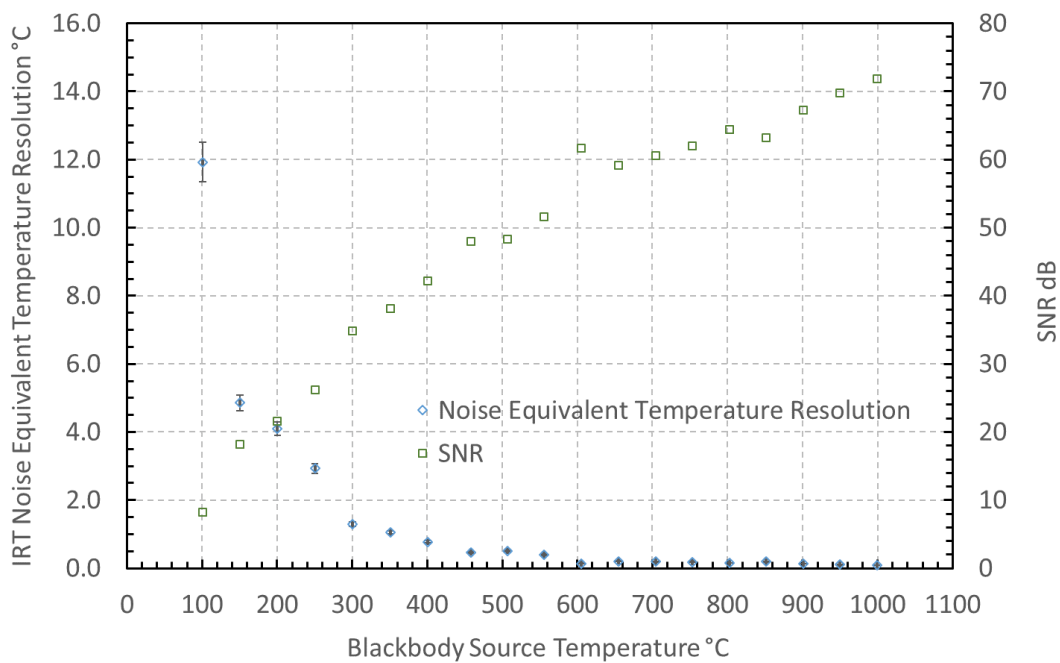


**Figure 4.6 Graph of noise limited equivalent temperature measurement resolution and signal to noise ratio calculated for prototype sapphire fibre optic coupled IRT**

The sapphire fibre optic limited the range of infrared wavelengths transmitted and the transimpedance resistor value used in the laboratory prototype thermometer limited the effective gain by which the photocurrent was multiplied. These constraints led to the limitation upon minimum temperature measurable and the noise limited equivalent temperature resolution calculated. Different fibre optics, affording a wider range of MWIR wavelengths to be transmitted and using a higher value of transimpedance in the amplifier could improve the capability of the thermometer to

measure lower temperatures and improve the resolution of the measurements. The fibre optic material would need to be capable of surviving the harsh conditions to which it would be subjected to provide useful coupling to the thermometer, of course. The effective gain achieved by increasing the transimpedance resistor value would need to maintain a stable output voltage from the thermometer for a steady-state source temperature measured, to be useful.

### 4.2.3 Thermometer output voltage modelling

The thermometer output voltage characteristic variation with object temperature was modelled based upon the Planck form of Sakuma–Hattori interpolation equation [6] with the limiting effective wavelength calculated from the Wien approximation, as described previously in chapter 2. The modelled and measured voltage outputs from the thermometer through the range of source temperatures 100 °C to 1000 °C are presented in figure 4.7. Comparison of the thermometer output voltage characteristic that was measured and the output voltage modelled, demonstrated that the curves were coincident within the uncertainty of the measurements above 200 °C but diverged below this temperature.

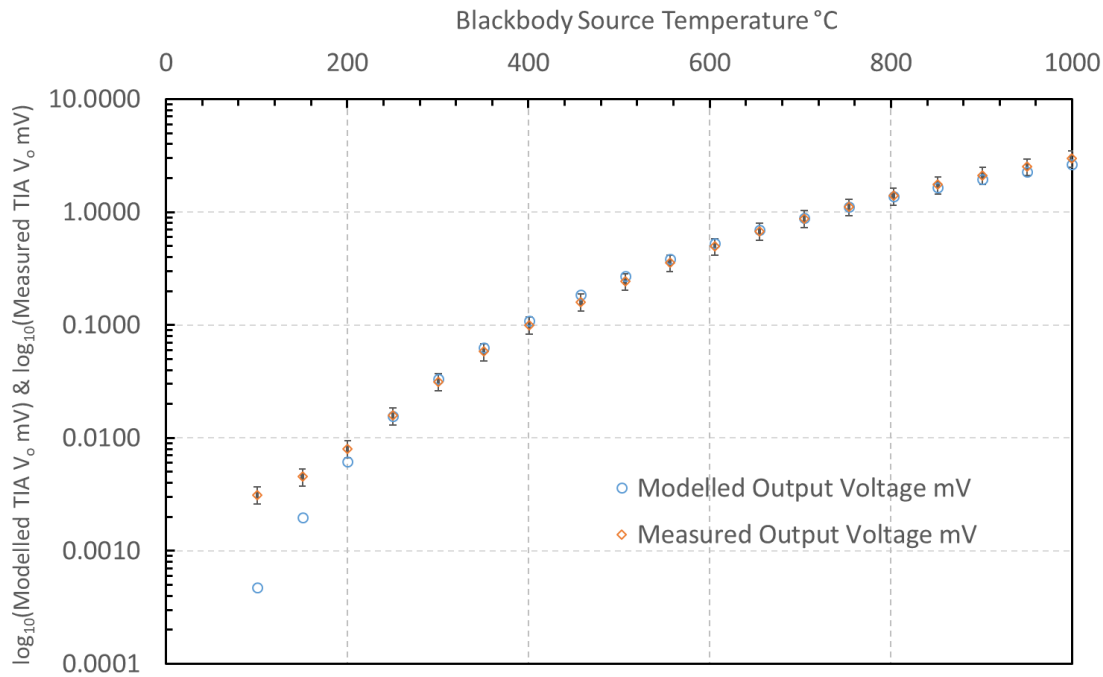


**Figure 4.7 Prototype thermometer measured and modelled output voltage versus source temperature curves with the standard deviation of output voltage measurements represented by error bars**

The similarity of the measured and modelled thermometer voltage output curves demonstrated that the thermometer characteristic based upon the laboratory calibration afforded estimation of the thermometer response and uncertainty around the measurement when applied to temperature measurements in a process.

The sapphire fibre optic coupled infrared thermometer achieved a Sakuma-Hattori curve fit [6], [7] with the scalar coefficient 0.1516 V (151.6 mV) through the temperature range 100-1000 °C for a limiting effective wavelength of 3.2  $\mu\text{m}$ . This scaling factor and limiting effective wavelength can be used to estimate the thermometer response expected when measuring any object temperature, for example, the expected output of the laboratory prototype sapphire fibre optic IRT measuring objects at 293 K (20 °C) and 1773 K (1500 °C) would be 5.7 nV and 9.55 mV, respectively. The photocurrent generated measuring an object at 20 °C would not translate to a readily measurable voltage, with the 1 M $\Omega$  transimpedance used in this configuration. The root mean square (RMS) noise magnitude observed from the measurements at ambient temperature was 10  $\mu\text{V}$ , therefore the noise was three orders of magnitude larger than

the signal at 20 °C. The initial laboratory prototype thermometer configuration would not be capable of measuring objects at temperatures approaching room temperature.

The fibre optic coupled thermometer achieved residual errors of less than or equal to  $\pm 5$  °C between the measured and calculated radiance temperatures between 250 °C and 1000 °C, as illustrated in figure 4.8.

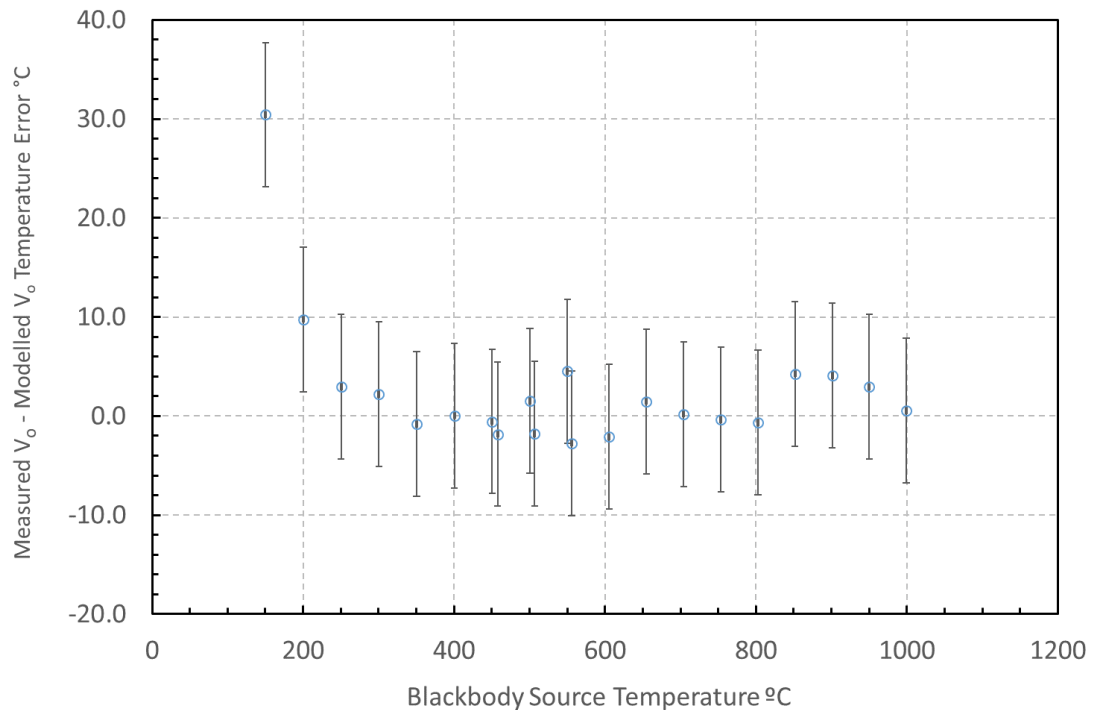


**Figure 4.8 Thermometer radiance temperature error calculated as (temperature measured – temperature modelled) and standard error of that calculation**

The error between the measured and modelled temperatures increased below 200 °C, with the uncertainty representing 30% of the measurement at 100 °C. The noise limited resolution of the thermometer, for which the signal magnitude fell below the noise magnitude, was reached at 200 °C therefore measurements below this temperature became increasingly uncertain and could not be measured without continuous and long duration averaging to extract the mean temperature signal.

#### 4.2.4 Evaluation of radiation coverage of photodiode active area

Field of view (FOV) measurements were undertaken to assess the proportion of the photodiode active area exposed to the incident infrared radiation and appraise

whether the signal could be increased by adjustment of the 'optical' coupling to provide maximum coverage of the photodiode without over-filling. The optimum condition would be to achieve 100% coverage so that the radiant power transfer was maximised, thereby optimising the signal intensity and SNR.

The FOV measurements, normalized with respect to the maximum photodiode output voltage, attributed to the incident signal intensity measured without an aperture obscuring part of the source, are presented in figure 4.9. These measurements demonstrated that the minimum aperture that did not cause more than 10% signal loss was approximately 20 mm diameter when mounted at 68 mm distance from the fibre optic receiving end. The linear FOV was evaluated from these measurements to be 3.4:1 to 90% power and this yields an equivalent planar included angle of the acceptance cone into the fibre optic of  $20.8^\circ$ . The conical angle inferred from the measurement contrasts with the specification for the numerical aperture of the fibre optic of 0.26, equivalent to  $25.4^\circ$  planar included angle of the acceptance cone. It may be inferred by comparison of these geometries, that the active area of the photodiode was overfilled by 48% in the test configuration. Ensuring that the active area was fully covered by radiation without over-filling would be expected to increase the signal to noise ratio, therefore enable measurement of lower temperatures than achieved during the characterization tests.

Installing a pair of aspheric lenses, positioned as a collimating lens pair, to collect and focus the infrared radiation onto the photodiode active area, could also provide full coverage of the photodiode by incident infrared radiation, thereby improved response to lower temperature objects. This would present additional mass and could increase the dimensions of the thermometer, so may not be ideal for applications that require the small size and mass of the prototype thermometer.

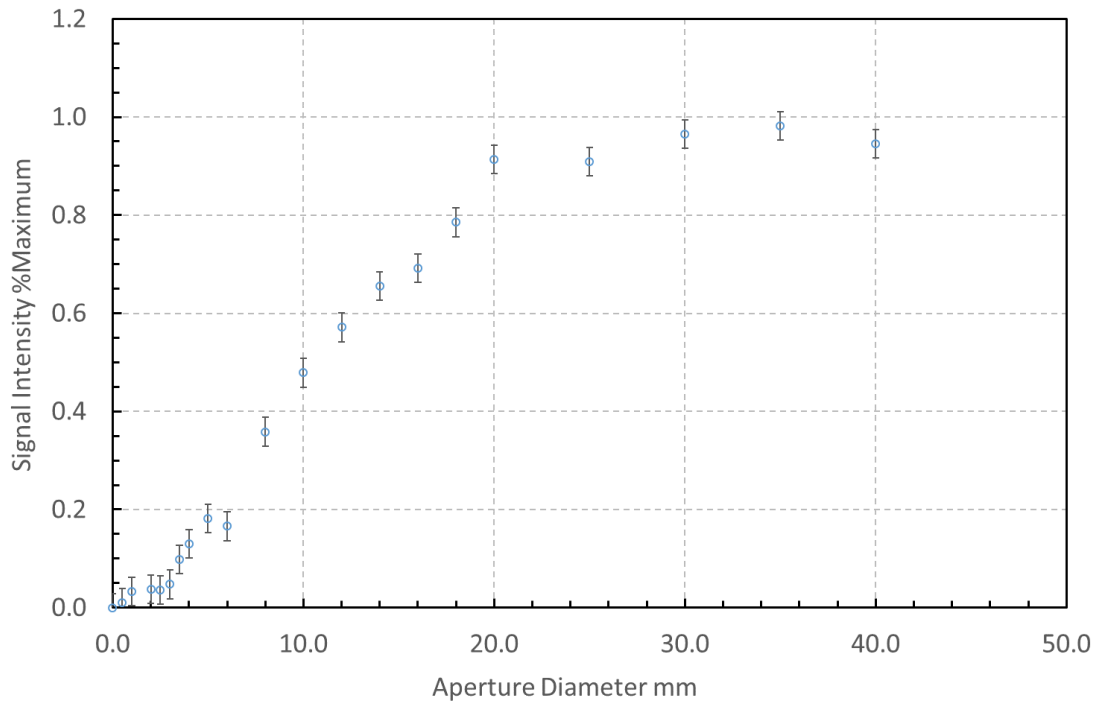


**Figure 4.9 Variation of field of view measured for fibre optic thermometer to assess proportion of photodiode that accepted radiation**

#### 4.2.5 Estimate of temperature measurement uncertainty of prototype thermometer

The uncertainty of individual measurements acquired using this thermometer system has been estimated, based upon the individual contributions from the equipment used in calibration and measurement, and from the measurements acquired using the thermometer during laboratory characterisation. The estimated contributions considered in the estimate and arising from the equipment and from the measurement are presented in Tables 4.1 and 4.2, respectively.

**Table 4.1 Contributions of calibration uncertainties to measurement uncertainty (K=2)**

Source Temperature °C	Calibration Thermocouple Uncertainty%	Calibration Blackbody Uncertainty%	Calibration Instrument Uncertainty%	Digital Multi-meter Uncertainty%
200	0.4	0.14	0.2	0.0085
1000	0.08	0.03	0.04	0.0085

**Table 4.2 Contributions of measurement uncertainties to measurement uncertainty (K=2)**

Source Temperature °C	Infrared Thermometer Variability in Usage%	Interpolation Error of Thermometer Mean Measurement%
200	1.2	2.0
1000	1.1	2.0

The overall uncertainty varied from 2.4% at 200 °C to 2.3% at 1000 °C. The largest individual contributions to the uncertainty arose from the variability in the infrared thermometer measurements and the error arising from the interpolation used to convert between the output voltage and temperature. The uncertainties that arose from the calibration equipment can be neglected without detriment to the uncertainty estimate, therefore the uncertainty estimation of the thermometer can be simplified. The uncertainty arising from the in-use variability of the measurements and interpolation error can be reported as the uncertainty of the thermometer.

Having demonstrated the capability of the thermometer under laboratory conditions and with no constraints upon the physical size of the thermometer PCB, this prototype was developed into a number of prototypes for trial applications. The prototypes were used in conditions that imposed constraints upon the size that the thermometer could occupy and required the infrared signal to be gathered from objects subjected to harsh conditions. Eliminating heatsinks, photodiode cooling and associated control circuit

and signal chopping afforded configuration of prototype thermometers on 25 mm x 25 mm footprint PCB that had the height of the surface mounted components only.

The prototype thermometers with fibre optic coupling developed for applications were characterised under laboratory conditions, using the methods described in chapter 3. The characterisation of the prototype thermometers was undertaken measuring radiation from blackbody sources within the temperature range 25 °C (for the lower temperature measuring prototype thermometer versions only) to 1100 °C (the maximum temperature for which calibration of the transfer standard thermometer was valid). This range of temperatures is useful for infrared thermometers intended for measuring material cutting temperatures [8], [9], battery cell temperatures during cycling and failure [10]–[12] and heating processes [13], [14]. A number of prototype, mid-wave infrared (MWIR) thermometers were used in applications, for which the fibre optic was embedded into the object being measured and the thermometer positioned externally.

## Summary of part I laboratory development and characterisation of IRT

The laboratory prototype thermometer demonstrated the feasibility of measuring object temperatures in the range 200-1000 °C, using an uncooled, mid-wave infrared photodiode that received unchopped radiation. The thermometer achieved measurement uncertainty within  $\pm 2.5\%$  throughout this temperature range.

The variation of the thermometer output voltage with multiple known source temperatures was measured to generate a working calibration of the thermometer. The output voltage variation with source temperature was characterised using Wien's approximation of Planck's Law of Thermal Radiation and modelled using the Planck form of Sakuma–Hattori curve fit. The model enabled interpolation of the characteristic to calculate any unknown source temperature from the output voltage measured within the range over which it was calibrated.

Further prototype thermometers, using similar designs were configured for application to processes that demanded a compact size, the ability to work under harsh conditions

and the capability of measuring over temperature ranges that were comparable to thermocouples embedded into a target object.

The feasibility of using a fibre-optic coupled, mid-wave infrared thermometer to substitute for thermocouple temperature measurements, when the target object incurs high temperature conditions, has been demonstrated under laboratory conditions.

## Part II: Application of prototype thermometer to cutting surface temperature measurement during end milling

### 4.3 Configuration and calibration of prototype application IRT

The first version of the prototype infrared thermometer (IRT) intended for application to a measurement undertaken in harsh conditions was based upon the laboratory prototype IRT. The application IRT used similar components and configuration to the laboratory prototype IRT but utilised the smaller sized surface-mount devices and excluded the switches and components that enabled testing of the development version thermometer.

#### 4.3.1 Configuration of end milling application thermometer

The prototype IRT developed for measuring end milling tool temperature used a fibre optic embedded into the tool insert to transmit infrared radiation from the cutting surface to the thermometer printed circuit board (PCB). This prototype thermometer used an Indium Fluoride ( $\text{InF}_3$ ) fibre optic with a 100  $\mu\text{m}$  diameter core. This fibre optic afforded wavelengths between 0.2  $\mu\text{m}$  and mid-wave infrared radiation at 5.5  $\mu\text{m}$  to be transmitted and was more flexible than the sapphire used in laboratory testing.

The thermometer PCB had a small size compared to the dimensions that would have been necessary to accommodate photodiode cooling components and optical signal chopping components and the controllers necessary to operate these. The reduction of the physical size of the thermometer PCB was essential to afford mounting of the device onto the rotating spindle of an end milling machine. This application required the thermometer to have a low mass to minimise the likelihood of causing either eccentricity of the shaft rotation or ejection of the thermometer PCB into the machine.

The fibre optic coupling between the cutting tool and IRT was embedded into a 'blind' hole comprising a cylindrical bore entering from the rear of a cutting tool 'insert' (the part of the tool that performs the cutting action) that ended approximately 0.5 mm from the surface of the insert. The IRT transimpedance amplifier (TIA) was positioned remotely from the cutting tool to obviate exposure of the electronics to the conditions at the milled surface.

The range of temperatures incurred within cutting processes, which has been suggested to be approximately 100 °C to 1000 °C [15] dictated that the thermometer should respond to mid-wavelength infrared (MWIR) radiation.

The short duration over which the tool would be cutting dictated that a thermometer suitable for measuring the transient temperature of the tool surface must have speed of response to a changing signal of 1 ms or faster [8].

The 'blind' hole into which the fibre optic would be inserted had a length to bore ratio exceeding five, with the fibre optic core exposed along the length of the embedded end for a similar ratio of length to diameter, thereby providing a means of collecting radiation from the internal surface area near to the end of the hole. The depth to bore ratio of this size of blind hole and using the exposed fibre optic tip embedded into it would ameliorate the problem of having to compensate the measured signal for the effect of the relative emissivity of the radiating object because the conditions approximate to a blackbody [16], [17].

#### 4.3.2 Prototype application thermometer characterisation.

The application prototype IRT with Indium Fluoride fibre optic coupling was characterised against approximate blackbody source temperatures between 100 °C and 1000 °C, using the same experimental method described in chapter three 'Experimental Methods' for characterising the laboratory prototype IRT. The application prototype IRT characteristic demonstrated monotonically increasing output voltage with temperature, similar to the laboratory prototype IRT. The application prototype thermometer had a higher magnitude output voltage at similar source temperatures owing to the wider range of wavelengths transmitted to the photodiode. The thermometer demonstrated similar magnitude of noise limited resolution

characteristics to the laboratory prototype thermometer, with elevated uncertainty at lower temperatures. The characteristics measured for this prototype thermometer are presented in figures 4.10 to 4.12.

The configuration of the first version of the application prototype thermometer was similar to the laboratory prototype thermometer, both having 1 M $\Omega$  transimpedance and using Linear Technologies LT1012 precision operational amplifiers (op-amps) for both the bootstrapping/voltage follower and transimpedance amplifier (TIA). The non-inverting input of the TIA was connected to the 0V line defined between the positive (+5 V regulated) and negative (-5 V regulated) power supplies. The principal differences between the two versions of the thermometer were: the use of surface mounted components for the application prototype thermometer, to create the 25 mm x 25 mm transimpedance amplifier PCB and the fibre optic material used to couple the sensor to the object being measured.

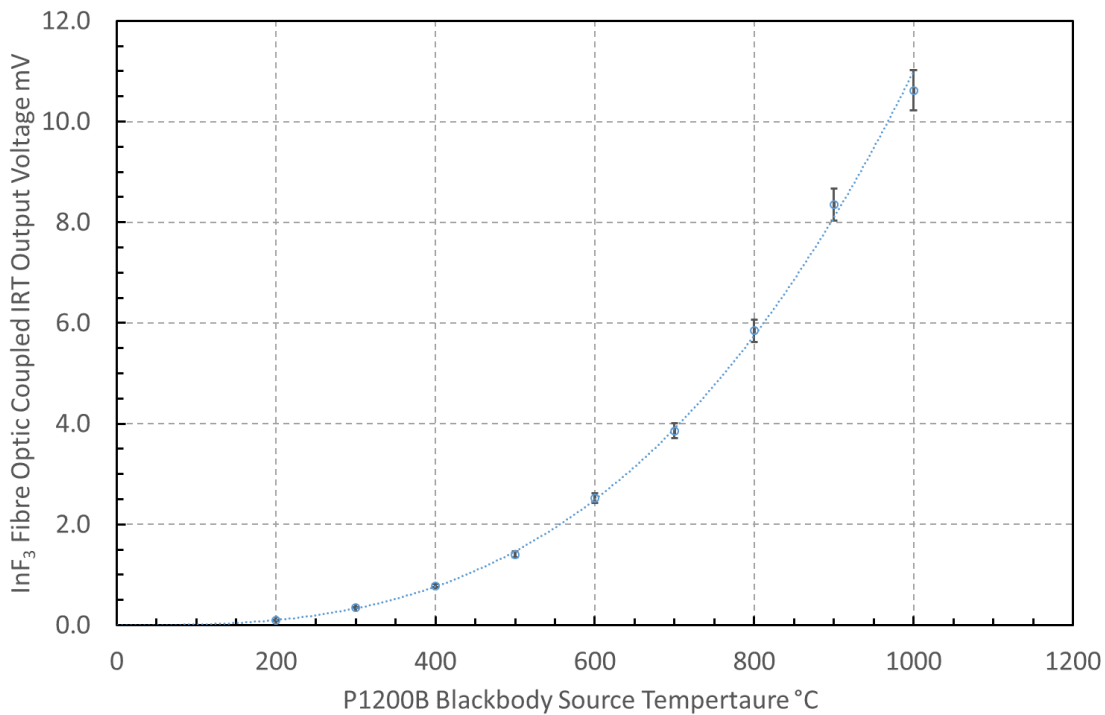


**Figure 4.10 InF<sub>3</sub> fibre optic coupled infrared thermometer TIA output voltage variation with blackbody source temperature characteristic**

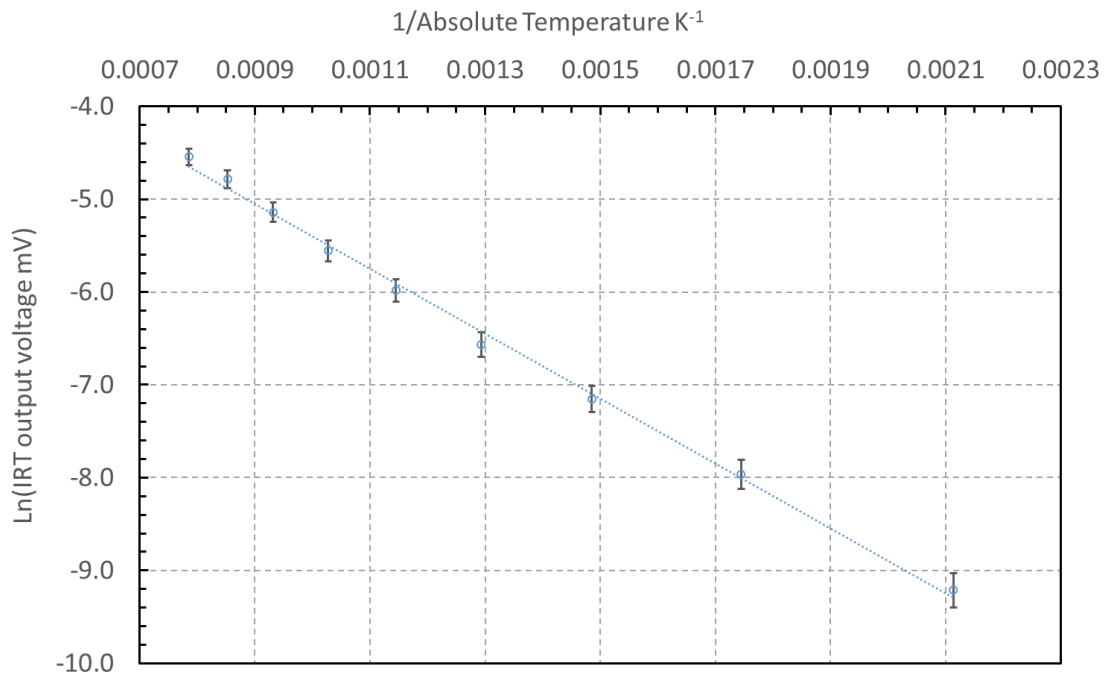


**Figure 4.11 Characteristic natural logarithm of the thermometer output voltage versus inverse of absolute temperature curve for the  $InF_3$  fibre optic coupled prototype infrared thermometer for machining applications**

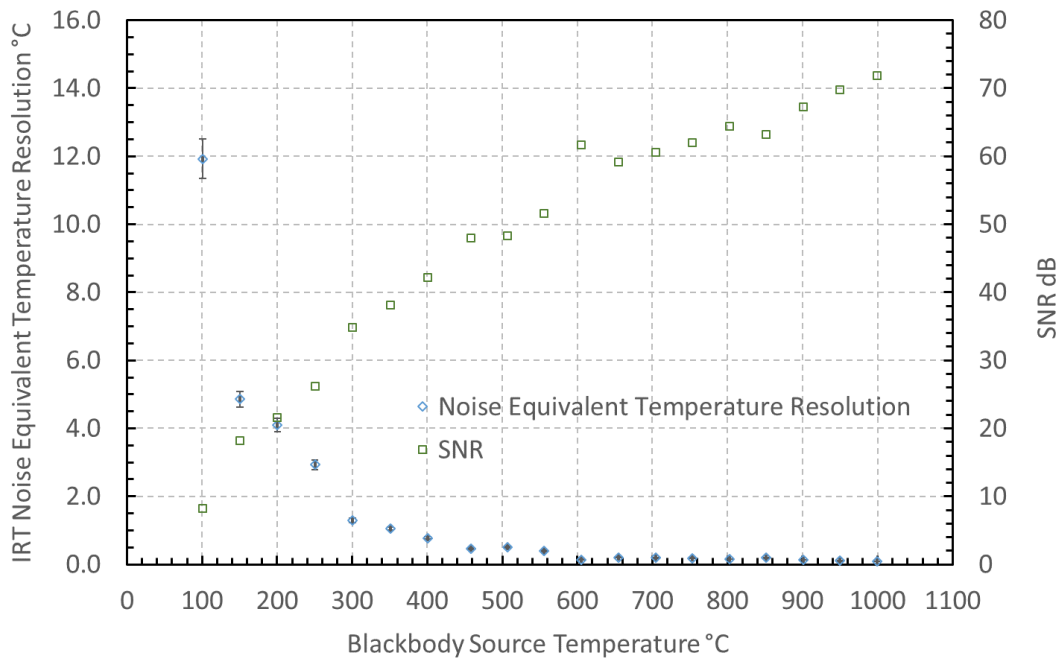


**Figure 4.12 Noise limited equivalent temperature resolution and SNR of InF<sub>3</sub> fibre optic coupled prototype IRT for end milling application**

The characteristic thermometer output voltage variation against source temperature, with extrapolation beyond the upper and lower blackbody source temperatures measured, was used as a practical calibration for the thermometer. A model of the output voltage versus temperature curve was defined using the Sakuma-Hattori equation for interpolation and extrapolation [6]. The curve fit achieved the scaling coefficient 141.6 mV through the temperature range 200-1000 °C at a limiting effective wavelength of 4.1 μm. This practical calibration of the thermometer afforded estimation of the cutting tool insert temperatures during end milling of a sample Titanium plate.

#### 4.4 Application of IRT to cutting tool temperature measurement

The application MWIR thermometer, with fibre optic coupling, was used to measure the surface temperature of a cutting tool insert during end-milling of Titanium plate. The tool holder rotated at several thousand revolutions per minute and the whole unit was swept along the length of the stationary work-piece, whilst varying the lateral depth of cut and vertical depth of cut/height of the tool. Four triangular-shaped tool

inserts (as illustrated in figure 4.14) mounted on the tool holder performed the actual cutting process as the holder was driven along the plate. The configuration of milling head, tool inserts and work-piece, along with the fibre optic embedded into the tool insert are illustrated in figures 4.13 and 4.14.

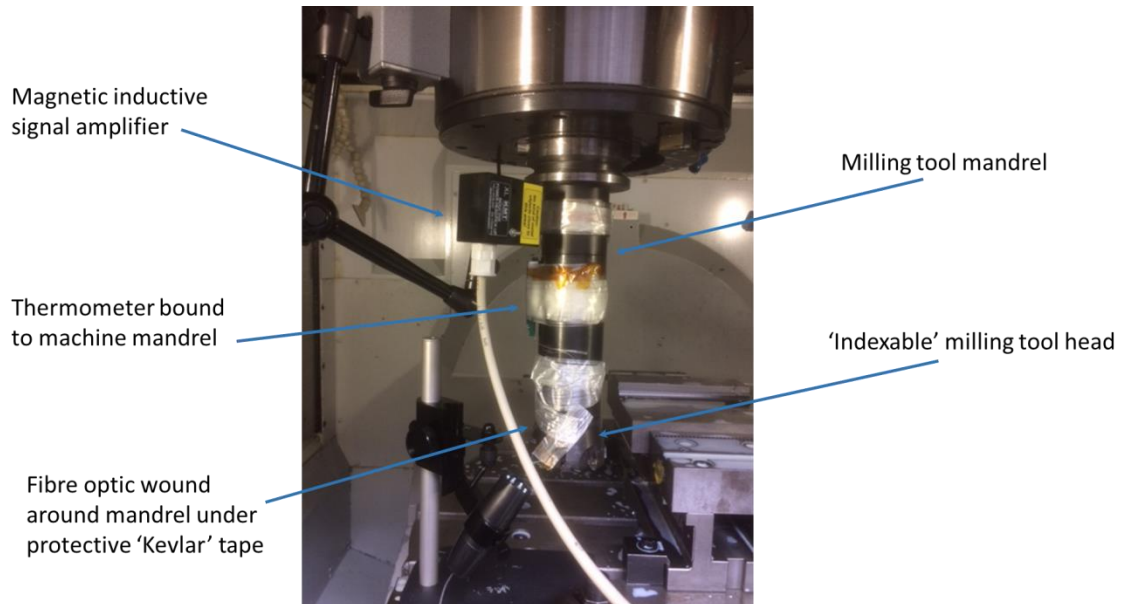


**Figure 4.13 Milling machine set up for trial of MWIR thermometer, with annotation of the key features of the trial arrangement.**

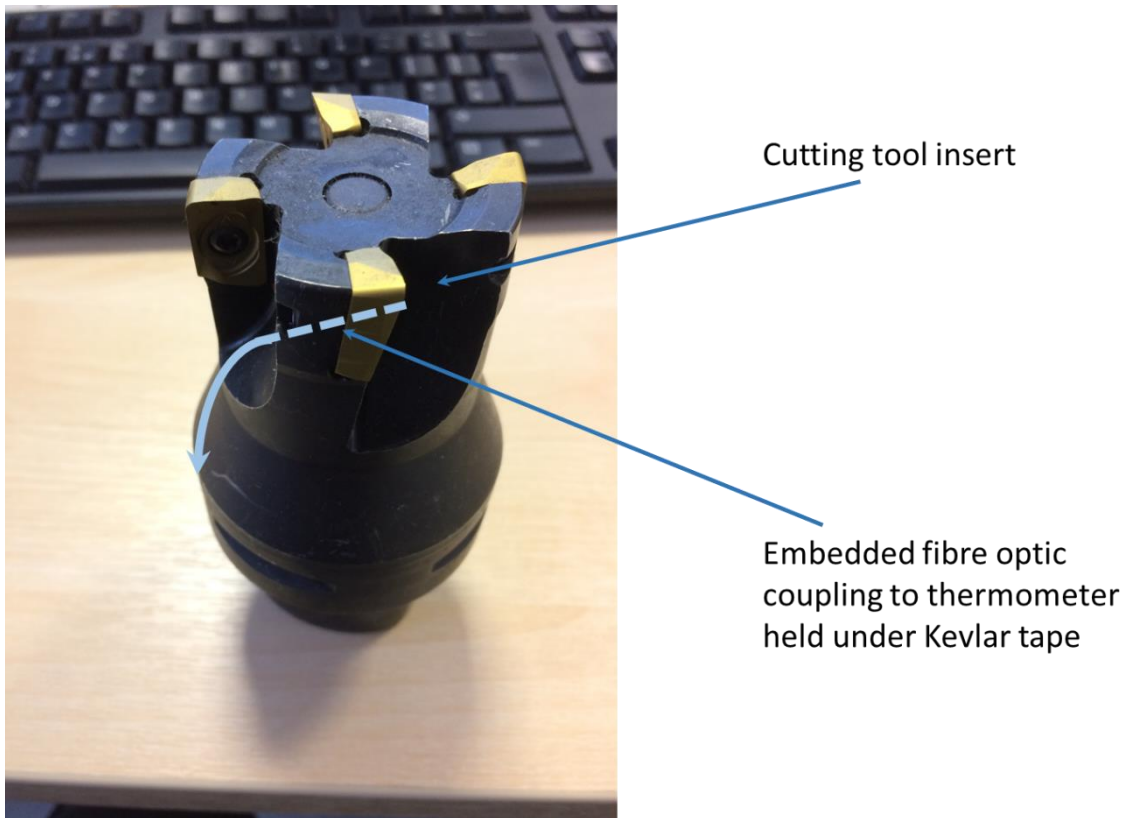


**Figure 4.14 'Indexable' milling tool head and cutting tool inserts, illustrating path of fibre optic embedded into the back of the tool insert and through the tool head, then exiting to pass along the machine driveshaft to the thermometer.**

Development of the laboratory prototype led to a successful configuration comprising two Linear Technologies LT1012 precision operational amplifiers (op-amps). The op-amps were eight-pin, surface mount, integrated circuit components and were used in the bootstrapping/voltage follower and transimpedance amplifier (TIA) stages, as described in chapters 2 and 3. The feedback to the inverting input of the TIA comprised 1 M $\Omega$  resistance and 10 pF capacitance positioned in parallel that formed a resistor-capacitor (R-C) network with an integration time constant of 10  $\mu$ s. The R-C network integration time constant determined an alternating signal cut-off frequency of 15.9 kHz, which was sufficiently high to capture signals from milling at the expected sample interval of 1 ms, that is equivalent to capturing a 1 kHz signal, without loss.

The thermometer PCB was mounted inside the milling machine, attached to the vertically-oriented, rotating spindle and coupled directly to the output end of the fibre

optic, the opposite end of which was embedded into the dead-end hole in the cutting tool insert. The inserted depth of the fibre optic that was also exposed to the inner surface of the dead-end hole represented measurement from a cavity that approximated blackbody conditions, similarly to the laboratory characterisation tests, described in chapter 3. The dead-end hole was formed to provide a clearance fit around the fibre optic, having a diameter that was marginally larger than a 'size-for-size fit' for the exposed fibre optic core diameter. This sizing was intended to minimise the chance of damaging the fibre optic during insertion and by movement once it was mounted in position. A silicone-based adhesive and sealant (Silicone 3145 from Dow Corning Chemical Company) was used to seal the fibre optic at the exit point of the hole and to secure the inner protective jacket to the back surface of the cutting tool insert. The sealant ensured that the fibre optic stayed in position during manipulation and testing, whilst minimising stresses that could break the short length of exposed core. The fibre optic was further protected by self-adhesive glass fibre reinforced tape that bound it to the milling machine tool holder, thereby restricting any movement that could occur and damage to the fibre optic caused by external bodies.

The cutting tool insert was subject to the harsh conditions of cyclic temperature and abrasion against the metal surface and impact from loose 'swarf' ejected by the milling operation. The thermometer system developed had 25 mm x 25 mm footprint and small mass to mitigate against any potential problems induced by mounting the thermometer on the rotating spindle within the machine, particularly: imposing eccentricity on the rotation of the spindle or the thermometer board becoming loose and being ejected into the machining chamber. The fibre optic used in the prototype trials was Indium Fluoride ( $\text{InF}_3$ ), which was capable of withstanding the temperature to which the cutting tool body was exposed and transmitted longer wavelengths than the original sapphire fibre optic. This enabled a lower temperature to be measured than the laboratory prototype allowed, with the voltage output versus temperature curve determined using extrapolation of the Sakuma – Hattori curve fitted to the calibration measurements.

The compact, InF<sub>3</sub> fibre optic coupled, infrared thermometer was used to measure the temperature of a milling tool insert during cutting passes of an end mill across a Titanium plate. The temperature measurements acquired during initial testing of the thermometer with an Indium Fluoride fibre optic embedded into the cutting tool insert and the continuously averaged mean are presented in figure 4.15.

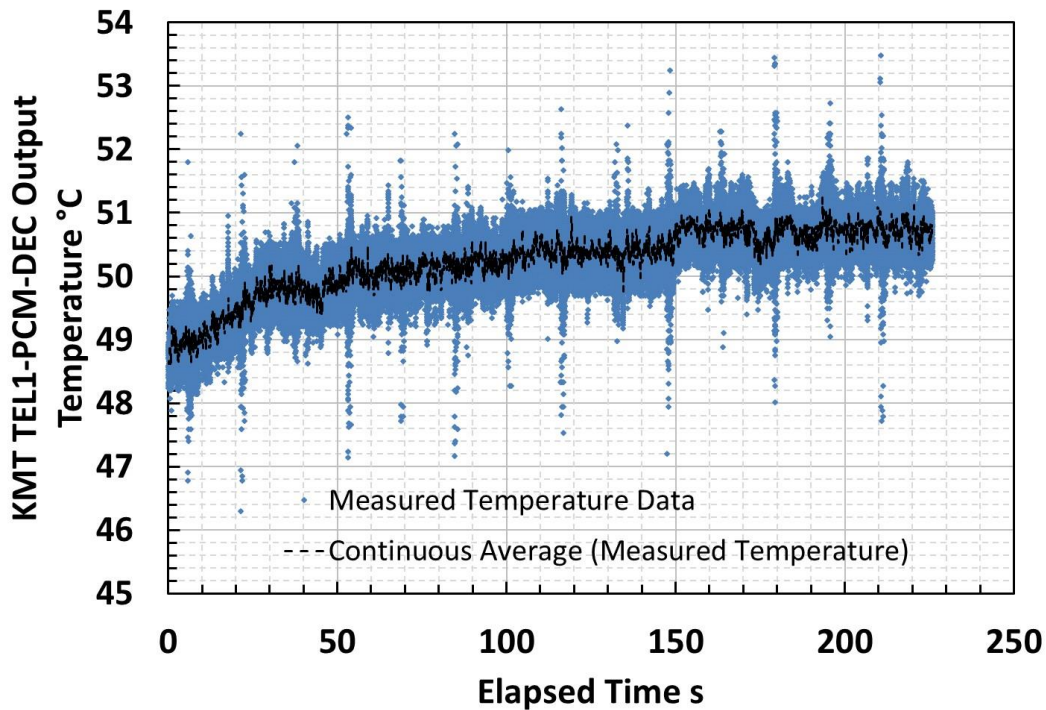


**Figure 4.15 Measurements and continuously averaged mean of cutting tool temperature during end milling of Titanium plate**

The continuously-averaged mean temperature demonstrated increasing cutting tool temperature during the milling head pass, with a similar shape observed to the time versus temperature characteristic measured using an embedded thermocouple during a separate set of cutting tests and with the measurement made using a different cutting tool insert and illustrated in figure 4.16. The signal measured using the prototype MWIR thermometer was noisy, with any cycles of the temperature present within the cutting progress being hidden by the peak-to-peak noise. There may be scope to increase the signal filtering or increase the duration over which continuous-averaging was undertaken to eliminate more of the noise, accepting that there would be a consequent loss of information because the upper and lower bounds of the signal could be clipped by filtering and the signal magnitude reduced by averaging.

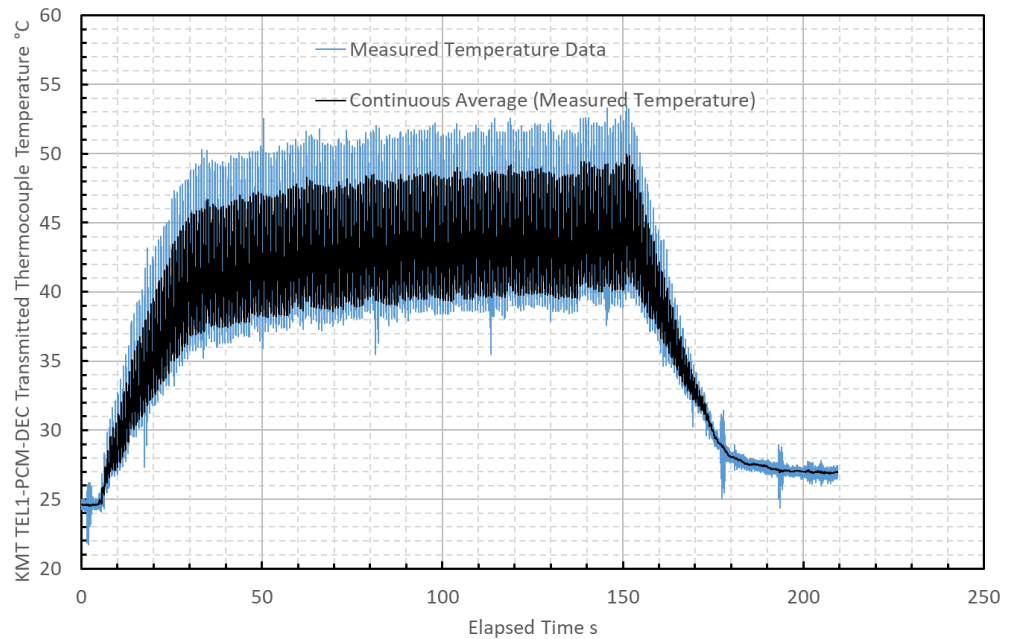


**Figure 4.16 Thermocouple measurements of cutting tool insert surface temperature during separate trials of end milling of Titanium plate.**

The shape of the temperature curve from the IRT in figure 4.15, rising from the initial temperature to a plateau compares with similar cutting operations measured by an embedded thermocouple and presented in figure 4.16. The IRT data had not captured the start and end points of the process or the variations fully but some part of the temperature curve only. Although not capturing the temperature changes of the tool fully during this trial, this graph demonstrated that it was feasible to measure temperatures from a fibre-optic cable embedded into a cutting tool insert, in principle.

The fibre optic used in the milling trials proved to be susceptible to damage by the metal ‘swarf’ that is formed during cutting and stress from being bound tightly to the rotating machine spindle. The swarf sometimes became caught temporarily by the rotating milling head and created a flailing length of metal that could be seen to present a risk to any sensitive equipment mounted on or adjacent to the milling head. The fibre optic was found to have broken at the position that it was embedded into the cutting tool insert, where a short length of the fibre was exposed from the outermost protective jacket to allow the adhesive to bond the fibre into the hole and seal the inner jacket onto the rear surface of the cutting tool. The prototype thermometer fibre optic embedding method proved to be insufficiently robust to capture multiple passes of the

cutting tool head along the plate. The weakness introduced by having the protective jacket stripped back to enable embedding of the fibre optic into the cutting tool insert and adhesion/sealing of the inner jacket onto the back of the tool insert surface would need to be improved to afford successful substitution for thermocouple temperature measurements in machining processes.

The sensitivity of the fibre optic coupled MWIR thermometer used in the cutting trials was low, achieving TIA output voltages of 13.7  $\mu\text{V}$  at 100  $^{\circ}\text{C}$  source temperature, 10.6 mV at 1000  $^{\circ}\text{C}$  source temperature and a mean value of  $\Delta V_o/\Delta T$  of 11.8  $\mu\text{V}/^{\circ}\text{C}$  through the source temperature range 100-1000  $^{\circ}\text{C}$ . The sensitivity of the thermometer was demonstrated have a similar order of magnitude to thermocouples, so would need to be increased to afford higher signal to noise ratio necessary for faster signal acquisition of low temperature radiation. The fibre optic used in the trial had a 100  $\mu\text{m}$  diameter Indium Fluoride glass core. Fluoride glass fibre material can be formed into larger diameters, providing signal throughput that increases by a factor of the square of the diameter. One consequence of increasing the fibre-optic cable diameter is that the minimum bend radius that can be accommodated before the glass of the fibre optic incurred fracturing increased, presenting additional challenges to mounting the cable inside a machine. Maximising the fibre optic core diameter that can be embedded into a process would provide the maximum signal to noise ratio possible for a given tool insert and hole diameter. The diameter chosen is compromised by the reduction in cable flexibility and increased minimum bend radius of larger diameter fibre optics.

Further improvement of the minimum temperature measurable by the thermometer could be achieved by increasing the transimpedance value to increase the effective gain of the TIA. The maximum value of the feedback resistor would be constrained to approximately 8 M $\Omega$  owing to the increased integration time of the R-C network and lower cut-off frequency for alternating signals that would occur in consequence.

## Summary of application of prototype IRT to end milling

The prototype MWIR thermometer was used to measure the surface temperature of a cutting tool insert on an end milling machine. The exposed tip of a small diameter fibre optic was embedded into a 0.5 mm diameter dead-end hole, that was bored from the back surface of the tool and finished at a position 0.5 mm below the cutting surface.

This hole acted as an approximate blackbody and the infrared radiation emitted from the surface of the tool whilst it was heated during contact with the work-piece was coupled to the thermometer via the fibre optic. The configuration of the hole into which the fibre optic was embedded replicated the configuration used for embedding thermocouples to measure temperatures of end milling tool inserts.

The thermometer PCB was mounted onto the shaft of the end milling machine and incurred rotation at speeds of several thousand revolutions per minute, thereby was constrained to have low mass and required binding to the shaft to prevent vibration of the rotating shaft and separation of the PCB from the shaft.

The feasibility of using the prototype IRT coupled to an embedded fibre optic to substitute for embedded thermocouple measurement of the cutting surface temperature of an end milling tool insert was demonstrated.

Application of the prototype thermometer to end milling would require that the fibre optic coupling be made more robust because the fibre was exposed to mechanical damage at the point of entry into the cutting tool insert. This weakness limited severely, the number of operations for which the thermometer could be used. In trial conditions, the fibre optic coupling to the thermometer survived only two passes of the cutting tool along a test plate, after which the fibre optic had been sheared through by metal swarf ejected from the milling process. Engineering more robust thermometers would be necessary to acquire measurements continuously from machining processes.

## REFERENCES

- [1] Hamamatsu Photonics, 'InAsSb photovoltaic detector P13243-11-MA Datasheet', *Hamamatsu P13243 Series Datasheet*. 2015.
- [2] Hamamatsu Photonics, 'S1087/S1133 Si Photodiodes Datasheet'. pp. 1–5, 2014.
- [3] J. W. Hahn and C. Rhee, 'Interpolation equation for the calibration of infrared pyrometers', *Metrologia*, vol. 31, no. 1, pp. 27–32, 1994.
- [4] Hamamatsu Photonics, 'InGaAs PIN photodiodes G12180 data sheet', no. 4. pp. 1–8, 2018.

- [5] W. M. Leach, 'Fundamentals of Low-Noise Analog Circuit Design', *Proc. IEEE*, vol. 82, no. 10, pp. 1515–1538, 1994.
- [6] F. Sakuma and S. Hattori, 'Establishing a practical temperature standard by using a narrow-band radiation thermometer with a silicon detector', in *TEMPERATURE: ITS MEASUREMENT AND CONTROL IN SCIENCE AND INDUSTRY, VOLUME 5, PART 1: Proceedings of the Sixth International Temperature Symposium*, 1982, vol. 5.1, pp. 421–427.
- [7] P. Saunders, 'General interpolation equations for the calibration of radiation thermometers', *Metrologia*, vol. 34, no. 3, pp. 201–210, 1997.
- [8] M. Bacci da Silva and J. Wallbank, 'Cutting temperature: prediction and measurement methods—a review', *J. Mater. Process. Technol.*, vol. 88, no. 1–3, pp. 195–202, 1999.
- [9] G. Le Coz, M. Marinescu, A. Devillez, D. Dudzinski, and L. Velnom, 'Measuring temperature of rotating cutting tools: Application to MQL drilling and dry milling of aerospace alloys', *Appl. Therm. Eng.*, vol. 36, no. 1, pp. 434–441, 2012.
- [10] Q. Wang, P. Ping, X. Zhao, G. Chu, J. Sun, and C. Chen, 'Thermal runaway caused fire and explosion of lithium ion battery', *J. Power Sources*, vol. 208, pp. 210–224, 2012.
- [11] X. Feng, M. Ouyang, X. Liu, L. Lu, Y. Xia, and X. He, 'Thermal runaway mechanism of lithium ion battery for electric vehicles : A review', *Energy Storage Mater.*, vol. 10, no. May 2017, pp. 246–267, 2018.
- [12] P. G. Balakrishnan, R. Ramesh, and T. Prem Kumar, 'Safety mechanisms in lithium-ion batteries', *J. Power Sources*, vol. 155, no. 2, pp. 401–414, 2006.
- [13] A. Queck, et al, 'Advanced measurements and dynamic modelling for improved furnace operation and control (DYNAMO)', European Commission Directorate-General for Research and Innovation, Final Report EUR 28146 EN, 2016. ISBN 978-92-79-62951-8 doi:10.2777/338050.
- [14] G. R. Peacock, 'Radiation Thermometers in Steel and Metals Processing', *AIP Conf. Proc.*, vol. 684, no. October, pp. 813–818, 2003.

- [15] D. Soler, T. H. C. Childs, and P. J. Arrazola, 'A note on interpreting tool temperature measurements from thermography', *Mach. Sci. Technol.*, vol. 19, no. 1, pp. 174–181, 2015.
- [16] E. M. Sparrow, L. U. Albers, and E. R. G. Eckert, 'Thermal radiation characteristics of cylindrical enclosures', *J. Heat Transfer*, vol. 84, no. 1, pp. 73–81, 1962.
- [17] J. Vollmer, 'Study of the effective thermal emittance of cylindrical cavities', *J. Opt. Soc. Am.*, vol. 47, no. 10, pp. 926–932, 1957.

## 5 DEVELOPMENT OF ZERO DRIFT, LOW TEMPERATURE RANGE, FIBRE OPTIC THERMOMETER AND APPLICATION TO BATTERY TEMPERATURE MEASUREMENTS

Thermocouples afford measurement over a wide range of temperatures, typically enabling continuous measurement from zero to many hundreds Celsius. Substitution of thermocouples by infrared radiation thermometers (IRTs) requires the capability to measure similar temperature ranges. The prototype mid-wave infrared (MWIR) thermometers of chapter 4 did not have sufficiently low minimum temperature measurable to substitute for thermocouples through all temperature ranges encountered in manufacturing and industrial processes. The MWIR thermometers were developed further to achieve measurement of lower minimum temperatures. The capability of measuring from ambient temperature was desirable for an IRT that could be substituted for thermocouples in lower temperature applications, for example: the measurement of battery cell temperatures during charging and discharging.

The Chemical and Biological Engineering (CBE) department at University of Sheffield operate a Lithium battery cell laboratory, in which cells can be manufactured and tested to understand the mechanisms incurred during real operating cycles. Temperature achieved by the components and electrolyte during charging and discharging of cells is an important parameter that affects the electrochemistry and longevity of cells. Typically, cell temperatures have been measured using

thermocouples bonded to the cell casing and internal temperatures measured using thermocouples embedded into the cell during construction. The CBE department have used infrared thermography cameras to image the temperature distribution of cell casings and wished to utilise infrared thermometry to measure the internal temperature of cells undergoing test cycles. The compact IRT developed within this project provided a prototype device that could use a fibre optic embedded into a cell and isolate the measurement electronics outside of a cell. This would enable the temperature adjacent to the reactive Lithium-ion electrolyte to be measured, whilst the cells were cycled within a controlled-environment test chamber. No such IRT existed commercially, therefore development of the prototype would enable the CBE researchers to measure internal temperatures better than embedded thermocouples and to apply this new knowledge to understanding the performance of cells undergoing test.

Typically, low temperature range infrared thermometers use either:

- Photo-electronic Mercury Cadmium Telluride (MCT) photodiodes that can be operated in the MWIR or long-wave infrared wavelength range, depending upon the alloy composition used and cooling applied
- Thermal detectors, such as, thermopiles and bolometers that respond to all radiation incident upon the surface, often referred to as broad spectrum or total radiation thermometers

Photodiodes and thermal detectors used to measure over longer wavelength ranges are subject to larger magnitude temperature measurement uncertainties arising from emissivity errors because of the relationship with wavelength that was presented in chapter 2:

$$\Delta T = \frac{\lambda T^2}{c_2} \frac{\Delta \varepsilon}{\varepsilon}$$

where:

$\Delta T$  is the error in the radiance temperature measured, K

$c_2$  is the second Planck radiation constant 0.014387752 m K

$\lambda$  is the limiting effective wavelength at which the IRT measured, m

$T$  is the absolute temperature of the object, K

$\Delta\epsilon$  is the difference in emissivity between the object and blackbody

It was desirable to use photodiodes that responded to the shortest range of wavelengths that would provide measurement over the low temperature range required to minimise this uncertainty.

MCT photon detectors have been used in low temperature thermometers but required thermoelectric cooling to reduce the dark current and Johnson noise, whilst increasing the photosensitivity to enable the measurement of low intensities of MWIR radiation. Cooling a photon detector increases the cost and size of thermometers, therefore disallowing their use in size-constrained locations. Thermopiles and bolometers, can measure within the MWIR spectral range but have slow response speeds and low sensitivity compared to photon detectors [1]. Both MCT and thermal detectors incur output drift, particularly related to thermometer ambient temperature, which leads to increased measurement uncertainty.

Typically, IRTs that use photodiodes have a transimpedance amplifier (TIA) to output a measurable voltage from the photocurrent generated. The low shunt resistance of MWIR photodiodes enables some of the photocurrent to flow through the photodiode, rather than generating output voltage via the TIA, as presented in chapters 1 and 2. The input voltage offset and noise are amplified by the transimpedance and combined at the TIA as an output voltage offset. Variation of the output voltage offset and shunted current cause non-linear thermometer characteristics that have constrained the capability of MWIR thermometers to achieve low temperature measurements with low uncertainties, particularly using uncooled detectors [2], [3].

Compromising between the capability to measure low intensity infrared emitted from low temperature sources and having a compact thermometer led to further development of the bootstrapped Indium Arsenide Antimony (InAsSb) thermometer of chapter 4. The noise and offset voltage of the TIA were identified as limiting the capability of the thermometer to measure lower temperatures [3]. Sakuma and Hattori noted that the amplifier noise and offset voltage were limiting the capability to measure low temperatures in their research into developing a standard infrared radiation thermometer [4] and this limitation was also noted during the development

of the laboratory prototype InAsSb thermometer [5]. Reduction of the input voltage offset of the TIA would enable the minimum temperature measurable by the IRT to be reduced [4], [6]. The minimum temperature measurable for the prototype IRT was defined as the temperature for which there was unity signal to noise ratio (SNR) at the TIA output [5]. Achieving lower minimum temperature measurable than the laboratory prototype demanded the use of higher transimpedance values, which presented higher effective gain to both the signal and noise. Reduction of the noise and offset magnitudes were essential to allow higher transimpedance values to be used. Using larger resistor values increased the integration time of the resistor-capacitor (R-C) feedback loop. Increasing the integration time over which the mean output voltage and the variation around the mean were evaluated also improved the SNR of the thermometer, in accordance with the analysis by Bielecki [7]:

$$SNR = \frac{V_o}{V_{RMS\ Noise}} = \frac{2V_i^2 t}{S_n}$$

where:

$V_o$  is the signal, determined as the mean output voltage of the TIA

$V_{RMS\ Noise}$  is the noise on the output voltage of the TIA

$V_i$  is the input voltage to the TIA

$t$  is the total integration time over which the mean and standard deviation of the output voltage were calculated (for discrete values this value would be  $mt$  where  $m$  represents the number of values and  $t$  the increment of time between measurements)

$S_n$  is the noise spectral density of the signal

For constant noise spectral density,  $S_n$  and input voltage to the TIA,  $V_i$  having an increased integration time of the R-C network (by increasing the transimpedance value by a factor of ten) also led to an increased SNR by the same factor.

## Part I: Zero Drift Op-amp Thermometer Development and Characterisation

### 5.1 Zero drift op-amp thermometer development

A zero drift operational amplifier (op-amp) incurs very low offset voltage, offset voltage drift and low noise magnitude. Zero drift op-amps modulate the input voltage with a square wave carrier signal and demodulate the resulting signal to isolate the output voltage from low frequency noise. This modulation and demodulation occurs within the amplifier integrated circuit, using transistor switches to afford kilohertz modulation frequencies. This modulation method results, ultimately, in the very low offset voltage and offset voltage drift offered by the zero-drift op-amp [8], [9]. Using a zero drift op-amp within an IRT that has an uncooled photodiode should enable the measurement of lower minimum temperatures without compromising the thermometer response speed, sensitivity or measurement uncertainty.

Different combinations of op-amps were trialled to identify the configuration that enabled low noise and voltage offset from candidate amplifiers selected from the results of modelling the TIA output voltage and noise. Typically, op-amps that offered the fastest response and lowest input noise voltage, incurred high offset voltage approaching 1.0 mV at the TIA input [10], therefore were considered a sub-optimal compromise. The offset voltage would require compensation to alleviate the consequent offset being propagated to the output voltage with amplification through the TIA. The offset voltage and noise voltage for each of the op-amps tested in the TIA circuit, Linear Technologies LT1012 and LTC2050 and Texas Instruments OPA627 and OPA657, were specified to be of the order of micro-Volts [8], [9], [11]–[13] thereby, presenting several orders of magnitude lower offset voltage than the high speed, low noise op-amps reviewed for transimpedance amplifiers in previous studies [10].

The combinations of Linear Technologies (designated as LT or LTC) and Texas Instruments (designated as TI) op-amps tested and the output voltage offset that limited the measurement resolution when amplified through 10 M $\Omega$  transimpedance are presented in table 5.1. The combinations presented had a range of offset voltages that would be acceptable but the combination of LT1012 or OPA 627 bootstrap and LTC2050 TIA (rows 2 and 6 of the table below) offered the lowest offset voltages

modelled. It was evident that having the zero drift op-amp TIA would be expected to provide the lowest offset voltage on the thermometer output.

**Table 5.1 Combinations of op-amps identified by modelling as offering lowest offset voltage and noise from modelling and subsequently tested at laboratory conditions**

Bootstrap Op-amp	TIA Op-Amp	Offset Voltage Modelled at Output with 10 M $\Omega$ R $_f$ $\mu$ V
LT1012	LT1012	1.0
LT1012	LTC2050 Zero Drift	0.6
TI OPA627	TI OPA657	2.7
LT1012	TI OPA627	5.5
LT1012	TI OPA657	5.5
TI OPA627	LTC2050 Zero Drift	0.4

These six candidate combinations were configured as low temperature prototype IRTs with the InAsSb photodiode and used 600  $\mu$ m diameter core ZBLAN glass fibre optic to couple infrared radiation. ZBLAN glass fibre optic transmitted radiation over the wavelength range 0.2 – 4.5  $\mu$ m [14] that included most of the MWIR wavelength range to which the InAsSb photodiode responded [15]. ZBLAN was available readily with core diameters that were larger than the Indium Fluoride fibre optic used for the measurements in chapter 4. The transmission range and diameter of the ZBLAN fibre optic combined to afford the lowest minimum temperature measurable of the configurations of fibre optics and photodiodes used, nominally 50 °C, as presented in table 2.1 of chapter 2.

These low temperature versions of the prototype IRT used 10 M $\Omega$  feedback resistors to increase the transimpedance and achieve an effective ‘gain’ between the photocurrent and TIA output voltage equivalent to 140 dB. The revised thermometers were evaluated to have lower maximum temperature measurable of 670 °C, above which temperature the TIA output voltage would saturate. This exceeded the maximum temperature expected from battery cell cycling, nominally 60 – 70 °C, by an order of

magnitude [16]. Evidently, the low temperature IRTs configured could be useful in this application. The maximum temperature that the thermometer could measure would be extendable by increasing the power supply voltage and deploying suitable op-amps.

## 5.2 Comparison of low temperature IRT configurations using zero drift and precision op-amps

Identical low temperature range prototype IRTs were configured except for the op-amp used in the TIA. The IRT versions tested used the LT1012 precision op-amp and LTC2050 zero drift op-amp in the TIAs. The TIA feedback resistance and capacitance was 10 M $\Omega$  and 10 pF in both IRT versions. The R-C time constant of this thermometer was calculated to be 100  $\mu$ s, thereby providing faster response than could be achieved by thermocouples or thermal detector based IRTs.

### 5.2.1 Comparison of precision op-amp and zero-drift op-amp IRTs measuring steady-state temperatures

Comparisons were undertaken to determine the capabilities of the IRTs to maintain a nominal zero value when the thermometers were blanked by a cover at ambient temperature and a steady-state value when the photodiodes were exposed to a source at an arbitrary steady-state temperature of 700 °C. The thermometers measured the same radiant source concurrently and from adjacent positions, thereby ensuring that no difference arose from systematic errors with the experimental configuration. The TIA output voltages were recorded on a pair of Keysight Technologies 34465A digital multi-meters with identical configurations to measure and store data. Measurements were recorded at 1 minute intervals for three consecutive durations of 100 hours each. The data sets were concatenated to provide contiguous thermometer output voltage measurements over 300 hours' duration.

The configuration of the blackbody source and photodiodes is illustrated in figure 5.1, noting that the photodiodes were connected to separate TIAs and multi-meters.

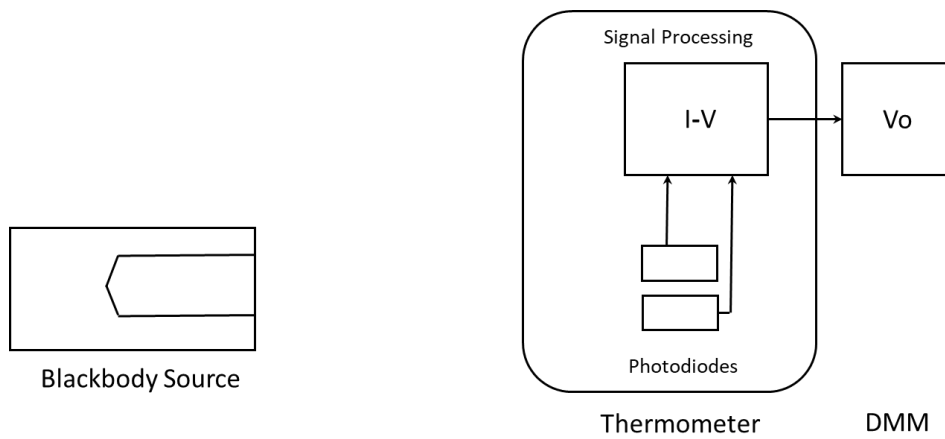


**Figure 5.1 Schematic diagram illustrating configuration used to test two prototype thermometers concurrently, viewing similar source temperatures**

The output voltages measured from the thermometers under the zero signal conditions were interpreted as resulting from the total of the offset voltage and noise. The source was changed from providing a zero signal condition to both of the thermometers receiving infrared radiation from an Ametek Land Instruments Landcal P1200B approximate blackbody source, set at an arbitrary and constant temperature of 700 °C. The noise power on the output voltage was represented by the variance around the mean in both zero signal and steady-state signal tests. It was not critical that identical conditions were achieved for each thermometer because small differences between the mean output voltages would not influence the variances. The excess kurtosis values of the measurements were evaluated to indicate whether the distributions had extensive or restricted tails and to indicate how much extremal values affected the variances.

### 5.2.2 Characterisation of precision op-amp and zero-drift op-amp IRTs over low temperature ranges

The output voltages of the IRTs configured using the zero drift op-amp and precision op-amp were characterised as a function of the temperature of an Ametek Land Instruments, Landcal P80P approximate blackbody source. The blackbody source temperature was calibrated prior to characterisation of the IRTs, using an Isothermal Technology Limited, milliK precision thermometer and transfer standard Platinum Resistance Thermometer, as described in chapter 3.

A 150 mm length of 600  $\mu\text{m}$  core diameter, ZBLAN fibre optic cable coupled infrared radiation from the calibration thermo-well in the blackbody source to the thermometers. The length was representative of the fibre optic to be embedded into Lithium-ion pouch cells, therefore characterisation of the thermometer voltage variation with source temperature provided a practical calibration of the IRT. The depth to diameter ratio of the calibration thermo-well and the exposed tip of the fibre exceeded 5:1, which afforded high relative emissivity, approaching blackbody conditions [17], [18].

The thermometer output voltages were measured and recorded using a Keysight Technologies 34465A data-logging, digital multi-meter. The temperature set point of the blackbody source was increased in 10  $^{\circ}\text{C}$  increments between 20  $^{\circ}\text{C}$  and 70  $^{\circ}\text{C}$  and the thermometer output voltages characterised against this sequence of temperatures. The thermometer output voltages at each source temperature were recorded at intervals of 1 s for a duration of ten minutes per measurement. The configuration of the equipment for undertaking thermometer characterisation was the same as presented in Figure 5.1, except that the fibre optic was inserted into the blackbody source thermo-well and coupled infrared radiation directly onto the photodiode.

The mean and standard deviation of the output voltages recorded from the IRTs were evaluated to abstract values that represented each temperature and the noise. The signal to noise ratio was evaluated as the ratio between the mean output voltage and standard deviation around that mean. The noise limited, equivalent temperature resolution of each thermometer was calculated from these measurements.

Wien's approximation enabled evaluation of the ratio between radiances arising from two temperatures to be compared and led to the expectation of a linear relationship between the natural logarithm of the thermometer output voltage ( $\ln(V_o)$ ) and the inverse of the absolute temperature of the source object ( $1/T$ ), as presented in chapter 2. The limiting effective wavelength, that is a monochromatic wavelength abstraction of the thermometer response at different temperatures over a broad wavelength range [19], was calculated from the gradient of the relationship between  $\ln(V_o)$  and  $1/T$ .

These measurements tested the capability of the IRTs to measure low temperatures likely to be encountered on industrial processes [20] and provided practical calibrations of the IRTs through the temperature range 20 °C to 70 °C.

### 5.2.3 Comparison of the capabilities of the IRTs to maintain 'zero' and steady-state output voltages

The capability of the IRTs to maintain steady-state output was determined based upon the variability of output voltage measurements recorded for a source radiating at ambient temperature and the arbitrary, steady-state 700 °C.

The zero drift op-amp TIA afforded a lower magnitude voltage offset apparent at the output than the precision op-amp version, measuring an ambient temperature. The offset voltages achieved mean values of: +0.024 mV for the zero drift op-amp IRT compared with -0.10 mV for the precision op-amp IRT. The output voltage variance of the zero drift op-amp IRT was approximately half the magnitude of the precision op-amp IRT, achieving values of  $8.6 \times 10^{-4} \text{ (mV)}^2$  and  $19.1 \times 10^{-4} \text{ (mV)}^2$ , respectively.

The measurements recorded and histograms for the two thermometers with the photodiodes having no signal are presented in figures 5.2 and 5.3 and exposure to a radiant source at a steady-state temperature of 700 °C in figures 5.4 and 5.5, respectively.

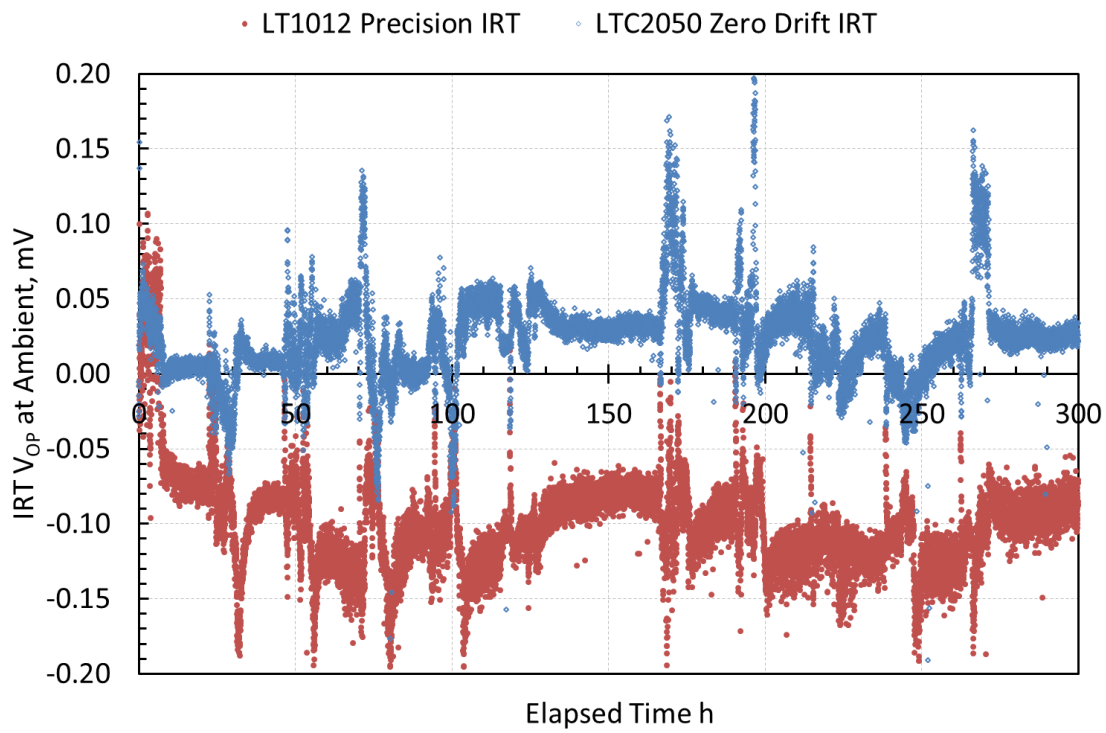


Figure 5.2 IRT Output Voltage with Zero Signal; Time Series Data

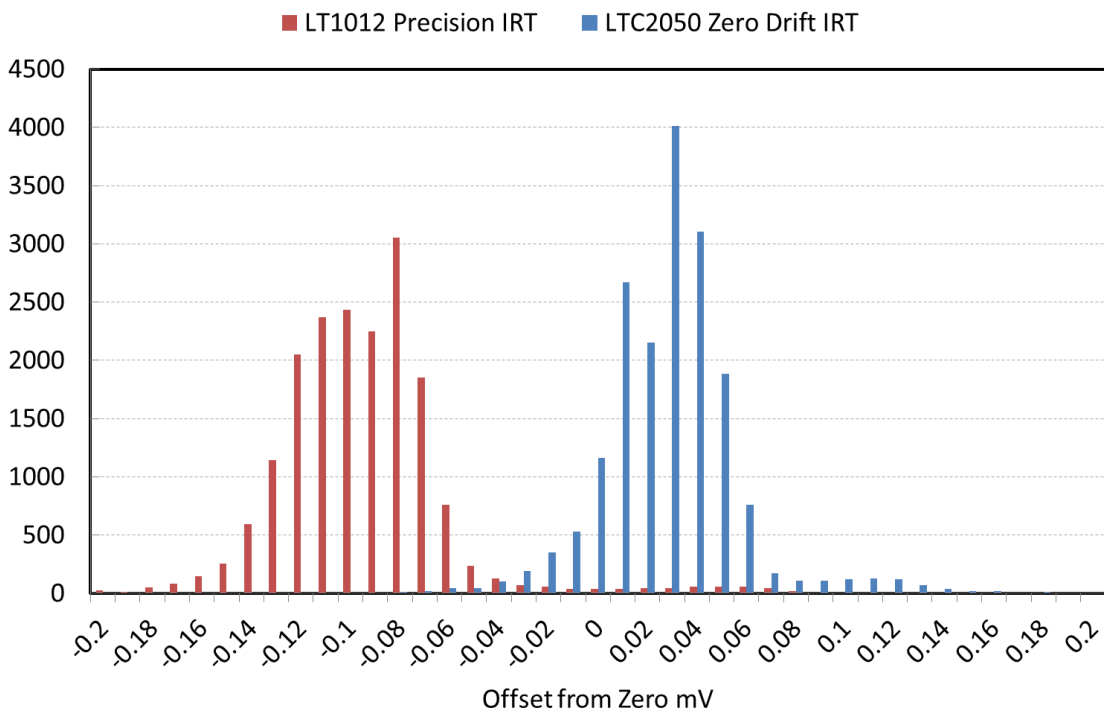
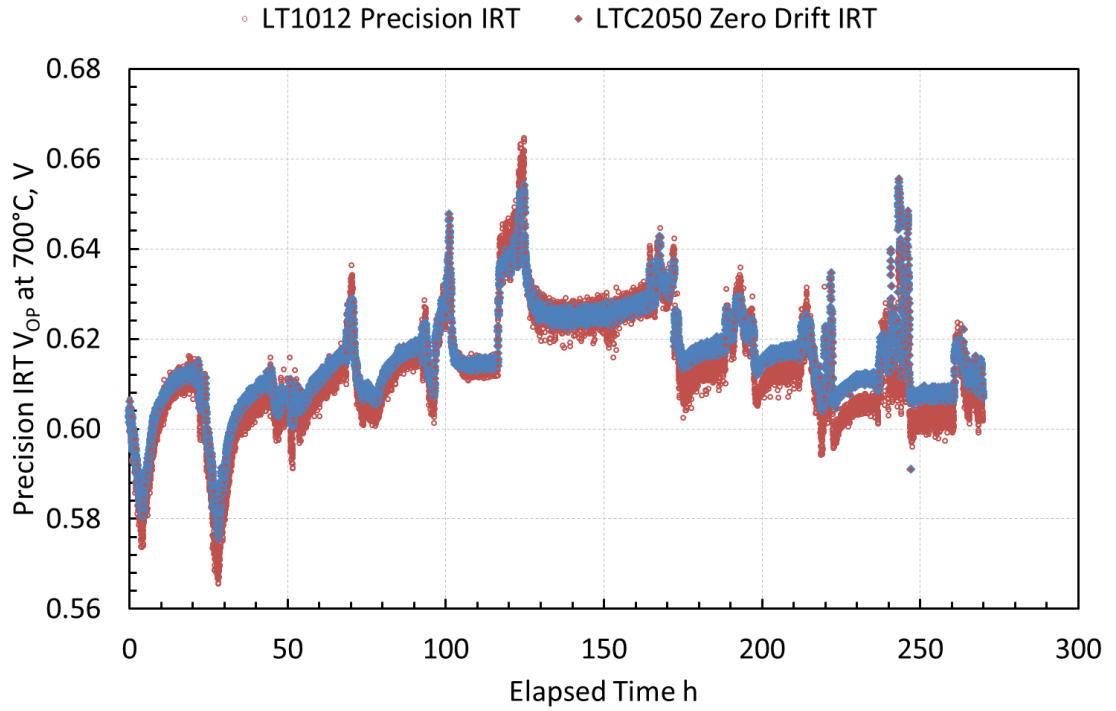
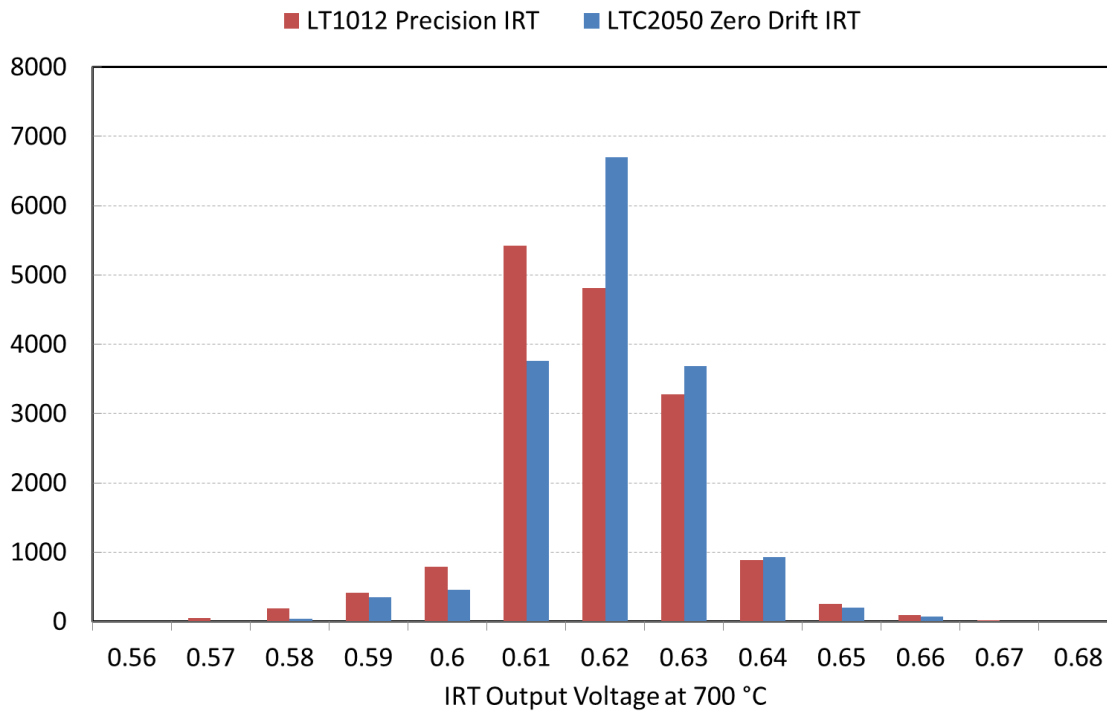


Figure 5.3 IRT Output Voltage with Zero Signal; Histogram of Measurements



**Figure 5.4 IRT Output Voltage Measuring 700 °C; Time Series Data**

graphs, voia.m consecutivem Ikhem lkargericult tonedd till but of course leaves open the question ed, for example:119119119119119119119119119119119119



**Figure 5.5 IRT Output Voltage Measuring 700 °C; Histogram of Measurements**

The variances for the zero drift op-amp IRT can be seen to be smaller than the variances incurred by the precision op-amp version, by inspection of the curves presented in figures 5.2 to 5.5. It was also evident by inspection of figures 5.2 and 5.3, that the zero drift op-amp IRT maintained the nominal ‘zero’ output voltage closer to actual zero millivolts than the precision op-amp version.

Both IRTs demonstrated larger magnitude changes in the output voltage than the noise incurred around the mean values and these had similar magnitudes and occurred concurrently during the steady-state 700 °C set point temperature tests, as illustrated by inspection of figures 5.4 and 5.5. The similarity of magnitude and occurrence of these output voltage changes for both thermometers implied that the cause was common. Comparison of one IRT output voltage variation with the steady-state temperature variation of the blackbody source is presented in figure 5.6.

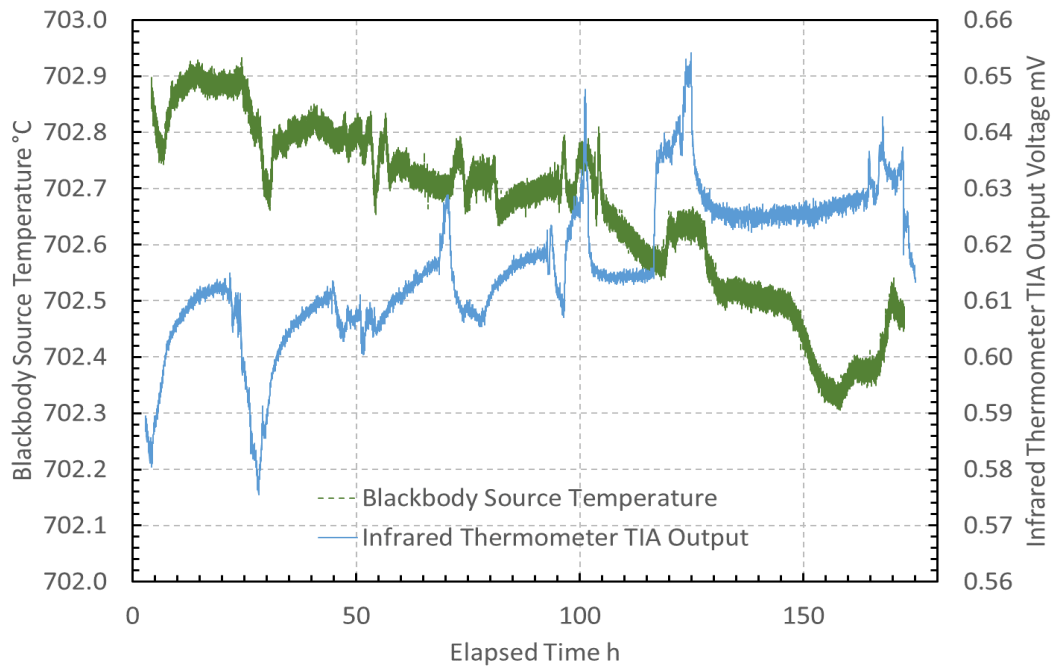


**Figure 5.6 Variation of blackbody source temperature at 700 °C steady-state set point and concurrent infrared thermometer output voltage**

A relationship between the changes in temperature of the blackbody source and changes of the thermometer output voltage existed, although there was only a weak correlation. The apparent relationship was obscured, at least partially, by an underlying drift of the source temperature by approximately 0.6 °C and consequent variation of the thermometer output by approximately 25% of the measured range. These variations caused the simple mean value of the thermometer output voltage to vary by more than would have arisen from true steady-state conditions. The variations in process conditions would not affect the variances around the continuously averaged mean values because these were measured over shorter durations than the time over which the changes occurred.

The precision op-amp IRT incurred a larger magnitude change of the zero than the zero drift op-amp IRT. Observation of the signals in figures 5.2 and 5.3 illustrated the larger drift and cycling incurred by the precision op-amp IRT, having most variation within the range -0.05 mV to -0.10 mV during these zero signal tests. The zero drift op-amp IRT incurred variations mostly between 0.00 mV and +0.05 mV during the same test. Both thermometers demonstrated some larger excursions that occurred randomly during the tests and were probably caused by interference. The precision op-amp IRT incurred more excursions than the zero drift op-amp version.

## 5.2.4 Statistics Describing the Distributions of Measurements

The measurements acquired from the two IRTs at the zero signal and 700 °C conditions were demonstrated to have arisen from independent systems, therefore differences between the mean values, variances and excess kurtosis values calculated were interpreted as arising from the different op-amps used to configure the TIAs.

The mean, variance and excess kurtosis values calculated for the IRT output voltage measurements at the two measuring conditions are presented in table 5.2.

**Table 5.2 Mean, Variance and Excess Kurtosis Values of Precision Op-amp and Zero Drift Op-amp Thermometer Versions.**

Condition	Thermometer Version	Mean V	Variance V <sup>2</sup>	Excess Kurtosis
Zero	Precision Op-Amp TIA	-1.000 x10 <sup>-4</sup>	1.906 x 10 <sup>-9</sup>	416.2
Signal	Zero Drift Op-Amp TIA	2.397 x10 <sup>-5</sup>	8.558 x 10 <sup>-10</sup>	121.4
700 °C	Precision Op-Amp TIA	0.613	1.645 x 10 <sup>-4</sup>	1.22
Signal	Zero Drift Op-Amp TIA	0.616	1.168 x 10 <sup>-4</sup>	1.33

The variances incurred by the measurements using the zero drift op-amp IRT were smaller than the variances incurred by the precision op-amp IRT by factors of 0.46 and 0.71, for the zero and steady-state temperature measurements, respectively.

The high excess kurtosis values demonstrated that extremal values within the measurements led to much of the variances calculated whilst the photodiodes were blanked and less so when measuring the blackbody source at 700 °C. Comparison of the excess kurtosis values indicated that the precision op-amp IRT was subject to more extreme variations from the mean value than the zero drift op-amp version.

The similarity of variance and excess kurtosis values evaluated for the IRTs measuring 700 °C steady-state temperature, indicated that the two configurations would work similarly well measuring higher temperature sources. The zero drift op-amp IRT did still achieve lower variance than the precision op-amp version but the difference between the prototypes was not as marked with higher intensity radiation.

The zero drift op-amp IRT would be expected to afford lower minimum resolvable temperature measurement whilst achieving similar maximum temperature measurable to the precision op-amp IRT.

### 5.3 Characterisation of low temperature IRTs against blackbody source

The two versions of low temperature range IRT developed were characterised against a low temperature blackbody source to determine practical calibrations and allow comparison of the thermometers.

The source temperature versus IRT output voltage characteristics measured for the zero drift op-amp and precision op-amp based IRTs are presented in figure 5.7.

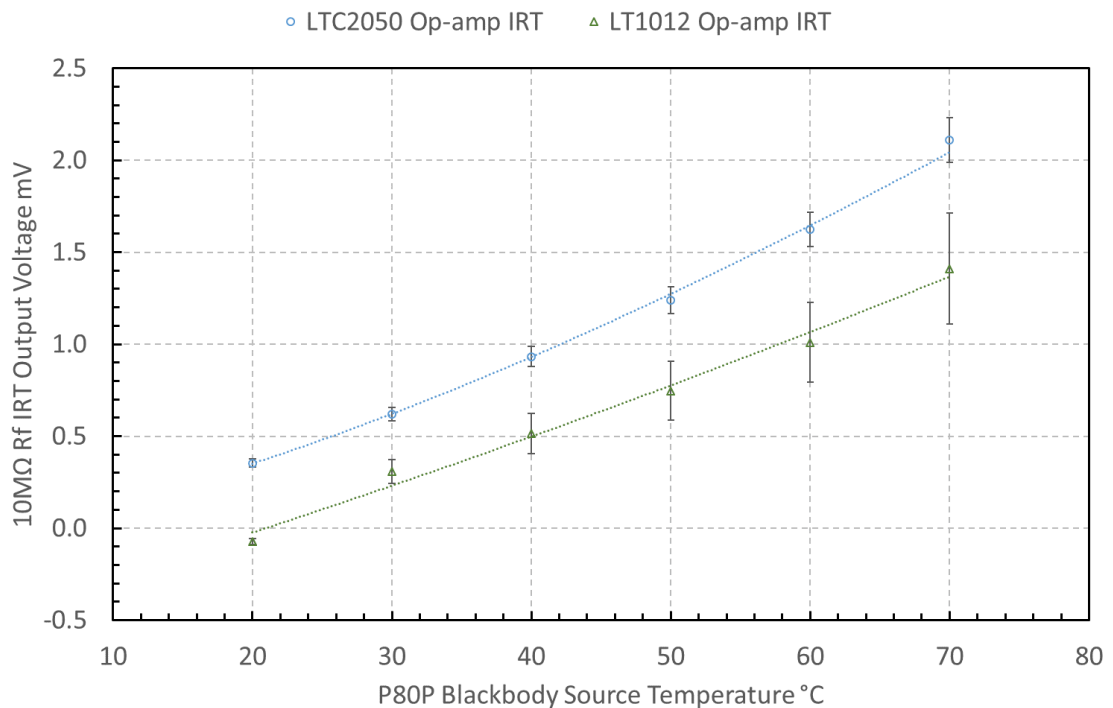


**Figure 5.7 Source temperatures versus voltage output characteristics of zero drift op-amp IRT and precision op-amp IRT**

The zero drift op-amp IRT measured 0.35 mV at 20 °C source temperature to 2.1 mV at 70 °C source temperature, with a mean uncertainty of 5.8%. The precision op-amp IRT measured -0.072 mV at 20 °C source temperature to 1.4 mV at 70 °C source temperature

with a mean uncertainty of 21.4%. Evidently, the zero drift op-amp IRT had lower uncertainty and marginally higher sensitivity than the precision op-amp version. The low temperature version of the prototype IRT achieved output voltages measuring source temperatures up to 70 °C that were comparable to the voltages achieved by the laboratory prototype measuring higher temperatures. The higher output voltage achieved by the low temperature version of the thermometer was consistent with having transimpedance that was an order of magnitude higher than the laboratory prototype thermometer. The curvature expected of the output voltage characteristic with the source temperature was not obvious in figure 6.5, owing to the limited range of temperatures over which the measurements were undertaken.

Curve fits to the  $\ln(V_o)$  variations with  $1/T$  for the two thermometer versions are presented in figure 5.8.

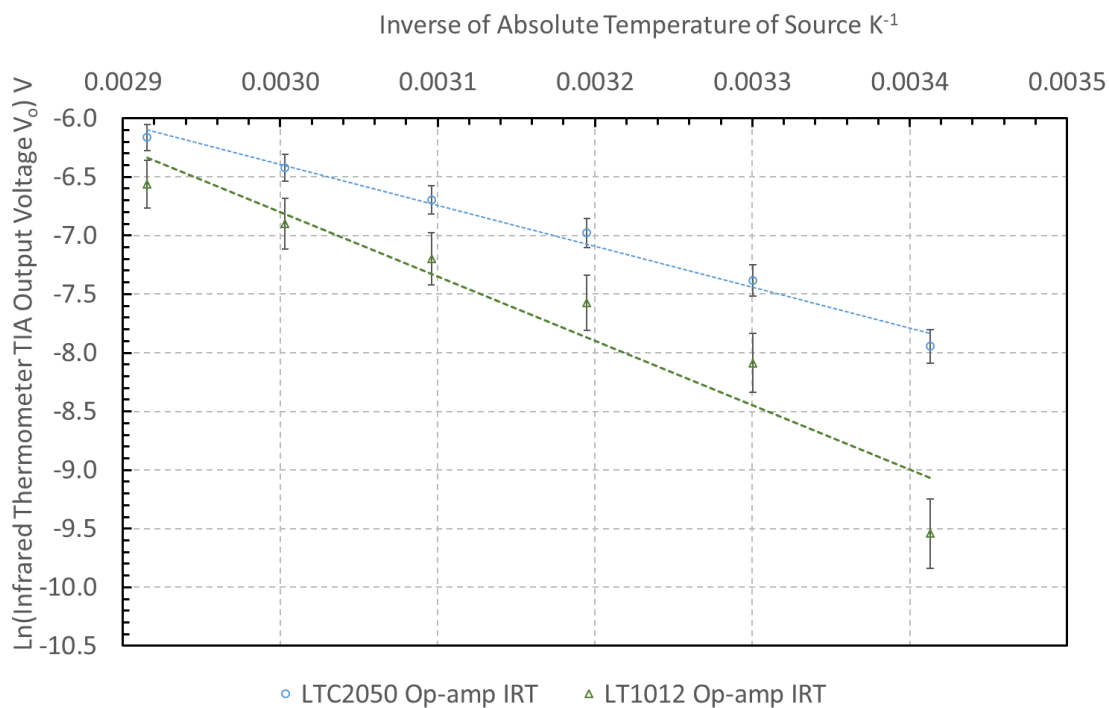


**Figure 5.8 Characteristics of  $\ln(V_o)$  variations with  $1/T$  for zero drift op-amp IRT and precision op-amp IRT**

Evaluation of the ratio of convolved radiances and spectral response curves from known and unknown temperatures using Wien's approximation led to the expectation

that the relationship between the  $\ln(V_o)$  and  $1/T$  should be linear [21]–[24], as presented in equation (2.13) from chapter 2.

$$\ln(V_o) = a + \frac{b}{T}$$

where:

$V_o$  is the output voltage of the thermometer, V

$T$  is the absolute temperature of the source being measured, K

$a$  and  $b$  are the intercept and gradient coefficients derived from a linear regression to the  $\ln(V_o)$  versus  $1/T$  curve.

The zero drift op-amp IRT adhered to the linear relationship expected between  $\ln(V_o)$  and  $1/T$  better than the precision op-amp version. The limiting effective wavelength for the thermometer configurations were calculated to be 4.12  $\mu\text{m}$ , for the zero drift op-amp IRT and 3.71  $\mu\text{m}$  for the precision op-amp IRT. The longer effective wavelength evaluated for the zero drift op-amp IRT should enable a lower minimum temperature to be measured than the precision op-amp IRT.

The practical calibrations of the thermometers were used to determine interpolation curves, according to the method of Sakuma and Hattori [4]. There was good agreement between the measured and modelled output voltages for the zero drift op-amp IRT at each temperature within the range, with only the lowest temperature having a deviation that exceeded 10% of the measured voltage. The precision op-amp IRT afforded reasonable agreement, with larger deviations between modelled and measured output voltages than recorded for the zero drift op-amp IRT. The difference between modelled and measured voltages for the precision op-amp IRT was 47.5% at 20 °C, reducing to circa 30% for source temperatures above 40 °C.

The noise limited equivalent temperature resolution of the zero drift op-amp IRT was evaluated to be 3.5 °C at 20 °C source temperature, reducing to less than 1.0 °C for source temperatures above 40 °C. The uncertainties of the measurements were less than  $\pm 10\%$  for source temperatures above 30 °C and less than  $\pm 3\%$  for source temperatures above 40 °C. The noise limited equivalent temperature resolution of the precision op-amp IRT was evaluated to be 14.7 °C at 20 °C source temperature,

reducing to 5.0 °C for source temperatures above 40 °C. The uncertainties of the measurements were  $\pm 30\%$  for source temperatures above 30 °C, reducing to  $\pm 11\%$  for source temperatures above 40 °C.

The signal to noise ratio (SNR) was near unity at the lowest temperature measured, representing the limit to which the thermometer could be expected to measure without employing signal processing to extract measurement from data having a higher magnitude of noise than useful signal.

The noise limited equivalent temperature resolution for the zero drift op-amp and precision op-amp versions of the low temperature prototype IRT are presented in figure 5.9 and 5.10, along with the SNR calculated for each measurement.

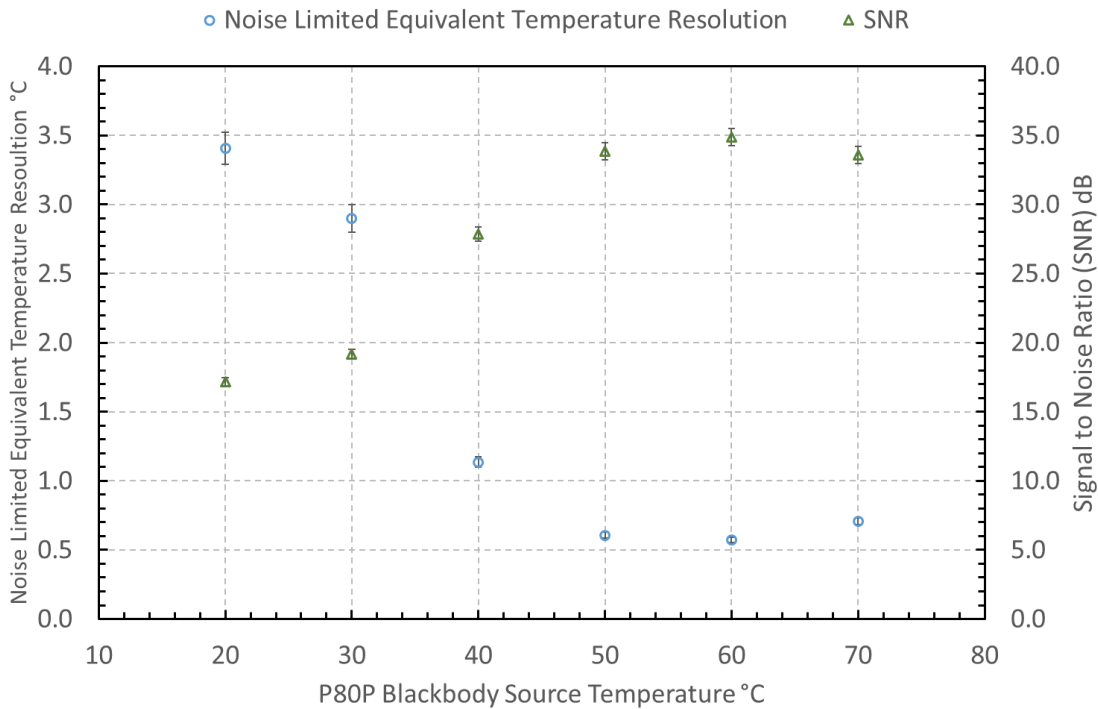


**Figure 5.9 Characteristic noise limited equivalent temperature resolution and SNR of zero drift op-amp IRT**

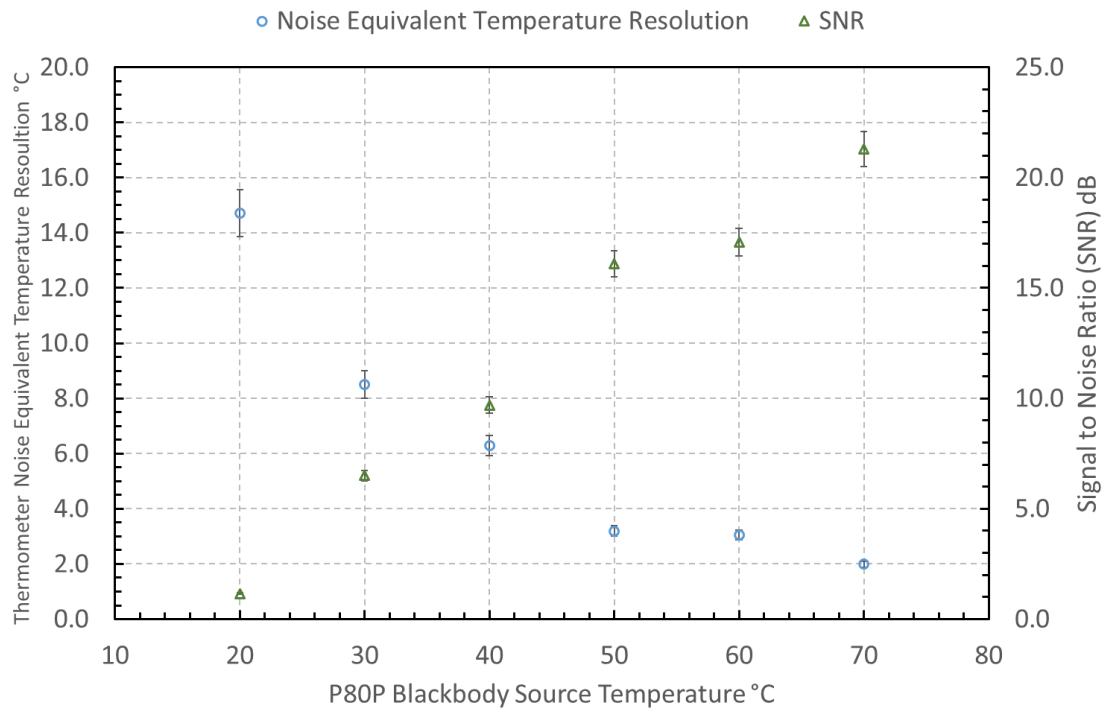


**Figure 5.10 Characteristic noise limited equivalent temperature resolution and SNR precision op-amp IRT**

The noise equivalent temperature resolution of the zero drift op-amp IRT was lower than the precision op-amp version throughout the low temperature range measured. The SNR was higher throughout the range. The zero drift op-amp IRT would be better than the precision op-amp version for measurement of lower temperatures.

The noise limited temperature resolution of 3.5 °C at 20 °C source temperature measured for the zero drift op-amp IRT indicated that there would be uncertainty of 17.5% (at 95% confidence level) introduced around the measurement of objects radiating near nominal room temperature. The zero drift op-amp IRT could be used to measure objects having room temperature but the noise limited temperature resolution characteristic demonstrated that the practical minimum temperature for which the prototype zero drift op-amp IRT should be deployed was between 30 °C and 40 °C. It would be preferable to specify the minimum source temperature from which the prototype thermometer should measure to be above 40 °C to maintain the noise limited measurement resolution within circa  $\pm 1$  °C. This recommendation represented a reduction in the minimum temperature measurable by a factor of five compared to the 200 °C minimum temperature measurement achieved with the laboratory prototype.

The output voltage measured for the low temperature prototype IRT had increased magnitude at lower source temperatures, compared to the laboratory and initial application prototype thermometers. The increased output voltage of the low temperature prototype IRT owed to the larger value of transimpedance resistor used, the range of wavelengths transmitted by the ZBLAN glass and the higher throughput of infrared radiation afforded by the larger diameter fibre optic core used to couple the source infrared radiation to the photodiode.

## Part II: Application of Low Drift Thermometer to Low Temperature Range Measurement.

### 5.4 Application of prototype IRT to Lithium-ion cell temperature measurements.

The low temperature prototype IRTs were used to measure battery cell temperatures in collaboration with the Chemical and Biological Engineering (CBE) Department at The University of Sheffield. The CBE Lithium-ion battery development laboratory provided the capability of assembling cells from components, thereby allowing the construction to be modified to embed a fibre optic into a cell.

Lithium-ion battery cell temperatures increase during charging and discharging, high current drain and failure events [25]–[28], owing to the electro-chemical reactions occurring. Typically, Lithium-ion cells can achieve temperatures in the range 30 °C to 70 °C during normal charging and discharging cycles, depending upon the rate of charge, ambient temperature conditions and capacity of the cell [29]. The reactions within a cell can achieve temperatures capable of inducing distortion and melting or burning of plastic if thermal runaway occurs. Lithium cell over-heating events have been reported in journals and have been recorded by aviation authorities [30]–[32]. Understanding of cell thermal behaviour has become increasingly important with the growing number and type of applications, ranging from mobile communications to power storage for supply networks, electrically powered vehicles and driving aerospace actuators [31]–[33]. The safety-critical nature of some applications of Lithium-ion cells [30], [32], [34] demanded that methods of measuring the cell temperature should be developed to help inform research into the operating and

failure modes of cells. Scientific investigations have been undertaken to measure normal thermal behaviours and compare with thermal runaway events in cells to understand more about these types of failures.

Presently the prominent methods of inferring the internal cell temperatures that have succeeded used measurement of the cell surface temperatures using attached thermocouples or thermal imaging, combined with modelling of the internal temperature that could lead to the external temperatures measured [25], [27], [28], [35]–[37]. The variations with temperature of known electrical parameters have also been used to infer internal temperatures, for example: using electro-chemical impedance spectroscopy [25], [26], [37], [38]. The internal temperature distribution and evolution have been modelled based upon the assumption that the impedance of the anode, cathode and electrolyte are uniform and resistance heating of the cell occurs at the anode and cathode only and then dissipates through the cell. These assumptions simplify the model sufficiently to enable its analytical solution but introduce additional uncertainties to calculation of the temperature of the cell [37]. A number of research groups have published work for which one or more fibre Bragg grating (FBG) sensors were embedded into a cell to measure temperature and other physical parameters [39]–[41]. FBG sensors enable temperature to be inferred by measuring the strain-induced change in the wavelength and width of the resonance peak around the mean value of reflected radiation [42]. FBG sensors have faster response than thermocouples, with response speeds capable of measuring at a frequency of 2 Hz reported [43]. Infrared radiation thermometers can have response times of micro-seconds to milli-seconds, which represents several orders of magnitude faster response than either mineral-insulated thermocouples or FBG sensors have achieved. A fast response IRT would enable measurement of the battery cell temperature cycles at higher temporal resolution than the competing methods. An infrared radiation thermometer can also be configured to have higher sensitivity to temperature changes than either thermocouples (order of 10  $\mu\text{V}/\text{K}$  sensitivity and 1 K uncertainty) or FBG sensors (order of 0.01 nm/K sensitivity and 1 K uncertainty). Having high values of resistance in the feedback loop of the TIA would afford the high sensitivity of the thermometer to temperature changes required to offer the highest resolution of low temperature measurements possible.

Objects inside a battery cell such as: electrodes, separator sheets and the pouch will all emit infrared radiation. It should be possible to measure the temperatures of specific components within the cell because of the narrow numerical aperture presented by a fibre optic, typically 0.2 – 0.3, that project to an included angle from which the fibre optic tip would accept radiation of 22.9 ° to 34.4 ° around the fibre axis. A temperature measurement attained directly from the infrared emissions rather than inference from the effect of temperature upon the electrical properties of the cell and modelling to characterise the internal heat distribution from surface measurements would improve understanding of cell thermal behaviour.

#### 5.4.1 Insertion of fibre optic into Lithium ion cells coupled to low temperature IRT

The thermometer printed circuit board (PCB) had the same 25 mm x 25mm dimensions used for the previous prototypes described in chapter 4, enabling variants of the IRT to be used within any of the applications with appropriate modifications. The low temperature range thermometer configured for battery cell measurements used the Linear Technologies LTC2050 zero drift op-amp in the TIA. This op-amp had been demonstrated to achieve lower minimum temperature measurable than the precision op-amp version. The zero drift op-amp afforded low output voltage offset of less than 1.0 mV with 10 M $\Omega$  transimpedance, without any zero trim applied. The thermometer was able to measure from a lower minimum temperature than previous prototype IRTs because of the low voltage offset and noise incurred in the TIA that enabled use of a high transimpedance value, combined with the higher throughput and range of MWIR wavelengths transmitted by the fibre optic.

This modification afforded a lower minimum temperature approaching room temperature to be measured and limited the maximum temperature that could be measured by this configuration of thermometer to an estimated 670 °C, beyond which the amplifier output voltage would saturate at the power supply limit of +2.5 V. The thermometer range could be extended by adapting the PCB to use a higher voltage or dual polarity power supply. Doubling the power supply voltage to +5 V maximum would extend the maximum temperature measurable to an estimated 855 °C and increasing the positive supply to +10 V would increase it to 1115 °C. This latter change

would enable the highest temperature measurable using the 10 M $\Omega$  transimpedance zero drift op-amp IRT to achieve 1100 °C, thereby affording a wide temperature range.

The thermometer was coupled to the battery cell using a 150 mm length of 600  $\mu$ m core diameter, ZBLAN fibre optic embedded inside the cell to transmit infrared radiation to the thermometer. Using ZBLAN glass fibre optic in this application afforded some immunity to degradation by electrochemical reaction with the electrolyte for durations that were sufficient to afford measurement of temperatures from several tests. The fibre optic would become more susceptible to reaction and degradation with increasing temperature, so damage may occur to the fibre during higher temperature cycles. The maximum temperature to which the ZBLAN fibre optic should be exposed is approximately 90 °C [44] which exceeds the temperature expected to be generated in a cell under typical charging and discharging conditions.

A method of inserting the fibre optic into a cell was developed for which the open end of the fibre optic was inserted between layers of separator that act to isolate the cell anode from the cathode. The point at which the fibre optic egressed the cell was sealed using heat sealing tape and adhesive applied externally that also held the fibre optic sheath in position.

Each cell contained the battery contacts, anode and cathode that aligned with external contacts and were held against them by physical pressure, insulating separator sheets between the electrodes inside the cell, spacer materials and liquid electrolyte. The pouches were sealed fully to prevent exposure of the cell materials to atmosphere, thereby preventing deleterious reaction of the electrolyte.

The construction of different Lithium-ion pouch cells with ZBLAN fluoride glass fibre optic embedded inside is illustrated in figures 5.11 through 5.13.

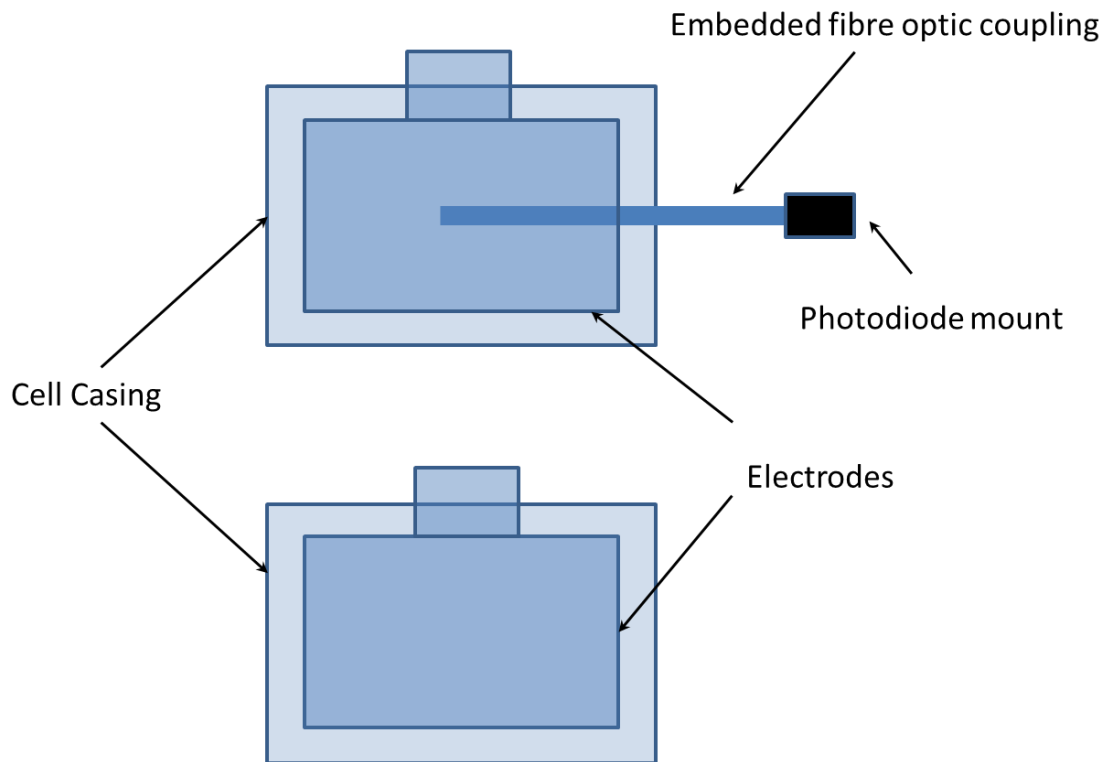


**Figure 5.11 Components of Lithium-ion pouch cells prior to assembly, illustrating the electrodes, contacts, Aluminium laminate sheet that forms the pouch casing (prior to sealing) and fibre optic for embedding into cell.**

The method of embedding fibre optic into a cell was similar for small capacity cells (having a footprint that was approximately the size of a palm of a hand) and larger capacity cells (having a footprint of approximately half a sheet of A4 paper). The large capacity cells used multiple electrodes and separator sheets arranged in layers. The fibre optic was inserted between one layer of electrodes and separator sheets, after assembly of the cell stack.

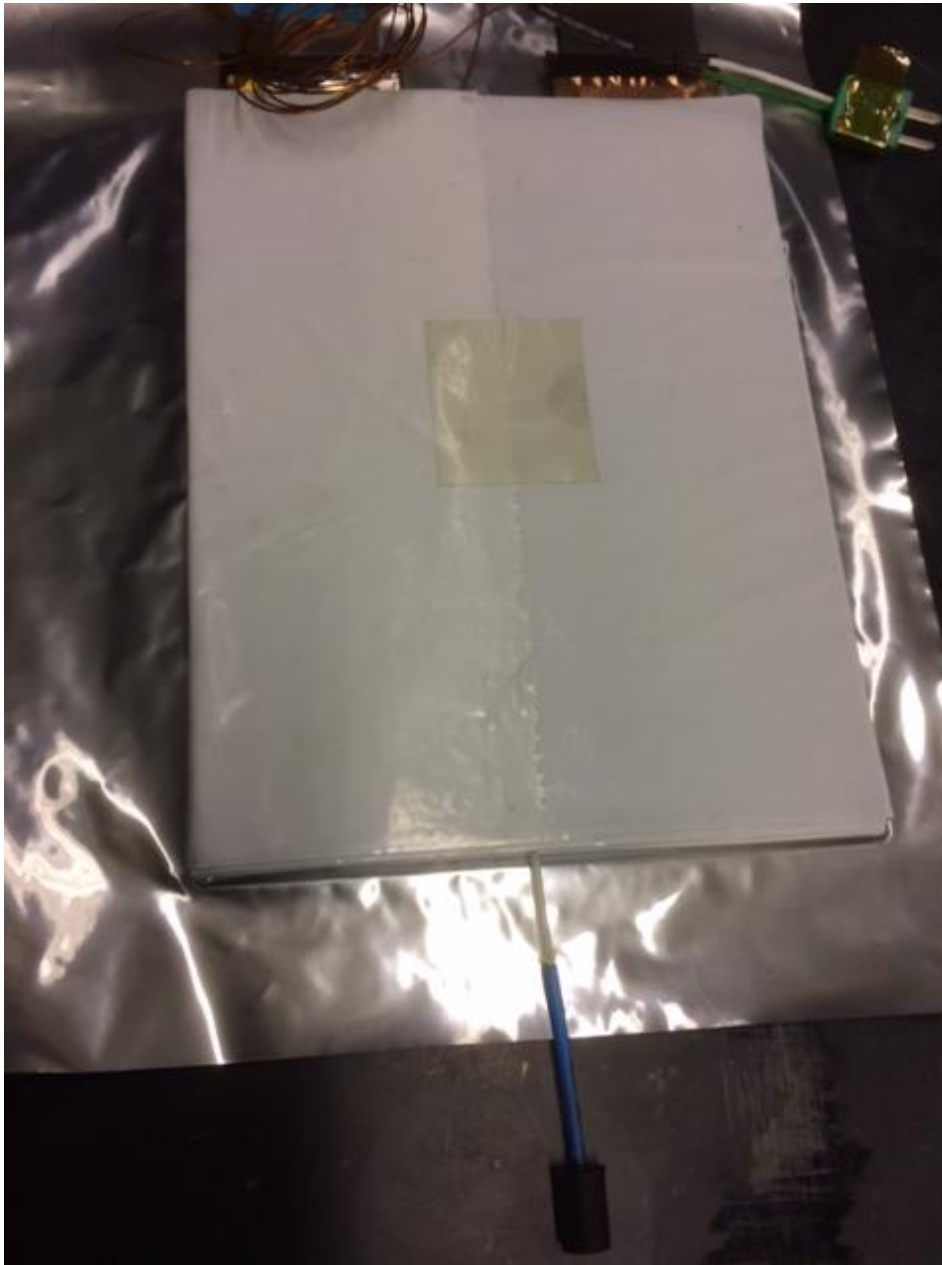


**Figure 5.12 Assembly of large capacity pouch cell with embedded ZBLAN fibre optic inserted into centre of electrode stack, prior to forming into active cell**

Sealing the pouch cell sheets around the fibre optic that was inserted into the cell stack required that the heat-sealing bar was modified to accommodate the diameter of the sheath, without crushing the fibre core inside.



**Figure 5.13 Completed large capacity Lithium ion pouch cell with embedded ZBLAN fibre optic and thermocouple inserted through opposite edges of pouch**

The seal between the pouch sheets around the fibre optic can be seen to have crimped the sheets in figure 5.13.

The electrolyte used inside the cell was one molar concentration of 'LP30' Lithium Hexafluorophosphate ( $\text{LiPF}_6$ ) salt solution in ethylene carbonate and dimethyl carbonate. The electrolyte filled the volume adjacent to the electrodes and surrounded the ZBLAN glass fibre optic that was embedded in the cell.

Initial fibre optic installations into small size Lithium-ion pouch cells incurred fractures of the core when heat-sealing the pouch, owing to the pressure required to ensure that a gas-tight seal was achieved around the fibre optic. The fractures were sufficiently complete in some cases to cause the total loss of the transmitted signal. The method of heat sealing the pouch cells was amended to use a manual heating bar with a round profile groove cut into the surface to accommodate the fibre optic sheath.

The temperatures achieved by cells at the charging and discharging rates achieved under test conditions did not generate sufficient heat to be measured by the IRT developed. Higher transimpedance would be necessary to amplify the small photocurrent generated at the low temperatures of the cells to measurable voltages. The noise and offset of the op-amps used to configure the thermometer would need to be reduced further to enable measurement of these lower temperatures with low uncertainty and at sufficiently fast response speed. It may also be necessary to cool the detector to achieve sufficiently low dark current and Johnson noise to be able to measure the low temperatures and small differences from ambient temperature arising during normal cell cycling.

#### 5.4.2 Proof of concept using laboratory tests

A small size dummy pouch cell containing no electrolyte or active electrodes but otherwise having identical construction to an operable Lithium-ion pouch cell was subjected to temperatures between 20 °C and 55 °C using an Ametek Land Landcal P80P blackbody source. The cell temperature was allowed to achieve steady-state conditions and the prototype IRT output voltage recorded for each temperature. The method used was similar to undertaking a practical calibration of the thermometer, except that the fibre optic was embedded into the dummy pouch cell that was inserted into the blackbody chamber rather than inserted into the thermo-well. The dummy cell temperature versus IRT output voltage characteristic measured is presented in figure 5.14. The uncertainty around these measurements was estimated to be 5.7 %.

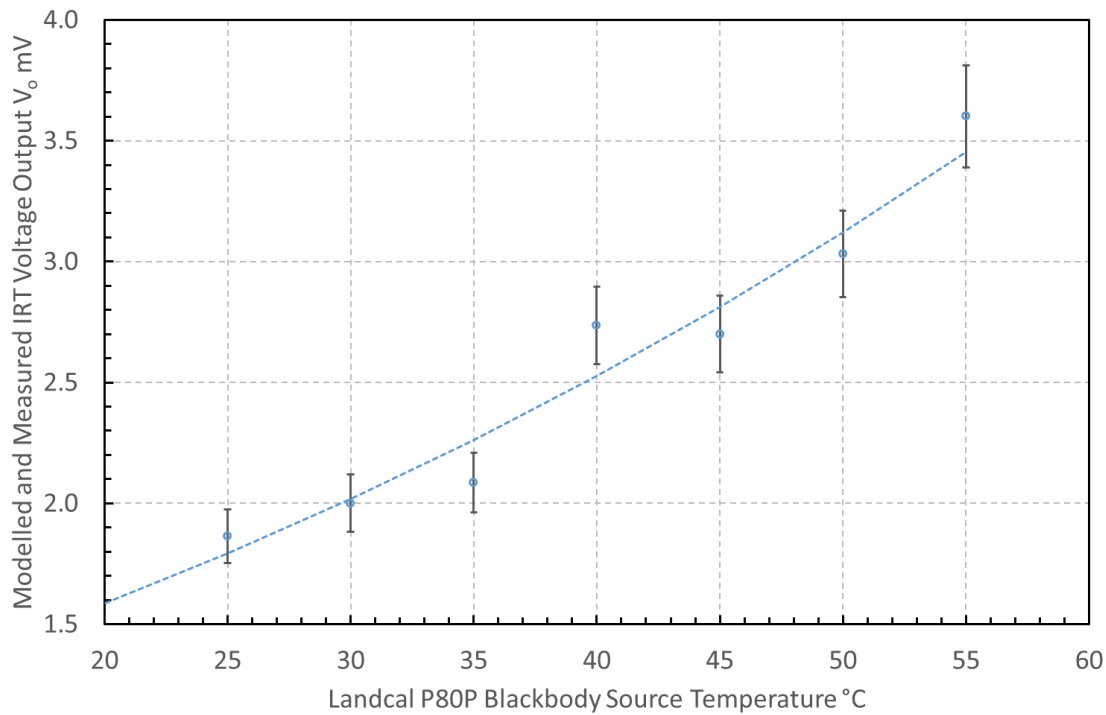


**Figure 5.14 Measurements of dummy pouch cell (containing no electrolyte) temperature using one of the low temperature IRTs**

The analogue signal was sampled at 5 s interval and these sample measurements were averaged continuously over a sliding window of twelve consecutive measurements. This data filtering enabled the low magnitude output voltage signal from the thermometer, that was associated with the low temperature measurements, to be identified from the noise. The long duration sampling limited the capability of the thermometer to respond to signals that incurred fast changes. The maximum frequency of alternating signal that the thermometer could respond to at the lowest temperature was 0.1 Hz, to allow averaging over the sliding window duration, and to comply with the Nyquist limit for signal aliasing [45]. The averaging period could be shortened for higher temperature measurements, allowing sampling in excess of the 2 Hz achieved with FBG sensors or similar for thermocouples.

The variations of thermometer voltage output from a smooth, monotonically increasing curve resulted from the low SNR achieved for the lowest source temperatures measured, at which the signal was approaching the noise limit of the op-amps. The noise and voltage offset from the TIA led to increased variability within the

measured data and increased uncertainty identifying the continuously-averaged mean temperature.

The 10 M $\Omega$  transimpedance, zero drift op-amp IRT has been demonstrated to be capable of measuring from low minimum temperatures, with large diameter ZBLAN fibre optic embedded into Lithium-ion cells. The IRT could measure from a practical minimum temperature of 30 °C with uncertainty of  $\pm 1$  °C without detriment to the response speed. The laboratory trials demonstrated measurement from 25 °C minimum temperature, achieved using continuous averaging of the thermometer output signal over sixty seconds duration sliding window.

## Summary of chapter

Application of the prototype thermometer to lower temperature range measurements, typical of the temperatures arising during battery cell charge and discharge cycling, required higher transimpedance than 1M $\Omega$  that was used for the laboratory prototype. A transimpedance of 10 M $\Omega$  was used in the low temperature version of the prototype thermometer to afford increased SNR. The higher transimpedance value in the resistor-capacitor network imposed a lower speed of response to a changing signal of 0.1 ms. The equivalent alternating signal frequency cut-off limit was 1.59 kHz. Ideally, the transimpedance used would be increased to afford the lowest minimum temperature measurable and the supply voltage maximised to provide the widest measurement range possible. The low temperature range IRT with ZBLAN fibre optic coupling developed was suitable for use as a probe embedded into Lithium cells but needed improvement to be able to measure the lowest temperatures during normal charging and discharging cycles.

Two prototype thermometers were configured that were identical apart from the op-amps used in the TIAs. The capabilities of each version of prototype IRT to maintain zero and mean output voltages were assessed by calculating the variances at an effective zero signal and whilst sighted at an approximate blackbody source at an arbitrary, steady-state temperature of 700 °C. Using a zero drift op-amp configuration of the TIA on the prototype thermometer achieved approximately 50% reduction of the output voltage noise, compared to using a precision op-amp. The zero drift op-amp

IRT maintained a lower offset voltage from zero than the precision op-amp IRT and was less susceptible to perturbation by extremal voltages.

The zero drift op-amp enabled an MWIR thermometer to be configured to measure a lower minimum temperature without compromising the response speed, sensitivity or range of temperature measurements. The zero drift op-amp IRT was demonstrated to be capable of measuring from 30 °C with a maximum  $\pm 10\%$  uncertainty, whilst the precision op-amp IRT achieved a minimum, practical measurement of 40 °C with similar uncertainty.

The measurement resolution of the zero drift op-amp IRT was 1 °C at 40 °C measured temperature, which was a five-fold improvement on the capability of the precision op-amp IRT that achieved 5 °C resolution at 40 °C.

A method of embedding fibre optic into a battery cell has been developed to enable laboratory testing of instrumented cells but a more robust design would need to be engineered to use the technology more generally. Protection against mechanical damage during assembly and manipulation into the battery cell test chamber (or installation into a battery stack) will be essential to successful longer term deployment. The machining application thermometer, described in chapter five and the battery cell thermometer, described within this chapter, needed to have more robust fibre optic installations for usage outside of laboratory conditions.

Ideally, higher charging and discharging rates, that would dissipate more heat from the Lithium-ion cell, would be used to test the capability of the IRT to measure internal cell temperatures. Using higher transimpedance would not necessarily be detrimental to the fast response from the thermometer compared to the inherently faster 1 M $\Omega$  transimpedance version, in practice because the measurement samples would not need to be averaged over as long a duration to be able to identify the useful signal magnitude from the noise.

Data filtering over extended durations allowed low intensity infrared radiation arising from source temperatures near to ambient to be measured by the InAsSb photodiode. The thermometer version for lower temperature measurements had transimpedance of 10 M $\Omega$  and afforded measurement from circa 25 °C (nominal room temperature) with higher magnitude of uncertainty. The thermometer was specified for practical

measurement of temperatures above 30 – 40 °C minimum to ensure that the measurement uncertainty attributable to the thermometer was maintained within the nominal specification of  $\pm 1$  °C. This magnitude of uncertainty was comparable to measurement by thermocouple over a useful temperature range. It should be possible to achieve lower measurement uncertainty and minimum temperature measurable by reducing the noise and offset of the op-amps used to configure the thermometer and increasing the transimpedance further.

## REFERENCES

- [1] A. Rogalski, 'Infrared detectors : an overview', *Infrared Phys. Technol.*, vol. 43, pp. 187–210, 2002.
- [2] J. P. Makai and J. J. Makai, 'Current-to-voltage converter for linearity correction of low shunt resistance photovoltaic detectors', *Rev. Sci. Instrum.*, vol. 67, no. 6, pp. 2381–2386, 1996.
- [3] S. E. Aleksandrov, G. A. Gavrilov, and G. Y. Sotnikova, 'Effect of low-frequency noise on the threshold sensitivity of middle-IR photodetectors in a broad frequency range', *Tech. Phys. Lett.*, vol. 40, no. 8, pp. 704–707, 2014.
- [4] F. Sakuma and S. Hattori, 'Establishing a practical temperature standard by using a narrow-band radiation thermometer with a silicon detector', in *TEMPERATURE: ITS MEASUREMENT AND CONTROL IN SCIENCE AND INDUSTRY, VOLUME 5, PART 1: Proceedings of the Sixth International Temperature Symposium*, 1982, vol. 5.1, pp. 421–427.
- [5] A. D. Heeley, M. J. Hobbs, H. Laalej, and J. R. Willmott, 'Miniature Uncooled and Unchopped Fiber Optic Infrared Thermometer for Application to Cutting Tool Temperature Measurement', *Sensors*, vol. 18, no. 3188, 2018.
- [6] B. Nguyen and W. D. Smith, 'Nulling Input Offset Voltage of Operational Amplifiers', *TI Appl. Rep.*, vol. SLOA045, no. August, pp. 1–15, 2000.
- [7] Z. Bielecki, 'Maximisation of Signal-to-Noise Ratio in Infrared Radiation Receivers', *Opto-Electronics Rev.*, vol. 10, no. 3, pp. 209–216, 2002.

- [8] Linear Technologies, 'LT1012A/LT1012 - Picoamp Input Current, Microvolt Offset, Low Noise Operational Amplifier Datasheet', *LW/TP 1202 1K Rev B*. pp. 1–20, 1991.
- [9] Linear Technologies, 'LTC2050/LTC2050HV Zero Drift Operational Amplifiers Datasheet', *LT0817 Rev D*. pp. 1–18, 1999.
- [10] S. M. A. Auckloo, 'Analog Frontend Circuits for Avalanche Photodiodes', University of Sheffield Doctor of Philosophy Thesis, 2016. Accessed September 2017.
- [11] Texas Instruments, 'LMH664x Low Power , 130 MHz , 75 mA Rail-to-Rail Output Amplifiers', *Datasheet*. 2014.
- [12] Texas Instruments, 'OPA627 and OPA637 Precision High-Speed Difet ® Operational Amplifiers', *Datasheet*. 2015.
- [13] Texas Instruments, 'OPA657 1 . 6-GHz , Low-Noise , FET-Input Operational Amplifier', *Datasheet*. 2015.
- [14] Thorlabs Inc, 'Thorlabs ZrF4 & InF3 Attenuation Comparison Spreadsheet', *Thorlabs webpage*. .
- [15] Hamamatsu Photonics, 'InAsSb photovoltaic detector P13243-11-MA Datasheet', *Hamamatsu P13243 Series Datasheet*. 2015.
- [16] T. Waldmann *et al.*, 'Influence of cell design on temperatures and temperature gradients in lithium-ion cells: An in operando study', *J. Electrochem. Soc.*, vol. 162, no. 6, pp. A921–A927, 2015.
- [17] E. M. Sparrow, L. U. Albers, and E. R. G. Eckert, 'Thermal radiation characteristics of cylindrical enclosures', *J. Heat Transfer*, vol. 84, no. 1, pp. 73–81, 1962.
- [18] J. Vollmer, 'Study of the effective thermal emittance of cylindrical cavities', *J. Opt. Soc. Am.*, vol. 47, no. 10, pp. 926–932, 1957.
- [19] P. Saunders, 'General interpolation equations for the calibration of radiation thermometers', *Metrologia*, vol. 34, no. 3, pp. 201–210, 1997.
- [20] H. Pfeifer, 'Industrial Furnaces-Status and Research Challenges', *Energy Procedia*, vol. 120, pp. 28–40, 2017.

- [21] J. W. Hahn and C. Rhee, 'Interpolation equation for the calibration of infrared pyrometers', *Metrologia*, vol. 31, no. 1, pp. 27–32, 1994.
- [22] P. B. Coates, 'Wavelength specification in optical and photoelectric pyrometry', *Metrologia*, vol. 13, no. 1, pp. 1–5, 1977.
- [23] British Standards Institute, 'BS 1041-5 Temperature measurement— Part 5: Guide to selection and use of radiation pyrometers', *British Standards Institute*, vol. 1041, no. 5. 1989.
- [24] J. Dixon, 'Radiation thermometry', *J Phys E Sci Instrum*, vol. 21, pp. 425–436, 1988.
- [25] H. P. G. J. Beelen, L. H. J. Raijmakers, M. C. F. Donkers, P. H. L. Notten, and H. J. Bergveld, 'A comparison and accuracy analysis of impedance-based temperature estimation methods for Li-ion batteries', *Appl. Energy*, vol. 175, pp. 128–140, 2016.
- [26] R. Srinivasan, B. G. Carkhuff, M. H. Butler, and A. C. Baisden, 'Instantaneous measurement of the internal temperature in lithium-ion rechargeable cells', *Electrochim. Acta*, vol. 56, no. 17, pp. 6198–6204, 2011.
- [27] R. Srinivasan, A. Carson Baisden, B. G. Carkhuff, and M. H. Butler, 'The five modes of heat generation in a Li-ion cell under discharge', *J. Power Sources*, vol. 262, pp. 93–103, Sep. 2014.
- [28] R. Srinivasan et al., 'Heat Generation in Li-ion Cells during Charge and Discharge', in *Proceedings of SPIE 8728 Energy Harvesting and Storage: Materials, Devices and Applications IV*, May, 2013.
- [29] S. J. Drake *et al.*, 'Heat generation rate measurement in a Li-ion cell at large C-rates through temperature and heat flux measurements', *J. Power Sources*, vol. 285, pp. 266–273, 2015.
- [30] Q. Wang, P. Ping, X. Zhao, G. Chu, J. Sun, and C. Chen, 'Thermal runaway caused fire and explosion of lithium ion battery', *J. Power Sources*, vol. 208, pp. 210–224, 2012.
- [31] P. G. Balakrishnan, R. Ramesh, and T. Prem Kumar, 'Safety mechanisms in lithium-ion batteries', *J. Power Sources*, vol. 155, no. 2, pp. 401–414, 2006.

- [32] S. Abada, G. Marlair, A. Lecocq, M. Petit, V. Sauvant-moynot, and F. Huet, 'Safety focused modeling of lithium-ion batteries : A review', *J. Power Sources*, vol. 306, pp. 178–192, 2016.
- [33] S. Gao, L. Wang, C. Feng, and K. D. Kipnetich, 'Analyzing the influence of combustion gas on a gas turbine by radiation thermometry', *Infrared Phys. Technol.*, vol. 73, pp. 184–193, 2015.
- [34] X. Feng, M. Ouyang, X. Liu, L. Lu, Y. Xia, and X. He, 'Thermal runaway mechanism of lithium ion battery for electric vehicles : A review', *Energy Storage Mater.*, vol. 10, no. May 2017, pp. 246–267, 2018.
- [35] D. Anthony, D. Wong, D. Wetz, and A. Jain, 'Non-invasive measurement of internal temperature of a cylindrical Li-ion cell during high-rate discharge', *Int. J. Heat Mass Transf.*, vol. 111, pp. 223–231, 2017.
- [36] E. McTurk, T. Amietszajew, J. Fleming, and R. Bhagat, 'Thermo-electrochemical instrumentation of cylindrical Li-ion cells', *J. Power Sources*, vol. 379, no. January, pp. 309–316, 2018.
- [37] R. R. Richardson, P. T. Ireland, and D. A. Howey, 'Battery internal temperature estimation by combined impedance and surface temperature measurement', *J. Power Sources*, vol. 265, pp. 254–261, 2014.
- [38] L. H. J. Rajmakers, D. L. Danilov, R. A. Eichel, and P. H. L. Notten, 'A review on various temperature-indication methods for Li-ion batteries', *Appl. Energy*, vol. 240, no. July 2018, pp. 918–945, 2019.
- [39] J. Fleming, T. Amietszajew, E. McTurk, D. Greenwood, and R. Bhagat, 'Development and evaluation of in-situ instrumentation for cylindrical Li-ion cells using fibre optic sensors', *HardwareX*, vol. 3, pp. 100–109, 2018.
- [40] S. Novais *et al.*, 'Internal and external temperature monitoring of a li-ion battery with fiber bragg grating sensors', *Sensors (Switzerland)*, vol. 16, no. 9, pp. 1–9, 2016.
- [41] A. Raghavan *et al.*, 'Embedded fiber-optic sensing for accurate internal monitoring of cell state in advanced battery management systems part 1: Cell embedding method and performance', *J. Power Sources*, vol. 341, pp. 466–473, 2017.

- [42] J. Fleming, T. Amietszajew, J. Charmet, A. J. Roberts, D. Greenwood, and R. Bhagat, 'The design and impact of in-situ and operando thermal sensing for smart energy storage', *J. Energy Storage*, vol. 22, no. January, pp. 36–43, 2019.
- [43] M. Nascimento, M. S. Ferreira, and J. L. Pinto, 'Real time thermal monitoring of lithium batteries with fiber sensors and thermocouples: A comparative study', *Meas. J. Int. Meas. Confed.*, vol. 111, no. March, pp. 260–263, 2017.
- [44] Thorlabs Inc, 'Thorlabs ZrF4 Fibre Properties'. [Online]. Available: <https://www.thorlabs.com/thorproduct.cfm?partnumber=MZ61L1>. [Accessed: 12-Mar-2018].
- [45] A. de Sa, *Principles of Electronic Instrumentation*, First Edition, Edward Arnold (Publishers) Ltd, London, 1981.

## 6 PROTOTYPE ZERO DRIFT, FIBRE OPTIC INFRARED THERMOMETER FOR THERMOCOUPLE SUBSTITUTION

Thermocouple temperature measurements are affected by calibration drift and irreversible hysteresis of the thermometer output with ageing and exposure to harsh process conditions [1]–[3]. Thermocouples have been configured with integral fixed point temperature calibration cells [4]–[6] which would allow in-operando assessment of thermocouple calibration. These developments offer some scope to overcome the ageing-related drift of thermocouples but may not address the detriment of thermoelectric stability caused by exposure to harsh conditions. The scope exists to substitute a fibre optic coupled, infrared thermometer with integral fixed point temperature calibration cells for such thermocouples, thereby obviating the problems caused by harsh measurement conditions. No such infrared radiation thermometer (IRT) with an integral fixed point material deposited onto a fibre optic probe exists, therefore the feasibility of creating a suitable IRT and probe was undertaken. The potential of an IRT to measure the small changes in the temperature history curves that were caused by absorption and release of the heat of transformation of tin, was demonstrated successfully. This feasibility study could lead to the development of IRTs with integral calibration capabilities, if pursued through subsequent projects.

A version of the fibre optic coupled, infrared thermometer (IRT) was configured that used an Indium Gallium Arsenide photodiode with response over an extended range

of wavelengths, nominally 0.9–2.6  $\mu\text{m}$  [7] (extended-InGaAs photodiode). This photodiode had photoresponsivity within the short-wave infrared (SWIR) band. The extended-InGaAs thermometer was coupled to a sapphire fibre optic, for which the nominal 0.75–3.5  $\mu\text{m}$  range of wavelengths transmitted [8], included the full wavelength range over which the photodiode responded. The capability of the fibre optic to transmit throughout the photodiode response wavelength range ensured that the thermometer achieved the broadest range of temperature measurement possible. The thermometer received unchopped infrared radiation and used the same configuration of uncooled and bootstrapped photodiode connected to the transimpedance amplifier that was proposed by Makai and Makai for low shunt resistance detectors [9] and used with the mid-wave infrared (MWIR) thermometers described in chapters 4 and 5.

The range of infrared wavelengths to which the extended-InGaAs photodiode responded favoured measurement of object temperatures from the low hundreds of Celsius, which emit sufficiently strongly at SWIR wavelengths to be measured readily.

## 6.1 SWIR thermometer configuration

The SWIR thermometer configured for measurement of the infrared radiation transmitted through the fibre optic probe used a ‘zero-drift’ operational amplifier (op-amp) for configuration of the transimpedance amplifier (TIA). The zero drift op-amp version of the prototype thermometer was demonstrated to afford low noise, offset voltage and offset voltage drift when applied to the low temperature version of the MWIR thermometer, described in chapter 5. The low noise of the zero drift op-amp TIA configuration enabled the measurement of small changes in infrared radiation that would be expected from small changes in temperature. This configuration of thermometer was suitable for identifying phenomena that cause small deviations in temperature, for example, the temperature inflections during phase transformations between solidus and liquidus states of pure metals used as calibration standards.

The photosensitivity of the extended-InGaAs detector, approximately 1.2 A/W and low minimum incident power to which it responded, approximately 1 pW, enabled low intensity infrared radiation to generate photocurrent. Amplification of the resulting pA

magnitude photocurrent to measurable voltage by 10 M $\Omega$  transimpedance, afforded measurement of the low intensity infrared radiation. The minimum TIA output voltage from the SWIR thermometer was expected to be 10  $\mu$ V at the lowest incident power that was capable of generating a response. This magnitude of output voltage was comparable to the noise measured for previous prototype IRTs and could arise from relatively low temperature sources at approximately 100 °C. The photosensitivity of the extended-InGaAs detector ensured that small magnitude changes of incident power generated sufficient photocurrent to cause a measurable change in output voltage. The shunt resistance of the extended-InGaAs photodiode is low, typically 10 – 15 k $\Omega$ , therefore it was essential to use a low offset voltage, low noise and low offset voltage drift op-amp to configure the TIA to be able to measure the photocurrent generated. Model calculations, reported in table 2.2 of chapter 2, demonstrated that the extended-InGaAs thermometer coupled to a short length sapphire fibre optic should be suitable for measurement from a minimum temperature of approximately 100 °C.

## 6.2 Configuration of fibre optic probe with tin coating forming a prototype integral temperature fixed point calibration cell

Pure tin has a melting temperature of 231.9 °C [10] and pure silver has a melting temperature of 961.8 °C [10], therefore tin may be melted whilst contained by silver without the risk of the molten metal breaching the encapsulating layer. Tin undergoing melting absorbs the heat of phase transformation and releases the same heat of transformation during solidification. The rates of change of temperatures measured during heating or cooling incur inflections during the solidus to liquidus and liquidus to solidus phase transformations, respectively. These inflections in the rate of change of temperature are manifest as an inflection in the time versus temperature history curves measured from the material during heating and cooling. Identifying the inflections in the increasing and decreasing temperature curve of tin can be used to define a calibration point of the output voltage of a thermometer at the precise temperature 231.9 °C. Measurement of the infrared radiation emitted during transition through the melting temperature inflections of tin is analogous to the method by which the International Temperature Scale of 1990 (ITS-90) standards have been defined. The

temperature calibration points above the triple point of water (0.01 °C) have been defined by the melting points of several pure metals, up to the highest temperature melting point material defined presently, pure copper at 1084.6 °C [10], [11]. The purity of metals used in fixed point temperature standard cells to define ITS-90 have been specified to comprise a minimum of 99.9999% of the elemental metal.

A rudimentary fixed point temperature calibration cell was created by coating the core of a sapphire fibre optic with layers of tin, that were encapsulated by layers of silver. A schematic diagram of the fibre optic arrangement, illustrating the fibre optic tip, with multiple reflections of infrared radiation that occurred within it from the tin deposit and infrared radiation that was coupled into and transmitted along the fibre optic, is presented in figure 6.1.

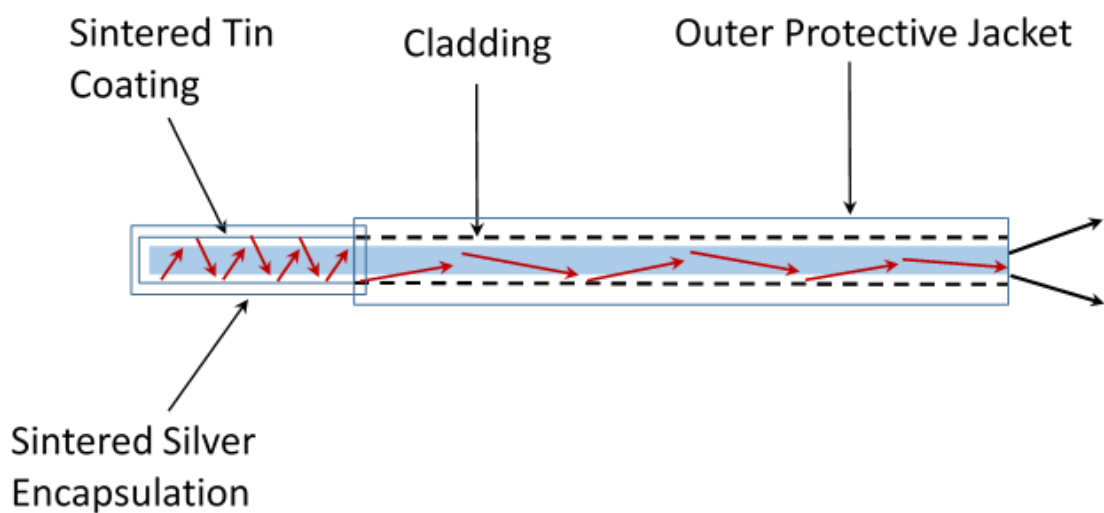


**Figure 6.1 Schematic diagram of silver encapsulated, tin coated sapphire fibre optic core used to create integral calibration point on fibre optic probe**

A sapphire fibre optic having a core of 425 µm diameter was exposed from the protective jacket for a length of approximately 40 mm from an open tip and coated with layers of tin nanoparticles suspended in water and ethylene glycol. The liquid acted as a carrier to deposit the solid tin nanoparticles onto the surface of the fibre optic core. The tin deposited onto the fibre optic surface was sintered after each layer was

applied to form a solid metal agglomeration on the fibre optic surface. Each layer of tin was sintered in a furnace set at 150 °C for ten minutes. After several layers of tin were deposited and sintered, the fibre optic tip was encapsulated in several layers of silver nanoparticles suspended in water and ethylene glycol mixture. Each layer of silver deposited was sintered at 150 °C for ten minutes, to form a layer of agglomerated silver that encapsulated the underlying tin. The sapphire fibre acted as a body on which to deposit the tin and a medium to transmit infrared radiation from the heated coating to an infrared radiation thermometer (IRT) positioned at the output end of the fibre. The silver layers acted to encapsulate the tin so that it remained in contact with the fibre optic surface and did not run off the surface when molten.

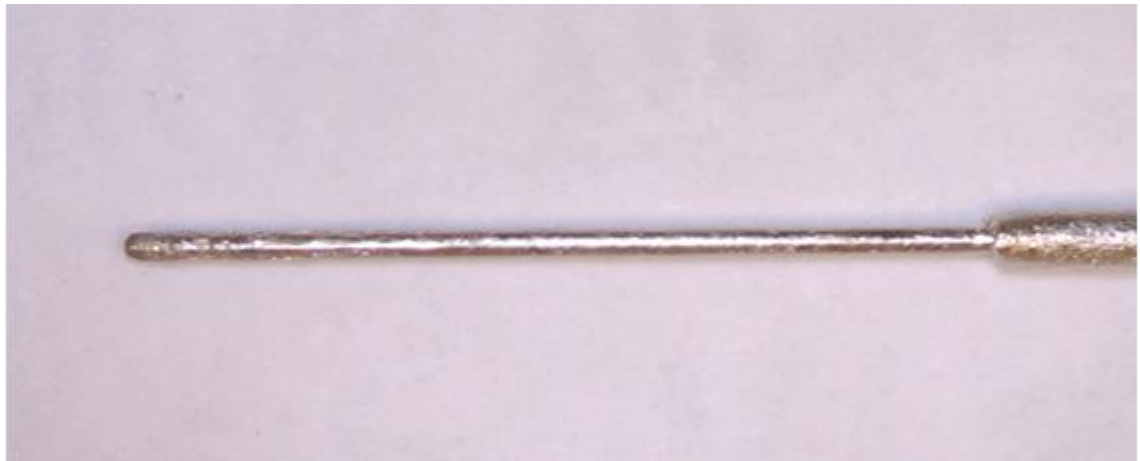
The tip of the fibre optic probe acted as an approximate blackbody, having a length to diameter ratio exceeding five and having multiple reflections of the infrared radiation throughout the fibre core from the heated tin coating, immediately adjacent to the surface of the core [12], [13].

The prototype thermometer coupled to a fibre optic probe that was developed was not traceable to ITS-90 standards because the materials used did not have certified compositions. The quantities of metals deposited were unknown, therefore, the magnitude of inflection within the temperature versus time history curve caused by the phase transformation was unknown. This prototype was intended only as a demonstration that making a thermometer coupled to a fibre optic probe with an integral fixed point temperature calibration cell was feasible.

An example short length of fibre optic coated with tin, encapsulated by silver coating and connected to a prototype thermometer to form an experimental thermometer with integral tin fixed point cell is illustrated in figures 6.2 to 6.4.



**Figure 6.2 Sintered tin nanoparticle coated sapphire fibre optic forming layers of**



**metal that adhered to the bared fibre optic surface**

**Figure 6.3 Sintered silver nanoparticle coated sapphire fibre optic, encapsulating underlying layers of tin within the silver coating**

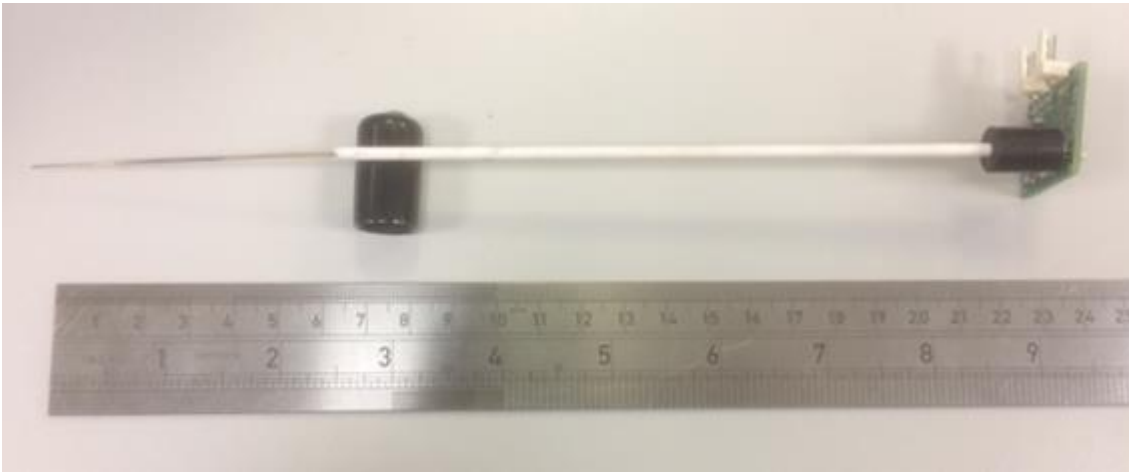


**Figure 6.4 Sintered tin and silver nanoparticle coated sapphire fibre optic coupled to compact infrared thermometer printed circuit board for laboratory testing of prototype thermometer with integral tin fixed point cell**

The fibre optic probe was mounted in a short length of ceramic tube to afford sufficient rigidity to the probe to be able to insert it into the centre of the thermo-well on a blackbody source and to afford supporting the assembly connected to the prototype SWIR thermometer printed circuit board (PCB). The SWIR thermometer with fibre optic probe assembly was characterised against a blackbody source through a series of known temperatures and the resulting calibrated thermometer used to measure the radiation emitted by the rudimentary fixed point temperature calibration cell.

### 6.3 Characterisation of sapphire fibre optic coupled, SWIR thermometer

The extended-InGaAs thermometer, coupled to the tin and silver coated sapphire fibre optic probe, was characterised against the temperature of an Ametek Land Landcal P550P approximate blackbody source at temperatures between 50 °C and 450 °C. The characteristic thermometer output voltage versus blackbody source temperature curve is presented in figure 6.5. The thermometer output voltage axis has been presented on a logarithmic scale to illustrate more clearly the wide range of output voltage that was measured using this thermometer configuration.

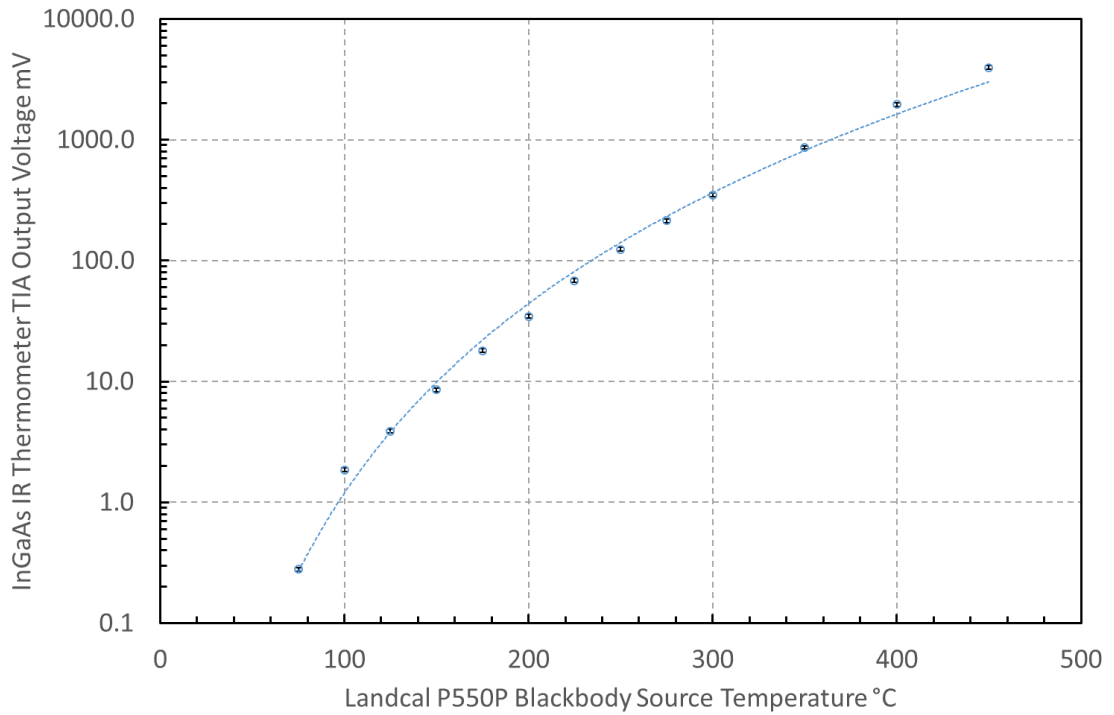


**Figure 6.5 Characteristic output voltage of thermometer transimpedance amplifier versus blackbody source temperature curve.**

The extended-InGaAs infrared thermometer with 10 MΩ transimpedance evidently could measure temperatures above a minimum of 100 °C up to a maximum of approximately 450 °C. The maximum temperature was constrained by saturation of the transimpedance amplifier output at the op-amp positive supply voltage of +5 V, for this version of the thermometer. It would be possible to extend the range to higher maximum temperature by using higher voltage power supplies and components that were capable of accepting these, enabling higher temperatures to be measured before the transimpedance amplifier output saturated.

The relationship between the output voltage and temperature should comply with the formulation determined for the ratio between band radiances from the Wien approximation, that was presented in chapter 2, equation (2.13). The natural logarithm of the output voltage,  $\ln(V_o)$  should have a linear relationship with the inverse of absolute temperature measured,  $1/T$ , to the first order approximation of this relationship. The relationship of  $\ln(V_o)$  against  $1/T$  evaluated from the characterisation measurements for this thermometer is presented in figure 6.6.

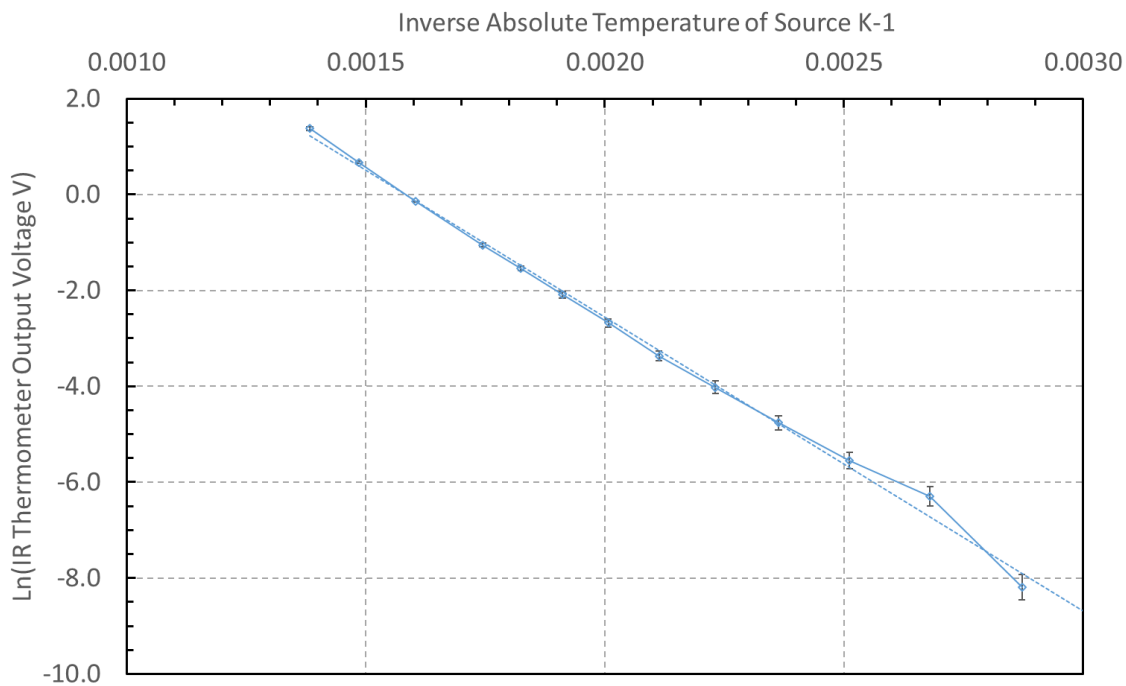


**Figure 6.6 Characteristic curve of thermometer  $\ln(V_o)$  versus  $1/T$  of blackbody source**

The variation of the thermometer output voltage with source temperature followed the expected linear relationship for source temperatures above 100 °C (inverse absolute temperature value 0.00268 /K) but became non-linear below this temperature. The non-linearity owed to the magnitude of the noise contributing increased variability within the total output voltage (signal + noise) measured, particularly as the noise limit of the op-amp used to configure the TIA was approached. This noise magnitude imposed a limit upon the capability of the thermometer to measure temperatures without additional signal processing to extract a useful signal.

The noise limited equivalent temperature resolution of the thermometer was calculated based upon applying Wien's approximation, that was also elaborated in chapter 2, equations (2.16) and (2.17). The variation of the noise limited equivalent temperature resolution calculated from the thermometer characterisation is presented in figure 6.7.

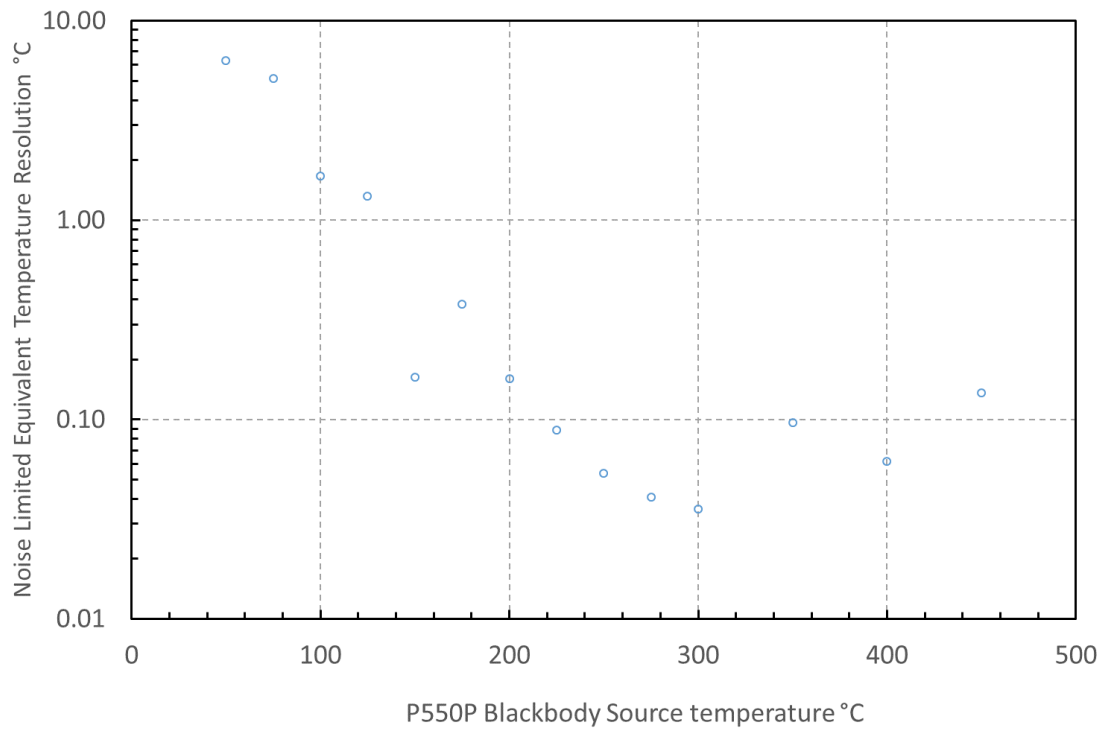


**Figure 6.7 Noise limited equivalent temperature resolution of the extended-InGaAs based thermometer with 10 MΩ transimpedance**

The signal to noise ratio (SNR) for the thermometer was defined as the ratio between the mean value of the output voltage and its standard deviation measured during characterisation. The variation of the thermometer SNR with source temperature measured is presented in figure 6.8.

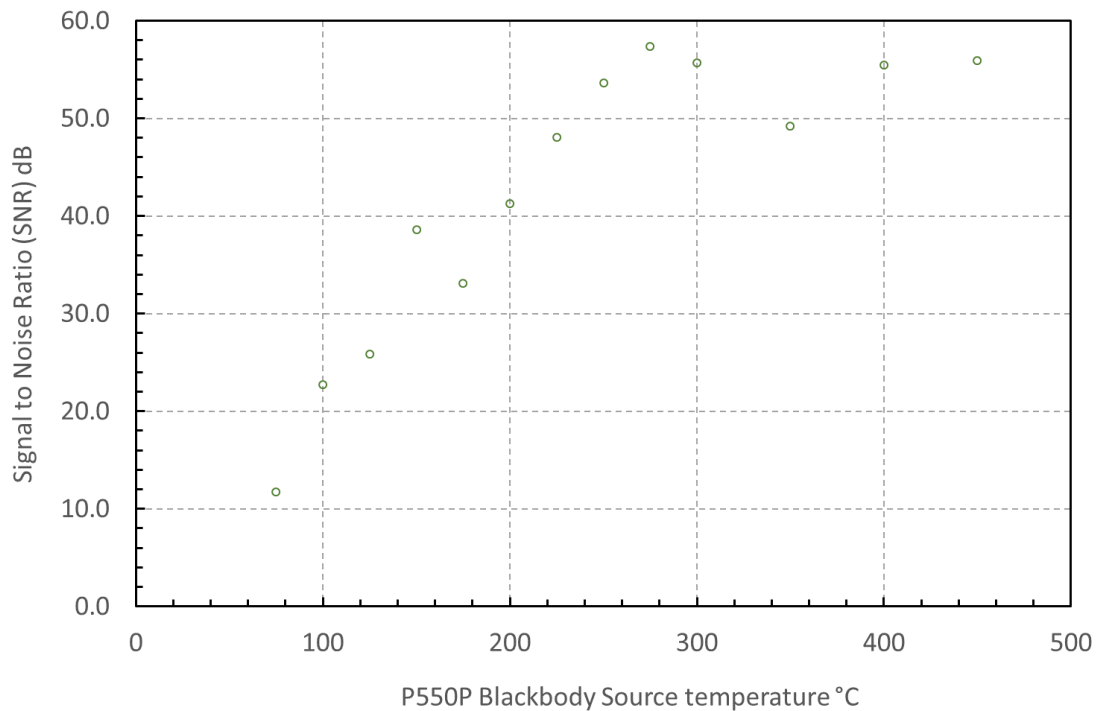


**Figure 6.8 Signal to noise ratio of the extended-InGaAs based IRT**

The noise limited equivalent temperature resolution and SNR variations with source temperature measured and presented within the graphs confirmed that the thermometer configured using the uncooled extended-InGaAs photodiode with 10 M $\Omega$  transimpedance amplifier and receiving unchopped infrared radiation through sapphire fibre optic was suitable for measuring source temperatures above 100 °C. The resolution of measurements acquired above 100 °C was 2 °C and reduced to 1 °C for measurements above 150 °C.

A Sakuma-Hattori curve fit to the characteristic infrared thermometer output voltage versus blackbody source temperature was determined, illustrating the capability to interpolate any temperature measurement between the known points from the output voltage measured. Curves illustrating the variations of modelled and measured output voltages and error between the modelled and measured values with source temperature are presented in figure 6.9.

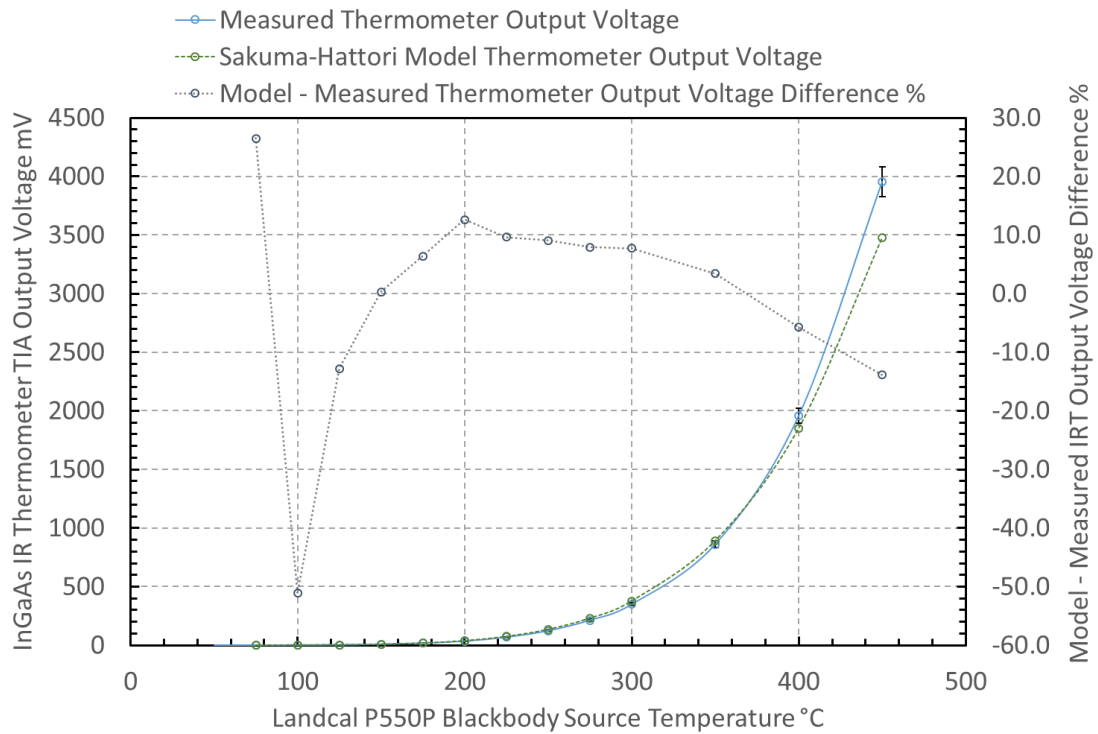


**Figure 6.9 Sakuma-Hattori curve fit to measured characteristic of the infrared thermometer based upon using the extended-InGaAs photodiode**

The Sakuma-Hattori model curve scale factor for this configuration of thermometer was determined to be 16.6 V at a limiting effective wavelength of 2.35  $\mu\text{m}$ . It was inferred that the thermometer had a high sensitivity to changes in source temperature measured and was estimated to be able to resolve 0.05  $^{\circ}\text{C}$  changes in source temperature measured using a bench-top digital multi-meter that provided 10  $\mu\text{V}$  resolution. The limiting voltage resolution applicable was inferred from the minimum output voltage noise measured from the prototype thermometer. The Keysight 34465A multi-meter used can measure smaller voltage signals but these would be dominated by the output voltage noise of the thermometer amplifier. The thermometer configured and characterised should be suitable for measuring the small variations in the infrared radiation as the rate of change of temperature varied during the melting phase transformation of tin deposited onto a sapphire fibre optic.

## 6.4 Application of prototype SWIR thermometer measuring temperature inflections during phase transformations of tin

The prototype tin coated and silver encapsulated fibre optic probe thermometer used the 10  $\text{M}\Omega$  transimpedance, zero drift op-amp version of the thermometer printed

circuit board, with the extended-InGaAs photodiode. The thermometer was used to measure the infrared radiation transmitted along the 425  $\mu\text{m}$  core diameter of a sapphire fibre optic from the metal coated end that was heated and cooled through the range of temperatures around the tin melting temperature.

The coated tip of the sapphire fibre optic was inserted into the calibration thermo-well on an Ametek Land Landcal P550P approximate blackbody source. The blackbody temperature set point was increased and decreased at a constant rate of 0.05  $^{\circ}\text{C}/\text{minute}$ , through the temperature range 230.0  $^{\circ}\text{C}$  to 235.0  $^{\circ}\text{C}$  and at constant rates of 0.1  $^{\circ}\text{C}/\text{minute}$  and 0.25  $^{\circ}\text{C}/\text{minute}$ , through the temperature range 225.0  $^{\circ}\text{C}$  to 240.0  $^{\circ}\text{C}$ . The heating and cooling regimes imposed passed through the temperature range over which the solidus to liquidus and inverse phase transformations of pure tin occurred. Using tin nanoparticles coated onto a sapphire fibre optic that was heated and cooled through the temperature ranges quoted afforded measurement of the tin melting phase transformation temperature change. The mean output voltage from repeated measurements using the fibre optic probe thermometer led to the characteristic presented in figures 6.10 to 6.12 for heating and cooling rates of 0.05  $^{\circ}\text{C}/\text{minute}$ , 0.1  $^{\circ}\text{C}/\text{minute}$  and 0.25  $^{\circ}\text{C}/\text{minute}$ , respectively. The fibre optic IRT output measurements have been compared to the interpolation curve between calibration measurements of the fibre optic probe IRT without the metal present, evaluated from Wien's approximation and shown as a black dashed line on each plot.

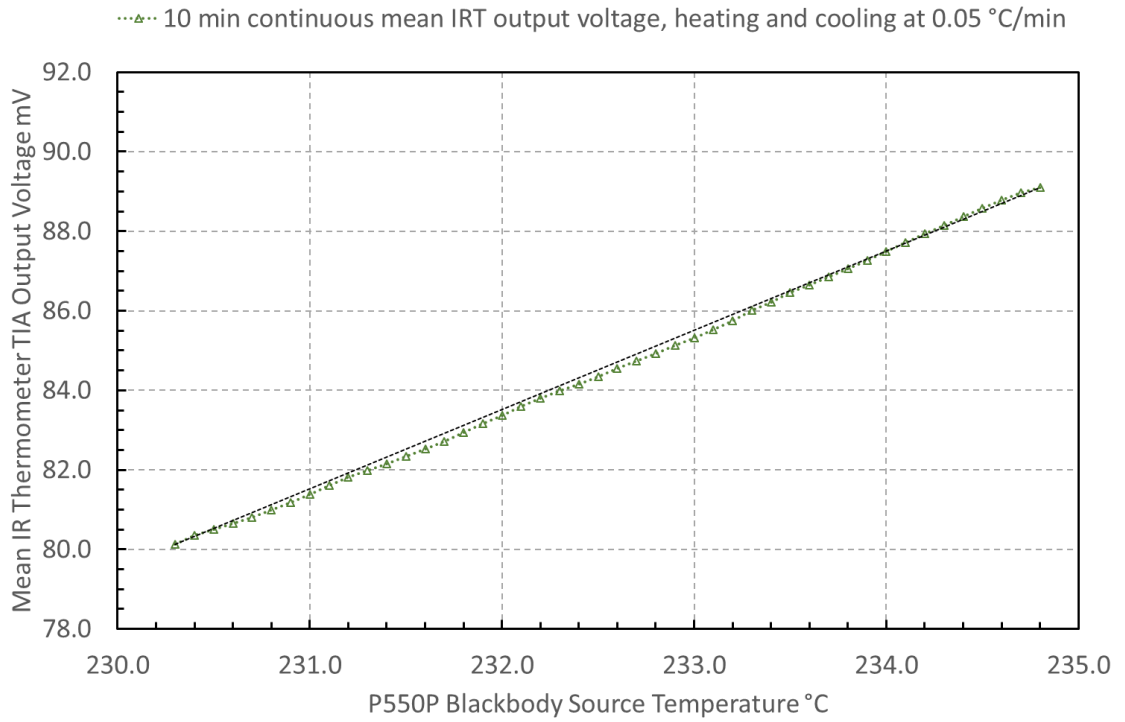


**Figure 6.10 Mean InGaAs thermometer output voltage whilst heating and cooling Tin coated fibre optic through transformation temperature at 0.05 °C/minute**

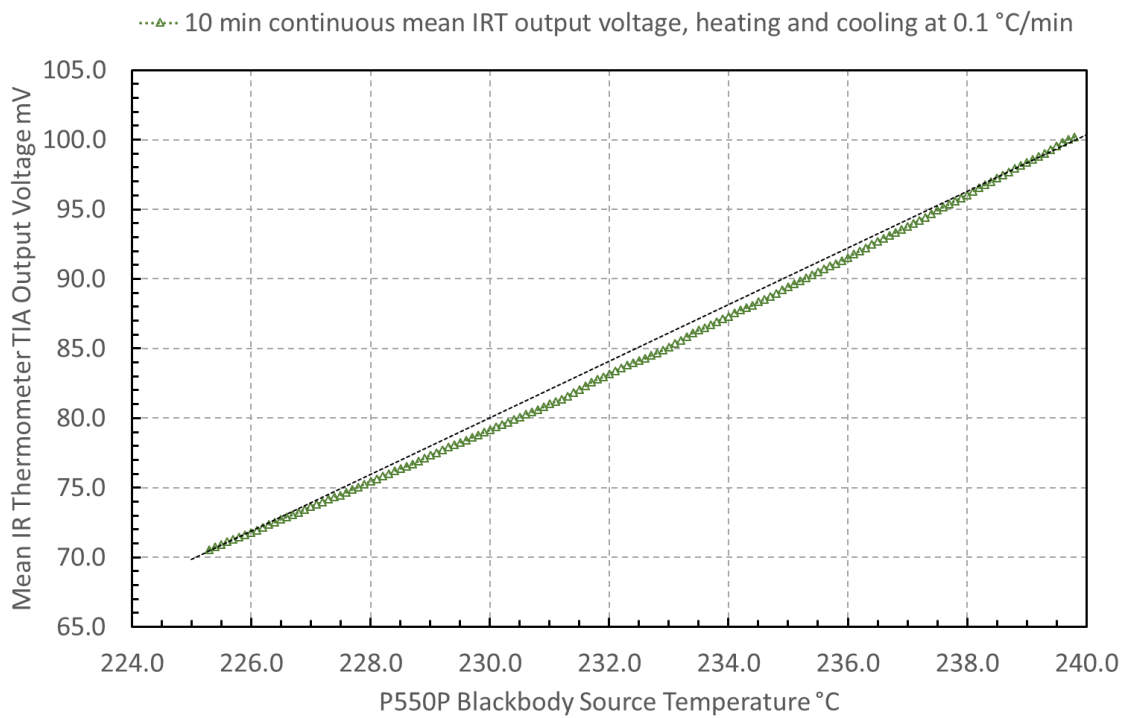


**Figure 6.11 Mean InGaAs thermometer output voltage whilst heating and cooling Tin coated fibre optic through transformation temperature at 0.1 °C/minute**

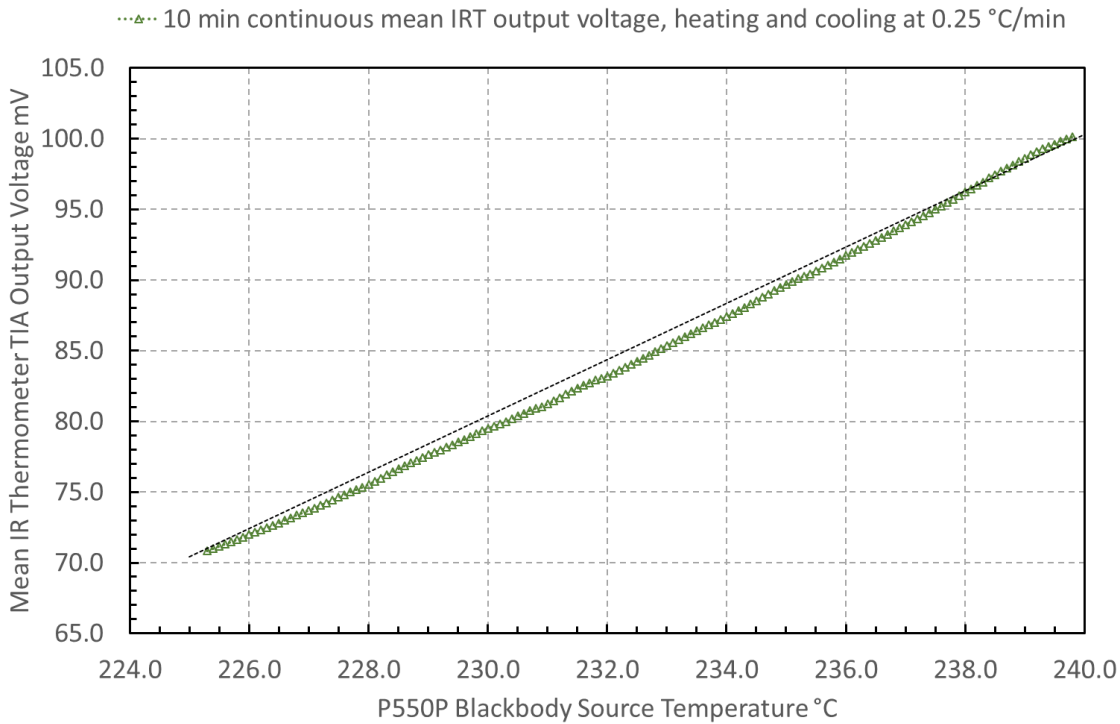


**Figure 6.12 Mean InGaAs thermometer output voltage whilst heating and cooling Tin coated fibre optic through transformation temperature at 0.25 °C/minute**

The thermometer incurred brief output voltage spikes that had a period of 1800 seconds (30 minutes), hence these were probably caused by an external source of electromagnetic interference. The thermometer continued to measure the infrared radiation arising from the heated probe at the same magnitude as prior to the excursions immediately following these periodic disturbances. The excursions were eliminated from the data analysed, thereby having no effect upon the mean values of the measurements calculated. The mean values of the thermometer output voltage evaluated from the measurements of thermometer output during heating and cooling of the fibre optic probe incurred peak-to-peak noise magnitude of 2.4 mV.

The extended-InGaAs version of the thermometer had low noise magnitude, owing to the zero drift op-amp used for the transimpedance amplifier and high output voltage,

owing to the photosensitivity of the photodiode and 10 M $\Omega$  transimpedance used. The infrared intensity emitted at the melting temperature of tin was lower at the short-wave infrared wavelengths to which the extended-InGaAs photodiode responded than the mid-wave infrared radiation to which the InAsSb photodiode responded, owing to the low temperature at which tin melts. The compromise between the higher photosensitivity of the extended-InGaAs photodiode compared to the InAsSb photodiode and the lower intensity of infrared radiation emitted in the SWIR waveband led to the necessity to measure small differences in thermometer output voltage to identify the inflection around the tin melting and freezing point temperature.

There were inflections from the linear increasing source temperature and modelled IRT output evident in the measurements, with maximum deviations of approximately 1.1 mV. The inflections observed in the mean output voltage versus source temperature curves had similar magnitude to the noise but demonstrated a consistent reduction of gradient through the temperature range 225.0 °C to 240.0 °C, as illustrated in figures 6.10 to 6.12. The thermometer output voltage versus source temperature curve when heating and cooling at rates of 0.1 °C/minute and 0.25 °C/minute demonstrated more pronounced inflections than the curve measured at a heating and cooling rate of 0.05 °C/minute. The temperature ranges over which the inflections in the gradients of the thermometer output voltage versus source temperature curves occurred were proximate to the temperature range over which tin would be expected to melt and freeze. The temperature ranges over which melting and solidification occurred were broadened, which indicated that there were impurities in the tin deposited [14]. The inflections away from the linear increasing temperature of the source indicated that the thermometer measured the effect of the tin phase transformation upon the intensity of infrared radiation transmitted to the thermometer. The lowest rate of heating and cooling tested was too slow to elucidate the temperature inflection well. The evidence of the weak inflection implied that the fibre optic tip temperature tracked the thermowell temperature more closely, which compensated partially for the heat absorption and release by the tin.

The deviations from the linear temperature gradient imposed by the source were not sufficiently distinct to provide a fixed point temperature calibration because of the broadened range over which the inflections occurred and the noise having comparable magnitude to the change of thermometer output voltage observed. Identifying the transition between solidus and liquidus states of tin relied upon averaging over multiple data sets to reduce the effect of noise. The inflections measured provided evidence that the tin coating on the fibre optic probe acted like a fixed point temperature standard cell. The prototype demonstrated the feasibility of creating a fibre optic probe thermometer with an integral fixed point temperature calibration cell, albeit the inflections observed in the temperature versus time history curves were weak. The change to the infrared radiation intensity derived from melting and solidifying the tin within the integral fixed point cell could be strengthened by having a larger mass of tin deposited undergoing the phase transformation. This adaptation would ensure that the temperature inflection, therefore, thermometer output voltage inflection, was more prominent within the variations caused by noise. Depositing pure tin and maintaining its purity during formation of cell on the probe would afford identification of the tin melting temperature more precisely, rather than incurring the broadened melting temperature range observed with the prototype device.

Burst noise was evident in the individual output voltage measurements and caused large, random but brief excursions in output voltage, rather than the smooth and slowly changing response to smooth changes in the blackbody source temperature. The burst noise sources were unknown and the noise obfuscated the measured response of the thermometer for brief durations only, so these data were eliminated from the calculations of mean output voltage. Grounding the thermometer printed circuit board reduced the magnitude of interference from external noise sources but did not eliminate the burst noise from the measurement.

The ideal thermometer would have higher SNR than the prototype thermometer using the uncooled extended-InGaAs photodiode, at the response speed necessary to identify the inflection in the temperature versus time history curve. It may be possible to achieve better resolution of the tin melting and freezing transformation temperature inflection by using a cooled photodiode to reduce the noise and boost the SNR and

chopping the infrared signal to afford amelioration of zero offset and drift. Such a thermometer would not be as compact as the prototype device but could be integrated into a measurement system that formed a self-calibrating thermometer.

The concept of having a thermometer coupled to a fibre optic probe with an integral fixed point temperature calibration cell could be extended to create a thermometer with multiple fixed point temperature metals deposited and ultimately, a self-calibrating thermometer. A thermometer with the ability to undergo in-operando calibration assessment, could also report upon the calibration drift incurred over time, thereby providing a step towards creating a thermometer probe with self-diagnostic capabilities.

## Summary of Chapter

A short-wave infrared version of the prototype thermometer that used an extended-InGaAs photodiode was used to measure the temperature inflections during melting and freezing of tin. The tin was deposited directly onto the surface of a 425  $\mu\text{m}$  diameter core sapphire fibre optic. The resulting fibre optic probe was heated and cooled through multiple cycles, over the temperature ranges:

- 230.0  $^{\circ}\text{C}$  to 235.0  $^{\circ}\text{C}$  at a rate of 0.05  $^{\circ}\text{C}/\text{minute}$
- 225.0  $^{\circ}\text{C}$  to 240.0  $^{\circ}\text{C}$  at rates of 0.1  $^{\circ}\text{C}/\text{minute}$  and 0.25  $^{\circ}\text{C}/\text{minute}$

The thermometer was able to measure the appearance of weak inflections that occurred within temperature ranges that were consistent with the solidus to liquidus and inverse phase transformations of tin. The evidence of this experiment indicated that it would be feasible to create an infrared thermometer coupled to a sapphire fibre optic probe that had an integral fixed point temperature calibration cell deposited onto the surface.

This demonstration provided an initial step towards creating a fibre optic coupled, infrared radiation thermometer with an integral and in-operando, temperature calibration capability. Ultimately, such a device could be developed further to afford a self-calibrating or self-correcting thermometer that would have application to long-term deployment in manufacturing and research.

## REFERENCES

- [1] R. E. Bentley, 'Long-term drift in mineral-insulated Nicrosil-sheathed type K thermocouples', *Sensors Actuators A. Phys.*, vol. 24, no. 1, pp. 21–26, 1990.
- [2] R. E. Bentley, 'Irreversible thermoelectric changes in type K and type N thermocouple alloys within Nicrosil-sheathed MIMS cable', *J. Phys. D. Appl. Phys.*, vol. 22, no. 12, pp. 1908–1915, 1989.
- [3] P. Pavlasek *et al.*, 'Hysteresis Effects and Strain-Induced Homogeneity Effects in Base Metal Thermocouples', *Int. J. Thermophys.*, vol. 36, no. 2–3, pp. 467–481, 2015.
- [4] O. Ongrai, J. V. Pearce, G. MacHin, and S. J. Sweeney, 'A miniature high-temperature fixed point for self-validation of type C thermocouples', *Meas. Sci. Technol.*, vol. 22, no. 10, 2011.
- [5] D. Tucker *et al.*, 'Integrated self-validating thermocouples with a reference temperature up to 1329 °C', *Meas. Sci. Technol.*, vol. 29, no. 10, 2018.
- [6] C. J. Elliott, A. D. Greenen, D. Tucker, T. Ford, and J. V. Pearce, 'A Slimline Integrated Self-Validating Thermocouple: Initial Results', *Int. J. Thermophys.*, vol. 38, no. 9, pp. 1–10, 2017.
- [7] Hamamatsu Photonics, 'InGaAs PIN photodiodes G12180 data sheet', no. 4. pp. 1–8, 2018.
- [8] SEDI-ATI Fibres Optiques, 'Special Fibers', *SEDI-ATI Datasheet*. SEDI-ATI webpage, Accessed May 2018.
- [9] J. P. Makai and J. J. Makai, 'Current-to-voltage converter for linearity correction of low shunt resistance photovoltaic detectors', *Rev. Sci. Instrum.*, vol. 67, no. 6, pp. 2381–2386, 1996.
- [10] International Committee for Weights and Measures, 'ITS-90 Published in the Procès-verbaux du Comité International des Poids et Mesures , 78th meeting, 1989', *Procès-verbaux du Com. Int. des Poids Mes.*, vol. 78th meeti, 1989.
- [11] H. Preston-Thomas, 'The International Temperature Scale of 1990 (ITS-90)', *Metrologia*, vol. 27, no. 107. pp. 3–10, 1990.

- [12] E. M. Sparrow, L. U. Albers, and E. R. G. Eckert, 'Thermal radiation characteristics of cylindrical enclosures', *J. Heat Transfer*, vol. 84, no. 1, pp. 73–81, 1962.
- [13] J. Vollmer, 'Study of the effective thermal emittance of cylindrical cavities', *J. Opt. Soc. Am.*, vol. 47, no. 10, pp. 926–932, 1957.
- [14] W. Joung, J. V. Pearce, and J. Park, 'Comparison between the liquidus temperature and triple-point temperature of tin realized by heat pulse-based melting', *Metrologia*, vol. 55, no. 3, pp. 17–24, 2018.

## 7 CONCLUSIONS

The thesis presented herewith has described the laboratory development and testing of compact, fibre optic coupled infrared thermometers (IRTs) that can substitute for embedded thermocouples. A number of the test applications incurred harsh conditions that would increase the uncertainty of temperature measurements acquired by thermocouples. Non-contact temperature measurements afford solutions to many of the problems associated with measurement by invasive thermocouples in such harsh conditions. The conditions are challenging to achieve mounting and operation of IRTs that are available commercially. The IRTs developed used uncooled photodiodes that received unchopped radiation via fibre optic coupling and had no lens systems deployed. The IRTs configured had low mass and were constructed using small footprint printed circuit boards (PCBs) and surface mounted components, thereby afforded the capability of being installed into constrained spaces or mounted onto moving equipment. Drift of thermocouple calibration causes increased uncertainty in temperature measurements, therefore disallows optimal control of processes and presents a challenge to the maintenance of consistent conditions and product quality in manufacturing. Addressing this challenge using low-drift or drift-free thermometers presents an opportunity to improve temperature measurements and optimise production. The capabilities of the thermometers developed to measure across different temperature ranges and the uncertainties attached to those measurements were characterised. Practical calibrations of the thermometers were derived from measurements of known temperatures. Models of the IRT response were calculated to

afford interpolation of the thermometer output voltage versus source temperature relationship between the temperature calibration points.

The following points summarise the key achievements and knowledge generated by the project.

1. A compact and high speed mid-wave infrared (MWIR) thermometer has been configured using:

- A commercially available Hamamatsu P13243-11-MA Indium Arsenide Antimony (InAsSb) semiconductor alloy photodiode
- A bootstrapping amplifier to enhance the apparent impedance of the photodiode and transimpedance amplifier to amplify the photocurrent to a measurable voltage
- Infrared transmitting fibre optic embedded into an object that coupled between the source and thermometer, using either sapphire or metal fluoride fibre optics

The MWIR thermometer used the InAsSb photodiode uncooled and received unchopped infrared radiation. This was the first demonstration of an uncooled InAsSb photodiode that received unchopped radiation being used to configure an MWIR thermometer for moderate and lower temperature range measurements. The thermometer did not need the ancillary components required for cooling and signal chopping that would be used, typically, in the configuration of IRTs for accurate measurement of low intensity radiation.

The initial prototype MWIR thermometer maintained measurements within an uncertainty of  $\pm 5$  °C, from a minimum temperature measurable of 200 °C and  $\pm 1$  °C above 350 °C. The temperature ranges over which the IRTs operated with low uncertainty and fast response speed, were useful for industrial process and product temperature measurement. Further versions of the thermometer PCB were configured to afford the measurement of different temperature ranges and to achieve increased signal to noise ratio.

2. The use of the prototype infrared radiation thermometers to substitute for thermocouples overcomes many of the problems associated with invasive thermometers by decoupling the measuring instrumentation from the source. Using

fibre optic coupling between the object being measured and the thermometer also provided immunity from electromagnetic interference and isolation of the object from the IRT. The speed with which the thermometer could respond to changing signals was faster than could be achieved by a thermocouple that incurs thermal inertia from the protective sheath and insulation used in its construction. The IRTs developed afforded temperature measurements with faster response speed than thermocouples and could be configured to have higher sensitivity.

3. The prototype fibre optic coupled IRTs have been applied to situations that incurred harsh conditions of high and rapidly changing temperatures and reactive chemical species at the measurement position. The harsh conditions incurred required that the thermometer PCB was placed remotely from the process and coupled to the harsh conditions via inert fibre optics. The small dimensions and low mass of the thermometer PCB, ensured that it could be mounted readily inside a process chamber or attached to an object and not interfere with the normal operation of the process or object. These tests demonstrated the feasibility of using the prototype IRT to substitute for thermocouples in applications that incurred harsh conditions.

4. The prototype IRTs were characterised against approximate blackbody sources that were set to known temperatures and working calibrations of the thermometers derived. The laboratory prototype IRT had a 1 M $\Omega$  resistance and 10 pF capacitance in the feedback network around the transimpedance amplifier inverting input. This feedback resistor–capacitor network enabled the response speed of the thermometer to be as short as 10  $\mu$ s, therefore, the thermometer could measure an alternating signal or equivalent rapidly changing signal having a maximum frequency of 15.9 kHz. The noise-limited equivalent temperature resolution, uncertainty around measurements and signal to noise ratio were characterised from the relationship of output voltage with known temperatures measured for calibration. An interpolation curve was derived using the Planck form of the Sakuma–Hattori equation that described the relationship between the thermometer output voltage and source temperature, thereby enabling unknown source temperatures to be determined from the resulting thermometer output voltages.

5. The prototype MWIR thermometer was amended to afford lower temperature range measurements to be acquired. The lower temperature range version of the thermometer used a zero drift op-amp to configure the transimpedance amplifier and incurred low offset voltage and low noise. The zero drift op-amp version of the transimpedance amplifier afforded more stable output voltage than the equivalent precision op-amp. The low temperature prototype thermometer also used a larger diameter ZBLAN metal fluoride fibre optic to couple the mid-wave infrared radiation to the photodiode. These changes improved the signal to noise ratio arising for lower temperatures, enabling the practically useful, minimum temperature measurable achieved by the thermometer to be reduced to 30 °C with a measurement uncertainty of  $\pm 1$  °C.

6. A variant of the compact IRT configuration using a Hamamatsu G12183-010K, extended range Indium Gallium Arsenide (extended-InGaAs) photodiode coupled to a sapphire fibre optic was constructed to configure a short-wave infrared (SWIR) thermometer. The configuration of the IRT was retained as being an uncooled photodiode receiving unchopped radiation. The product of the extended-InGaAs photosensitivity and sapphire fibre optic transmission curves maximised the intensity of incident radiation upon the photodiode within the wavelength range to which it responded. The open-ended tip of the sapphire fibre optic was coated with layers of tin and encapsulated in layers of silver. The resulting fibre optic probe was heated and cooled through multiple cycles around the tin melting temperature of 231.9 °C. The response of the thermometer measured during heating and cooling, demonstrated weak inflections around the tin melting and freezing temperature. The inflections indicated that the heat of phase transformation of the small volume of tin present on the fibre optic surface had been absorbed (during heating) and released (during cooling). This thermometer demonstrated that it would be feasible to use a fibre optic probe coated with metal to create an integral fixed point temperature calibration cell. Such a thermometer could be corrected for drift and provide self-calibration, in-operando.

7. A version of the prototype IRT was configured using the extended-InGaAs photodiode with 1 M $\Omega$  transimpedance, coupled to a sapphire fibre optic and was

intended for undertaking higher temperature range measurements. This SWIR version of the compact IRT would be suitable for measurements of industrial furnace temperatures, typically having minima above 300 °C and maxima above 1000 °C. The prototype thermometer was suitable for process monitoring of industrial furnaces that need to control temperatures exceeding a few hundred Celsius.

8. The feasibility of substituting infrared thermometers, coupled to fibre optics that were embedded into objects, for thermocouples has been demonstrated successfully. The IRTs configured and tested were prototype versions that would need to be engineered to afford more robust construction that could survive for longer durations in the physically damaging conditions to which they were exposed. Improvement of the longevity of the instruments configured will be essential to implement thermometers that can be used continuously and for long durations in harsh conditions, within industrial applications.

The project objectives to substitute infrared radiation thermometers for thermocouples used for measurements from harsh conditions that were met fully or partially were:

- the creation of the first IRT that used an uncooled MWIR photodiode and received unchopped radiation via fibre optic coupling
- the extension of the range of temperature measurements measurable to include near ambient room temperature
- the first demonstration of a chopper-stabilised op-amp used to create a 'zero drift' IRT that adhered to zero offset better than an equivalent precision op-amp configuration and incurred low noise, enabling small magnitude signals to be measured successfully
- creation of a compact device that had sufficiently low manufacturing and installation cost that total loss in harsh conditions would not be critical
- the first demonstration of the feasibility of embedding fibre optics into Lithium-ion cells to acquire measurements from the components inside a cell
- the first demonstration of the feasibility of applying fixed point cell materials to a fibre optic probe IRT and measuring the small effect upon measured

temperature of having a mass of metal undergoing solid to molten phase transformation

The partial failures and the artefacts that needed improvement from the outcomes achieved within this project were:

- robustness of the protective covering for the fibre optic coupling embedded into cutting tools on the end milling machine to ensure that metal swarf could not shear through the protective layer and fibre
- the size of the PCB and surface-mounted components would ideally be reduced for a re-usable device that would also be encapsulated in a body affording improved rigidity and protection of the circuit from electromagnetically coupled (EMC) interference, along with component guarding and shortest track lengths used to minimise noise
- the lower temperature range IRT will need to have lower noise components used and higher transimpedance, effectively giving a higher 'gain' to increase the signal to noise ratio, affording measurement from lower temperatures, with the aim of achieving zero degrees Celsius minimum
- the development of integral calibration fixed point cells on a fibre optic probe IRT will require some collaborative research with materials scientists to understand the effects of different potential metal deposition methods and the effects upon the phase transformation temperature of using nano-particle suspensions to supply the metal elements

Developments from the novel prototype IRTs demonstrated in this project could provide devices suitable for thermocouple substitution in many applications, particularly scenarios requiring deployment of thermometers into harsh physical or chemical conditions. Substituting robust IRTs for thermocouples could reduce the manufacturing costs of products, resulting from improved understanding of the processes, the pertinent factors that affect temperature variations and control of processes to tighter tolerances. Typical improvements to process control achievable

with present technologies can lead to significant cost benefits, reaching many millions of pounds for continuous, large-scale production of basic materials.

Further research and development of fibre optic probe IRTs with integral calibration fixed point cells could lead to the creation of thermometers with in-operando or self-calibrating capabilities, particularly if the IRT artefact could be combined with artificial intelligence or machine learning software to create a 'smart' thermometer. Such devices should become standard in distributed control systems and inter-connected measurement and recording systems in advanced manufacturing facilities. The capability to maintain production whilst checking calibration or interfacing measurements to a downstream process has the potential to save significant amounts of unproductive time and reduce costs in manufacturing.

## 8 FUTURE WORK TO EXTEND THE CAPABILITIES OF FIBRE OPTIC COUPLED INFRARED THERMOMETERS

### 8.1 Indium Arsenide avalanche photodiode to increase sensitivity

The potential exists to use an Indium Arsenide avalanche photodiode (InAs APD) that responds with higher magnitude photocurrent than achieved by the prototype within the 3.0-3.5  $\mu\text{m}$  waveband. The InAs APD would need to be cooled to enable avalanche gain and minimise the dark current of the device, thereby constraining its use as a small footprint device. The InAs APD could provide increased response to lower temperature sources, therefore affording lower minimum temperature measurable than achieved using the uncooled InAsSb photodiode. Static positioning of a prototype InAs APD thermometer externally to a process, with sufficient space to afford the larger size necessary for photodiode cooling, would be necessary for such a thermometer. The combination of InAs APD with fibre optic coupling should be evaluated as a potential improvement to the prototype thermometer.

### 8.2 Transimpedance amplifier with lower noise and input voltage offset

Development of lower noise, higher speed and higher sensitivity transimpedance amplifiers with higher signal to noise ratio would enable the thermometer to measure

over wider temperature ranges and afford substitution for thermocouples in further applications. The potential exists to extend the prototype thermometer that used zero-drift operational amplifiers to configure the transimpedance amplifiers from this project to thermometers with wider measurement range and higher sensitivity.

### 8.3 Self-calibrating fibre optic probe thermometer

Further research should be undertaken concerning the development of infrared thermometers that have integral, fixed point temperature calibration cells deposited onto the core of fibre optic probes. Successful implementation could lead to the creation of 'self-calibrating' thermometers that afford continuous temperature measurement whilst undergoing in-operando calibration.

Development of a self-calibrating IRT would require several strands of research to be undertaken to understand: the effects of material types upon properties (for example: the effects of using nanoparticle suspensions upon melting temperature range), deposition methods to ensure that consistent and accurate mass and distribution of metal is achieved and artificial intelligence technologies to interpret and respond to changes in the temperature history curve. National and international calibration standards, based upon the ITS-90 temperature scale definition define the purity requirements of the metal and temperatures at which the solidus to liquidus phase transformations occur [Preston-Thomas ITS-90]. These standards will have to be adhered to or adapted to enable metal deposition onto a fibre optic core to be used as a secondary calibration standard. Further standards that will need to be adhered to or amended define the capabilities and limitations of equipment and the schedule to maintain traceable measurements, for example standards concerning: fibre optic probes for distributed temperature measurement [BS EN 61757], utilisation of electronic devices and software in temperature measurement systems [BS EN 61987] and temperature measurement equipment calibration requirements [ISO 9001:2008].

Such a thermometer could be used in situations that demanded small temperature measurement uncertainties or that were critical to safe operation, for example: chemical refining, medical sterilisation and materials manufacturing processes. A self-

calibrating thermometer of this type with traceable calibration could also act as a secondary standard.

## 8.4 Higher temperature prototype SWIR thermometer configuration

The initial development of the prototype SWIR thermometer with an uncooled, extended-InGaAs photodiode that received unchopped radiation was intended for the measurement of higher temperature ranges, above a few hundred Celsius.

The higher temperature version of the SWIR thermometer was configured using the same arrangement of operational amplifiers described for the prototype mid-wave infrared thermometer of chapter 4 but using the extended-InGaAs photodiode that responded through the range of wavelengths 0.9 – 2.6  $\mu\text{m}$ . This thermometer would be suitable for measuring higher temperatures presented by industrial processes, for example, metallurgical furnaces. The higher temperature range thermometer was configured with 1 M $\Omega$  transimpedance and consequent fast response speed.

The characteristic voltage output versus approximate blackbody source temperature curve for the thermometer comprising extended-InGaAs photodiode with 425  $\mu\text{m}$  diameter core sapphire fibre optic coupling is presented in figure 8.1.

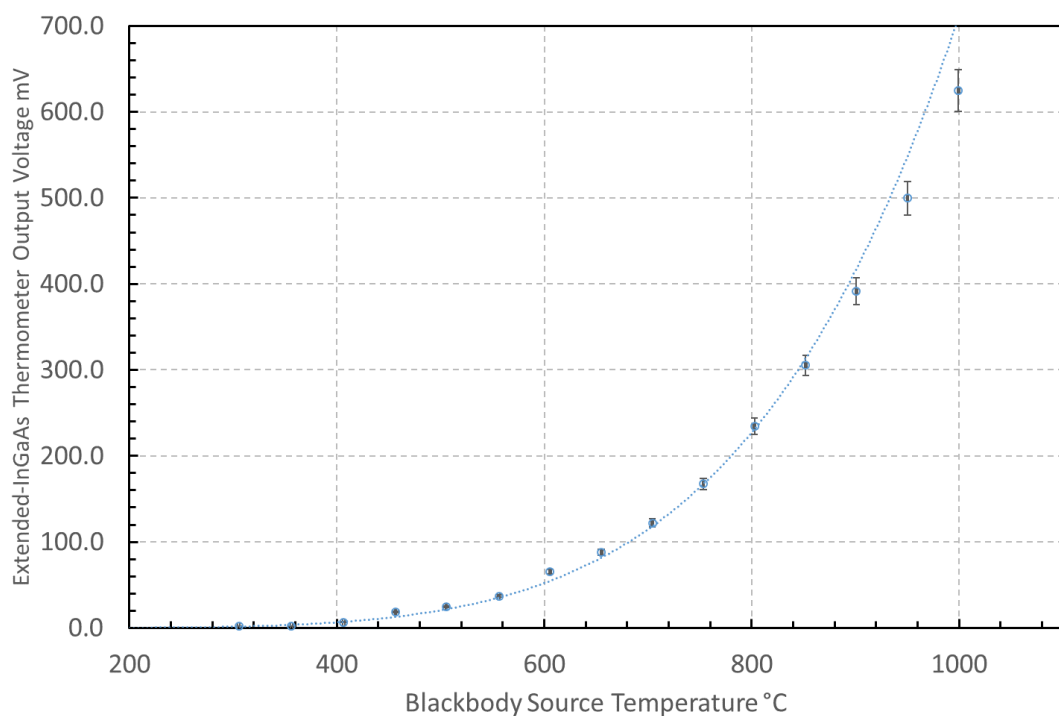


**Figure 8.1 Characteristic curve of 1 M $\Omega$  transimpedance, sapphire fibre optic coupled extended-InGaAs IRT against known blackbody source temperatures**

The output voltage generated by the IRT was higher than the equivalent InAsSb thermometer measuring similar source temperatures, owing to the higher photoresponsivity of the extended-InGaAs photodiode and better match of wavelengths transmitted by the sapphire fibre optic. It was evident that the minimum temperature measurable with this configuration would be between 200 °C and 300 °C. The maximum temperature measurable by the thermometer, with  $\pm 5$  V power supplies, was estimated to be approximately 1200 °C. Typical industrial furnaces operate at temperatures from several hundred Celsius to over one thousand Celsius, therefore can be measured readily by the SWIR extended-InGaAs thermometer. The SWIR thermometer should be applied to industrial furnace temperature measurements, providing further example applications of the compact thermometers.

## APPENDIX 1. PLANCK BLACKBODY CURVE CALCULATIONS

The method used for calculating blackbody radiation outlined in chapter 2 has been formulated as a spreadsheet enabling calculation of infrared spectral radiance, hemispherical band radiance, radiant power incident upon a detector, photocurrent generated and transimpedance amplifier output voltage. The spreadsheet calculations are described in the following.

Spectral radiance was calculated according to the frequency formulation of Widger and Woodall [1], as follows:

$$L_{\nu}(T) = \left( \frac{2h\nu^3}{c^2} \right) \left[ \frac{1}{\left( e^{\frac{h\nu}{kT}} - 1 \right)} \right]$$

where:

$L_{\nu}(T)$  is the spectral radiance of an object at absolute temperature, T

$h$  is the Planck constant  $6.6261 \times 10^{-34}$  J s

$\nu$  is the frequency of radiation, Hz

$c$  is the speed of light in vacuum  $2.9979 \times 10^8$  m/s

$k$  is Boltzmann's constant  $1.3806 \times 10^{-23}$  J/K

$T$  is the absolute temperature of the radiation object, K

The spectral radiance equation was rearranged and the following two constant values extracted from the integration, according to the numerical solution method used:

$$\frac{2k^4}{h^3 c^2} \tag{A2.1}$$

and

$$\frac{h}{k} \tag{A2.2}$$

were calculated from the fundamental constants:  $k$ ,  $h$  and  $c$ .

Wavelengths between 0.2  $\mu\text{m}$  and 5.0  $\mu\text{m}$  were tabulated in rows at increments of 0.2  $\mu\text{m}$  and the frequency of radiation,  $\nu$  calculated for each wavelength.

Temperatures between 300 K and 1750 K were tabulated in columns at increments of 50 K, with 273 K (0°C) and 293 K as additional temperature calculation points.

The constant of equation (A2.1) was multiplied by each absolute temperature value raised to the fourth power,  $T^4$  and the constant of equation (A2.2) was divided by each of the absolute temperature values.

The resulting variables were multiplied by the frequency of radiation related to each wavelength and tabulated in a look-up table referenced by the wavelength rows and temperature columns. These values represented the substitution by a new variable,  $x$  for the exponent  $\left(\frac{hv}{kT}\right)$ .

The series expansion  $\sum_{n=1}^{\infty} e^{-nx} \left[ \frac{x^3}{n} + \frac{3x^2}{n^2} + \frac{6x}{n^3} + \frac{6}{n^4} \right]$  for the substitute variable,  $x$  defined above, was calculated for the truncated series  $n = 1$  to 10, at the upper and lower limiting wavelengths between which the band radiance was required. These calculations were undertaken at each temperature increment. The resulting values were the spectral radiances at each wavelength and temperature increment, which were presented as separate rows for the two wavelength conditions.

The band radiance at each temperature increment was calculated by the difference between the spectral radiance values for the two wavelengths at each temperature increment. The wavelengths between which the band radiance was calculated were determined from the overlap of the photodiode photosensitivity curve and infrared fibre optic transmission curve. The photodiode photosensitivity and fibre optic transmission curves were represented as 'top-hat' functions with infinite cut-off gradients, as illustrated in figure A2.1

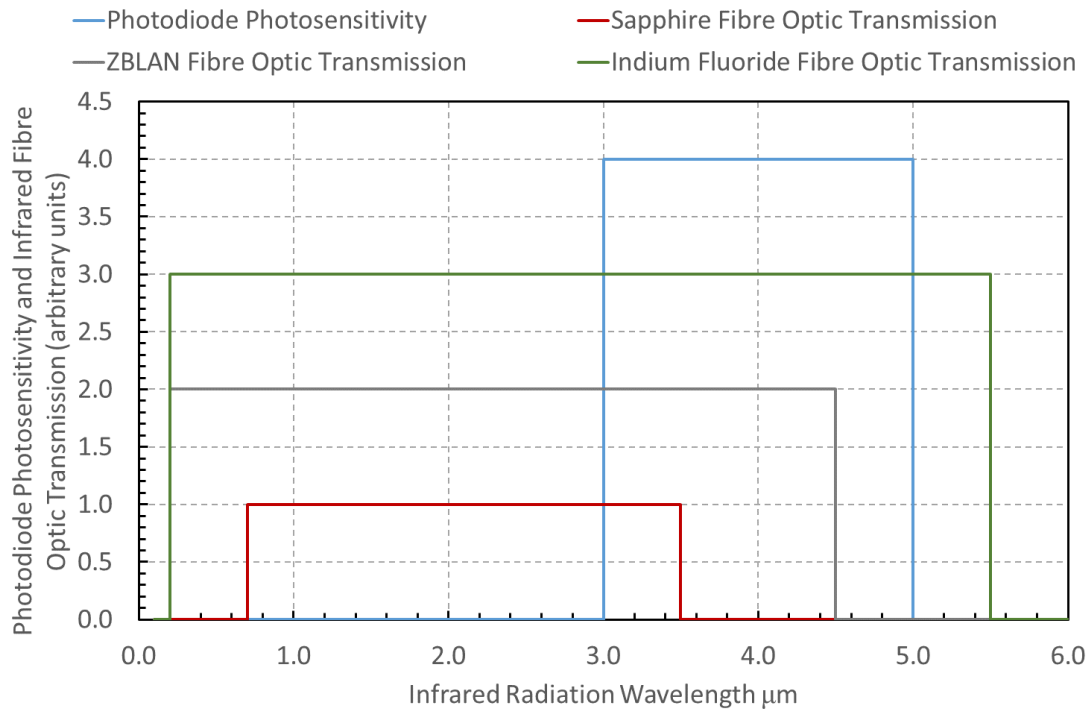


**Figure A1.8.2 Illustration of ‘top-hat’ functions used to represent photodiode photosensitivity and infrared fibre optic transmission curves in calculations**

The values of band radiance calculated were multiplied by the solid angle into which the object emitted and the fibre optic received infrared radiation to calculate the hemispherical band radiance coupled into the fibre optic, calculated according to Fresnel’s law of normal incidence. The resultant hemispherical band radiance coupled into the fibre optic was multiplied by the étendue of the specific diameter and length of fibre optic chosen to couple the object to the thermometer. This allowed evaluation of the power incident upon the photodiode and multiplying the resultant values by the photosensitivity of the detector enabled an estimate of the photocurrent generated to be calculated for each temperature increment. The output voltage of a specific thermometer configuration, measuring different temperatures, could then be estimated by multiplying the photocurrent by the transimpedance value used in the thermometer amplifier.

## REFERENCE

- [1] W. K. Widger Jr and M. P. Woodall, ‘Integration of the Planck blackbody radiation function’, *Bull. Am. Meteorol. Soc.*, vol. 57, no. 10, pp. 1217–1219, 1976.

## APPENDIX 2. EQUIPMENT USED AND FACTORY CALIBRATION UNCERTAINTIES FOR MEASURING INSTRUMENTATION.

### A2.1 TENMA dual output power supplies, type 72-10500 serial numbers: 08250079315 and 08250079241

Supplies configured to provide: positive d.c. voltage, negative d.c. voltage and zero Volts to thermometer printed circuit board power rails, when connected to dual supply printed circuit boards. The zero voltage point was defined as the mid-point of the positive and negative supplies. Maximum voltages and currents supplied were constrained to be  $\pm 8$  V and 0.5 A when connected to  $\pm 5$  V regulated rails.

Positive d.c. voltage and zero Volts when connected to single-side supplied printed circuit board power rails. The maximum voltage and current supplied were +5 V and 0.5 A in this configuration. A TLE2426 virtual ground rail splitter provided  $\pm 2.5$  V and 0 V from the single-side supply, with zero Volts defined as the mid-point of the 0 – 5 V supply. The virtual ground rail splitter could be used with higher positive d.c. voltage to provide a wider range of voltage to the operational amplifiers.

### A2.2 Keysight 34465A digital multi-meters (DMM) serial numbers: MY54503080, MY57500347 and MY54503021

Factory calibration details in tables A2.1a – c for the measurement ranges used.

**Table A2.1a Keysight DMM Serial Number MY54503080 d.c. Volt measurements**

Range	Value	Measurement	Error	1-year Specification
V	V	V	%	%
0.1	0.1	0.1000016	+0.0016	0.0085
1.0	1.0	0.9999999	0.0000	0.0039
10	10	9.9999949	-0.0001	0.0034
10	-10	-10.000002	0.0000	0.0034

**Table A2.1b Keysight DMM Serial Number MY57500347 d.c. Volt measurements**

Range	Value	Measurement	Error	1-year Specification
V	V	V	%	%
0.1	0.1	0.1000009	+0.0009	0.0085
1.0	1.0	1.0000011	+0.0001	0.0039
10	10	9.9999993	0.0000	0.0034
10	-10	-10.0000004	0.0000	0.0034

**Table A2.1c Keysight DMM Serial Number MY54503021 d.c. Volt measurements**

Range	Value	Measurement	Error	1-year Specification
V	V	V	%	%
0.1	0.1	0.1000014	+0.0014	0.0085
1.0	1.0	0.9999989	-0.0001	0.0039
10	10	9.9999908	-0.0001	0.0034
10	-10	-9.9999979	0.0000	0.0034

### A2.3 Approximate blackbody furnaces, used as radiant temperature sources through the range of temperatures 25 °C to 1100 °C

The voltages generated by the prototype thermometer transimpedance amplifiers were characterised against the approximate blackbody furnaces, having the specifications as follows:

#### A2.3.1 Ametek-LAND P1200B three-zone, tube furnace serial number 1078

Uniformity +/- 0.2°C of radiance temperature across the central 40mm of the infrared emitting target surface area between 200 °C and 1100 °C temperature set point when controlling at temperature

Stability  $\pm 0.2$  °C of radiance temperature over 60 minutes duration

Emissivity = 0.998

### A2.3.2 Ametek-LAND P80P compact calibrator; serial number 195671

Emissivity  $>0.995$

Uniformity  $\pm 0.2$ °C across the central 40mm of the radiant target surface area when controlling at temperature

Stability  $\pm 0.5$ °C of radiance temperature over 30 minutes duration when controlling at steady-state temperature

### A2.3.3 Ametek-LAND P550P compact calibrator; RMA 56188 serial number 35612-1

Emissivity  $>0.995$

Uniformity  $\pm 0.2$ °C across the central 50mm of the radiant target surface area at 150°C set point temperature when controlling at temperature, increasing to  $\pm 0.5$ °C across the central 50mm of the radiant target surface area at 500 °C set point when controlling at temperature

Stability  $\pm 0.5$ °C of radiance temperature over 30 minutes duration when controlling at steady-state temperature

Radiance temperature tolerances around set point when controlling at steady-state temperature

$\pm 1$ °C between 50-350°C

$\pm 2$ °C between 350-500°C

$\pm 3$ °C above 500°C

### A2.4 Isothermal Technology Limited (ISOTECH) milliK precision digital thermometer serial number 36267/1

Factory calibration of the channels and ranges used that were calibrated to traceable ISO/IEC standard 17025:2005 at the time of supply are presented in tables A2.2 to A2.4.

**Table A2.2 Factory Calibration Data for ISOTECH milliK Thermometer for both Channels with Type R Thermocouple Inputs Referenced to BS EN 60584-1:1996**

Simulated Temperature °C	milliK Channel 1 °C	milliK Channel 2 °C	Uncertainty of Measurement °C
0.0	0.22	0.17	0.4
800.0	800.23	800.18	0.4
1600.0	1600.24	1600.17	0.4

**Table A2.3 Factory Calibration Data for ISOTECH milliK Thermometer Channel 1 with PT-100 RTD Input Referenced to BS EN 60584-1:1996**

Nominal Value °C	Actual Value Applied Ω	Equivalent IEC-60751-2008 °C	milliK Channel 1			
			Measured °C	Error mK	Measured Ω	Error mΩ
-200	18.520274	-199.9995	-199.9995	0.0	18.52030	0.0
-100	60.260154	-99.9894	-99.9894	0.0	60.26007	-0.1
0	99.999748	-0.0006	-0.0011	-0.5	99.99955	-0.2
100	138.512807	100.0193	100.0186	-0.7	138.51250	-0.3
250	194.099290	250.0032	250.0022	-1.0	194.09877	-0.5
400	247.088744	399.9905	399.9886	-1.9	247.08811	-0.6
660	332.788970	659.9907	659.9882	-2.5	332.78820	-0.8
850	390.484578	850.0119	850.0074	-4.5	390.48332	-1.3

**Table A2.4 Factory Calibration Data for ISOTECH milliK Thermometer Channel 2 with PT-100 RTD Input Referenced to BS EN 60584-1:1996**

Nominal Value	Actual Value Applied	Equivalent IEC-60751-2008	milliK Channel 2			
			Measured	Error	Measured	Error
°C	Ω	°C	°C	mK	Ω	mΩ
-200	18.520264	-199.9996	-199.9995	0.1	18.52028	0.0
-100	60.260169	-99.9893	-99.9893	0.0	60.26019	0.0
0	99.999718	-0.0007	-0.0009	-0.2	99.99969	0.0
100	135.512778	100.0192	100.0194	0.2	138.51262	-0.2
250	194.099403	250.0035	250.0038	0.3	194.09951	0.1
400	247.089233	399.9920	399.9921	0.1	247.08932	0.1
660	332.789358	659.9919	659.9920	0.1	332.78928	-0.1
850	390.485264	850.0142	850.0125	-1.7	390.48482	-0.4

**A2.5 Isothermal Technology Limited (ISOTECH) transfer standard Platinum Resistance Temperature Detector (Pt-100 RTD) serial number 36267/2**

An Isothermal Technology Limited transfer standard Platinum resistance thermometer having the factory calibration in table A2.5 that was traceable to UKAS standards at time of supply.

**Table A2.5 Factory Calibration Data for ISOTECH PT-100 RTD Input Referenced to BS EN 60584-1:1996**

Measured Temperature	Measured Output of The Calibrated Thermometer	Uncertainty of Measurement
° C	Ω	° C
0.010	99.993348	0.015
-50*	80.262505	0.025
0.010	99.989608	0.015
660.323*	333.167664	0.050
419.532*	253.965198	0.040
0.010*	99.991218	0.015

A stirred liquid bath was used to calibrate the -50° C point, a water triple point cell was used to calibrate the 0.01°C point and fixed point cells containing Zinc and Aluminium were used to calibrate the 419.9°C and 660.3°C points, respectively.

Uncertainty of measurement by laboratory standard Platinum resistance thermometer +/- 0.0008 Ω, which is equivalent to +/- 0.002 °C referenced to BS EN 60751:2008

Callendar – van Dusen coefficients were derived from the results marked with asterisks in table A2.5 for use in the Callendar – van Dusen equation describing PRT-100 resistance, R.

$$R = R_0 [ 1 + AT + BT^2 + (T-100) CT^3 ]$$

Where:

$R_0 = 99.98731\Omega$  and which represented the resistance of the PRT-100 at 0 °C

$$A = 3.912772 \times 10^{-3}$$

$$B = -5.770136 \times 10^{-7}$$

$$C = -1.024102 \times 10^{-11}$$

**A2.6 Isothermal Technology Limited (ISOTECH) transfer standard type R thermocouple serial number 36267/3**

Factory calibration, traceable to UKAS standard at time of supply and referenced to BS EN 60584-1:1996 standard for thermocouple electro-motive force (EMF) versus temperature relationship.

**Table A2.6 Factory Calibration of electromotive force (emf), E for each temperature measured with reference to the expected emf, E<sub>ref</sub> from BS EN 60584-1:1996 standard for thermocouples at the temperatures recorded.**

Temperature	Measured emf (E)	E – E <sub>ref</sub> Difference	Uncertainty of Measurement
°C	µV	µV	°C
350.48	2892	-9	0.8
599.96	5578	-5	0.8
850.05*	8577	5	0.8
1099.88*	11860	12	0.8
350.87*	2897	-8	0.8

A deviation equation for the error E – E<sub>ref</sub>, referenced to BS EN 60584-1:1996 was derived from the results marked with asterisks in table YY.

$$E - E_{ref} = ct^3 + bt^2 + at$$

Where:

$$a = -0.0574629577862073$$

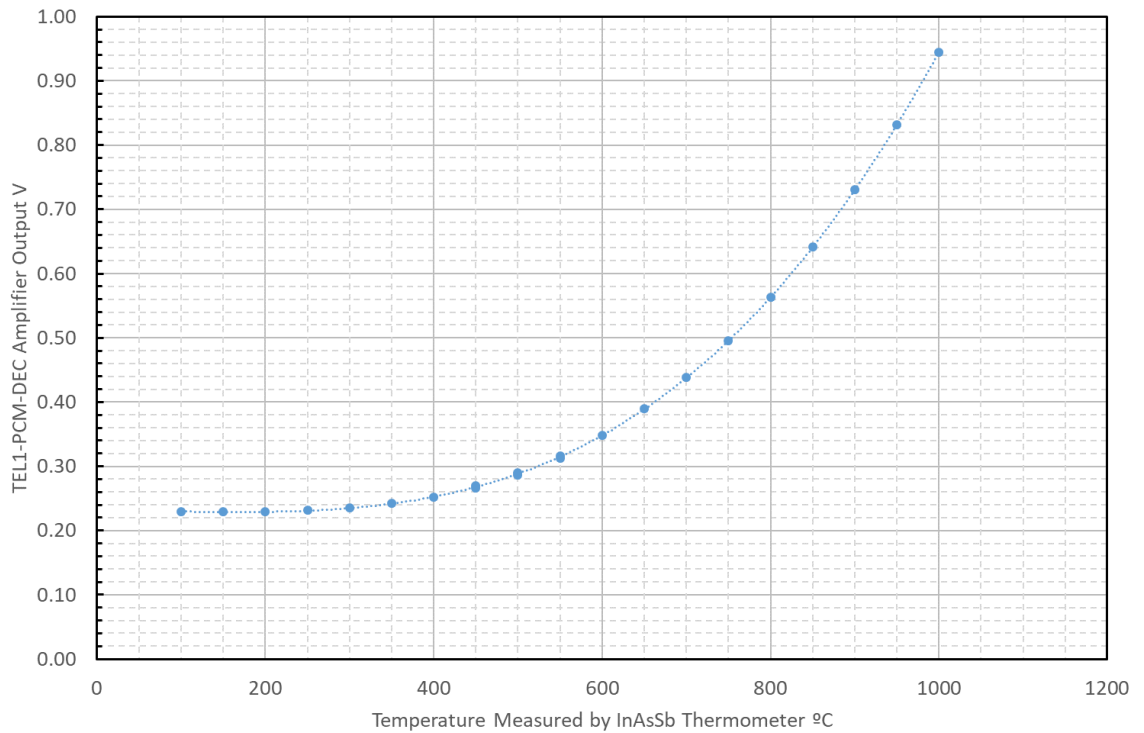
$$b = 0.000115947320198002$$

$$c = -4.88990150970532 \times 10^{-8}$$

**A2.7 Krauss-Messtechnik (KMT) inductive data transmission system type TEL1-PCM-DEC, serial number 170249-01/Alarm\_10V**

The calibration of the output from the inductively-coupled amplifier used in the machining application when the Indium Arsenide Antimony photodiode based

thermometer was connected to the input is presented in figure A2.1. The inductively-coupled amplifier output would achieve up to 10V output with a higher input voltage provided by the thermometer, for example: from voltage amplification after the transimpedance amplifier or higher transimpedance in the feedback loop. It was evident that the output voltage from the thermometer could be multiplied by a factor



of ten without saturating the inductively-coupled signal amplifier.

**Figure A2.1 calibration of inductively-coupled amplifier output connected to infrared radiation thermometer output**

### APPENDIX 3. TRACK AND COMPONENT LAYOUT DRAWINGS FOR THERMOMETER PRINTED CIRCUIT BOARD.

The prototype printed circuit board was prepared using Proteus Design Suite 8.8 computer-aided PCB design software. The top and bottom layer drawings, illustrating the tracks, ground planes and component positions and orientations are presented in figures A3.1 and A3.2.

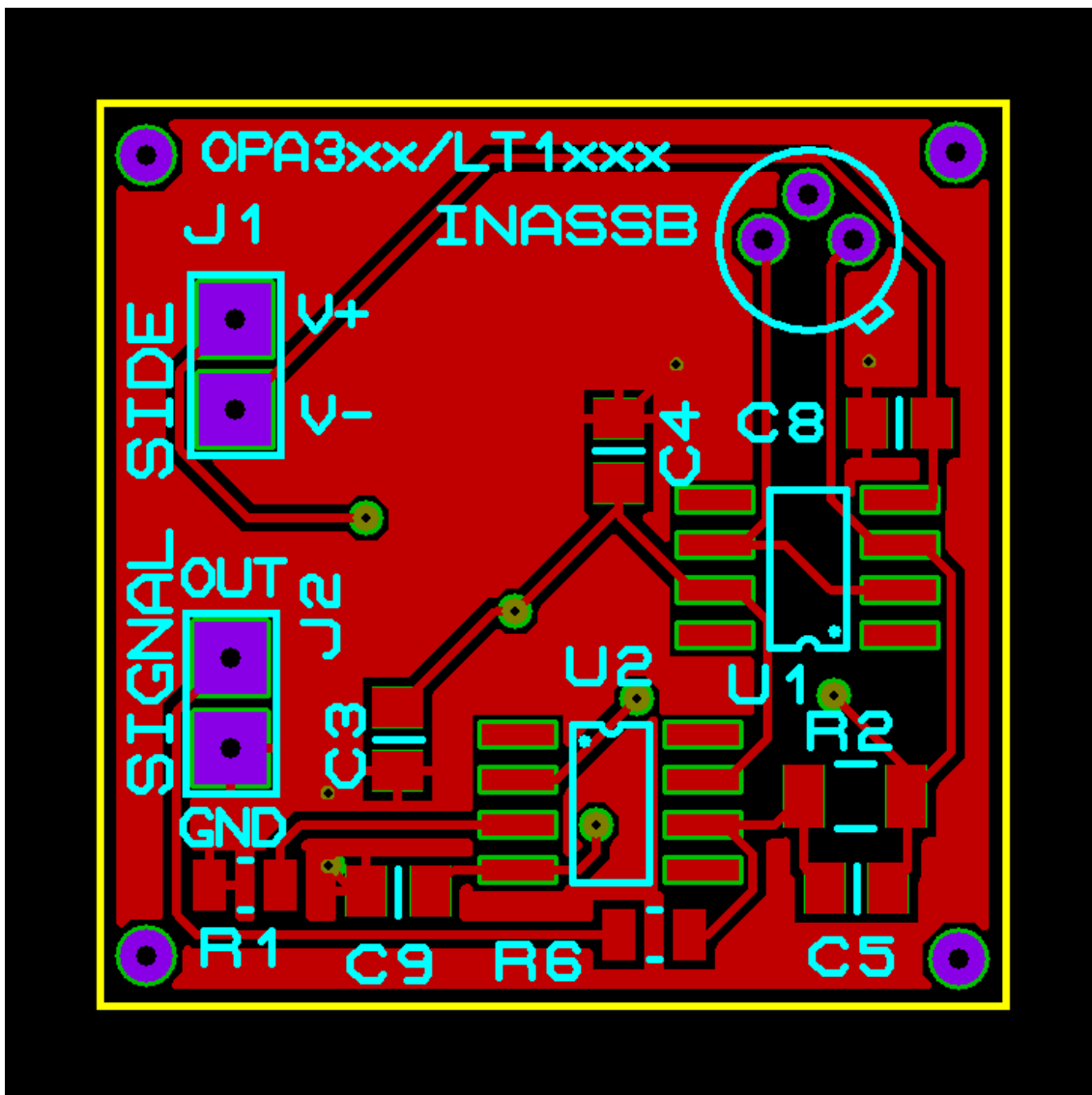


Figure A3.1 PCB Top Layer

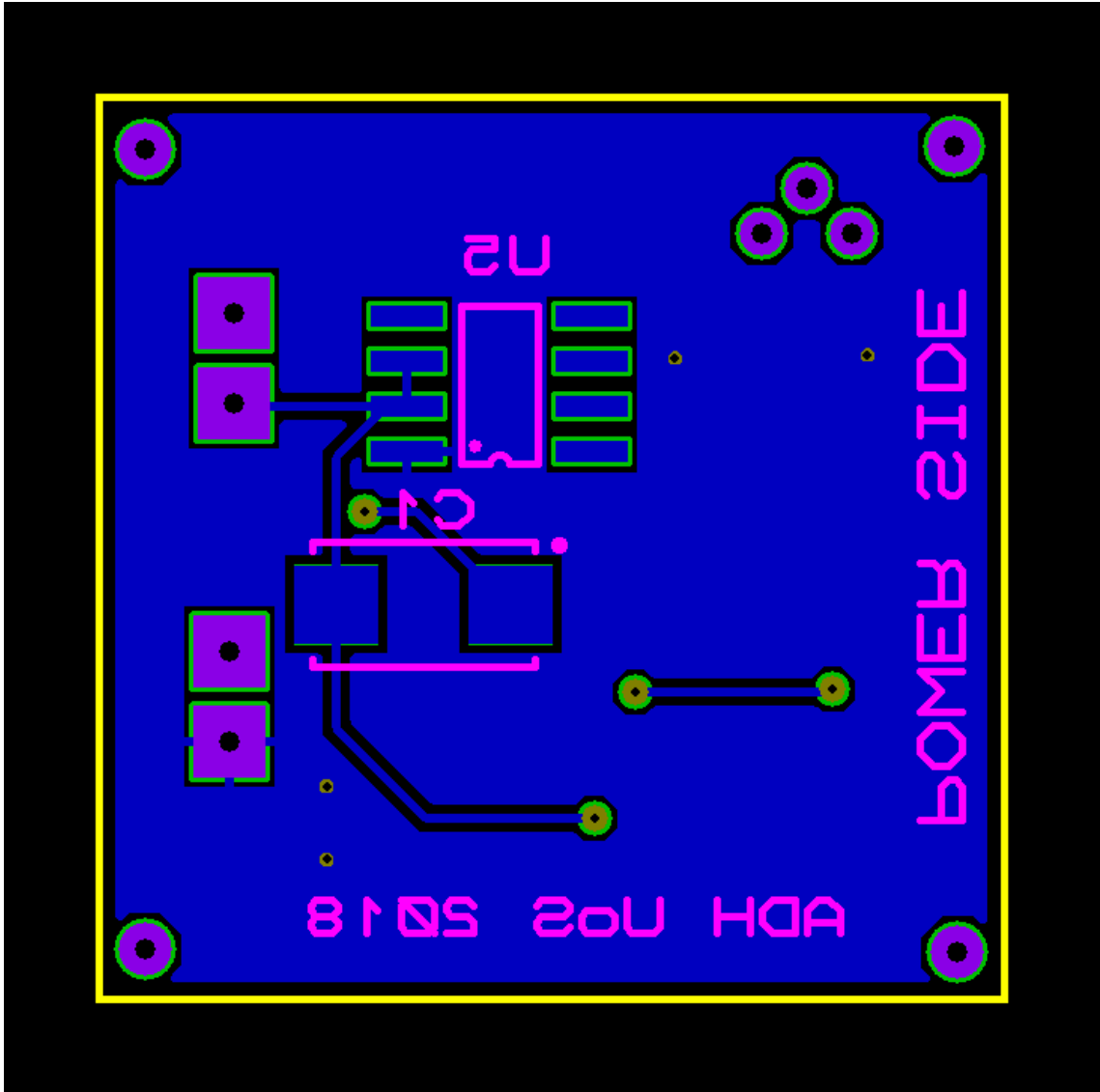


Figure A3.2 PCB Bottom Layer